UNIVERSITY OF CALIFORNIA SAN DIEGO

The role of microglial TAM receptors in neurodegenerative diseases

A dissertation submitted in partial satisfaction of the
requirements for the degree Doctor of Philosophy

in

Biology

by

Youtong Huang

Committee in charge:

Professor Greg Lemke, Chair
Professor Elina Zúñiga, Co-Chair
Professor Axel Nimmerjahn
Professor Robert Rissman
Professor Nicholas Spitzer

2020

The Dissertation of Youtong Huang is approved, and it is acceptable in quality and form for publication on microfilm and electronically:

_____

_____

_____

_____
Co-Chair

_____
Chair

University of California San Diego

2020

EPIGRAPH

“There is some good in this world, and it’s worth fighting for.”

Samwise Gamgee

-- J.R.R. Tolkien*, The Lord of the Rings: The Two Towers*

TABLE OF CONTENTS

LIST OF SUPPLEMENTAL FILES

Huang_Supplemental_Video_1

Huang_Supplemental_Video_2

Huang_Supplemental_Video_3

Huang_Supplemental_Video_4

LIST OF FIGURES

ACKNOWLEDGEMENTS

First, I would like to express my sincere gratitude to my mentor Greg Lemke for always guiding and inspiring me to become a better scientist and a better person. Greg, for the past five years of my life, there simply has been no better place for me to be than in your lab at Salk. You have greatly inspired me with your passion for science, your dedication for your trainees by always making yourself available to us and caring for our careers and lives, and for providing us with a healthy sanctuary to freely explore questions and wonders. I am beyond grateful for the training opportunities you have given me and the challenges you have encouraged me to pursue. Despite your denial of your niceness, I believe (and everyone would agree that) you are also a mentor who brings about the flourishing of his mentees to their full capacities. Over the years in the Lemke lab, I have witnessed countless instances of your selfless generosity and your compassionate heart, always standing up for the weak and the underrepresented. I am deeply touched by the care you have for each of us. I look forward to further improving my scientific and interpersonal skills working with you and to living up to the name of a “Lemkoid” for years to come.

I thank all the Lemke lab members, Kaisa, Lidia, Sheng, Patrick, Joe and Paqui, of course our “foster siblings” Graziana and Stefania, for being practically like family to me. I have learned so much in science and in life from each and one of you and I wish endless happiness and success for your futures. Kaisa, thank you for constantly radiating positivity and brilliance, for your kind guidance leading me onto the path of research, for our teamwork, and for our friendship. You have truly been a great role model for me both as a scientist and as a big sister. Lidia, you are like the first ray of sunshine in a forest, full of bright hope and contagious joy. Hay una amiga en mi! Having witnessed your metamorphosis in the U.S., I know you can achieve anything in the future with your dedicated attitude and curiosity

towards science and the world. Sheng, thank you for always making time for me and my projects. I am constantly inspired by your patience and rigorous attitude in research and will always be grateful for your help in the establishment of my AD project. Patrick, thank you for your generous time and help in making things work perfectly for my projects, for fostering a cheerful lab atmosphere, and for sharing your positive attitude in many aspects in life. I love the many sweet things each of you has done for the lab to make it a home. Because of you all, I'm proud to be a Lemkoid.

I would like to thank my committee members, Axel Nimmerjahn, Elina Zúñiga, Nicholas Spitzer and Robert Rissman for your time, helpful discussions, scientific insights, and generous support throughout my graduate career. I would like to especially thank Axel for his collaboration on my AD project, for his dedication to my education and for his very insightful guidance in my research and in teaching me about two-photon microscopy. He has demonstrated and shared with me the kind of pure joy of simply making things work and finding out how they work, the kind that Richard Feynman possibly refers to. Our discussions have benefited my research and career till today and certainly for many years onwards, for which I'm deeply grateful.

I would like to thank my friends and family who have been the supply of my core power. I thank my grandmother, the most optimistic and kind woman whom I had the luck to grew up close to. I will count myself lucky if I'm half as contented as she is when I am at her age. My ultimate inspiration comes from my mother and father. They are the twin pillars of my life without whom I cannot stand. They never gave me any ideas of what I cannot do and have constantly supported me and my decisions with complete understanding and unfailingly love. I am proud to be their child. My sincere gratitude also goes to my "American mother"

also the first person I know from the US, Mima, who has sheltered me during every college spring break, cared for my physical and spiritual nourishment, and taught me how to love. I thank my friends in my PhD program and at Salk, Jacey, Ye, Nancy and my “foodies” friends for making SD a home away from home. I also thank my friends far and near for their support throughout my PhD journey, especially my UCLA besties, Lushin, Sarah, Cynthia and Sara, and my soul mate, Cornelia. Last but not least, I am grateful for my boyfriend, Joshua, whom has gracefully provided me with incredible patience and support during my most anxious times. We are on our way to being life-long learners.

Chapter 2 is largely adapted from the material as it appears in **Huang, Y.,** Happonen, K.E., Burrola, P.G., O’Connor, C., Hah N., Huang, L., Nimmerjahn, A. & Lemke, G. Microglia use TAM receptors to detect and engulf amyloid beta plaques. *Nature Immunology*, In revision. (2020). The dissertation author was a primary investigator and the first author of this material. The authors would like to thank Joseph Hash for excellent technical assistance; Dr. Marc Mercken (Janssen Pharmaceuticals) for $A\beta_{42}$ antibodies; Dr. Robert Rissman and the Alzheimer’s Disease Research Center at UCSD for AD brain sections; Dr. Maxim Shokhirev for advice on bioinformatic analyses; Shijia Liu (Han lab) for technical assistance; Dr. Sarah Parylak (Gage lab), Dr. Isabel Salas and Jillybeth Burgado (Allen lab), for technical assistance and useful discussion; and members of the Lemke laboratory, Molecular Neurobiology Laboratory and Nomis Center for helpful discussions. Supported by grants from the US National Institutes of Health (RF1 AG060748 and R01 AI101400 to G.L., DP2 NS083038, R01 NS108034, and U01 NS103522 to A.N., P30 AG062429 to the UCSD ADRC, and P30 CA014195 and S10-OD023689 to the Salk Institute), the Cure Alzheimer’s Fund (to G.L.), and the Leona M. and Harry B. Helmsley Charitable Trust (to the Salk Institute); by Marguerite Vogt and H.A and Mary K. Chapman Charitable Trust graduate and

Goeddel Chancellor's graduate fellowships (to Y.H.), and by Anderson, Nomis, and Sweden-America Foundation postdoctoral fellowships (to K.E.H.).

Chapter 3, in part, is currently being prepared for submission for publication of the material. The working citation is: **Huang, Y** and Lemke, G. TAM receptors are crucial mediators of ALS pathology. The dissertation author was a primary investigator and the first author of this material. The authors would like to thank Joseph Hash for excellent technical assistance; Dr. L.Sweeney (Kintner lab, now at IST Austria) for providing MMP9 antibody and useful discussion, Dr. Graziana Gatto and Xiangyu Ren (Goulding lab) for antibodies and useful discussion. Supported by grants from the US National Institutes of Health (RF1 AG060748 and R01 AI101400 to G.L., and P30CA014195 to the Salk Institute), the Leona M. and Harry B. Helmsley Charitable Trust (to the Salk Institute) and by Marguerite Vogt, H.A and Mary K. Chapman Charitable Trust, Goeddel Chancellor's graduate fellowships and Salk Women and Science award (to Y.H.).

VITA

2011 - 2015 B.S. in Neuroscience (honors), University of California Los Angeles

2015 - 2020 Ph.D. in Biological Sciences, University of California San Diego

Thesis advisor: Greg Lemke (Salk Institute for Biological Studies)

PUBLICATION

Huang, Y., Happonen, K.E., Burrola, P.G., O'Connor, C., Hah N., Nimmerjahn, A. & Lemke, G. Microglia use TAM receptors to detect and engulf amyloid beta plaques. *Nature Immunology*, In revision. (2020).

MANUSCRIPT IN PREPARATION

Huang, Y. & Lemke, G. TAM receptors are crucial mediators of ALS pathology. *Manuscript in preparation.*

ABSTRACT OF THE DISSERTATION

The role of microglial TAM receptors in neurodegenerative diseases

by

Youtong Huang

Doctor of Philosophy in Biology

University of California San Diego, 2020

Professor Greg Lemke, Chair
Professor Elina Zúñiga, Co-Chair

Many neurodegenerative risk genes are predominantly expressed in microglia, the primary immune cells in the central nervous system. Our lab has demonstrated that two microglial TAM receptor tyrosine kinases - Axl and Mer – control multiple features of microglia physiology. Importantly, recent transcriptomic analysis has linked TAM receptors to Alzheimer's disease (AD) and Amyotrophic lateral sclerosis (ALS). This thesis dissertation describes original work that examines the expression and function of TAM receptors and their ligands in AD and ALS. We find that in AD and its mouse models, induced expression of Axl and Mer in amyloid plaque-associated microglia is coupled to induced plaque decoration

by the TAM ligand Gas6 and its co-ligand phosphatidylserine. Prior to plaque deposition in the *APP/PS1* AD model, genetic ablation of Mer alone leads to a marked increase incidence of lethal epileptic seizures. After deposition of plaques, ablation of Axl and Mer results in microglia that are unable to normally detect, respond to, organize, or phagocytose amyloid beta plaques, a hallmark of AD pathology. These major deficits notwithstanding, TAM-deficient AD mice develop fewer dense-core plaques than AD mice. Our findings reveal that the TAM system is an essential mediator of microglial recognition and engulfment of plaques, and that TAM-driven microglial phagocytosis does not constrain, but rather promotes, plaque development. In an ALS model, we find that TAM system is similarly strongly activated in microglia during disease progression. ALS mice in the absence of Axl and Mer have significantly advanced symptom onset, but their disease course is almost twice as long as that of TAM-expressing ALS mice. This delayed arrival of the end stage of disease may be accompanied by dampened inflammation and an increased survival of ALS-vulnerable motor neurons as a result of TAM deficiency. Original work in this dissertation suggests a critical and differential involvement of TAM receptors in early and late stages of both AD and ALS. With several whole-body TAM receptor antagonists already in development and clinical trials as cancer therapeutics, a thorough understanding of the roles of microglial TAM receptors in neurodegeneration is of genuine importance to public health.

Chapter 1: Introduction

1.1 The role of microglia in health and disease

Microglia are the distinctive tissue macrophages of the central nervous system (CNS)[1-10]. These immune sentinels, which constitute ~10% of the cells in the CNS[9], tile the parenchyma of the brain and spinal cord. Microglia are a unique class of cells in the CNS in terms of their origin, characteristics, and functions in contrast to other glial cell types, such as astrocytes and oligodendrocytes. They originate during primitive hematopoiesis in the fetal yolk sac and enter and reside in the CNS during early fetal development between E9.5 to E10.5, before the formation of the blood-brain barrier (BBB) [11,12]. Because of their yolk sac origin, these cells are maintained for very extended periods through continuous self-renewal. In a normal, healthy CNS, microglia continuously scan their immediate environment, exhibiting a ramified morphology, with many locally motile processes[13,14].

Microglia have gained increasing recognition over the last decade as to their critical roles in the development, homeostasis, and response to CNS injury and disease. They are most known for the roles they play in immune surveillance and the phagocytic removal of apoptotic cells (ACs) and microbes as professional phagocytes, similar to many tissue resident macrophages. Microglia are the first and primary front of cells to mount a response towards pathogens and the clearance of debris. In addition, microglia at steady-state are also known to provide CNS-specialized functions that are tightly associated with the maintenance of brain homeostasis[15], such as contributing to circuit plasticity by phagocytic pruning of exuberant synaptic elements during development[5,16,17], secreting neurotrophic factors such as IGF1, BDNF and TGFβ [18 19], modulating neuronal activity by sensing ATP [20,21] and phagocytosing ACs after adult neurogenesis[22 23,24]. In response to trauma or infection, these cells transform into amoeboid cells. They sense chemokine/nucleotide gradients radiating

from sites of injury and infection, migrate to these sites, and produce a panoply of proinflammatory effectors such as TNFα, IL-1β, and nitric oxide.

While the CNS was once viewed as a 'privileged environment devoid of classical immune signaling, chronic neuroinflammation is now known to be a hallmark of many neurodegenerative diseases (NDs), including Alzheimer's Disease (AD)[25,26], Multiple Sclerosis (MS)[27], Parkinson's Disease(PD)[26], and Amyotrophic Lateral Sclerosis (ALS)[28]. Emerging evidence suggest that neuroinflammation is not only both induced and regulated locally in the CNS, but also actively contributes to pathogenesis in NDs. Microglia, along with other glial cells such as astrocytes, are the key cells that produce and respond with neuroinflammation, typically recognized as reactive microglia at pathology-impacted regions [29-31].

However, despite unequivocal acknowledgement of the participation of microglia in NDs, whether activated microglia in NDs play a protective or detrimental role in the course of neurodegeneration, especially during the chronic progression of disease, is still largely unknown. On one hand, reactive microglia may play an active neuroprotective role by engulfing pathological structures such as aberrant protein aggregates, recruiting more phagocytes with the release of inflammatory cytokines while concomitantly clearing the AC corpses that are produced at sites of injury or neurodegenerative lesions. On the other hand, while these effectors are critical to an effective immune response, chronic activation of these cells due to sustained exposure to accumulated unresolved pathological features can lead to functional impairment of microglia. This may inflict secondary cytotoxic damage to neuronal function and survival, thus exacerbating neurodegeneration. Elucidating the role of microglia

in NDs, specifically the molecular mechanisms whereby microglia mediate responses towards disease pathology, is one of the main goals of this thesis.

The degree of contribution of infiltrated monocyte-derived macrophages in NDs is an unsettled argument, and studies have shown contradictory results [32,33], in part because molecular markers distinguishing resident microglia from blood-derived macrophages have also been lacking in disease settings. Though it may be that infiltrated macrophages present higher expression of CD45 when evaluated by FACS comparing to resident microglia[34], CD45 expression also increases in activated myeloid cells thereby obscuring the separation of the two populations[35,36]. In addition, although resident microglia have been shown to specifically express Tmem119 as a homeostatic marker[37], we and others[38] have shown that reactive microglia such as those near Aβ plaques, a classical hallmark of AD pathology, significantly downregulate Tmem119 in AD and other NDs (Fig. 2.3.1-3). Therefore, we have not attempted to distinguish resident microglia from infiltrated blood-derived macrophages during disease, or from other CNS macrophages found in the meninges, choroid plexus, and perivasculature. We have instead studied Iba1+ cells in brain and spinal cord in mouse models of AD and ALS – these cells are loosely termed 'microglia' in this thesis. This is primarily due to the limiting scope of these projects and the available genetic tools when the projects started, but also because 1) microglia and infiltrated macrophages are all positive for TAM receptors, which is the signaling pathway upon which our project is focused; and 2) microglia are the most abundant immune cell type in the CNS (monocytes constitute ~1% of all CD45+ cells at even the peak stage of AD[39]). Several lines of evidence indicate that the Iba1+ (or Cx3cr1+) CNS cells we are studying are microglia.

1.2 TAM system in microglia and other immune sentinels

Our laboratory discovered a signaling system that controls two fundamental activities – the inhibition of the innate immune inflammatory response and the phagocytosis of ACs and membranes – in immune sentinels[40-54]. This system is composed of the TAM receptor tyrosine kinases (RTKs) Tyro3, Axl, and Mer[42,46] and their ligands Gas6 and Protein S (Pros1)[46,55] (**Fig.1.2-1**).

Our group first identified the TAM RTK family[42]. We demonstrated that TAM signaling operates as the ultimate arm of the innate response to pathogens in immune sentinels, where it inhibits the expression and activity of inflammatory cytokines[45,46,48,49,56]. In dendritic cells (DCs), we showed that pathogen detection by pattern recognition receptors activates the genes for type I interferons (IFNs), which subsequently induce Axl. Axl in turn binds to the R1 chain of type I IFN receptors (IFNARs), and a hybrid Axl-IFNAR complex then activates *suppressor of cytokine signaling* (*SOCS*) genes 1 and 3, whose products shut down Toll-like receptor (TLR) and cytokine receptor signaling[49]. Thus, Axl is a pleiotropic inhibitor of the innate immune response, and its induction is intrinsic to that response[46]. TAM-mediated immune suppression in both DCs and macrophages has subsequently been demonstrated by many groups.

Concomitantly, TAM receptors and their ligands mediate the phagocytic clearance of ACs and phosphatidylserine (PtdSer)-rich membranes from nearly all mature tissues[44-46,57]. This phagocytosis is generally driven by Mer in healthy tissues, but is additionally mediated by Axl and Tyro3 in infected, damaged, or degenerating tissues[44,46,51,52,56,58]. It has been documented for DCs and macrophages of the immune system, Sertoli cells of the testis, retinal pigment epithelial (RPE) cells of the eye, and microglia[23,44,46,47,59-61] (**Fig. 1.2-2**). TAM-

mediated phagocytosis of membranes and cells requires the N-terminal 'Gla domains' of Gas6 and Pros1 (Fig.1.2-1): ~40 amino-acid modules, rich in γ-carboxylated glutamic acid residues, which mediate binding to PtdSer[52,62]. This phospholipid is confined to the inner leaflet of the plasma membrane in all normal cells, but is displayed on the outer leaflet of ACs[63-66]. It is the most common and potent of the *'eat-me'* signals by which dead cells are recognized by phagocytes[67,68]. Gas6 and Pros1 thus serve as 'bridging molecules' that link PtdSer on the surface of phagocytic cargo to the TAM receptors expressed by phagocytes (Fig. 1.2-2)[54]. In their action, Gas6 and Pros1 resemble other PtdSer bridging molecules[69-72]. However, these ligands have the unique ability, via their C-termini, to also bind the TAMs and thereby activate their tyrosine kinases (Fig. 1.2-2). This is key to TAM action[54,56], since ligand-opsonized ACs concomitantly trigger *both* immune suppression *and* their own phagocytic engulfment. We have shown that *Tyro3*$^{-/-}$*Axl*$^{-/-}$*Mertk*$^{-/-}$ triple knock-out (TAM TKO) mice[47] are viable, but autoimmune[44,45,48,58], infertile[47], and blind[47,59,60,73,74], because TAM function is required for phagocytosis and immune suppression in macrophages/DCs, Sertoli cells, and the RPE (Fig. 1.2-2).

We have recently shown that microglia normally express high levels of Mer and low levels of Axl, and are Tyro3-negative[23]. Importantly, we have also shown that microglial Axl is strongly up-regulated in response to neuroinflammatory stimuli, and in a transgenic mouse model of Parkinson's disease (PD)[23]. In this respect, microglia are very similar to tissue macrophages generally, in that we have previously shown that tissue macrophages *in vivo* express high levels of Mer (in concert with the high affinity $F_c\gamma$ receptor, Mer is now a consensus tissue macrophage marker[75]) and low levels of Axl[51]. Axl, however, is an extremely sensitive inflammation indicator, and its expression in macrophages and DCs is

up-regulated from 20- to 100-fold by type I IFNs, IFNγ, LPS, and many other inflammatory stimuli[49,51].

We have further shown that microglia require Mer predominantly and Axl secondarily for CNS phagocytosis in two distinct settings – the engulfment of the large number of ACs that are generated during adult neurogenesis in the hippocampus and subventricular zone[23], and the phagocytosis of neural cells that have been infected by viruses[61]. The neurogenic regions of *Mertk*$^{-/-}$ and *Axl*$^{-/-}$*Mertk*$^{-/-}$ mice have 10-fold and 40-fold more cleaved caspase3^{+} ACs, respectively, than do those of WT mice[23], a phenotype that we showed is due to the loss of TAM signaling specifically in microglia[23]. Both Gas6 and Pros1 function as TAM ligands in these cells[23]. Similarly, in a study published together with colleagues in Axel Nimmerjahn's laboratory, we showed that neural cells transduced with Adenovirus 5-based vectors are phagocytically cleared within days of transduction by TAM-dependent microglial phagocytosis. Both of these phagocytic events require PtdSer exposure on the surface of cells that are to be engulfed[23,61]. Remarkably, several lines of evidence indicate that many of these engulfed cells are not dead, but rather are eaten alive, by microglia, simply because they display PtdSer on their surface[54,61,76,77].

1.3 Neurodegenerative diseases

1.3.1 Alzheimer's Disease (AD)

More than 3 million Americans and 50 million people worldwide are currently suffering from AD, one of the most prevalent and devastating neurodegenerative diseases. It is the most common form of dementia and the sixth leading cause of death in the US adults according to the CDC (https://www.cdc.gov/aging/aginginfo/alzheimers.htm). The cost of treatment, caregiving and the living of patients' and their families is tremendous, yet since its first case diagnosis by Dr. Alois Alzheimer in 1906[78], there is still no therapy that effectively prevents, halts, or reverses the progression of the disease.

The two classic histopathological hallmarks of AD are the deposition of amyloid beta plaques, an aggregation of Aβ that is generated from amyloidogenic cleavage of the amyloid precursor protein (APP), and the development of intracellular neurofibrillary tangles. Despite being first identified by Dr. Alzheimer back in 1900s, how these classical hallmarks give rise to the massive loss of neurons and synapses in cognition-related regions such as cerebral cortex and hippocampus and the loss of memory capacity among other deficits, is still not clear. The amyloid cascade hypothesis postulates that deposition of extracellular Aβ is the initial pathological event in AD. This is thought to lead to the formation of senile plaques, which umbrella all other pathological characteristics[79]. This hypothesis is strongly supported by compelling evidence including the identification of AD pathology in familial AD patients carrying various mutations on the *APP* gene, as well as in the *PSEN1/2* gene that encodes part of the gamma-secretase complex[80] that processes the C-terminal cleavage of Aβ. In fact, in parallel to this, transgenic mouse models of AD that carry these familial AD mutations[81-83] reproduce many features of human AD[84,85]. These transgenic mice include the principal model in our studies, the *B6.Cg-Tg(APPSwePSEN1dE9)* mouse[86,87], which carries a

humanized APP695swe 'Swedish mutation' transgene (K595N/M596L) paired with a mutant human presenilin gene in which exon 9 is deleted (https://www.jax.org/strain/005864). Our second model, the *APP41* (B6 congenic) mouse, which expresses a 'Swedish' + 'London' (V717I) mutant human APP under the Thy-1 promoter[88-90], has an earlier disease onset, where amyloid plaques can first be detected at 3 months of age. Another commonly adopted AD mouse model, 5XFAD[91], is loaded with five AD-linked mutations on APP and PSEN1 genes and presents precipitous pathology development[92].

Despite the supporting evidence for the amyloid cascade hypothesis, studies have shown that smaller oligomeric Aβ moieties can mediate neuronal death and impair synaptic neurotransmission *in vitro* and *in vivo*; these Aβ oligomers are proposed to be comparatively more neurotoxic than plaques[93,94 95], and emerging therapeutics have been redirected to target Aβ oligomers[96]. Others have reported a non-linear correlation between amyloid burden and cognition in AD individuals[97], suggesting a temporal gap between these two events. In addition, many AD-linked risk genes have been uncovered, including the epsilon 4 allele of the apolipoprotein E (APOE) gene[98 99]. Of interest, GWAS studies show many AD risk genes are expressed abundantly in microglia[32,33,100,101], providing novel therapeutic targets and an alternative angle for studying neuron non-autonomous contributions to disease. The strong link of an active role played by microglia and innate immunity to AD pathogenesis essentially begot the project that is covered in detail in section 1.4 and chapter 2 of this thesis. Clearly, the amyloid cascade hypothesis cannot encompass the whole story of AD pathogenesis.

Largely based on the component targeted in the amyloid cascade theory – amyloid β plaques - AD clinical trials have not been fruitful despite collective efforts from bench science, industries, and governments. Over the past 20 years, active and passive

immunotherapy have mainly been focused on developing drugs that decrease the production of Aβ, either by inhibiting activities of gamma[102-106] or beta-secretase[107,108], and those that promotes clearance of plaques from the brain such as anti- Aβ monoclonal antibodies[109,110]. Though a few drugs were shown effective in clearance of Aβ plaques in patients' brains, together with the ongoing Biogen Aducanumab in both EMERGE and ENGAGE trials, these treatments have almost uniformly failed to efficiently prevent or slow down cognitive decline in patients. This only rising star showed a minimally significant improvement in cognition outcome but more than 30% of its patients that received the drug developed amyloid-related imaging abnormalities, in an *APOEε4*-aggravating dose-dependent manner, which made it impossible for maintaining the double-blind unbiasedness of the clinical study. Not only that, some drugs even worsened cognition and increased mortality compared to the placebo, which resulted in early termination of those studies[104-106,111]. Much is to be learned from the failed clinical trials. One emerging possibility is that Aβ aggregation in forms of dense-core plaques could be a compensatory response to toxic species of Aβ-induced or idiopathic neuronal damage, which may require active engagement of microglia, the validation and mechanism of which is explored in detail in chapter 2 of this thesis work. Alternative strategies focusing on newly identified AD risk factors and more precisely druggable molecular pathways might be considered for therapeutic advancement to combat AD.

1.3.2 Amyotrophic Lateral Sclerosis (ALS)

ALS is one of the most rapidly progressive neurodegenerative diseases, and is the most common form of motor neuron disease in adults. First described by the French neurobiologist and physician Jean-Martin Charcot in 1869, ALS has since become well-known in the United States - first as Lou Gehrig's disease, in remembrance of the Yankee baseball player Lou Gehrig diagnosed in 1939, and more recently following the diagnosis of cosmologist Stephen Hawking in 1963. The disease is known to be fast progressing, uniformly fatal and devastating to patients' well-being. ALS patients live from 2 to 5 years from the time of diagnosis, during which they suffer from progressive muscle atrophy and loss of control and initiation of nearly all voluntary movements. ALS patients die from respiratory failure in most cases. According to NINDS's fact sheet, ~30,000 people in the U.S. currently have the disease (https://www.ninds.nih.gov/Disorders/Patient-Caregiver-Education/Fact-Sheets/Amyotrophic-Lateral-Sclerosis-ALS-Fact-Sheet). The socioeconomic costs for the care of ALS patients are astronomical. Despite a lack of consensus as to the cause, pathological hallmarks of ALS include progressive muscle weakness, spasms, and muscle atrophy, usually beginning with one limb and then spreading to all body parts. Atrophy is observed in the muscles that mediate speech and swallowing, which are tied to the degeneration of upper and lower motor neurons (MNs) in the brain and spinal cord. Despite years of efforts and many clinical trials[112,113], there are no therapies that halt or reverse this deadly disease.

Over the past three decades, researchers have made tremendous progress in understanding the pathogenesis of ALS. Like many other neurodegenerative diseases, in more than 90% of cases, ALS occurs sporadically and has no genetic linkage in patients. The other 5%-10% cases, the so-called 'familial' cases, display dominant inheritance, which

is where breakthroughs in ALS first appeared. A primary cause of familial ALS are missense mutations in the gene encoding the enzyme Cu^{2+}/Zn^{2+} superoxide dismutase (*SOD1*). first discovered in 1993. These mutations promote disease due to toxic gain of function of misfolded aggregated proteins, rather than a loss of enzymatic activity[114 115]. The first mouse model of ALS with transgenic expression of a G93A mutant form of the human *SOD1* gene was made in 1994, and has been thus far the most widely used ALS transgenic mouse line in pre-clinical research[116]. Since then, clinical studies have uncovered more mutations in TAR DNA-binding protein 43 (*TARDBP*), chromosome 9 open reading frame 72 (*C9orf72*), and the *FUS* gene, all of which are represented in familial and even in some sporadic cases[117]. Despite diverse genetic mutations, ALS cases have converging pathological hallmarks that underlie the devastating clinical symptoms. These include aberrant protein aggregates and impaired degradation of these aggregates, marked neuroinflammation, and selective MN death.

Neurodegeneration underlying ALS is highly target selective. The disease only affects certain MN subsets, and is relatively forgiving on other cell types[118] In addition, different motor pools are differentially affected: spinal MNs in lateral motor column (LMC) innervating limbic skeletal muscle are preferentially more affected than MNs in medium motor column (MMC) innervating axial muscles. In addition, MNs in the III, IV, VI nuclei in midbrain and brainstem as well as Onuf's nucleus in lumbosacral spinal cord, controlling eye movements and sexual functions respectively, are relatively spared despite loss of all other voluntary motor functions at late stage of ALS[119,120]. Moreover, subtypes of MN with different morphological, transcriptional and biophysical properties are selectively resistant to ALS based on their corresponding muscle contractile properties. As such, motor units can be classified as fast fatigable (FF), fast fatigable-resistant (FR), and slow (S), whose MNs have

been found to range from high to low, respectively, in terms of their susceptibility in ALS[121]. The distinction of different lower motor neuron sub-populations primarily relies on distinguishing between molecular markers. For example, matrix metalloproteinase 9 (MMP9) is only expressed specifically in FF alpha MNs but is absent from FR alpha MNs and ALS-resistant S MN subpopulations. These are the largest, most-excitable MNs, and are involved in producing short-lasting bursts of forceful muscle contraction such as running[122,123-125]. Studies suggest almost all MMP9-expressing MNs are selectively lost at the end stage of disease in $SOD1^{G93A}$ mice, while the residual 50% MNs are MMP9-negative[122]. In addition, NeuN is found in ChAT+ alpha MNs but is largely absent in ChAT+ gamma MNs[126 127]. ERRγ is often used as a marker for S gamma MNs, which innervate small and slow-contracting muscle fibers that typically control behaviors such as keeping the body upright[126,128,123]. Multiple MN-autonomous and non-cell-autonomous mechanisms that mediate the selective loss of MNs have been proposed. Among these mechanisms, a role of excessive glutamate-mediated excitotoxicity and neuroinflammation in forms of compromised glial response[29] have been strongly indicated in ALS pathogenesis, both of which will be discussed further in Chapter 3.

Despite increasing depth of research and social awareness of the disease, one of the most famous one being the Ice Bucket Challenge in 2014, there is still much to learn and explore about the disease itself, its causes, mechanisms, and its treatments. There are only two FDA-approved interventional drugs and there is no remedy that halts, reverses. or cures the disease. Riluzole, an anti-excitatory therapy approved in 1995 that blunts excessive presynaptic glutamate signaling, has been proven to modestly extend median survival by about 3 months[129]. The more recent antioxidant edaravone, though having showed efficacy for prolonging tracheostomy-free survival in a skewed sample of regional ALS patients, is still

under investigation for its overall effect on survival[130 131]. On other fronts, despite a clear participation of immune activation in pathogenesis of ALS[132-134], all anti-inflammatory drugs so far have failed clinical trials due to either futility or safety concerns, including Masitinib[135] (an inhibitor of CSF-1R that prevents microglia proliferation), Minocycline[136] (inhibitor of microglia cytokine production), Thalidomide[137] (TNFα inhibitor) and Pioglitazone[138] (PPARγ agonist that acts to suppress NFkB pathway). These failed trials, together with failed clinical trials on this front in AD discussed in section 1.3.1, teach a valuable lesson: perhaps directly suppressing proinflammatory cytokine production or functionally ablating all microglia has more repercussions than it has benefits in human trials. Instead, more pre-clinical studies that aim to unravel the neurodegenerative nature of these active players in neuroinflammation and target more precisely defined molecular pathways that can modulate diverse aspects of disease progression should be warranted.

1.4 Significance

Neurodegenerative diseases by definition are characterized by neuronal dysfunction and cell death, usually selective, of the CNS. This leads to functional deficits that often lead to irreversible and deleterious damage. Though many diseases have been well characterized in pathology from postmortem patient samples, the cause and mechanistic basis of the pathogenesis and progression of these NDs remain unclear. Despite this lack of knowledge, it's been shown that common pathological hallmarks such as prominent neuroinflammation, abnormal or misfolded protein aggregates, and neuronal excitotoxicity, prevail throughout all NDs. It is likely then that there are converging cellular and molecular pathways that regulate these common features underlying NDs and that uncovering such fundamental mechanisms and their contributions in neurodegeneration hold the key for understanding pathogenesis of NDs and identifying potential targets for developing therapeutic intervention.

More compelling evidence that links microglia with NDs has been gathered over the past ten years from GWAS and RNAseq studies. Mounting genetic evidence shows that ND gene risk alleles are preferentially expressed in microglia compared to other CNS cell types[139,140]. Indeed, microglia are demonstrably important to the biology and pathology of AD[32,33,100,101] and ALS[141]. This is perhaps best illustrated by the fact that the *Trem2* gene, variants of which strongly predispose to the development of AD, is expressed by microglia and other myeloid cells, but not by neurons[142-145]. A role for microglial Trem2 in ALS and MS has also been implicated. Microglial activation is observed in the CNS in mouse models of ALS[29] and ALS postmortem samples[146]. Interestingly, microglia isolated at late stage of disease from SOD1G93A mouse model of ALS show neither an M1 nor M2 signature, suggesting a unique genetic landscape of these reactive microglia in NDs. This led to recent transcriptomic analyses[39,139,141,147] that have identified a distinct group of 'disease-associated

microglia' that expresses a set of core neurodegenerative genes that are shared across AD, ALS and MS and their animal models.

The TAM receptor tyrosine kinases Axl and Mer have been strongly linked to neurodegeneration. First, microglial *Axl* mRNA has been found to be dramatically upregulated in both AD and its mouse models[39,148,149]. An ~20-fold up-regulation of *Axl* mRNA has been measured in laser-captured plaque-associated microglia in early-onset human AD patients[148]. More recently, in RNAseq and single-cell RNAseq analyses of the 5xFAD mouse model of AD as well as in the $SOD1^{G93A}$ mouse model of ALS[91], *Axl* mRNA was up-regulated 25- to 40-fold in 'disease-associated microglia' at 6 months of age[39,148]. An elevated level of the soluble Axl ectodomain (sAxl, see below) in cerebrospinal fluid (CSF) and blood has been found to be among the most reliable biomarkers of human AD progression[150,151] and hippocampal sclerosis[152] in humans. Indeed, a recent report now classifies *Axl* as an 'AD-associated gene'[148]. In addition, nuclear receptor (e.g., PPARγ) agonists, which elevate both Mer expression and phagocytosis in microglia and macrophages[51,153,154], have been shown to ameliorate disease in mouse neurodegeneration models[154-157]; and these agonist benefits may be Mer-dependent[158]. Finally, our lab has reported prominent up-regulation of Axl specifically in microglia in the *Thy1-A53T a-synuclein* mouse model of PD[23].

The TAM receptors Mer and Axl control multiple features of microglia physiology that may indeed impact pathogenesis of NDs. These findings notwithstanding, experimental tests of the functional role of microglial TAM signaling in NDs have yet to be performed. In this thesis project, we have examined the expression and function of TAM receptors and their ligands in AD and in mouse models of AD (Chapter 2), and in a mouse model of ALS (Chapter 3). Our studies have shown that TAM signaling is critically involved in both AD and

ALS, and the TAM system might emerge as one of the converging mechanisms that microglia use in response to common disease associated pathologies in NDs. With several whole-body TAM receptor antagonists – including small molecule inhibitors of the TAM tyrosine kinases – already in development and clinical trials for the treatment of cancers[159], exploiting a mechanistic understanding of the role of TAM receptors and their ligands in neurodegeneration and their therapeutic potential is of great importance to public health.

1.5 References

1. Ransohoff, R.M. & Brown, M.A. Innate immunity in the central nervous system. *J Clin Invest* **122**, 1164-1171 (2012).

2. Wake, H., Moorhouse, A.J., Miyamoto, A. & Nabekura, J. Microglia: actively surveying and shaping neuronal circuit structure and function. *Trends Neurosci* (2012).

3. Luo, X.G. & Chen, S.D. The changing phenotype of microglia from homeostasis to disease. *Transl Neurodegener* **1**, 9 (2012).

4. Ousman, S.S. & Kubes, P. Immune surveillance in the central nervous system. *Nat Neurosci* **15**, 1096-1101 (2012).

5. Schafer, D.P., Lehrman, E.K. & Stevens, B. The "quad-partite" synapse: Microglia-synapse interactions in the developing and mature CNS. *Glia* **61**, 24-36 (2013).

6. Tremblay, M.E., Stevens, B., Sierra, A., Wake, H., Bessis, A. & Nimmerjahn, A. The role of microglia in the healthy brain. *J Neurosci* **31**, 16064-16069 (2011).

7. Ransohoff, R.M. & Perry, V.H. Microglial physiology: unique stimuli, specialized responses. *Annu Rev Immunol* **27**, 119-145 (2009).

8. Kettenmann, H., Hanisch, U.K., Noda, M. & Verkhratsky, A. Physiology of microglia. *Physiol Rev* **91**, 461-553 (2011).

9. Kettenmann, H., Kirchhoff, F. & Verkhratsky, A. Microglia: New roles for the synaptic stripper. *Neuron* **77**, 10-18 (2012).

10. Salter, M.W. & Stevens, B. Microglia emerge as central players in brain disease. *Nat Med* **23**, 1018-1027 (2017).

11. Saijo, K. & Glass, C.K. Microglial cell origin and phenotypes in health and disease. *Nat Rev Immunol* **11**, 775-787 (2011).

12. Kierdorf, K., Masuda, T., Jordao, M.J.C. & Prinz, M. Macrophages at CNS interfaces: ontogeny and function in health and disease. *Nat Rev Neurosci* **20**, 547-562 (2019).

13. Nimmerjahn, A., Kirchhoff, F. & Helmchen, F. Resting microglial cells are highly dynamic surveillants of brain parenchyma in vivo. *Science* **308**, 1314-1318 (2005).

14. Davalos, D., Grutzendler, J., Yang, G., Kim, J.V., Zuo, Y., Jung, S., Littman, D.R., Dustin, M.L. & Gan, W.B. ATP mediates rapid microglial response to local brain injury in vivo. *Nat Neurosci* **8**, 752-758 (2005).

15. Ginhoux, F. & Prinz, M. Origin of microglia: current concepts and past controversies. *Cold Spring Harb Perspect Biol* **7**, a020537 (2015).

16. Paolicelli, R.C., Bolasco, G., Pagani, F., Maggi, L., Scianni, M., Panzanelli, P., Giustetto, M., Ferreira, T.A., Guiducci, E., Dumas, L., Ragozzino, D. & Gross, C.T. Synaptic pruning by microglia is necessary for normal brain development. *Science* **333**, 1456-1458 (2011).

17. Schafer, D.P., Lehrman, E.K., Kautzman, A.G., Koyama, R., Mardinly, A.R., Yamasaki, R., Ransohoff, R.M., Greenberg, M.E., Barres, B.A. & Stevens, B. Microglia sculpt postnatal neural circuits in an activity and complement-dependent manner. *Neuron* **74**, 691-705 (2012).

18. Polazzi, E. & Monti, B. Microglia and neuroprotection: from in vitro studies to therapeutic applications. *Prog Neurobiol* **92**, 293-315 (2010).

19. Olefsky, J.M. & Glass, C.K. Macrophages, inflammation, and insulin resistance. *Annu Rev Physiol* **72**, 219-246 (2010).

20. Eyo, U.B., Peng, J., Swiatkowski, P., Mukherjee, A., Bispo, A. & Wu, L.J. Neuronal hyperactivity recruits microglial processes via neuronal NMDA receptors and microglial P2Y12 receptors after status epilepticus. *J Neurosci* **34**, 10528-10540 (2014).

21. Eyo, U.B., Peng, J., Murugan, M., Mo, M., Lalani, A., Xie, P., Xu, P., Margolis, D.J. & Wu, L.J. Regulation of Physical Microglia-Neuron Interactions by Fractalkine Signaling after Status Epilepticus. *eNeuro* **3**(2016).

22. Sierra, A., Encinas, J.M., Deudero, J.J., Chancey, J.H., Enikolopov, G., Overstreet-Wadiche, L.S., Tsirka, S.E. & Maletic-Savatic, M. Microglia shape adult hippocampal neurogenesis through apoptosis-coupled phagocytosis. *Cell Stem Cell* **7**, 483-495 (2010).

23. Fourgeaud, L., Traves, P.G., Tufail, Y., Leal-Bailey, H., Lew, E.D., Burrola, P.G., Callaway, P., Zagorska, A., Rothlin, C.V., Nimmerjahn, A. & Lemke, G. TAM receptors regulate multiple features of microglial physiology. *Nature* **532**, 240-244 (2016).

24. Diaz-Aparicio, I., Paris, I., Sierra-Torre, V., Plaza-Zabala, A., Rodriguez-Iglesias, N., Marquez-Ropero, M., Beccari, S., Huguet, P., Abiega, O., Alberdi, E., Matute, C., Bernales, I., Schulz, A., Otrokocsi, L., Sperlagh, B., Happonen, K.E., Lemke, G., Maletic-Savatic, M., Valero, J. & Sierra, A. Microglia Actively Remodel Adult Hippocampal Neurogenesis through the Phagocytosis Secretome. *J Neurosci* **40**, 1453-1482 (2020).

25. Akiyama, H., Barger, S., Barnum, S., Bradt, B., Bauer, J., Cole, G.M., Cooper, N.R., Eikelenboom, P., Emmerling, M., Fiebich, B.L., Finch, C.E., Frautschy, S., Griffin, W.S., Hampel, H., Hull, M., Landreth, G., Lue, L., Mrak, R., Mackenzie, I.R., McGeer, P.L., O'Banion, M.K., Pachter, J., Pasinetti, G., Plata-Salaman, C., Rogers, J., Rydel, R., Shen, Y., Streit, W., Strohmeyer, R., Tooyoma, I., Van Muiswinkel, F.L., Veerhuis, R., Walker, D., Webster, S., Wegrzyniak, B., Wenk, G. & Wyss-Coray, T. Inflammation and Alzheimer's disease. *Neurobiol Aging* **21**, 383-421 (2000).

26. Hirsch, E.C. & Hunot, S. Neuroinflammation in Parkinson's disease: a target for neuroprotection? *Lancet Neurol* **8**, 382-397 (2009).

27. Siffrin, V., Vogt, J., Radbruch, H., Nitsch, R. & Zipp, F. Multiple sclerosis - candidate mechanisms underlying CNS atrophy. *Trends Neurosci* **33**, 202-210 (2010).

28. Philips, T. & Robberecht, W. Neuroinflammation in amyotrophic lateral sclerosis: role of glial activation in motor neuron disease. *Lancet Neurol* **10**, 253-263 (2011).

29. Beers, D.R., Zhao, W., Liao, B., Kano, O., Wang, J., Huang, A., Appel, S.H. & Henkel, J.S. Neuroinflammation modulates distinct regional and temporal clinical responses in ALS mice. *Brain Behav Immun* **25**, 1025-1035 (2011).

30. Boillee, S., Yamanaka, K., Lobsiger, C.S., Copeland, N.G., Jenkins, N.A., Kassiotis, G., Kollias, G. & Cleveland, D.W. Onset and progression in inherited ALS determined by motor neurons and microglia. *Science* **312**, 1389-1392 (2006).

31. Heneka, M.T., Kummer, M.P. & Latz, E. Innate immune activation in neurodegenerative disease. *Nat Rev Immunol* **14**, 463-477 (2014).

32. Heneka, M.T., Carson, M.J., El Khoury, J., Landreth, G.E., Brosseron, F., Feinstein, D.L., Jacobs, A.H., Wyss-Coray, T., Vitorica, J., Ransohoff, R.M., Herrup, K.,

Frautschy, S.A., Finsen, B., Brown, G.C., Verkhratsky, A., Yamanaka, K., Koistinaho, J., Latz, E., Halle, A., Petzold, G.C., Town, T., Morgan, D., Shinohara, M.L., Perry, V.H., Holmes, C., Bazan, N.G., Brooks, D.J., Hunot, S., Joseph, B., Deigendesch, N., Garaschuk, O., Boddeke, E., Dinarello, C.A., Breitner, J.C., Cole, G.M., Golenbock, D.T. & Kummer, M.P. Neuroinflammation in Alzheimer's disease. *Lancet Neurol* **14**, 388-405 (2015).

33. Meyer-Luehmann, M. & Prinz, M. Myeloid cells in Alzheimer's disease: culprits, victims or innocent bystanders? *Trends Neurosci* **38**, 659-668 (2015).

34. Ford, A.L., Goodsall, A.L., Hickey, W.F. & Sedgwick, J.D. Normal adult ramified microglia separated from other central nervous system macrophages by flow cytometric sorting. Phenotypic differences defined and direct ex vivo antigen presentation to myelin basic protein-reactive CD4+ T cells compared. *J Immunol* **154**, 4309-4321 (1995).

35. Jay, T.R., Miller, C.M., Cheng, P.J., Graham, L.C., Bemiller, S., Broihier, M.L., Xu, G., Margevicius, D., Karlo, J.C., Sousa, G.L., Cotleur, A.C., Butovsky, O., Bekris, L., Staugaitis, S.M., Leverenz, J.B., Pimplikar, S.W., Landreth, G.E., Howell, G.R., Ransohoff, R.M. & Lamb, B.T. TREM2 deficiency eliminates TREM2+ inflammatory macrophages and ameliorates pathology in Alzheimer's disease mouse models. *J Exp Med* **212**, 287-295 (2015).

36. Plemel, J.R., Stratton, J.A., Michaels, N.J., Rawji, K.S., Zhang, E., Sinha, S., Baaklini, C.S., Dong, Y., Ho, M., Thorburn, K., Friedman, T.N., Jawad, S., Silva, C., Caprariello, A.V., Hoghooghi, V., Yue, J., Jaffer, A., Lee, K., Kerr, B.J., Midha, R., Stys, P.K., Biernaskie, J. & Yong, V.W. Microglia response following acute demyelination is heterogeneous and limits infiltrating macrophage dispersion. *Sci Adv* **6**, eaay6324 (2020).

37. Bennett, M.L., Bennett, F.C., Liddelow, S.A., Ajami, B., Zamanian, J.L., Fernhoff, N.B., Mulinyawe, S.B., Bohlen, C.J., Adil, A., Tucker, A., Weissman, I.L., Chang, E.F., Li, G., Grant, G.A., Hayden Gephart, M.G. & Barres, B.A. New tools for studying microglia in the mouse and human CNS. *Proc Natl Acad Sci U S A* **113**, E1738-1746 (2016).

38. Unger, M.S., Schernthaner, P., Marschallinger, J., Mrowetz, H. & Aigner, L. Microglia prevent peripheral immune cell invasion and promote an anti-inflammatory environment in the brain of APP-PS1 transgenic mice. *J Neuroinflammation* **15**, 274 (2018).

39. Keren-Shaul, H., Spinrad, A., Weiner, A., Matcovitch-Natan, O., Dvir-Szternfeld, R., Ulland, T.K., David, E., Baruch, K., Lara-Astaiso, D., Toth, B., Itzkovitz, S., Colonna,

M., Schwartz, M. & Amit, I. A Unique Microglia Type Associated with Restricting Development of Alzheimer's Disease. *Cell* **169**, 1276-1290 e1217 (2017).

40. Burstyn-Cohen, T., Heeb, M.J. & Lemke, G. Lack of protein S in mice causes embryonic lethal coagulopathy and vascular dysgenesis. *J Clin Invest* **119**, 2942-2953; PMC2752078 (2009).

41. Caraux, A., Lu, Q., Fernandez, N., Riou, S., Di Santo, J.P., Raulet, D.H., Lemke, G. & Roth, C. Natural killer cell differentiation driven by Tyro3 receptor tyrosine kinases. *Nat Immunol* **7**, 747-754 (2006).

42. Lai, C. & Lemke, G. An extended family of protein-tyrosine kinase genes differentially expressed in the vertebrate nervous system. *Neuron* **6**, 691-704 (1991).

43. Lemke, G. Biology of the TAM receptors. *Cold Spring Harbor Perspectives* **J. Schlessinger and M. Lemmon, Eds.**(2012).

44. Lemke, G. & Burstyn-Cohen, T. TAM receptors and the clearance of apoptotic cells. *Ann N Y Acad Sci* **1209**, 23-29. PMC3061224 (2010).

45. Lemke, G. & Lu, Q. Macrophage regulation by Tyro 3 family receptors. *Curr Opin Immunol* **15**, 31-36 (2003).

46. Lemke, G. & Rothlin, C.V. Immunobiology of the TAM receptors. *Nat Rev Immunol* **8**, 327-336; PMC2856445 (2008).

47. Lu, Q., Gore, M., Zhang, Q., Camenisch, T., Boast, S., Casagranda, F., Lai, C., Skinner, M.K., Klein, R., Matsushima, G.K., Earp, H.S., Goff, S.P. & Lemke, G. Tyro-3 family receptors are essential regulators of mammalian spermatogenesis. *Nature* **398**, 723-728 (1999).

48. Lu, Q. & Lemke, G. Homeostatic regulation of the immune system by receptor tyrosine kinases of the Tyro 3 family. *Science* **293**, 306-311 (2001).

49. Rothlin, C.V., Ghosh, S., Zuniga, E.I., Oldstone, M.B. & Lemke, G. TAM receptors are pleiotropic inhibitors of the innate immune response. *Cell* **131**, 1124-1136 (2007).

50. Rothlin, C.V. & Lemke, G. TAM receptor signaling and autoimmune disease. *Curr Opin Immunol* **22**, 740-746. (2010).

51. Zagórska, A., Través, P.G., Lew, E.D., Dransfield, I. & Lemke, G. Diversification of TAM receptor tyrosine kinase function. *Nat Immunol* **15**, 920-928 (2014).

52. Lew, E.D., Oh, J., Burrola, P.G., Lax, I., Zagórska, A., Través, P.G., Schlessinger, J. & Lemke, G. Differential TAM receptor-ligand-phospholipid interactions delimit differential TAM bioactivities. *eLife* **3:e03385**(2014).

53. Miner, J.J., Daniels, B.P., Shrestha, B., Proenca-Modena, J.L., Lew, E.D., Lazear, H.M., Gorman, M.J., Lemke, G., Klein, R.S. & Diamond, M.S. The TAM receptor Mertk protects against neuroinvasive viral infection by maintaining blood-brain barrier integrity. *Nat Med* **21**, 1464-1472 (2015).

54. Lemke, G. Phosphatidylserine Is the Signal for TAM Receptors and Their Ligands. *Trends Biochem Sci* **42**, 738-748 (2017).

55. Stitt, T.N., Conn, G., Gore, M., Lai, C., Bruno, J., Radziejewski, C., Mattsson, K., Fisher, J., Gies, D.R., Jones, P.F., Maslakowski, P., Ryan, T.E., Tobkes, N.J., Chen, D.H., DiStefano, P.S., Long, G.L., Basilico, C., Goldfarb, M.P., Lemke, G., Glass, D.J. & Yancopoulos, G.D. The anticoagulation factor protein S and its relative, Gas6, are ligands for the Tyro 3/Axl family of receptor tyrosine kinases. *Cell* **80**, 661-670 (1995).

56. Lemke, G. Biology of the TAM receptors. *Cold Spring Harbor Perspectives* **5(11)**, doi: 10.1101/cshperspect.a009076. (2013).

57. Nagata, S., Hanayama, R. & Kawane, K. Autoimmunity and the clearance of dead cells. *Cell* **140**, 619-630 (2010).

58. Scott, R.S., McMahon, E.J., Pop, S.M., Reap, E.A., Caricchio, R., Cohen, P.L., Earp, H.S. & Matsushima, G.K. Phagocytosis and clearance of apoptotic cells is mediated by MER. *Nature* **411**, 207-211 (2001).

59. Prasad, D., Rothlin, C.V., Burrola, P., Burstyn-Cohen, T., Lu, Q., Garcia de Frutos, P. & Lemke, G. TAM receptor function in the retinal pigment epithelium. *Mol Cell Neurosci* **33**, 96-108 (2006).

60. Burstyn-Cohen, T., Lew, E.D., Traves, P.G., Burrola, P.G., Hash, J.C. & Lemke, G. Genetic dissection of TAM receptor-ligand interaction in retinal pigment epithelial cell phagocytosis. *Neuron* **76**, 1123-1132 (2012).

61. Tufail, Y., Cook, D., Fourgeaud, L., Powers, C.J., Merten, K., Clark, C.L., Hoffman, E., Ngo, A., Sekiguchi, K.J., O'Shea, C.C., Lemke, G. & Nimmerjahn, A.

Phosphatidylserine Exposure Controls Viral Innate Immune Responses by Microglia. *Neuron* **93**, 574-586 e578 (2017).

62. Huang, M., Rigby, A.C., Morelli, X., Grant, M.A., Huang, G., Furie, B., Seaton, B. & Furie, B.C. Structural basis of membrane binding by Gla domains of vitamin K-dependent proteins. *Nat Struct Biol* **10**, 751-756 (2003).

63. Balasubramanian, K. & Schroit, A.J. Aminophospholipid asymmetry: A matter of life and death. *Annu Rev Physiol* **65**, 701-734 (2003).

64. Fadok, V.A., Bratton, D.L. & Henson, P.M. Phagocyte receptors for apoptotic cells: recognition, uptake, and consequences. *J Clin Invest* **108**, 957-962 (2001).

65. Fadok, V.A., Voelker, D.R., Campbell, P.A., Cohen, J.J., Bratton, D.L. & Henson, P.M. Exposure of phosphatidylserine on the surface of apoptotic lymphocytes triggers specific recognition and removal by macrophages. *J Immunol* **148**, 2207-2216 (1992).

66. Mirnikjoo, B., Balasubramanian, K. & Schroit, A.J. Mobilization of lysosomal calcium regulates the externalization of phosphatidylserine during apoptosis. *J Biol Chem* **284**, 6918-6923 (2009).

67. Ravichandran, K.S. Find-me and eat-me signals in apoptotic cell clearance: progress and conundrums. *J Exp Med* **207**, 1807-1817 (2010).

68. Ravichandran, K.S. Beginnings of a good apoptotic meal: the find-me and eat-me signaling pathways. *Immunity* **35**, 445-455 (2011).

69. Hanayama, R., Tanaka, M., Miwa, K. & Nagata, S. Expression of developmental endothelial locus-1 in a subset of macrophages for engulfment of apoptotic cells. *J Immunol* **172**, 3876-3882 (2004).

70. Hanayama, R., Tanaka, M., Miwa, K., Shinohara, A., Iwamatsu, A. & Nagata, S. Identification of a factor that links apoptotic cells to phagocytes. *Nature* **417**, 182-187 (2002).

71. Hanayama, R., Tanaka, M., Miyasaka, K., Aozasa, K., Koike, M., Uchiyama, Y. & Nagata, S. Autoimmune disease and impaired uptake of apoptotic cells in MFG-E8-deficient mice. *Science* **304**, 1147-1150 (2004).

72. Miyasaka, K., Hanayama, R., Tanaka, M. & Nagata, S. Expression of milk fat globule epidermal growth factor 8 in immature dendritic cells for engulfment of apoptotic cells. *Eur J Immunol* **34**, 1414-1422 (2004).

73. D'Cruz, P.M., Yasumura, D., Weir, J., Matthes, M.T., Abderrahim, H., LaVail, M.M. & Vollrath, D. Mutation of the receptor tyrosine kinase gene Mertk in the retinal dystrophic RCS rat. *Hum Mol Genet* **9**, 645-651 (2000).

74. Gal, A., Li, Y., Thompson, D.A., Weir, J., Orth, U., Jacobson, S.G., Apfelstedt-Sylla, E. & Vollrath, D. Mutations in MERTK, the human orthologue of the RCS rat retinal dystrophy gene, cause retinitis pigmentosa. *Nat Genet* **26**, 270-271 (2000).

75. Gautier, E.L., Shay, T., Miller, J., Greter, M., Jakubzick, C., Ivanov, S., Helft, J., Chow, A., Elpek, K.G., Gordonov, S., Mazloom, A.R., Ma'ayan, A., Chua, W.J., Hansen, T.H., Turley, S.J., Merad, M. & Randolph, G.J. Gene-expression profiles and transcriptional regulatory pathways that underlie the identity and diversity of mouse tissue macrophages. *Nat Immunol* **13**, 1118-1128 (2012).

76. Brown, G.C. & Neher, J.J. Microglial phagocytosis of live neurons. *Nat Rev Neurosci* **15**, 209-216 (2014).

77. Neher, J.J., Emmrich, J.V., Fricker, M., Mander, P.K., Thery, C. & Brown, G.C. Phagocytosis executes delayed neuronal death after focal brain ischemia. *Proc Natl Acad Sci U S A* **110**, E4098-4107 (2013).

78. Hippius, H. & Neundorfer, G. The discovery of Alzheimer's disease. *Dialogues Clin Neurosci* **5**, 101-108 (2003).

79. Hardy, J.A. & Higgins, G.A. Alzheimer's disease: the amyloid cascade hypothesis. *Science* **256**, 184-185 (1992).

80. De Strooper, B. Aph-1, Pen-2, and Nicastrin with Presenilin generate an active gamma-Secretase complex. *Neuron* **38**, 9-12 (2003).

81. Sasaguri, H., Nilsson, P., Hashimoto, S., Nagata, K., Saito, T., De Strooper, B., Hardy, J., Vassar, R., Winblad, B. & Saido, T.C. APP mouse models for Alzheimer's disease preclinical studies. *EMBO J* **36**, 2473-2487 (2017).

82. Esquerda-Canals, G., Montoliu-Gaya, L., Guell-Bosch, J. & Villegas, S. Mouse Models of Alzheimer's Disease. *J Alzheimers Dis* **57**, 1171-1183 (2017).

83. Bales, K.R. The value and limitations of transgenic mouse models used in drug discovery for Alzheimer's disease: an update. *Expert Opin Drug Discov* **7**, 281-297 (2012).

84. Morrissette, D.A., Parachikova, A., Green, K.N. & LaFerla, F.M. Relevance of transgenic mouse models to human Alzheimer disease. *J Biol Chem* **284**, 6033-6037 (2009).

85. Minkeviciene, R., Rheims, S., Dobszay, M.B., Zilberter, M., Hartikainen, J., Fulop, L., Penke, B., Zilberter, Y., Harkany, T., Pitkanen, A. & Tanila, H. Amyloid beta-induced neuronal hyperexcitability triggers progressive epilepsy. *J Neurosci* **29**, 3453-3462 (2009).

86. Jankowsky, J.L., Fadale, D.J., Anderson, J., Xu, G.M., Gonzales, V., Jenkins, N.A., Copeland, N.G., Lee, M.K., Younkin, L.H., Wagner, S.L., Younkin, S.G. & Borchelt, D.R. Mutant presenilins specifically elevate the levels of the 42 residue beta-amyloid peptide in vivo: evidence for augmentation of a 42-specific gamma secretase. *Hum Mol Genet* **13**, 159-170 (2004).

87. Jankowsky, J.L., Slunt, H.H., Ratovitski, T., Jenkins, N.A., Copeland, N.G. & Borchelt, D.R. Co-expression of multiple transgenes in mouse CNS: a comparison of strategies. *Biomol Eng* **17**, 157-165 (2001).

88. Rockenstein, E., Mallory, M., Mante, M., Sisk, A. & Masliaha, E. Early formation of mature amyloid-beta protein deposits in a mutant APP transgenic model depends on levels of Abeta(1-42). *J Neurosci Res* **66**, 573-582 (2001).

89. Hutter-Paier, B., Huttunen, H.J., Puglielli, L., Eckman, C.B., Kim, D.Y., Hofmeister, A., Moir, R.D., Domnitz, S.B., Frosch, M.P., Windisch, M. & Kovacs, D.M. The ACAT inhibitor CP-113,818 markedly reduces amyloid pathology in a mouse model of Alzheimer's disease. *Neuron* **44**, 227-238 (2004).

90. Imbimbo, B.P., Hutter-Paier, B., Villetti, G., Facchinetti, F., Cenacchi, V., Volta, R., Lanzillotta, A., Pizzi, M. & Windisch, M. CHF5074, a novel gamma-secretase modulator, attenuates brain beta-amyloid pathology and learning deficit in a mouse model of Alzheimer's disease. *British journal of pharmacology* **156**, 982-993 (2009).

91. Oakley, H., Cole, S.L., Logan, S., Maus, E., Shao, P., Craft, J., Guillozet-Bongaarts, A., Ohno, M., Disterhoft, J., Van Eldik, L., Berry, R. & Vassar, R. Intraneuronal beta-amyloid aggregates, neurodegeneration, and neuron loss in transgenic mice with five familial Alzheimer's disease mutations: potential factors in amyloid plaque formation. *J Neurosci* **26**, 10129-10140 (2006).

92. Jawhar, S., Trawicka, A., Jenneckens, C., Bayer, T.A. & Wirths, O. Motor deficits, neuron loss, and reduced anxiety coinciding with axonal degeneration and intraneuronal Abeta aggregation in the 5XFAD mouse model of Alzheimer's disease. *Neurobiol Aging* **33**, 196 e129-140 (2012).

93. Lambert, M.P., Barlow, A.K., Chromy, B.A., Edwards, C., Freed, R., Liosatos, M., Morgan, T.E., Rozovsky, I., Trommer, B., Viola, K.L., Wals, P., Zhang, C., Finch, C.E., Krafft, G.A. & Klein, W.L. Diffusible, nonfibrillar ligands derived from Abeta1-42 are potent central nervous system neurotoxins. *Proc Natl Acad Sci U S A* **95**, 6448-6453 (1998).

94. Lesne, S., Koh, M.T., Kotilinek, L., Kayed, R., Glabe, C.G., Yang, A., Gallagher, M. & Ashe, K.H. A specific amyloid-beta protein assembly in the brain impairs memory. *Nature* **440**, 352-357 (2006).

95. Shankar, G.M., Li, S., Mehta, T.H., Garcia-Munoz, A., Shepardson, N.E., Smith, I., Brett, F.M., Farrell, M.A., Rowan, M.J., Lemere, C.A., Regan, C.M., Walsh, D.M., Sabatini, B.L. & Selkoe, D.J. Amyloid-beta protein dimers isolated directly from Alzheimer's brains impair synaptic plasticity and memory. *Nat Med* **14**, 837-842 (2008).

96. Panza, F., Lozupone, M., Solfrizzi, V., Watling, M. & Imbimbo, B.P. Time to test antibacterial therapy in Alzheimer's disease. *Brain* **142**, 2905-2929 (2019).

97. Price, J.L., McKeel, D.W., Jr., Buckles, V.D., Roe, C.M., Xiong, C., Grundman, M., Hansen, L.A., Petersen, R.C., Parisi, J.E., Dickson, D.W., Smith, C.D., Davis, D.G., Schmitt, F.A., Markesbery, W.R., Kaye, J., Kurlan, R., Hulette, C., Kurland, B.F., Higdon, R., Kukull, W. & Morris, J.C. Neuropathology of nondemented aging: presumptive evidence for preclinical Alzheimer disease. *Neurobiol Aging* **30**, 1026-1036 (2009).

98. Corder, E.H., Saunders, A.M., Strittmatter, W.J., Schmechel, D.E., Gaskell, P.C., Small, G.W., Roses, A.D., Haines, J.L. & Pericak-Vance, M.A. Gene dose of apolipoprotein E type 4 allele and the risk of Alzheimer's disease in late onset families. *Science* **261**, 921-923 (1993).

99. Strittmatter, W.J., Saunders, A.M., Schmechel, D., Pericak-Vance, M., Enghild, J., Salvesen, G.S. & Roses, A.D. Apolipoprotein E: high-avidity binding to beta-amyloid and increased frequency of type 4 allele in late-onset familial Alzheimer disease. *Proc Natl Acad Sci U S A* **90**, 1977-1981 (1993).

100. Ransohoff, R.M. How neuroinflammation contributes to neurodegeneration. *Science* **353**, 777-783 (2016).

101. Wes, P.D., Sayed, F.A., Bard, F. & Gan, L. Targeting microglia for the treatment of Alzheimer's Disease. *Glia* **64**, 1710-1732 (2016).

102. Green, R.C., Schneider, L.S., Amato, D.A., Beelen, A.P., Wilcock, G., Swabb, E.A., Zavitz, K.H. & Tarenflurbil Phase 3 Study, G. Effect of tarenflurbil on cognitive decline and activities of daily living in patients with mild Alzheimer disease: a randomized controlled trial. *JAMA* **302**, 2557-2564 (2009).

103. Kirk, R. Clinical trials in CNS--SMi's eighth annual conference. *IDrugs* **13**, 66-69 (2010).

104. Doody, R.S., Raman, R., Farlow, M., Iwatsubo, T., Vellas, B., Joffe, S., Kieburtz, K., He, F., Sun, X., Thomas, R.G., Aisen, P.S., Alzheimer's Disease Cooperative Study Steering, C., Siemers, E., Sethuraman, G., Mohs, R. & Semagacestat Study, G. A phase 3 trial of semagacestat for treatment of Alzheimer's disease. *N Engl J Med* **369**, 341-350 (2013).

105. Coric, V., van Dyck, C.H., Salloway, S., Andreasen, N., Brody, M., Richter, R.W., Soininen, H., Thein, S., Shiovitz, T., Pilcher, G., Colby, S., Rollin, L., Dockens, R., Pachai, C., Portelius, E., Andreasson, U., Blennow, K., Soares, H., Albright, C., Feldman, H.H. & Berman, R.M. Safety and tolerability of the gamma-secretase inhibitor avagacestat in a phase 2 study of mild to moderate Alzheimer disease. *Arch Neurol* **69**, 1430-1440 (2012).

106. Coric, V., Salloway, S., van Dyck, C.H., Dubois, B., Andreasen, N., Brody, M., Curtis, C., Soininen, H., Thein, S., Shiovitz, T., Pilcher, G., Ferris, S., Colby, S., Kerselaers, W., Dockens, R., Soares, H., Kaplita, S., Luo, F., Pachai, C., Bracoud, L., Mintun, M., Grill, J.D., Marek, K., Seibyl, J., Cedarbaum, J.M., Albright, C., Feldman, H.H. & Berman, R.M. Targeting Prodromal Alzheimer Disease With Avagacestat: A Randomized Clinical Trial. *JAMA Neurol* **72**, 1324-1333 (2015).

107. Lahiri, D.K., Maloney, B., Long, J.M. & Greig, N.H. Lessons from a BACE1 inhibitor trial: off-site but not off base. *Alzheimers Dement* **10**, S411-419 (2014).

108. Yan, R. Stepping closer to treating Alzheimer's disease patients with BACE1 inhibitor drugs. *Transl Neurodegener* **5**, 13 (2016).

109. Doody, R.S., Thomas, R.G., Farlow, M., Iwatsubo, T., Vellas, B., Joffe, S., Kieburtz, K., Raman, R., Sun, X., Aisen, P.S., Siemers, E., Liu-Seifert, H., Mohs, R.,

Alzheimer's Disease Cooperative Study Steering, C. & Solanezumab Study, G. Phase 3 trials of solanezumab for mild-to-moderate Alzheimer's disease. *N Engl J Med* **370**, 311-321 (2014).

110. Ostrowitzki, S., Lasser, R.A., Dorflinger, E., Scheltens, P., Barkhof, F., Nikolcheva, T., Ashford, E., Retout, S., Hofmann, C., Delmar, P., Klein, G., Andjelkovic, M., Dubois, B., Boada, M., Blennow, K., Santarelli, L., Fontoura, P. & Investigators, S.C.R. A phase III randomized trial of gantenerumab in prodromal Alzheimer's disease. *Alzheimers Res Ther* **9**, 95 (2017).

111. Egan, M.F., Kost, J., Tariot, P.N., Aisen, P.S., Cummings, J.L., Vellas, B., Sur, C., Mukai, Y., Voss, T., Furtek, C., Mahoney, E., Harper Mozley, L., Vandenberghe, R., Mo, Y. & Michelson, D. Randomized Trial of Verubecestat for Mild-to-Moderate Alzheimer's Disease. *N Engl J Med* **378**, 1691-1703 (2018).

112. Wobst, H.J., Mack, K.L., Brown, D.G., Brandon, N.J. & Shorter, J. The clinical trial landscape in amyotrophic lateral sclerosis-Past, present, and future. *Med Res Rev* **40**, 1352-1384 (2020).

113. Mitsumoto, H., Brooks, B.R. & Silani, V. Clinical trials in amyotrophic lateral sclerosis: why so many negative trials and how can trials be improved? *Lancet Neurol* **13**, 1127-1138 (2014).

114. Borchelt, D.R., Lee, M.K., Slunt, H.S., Guarnieri, M., Xu, Z.S., Wong, P.C., Brown, R.H., Jr., Price, D.L., Sisodia, S.S. & Cleveland, D.W. Superoxide dismutase 1 with mutations linked to familial amyotrophic lateral sclerosis possesses significant activity. *Proc Natl Acad Sci U S A* **91**, 8292-8296 (1994).

115. Rosen, D.R., Siddique, T., Patterson, D., Figlewicz, D.A., Sapp, P., Hentati, A., Donaldson, D., Goto, J., O'Regan, J.P., Deng, H.X., Rahmani, Z., Krizus, A., McKenna-Yasek, D., Cayabyab, A.,Gaston, S.M., Berger, R., Tanzi, R.E., Halperin, J.J., Herzfeldt, B., Den Bergh, R.V., Hung, W.Y., Bird, T., Deng, G., Mulder, D. W., Smyth, C., Laing, N. G., Soriano, E, Pericak-Vance, M. A., Haines, J, Rouleau, G. A., Gusella, J. S., Horvitz, H. R & Brown, R.H. Mutations in Cu/Zn superoxide dismutase gene are associated with familial amyotrophic lateral sclerosis. *Nature* **362**, 59-62 (1993).

116. Gurney, M.E., Pu, H., Chiu, A.Y., Dal Canto, M.C., Polchow, C.Y., Alexander, D.D., Caliendo, J., Hentati, A., Kwon, Y.W., Deng, H.X., Chen, W., Ping, Z., Sufit, R.L. & Siddique, T. Motor neuron degeneration in mice that express a human Cu,Zn superoxide dismutase mutation. *Science* **264**, 1772-1775 (1994).

117. Brown, R.H. & Al-Chalabi, A. Amyotrophic Lateral Sclerosis. *N Engl J Med* **377**, 162-172 (2017).

118. Cleveland, D.W. & Rothstein, J.D. From Charcot to Lou Gehrig: deciphering selective motor neuron death in ALS. *Nat Rev Neurosci* **2**, 806-819 (2001).

119. Iwata, M. & Hirano, A. Sparing of the Onufrowicz nucleus in sacral anterior horn lesions. *Ann Neurol* **4**, 245-249 (1978).

120. Mannen, T., Iwata, M., Toyokura, Y. & Nagashima, K. Preservation of a certain motoneurone group of the sacral cord in amyotrophic lateral sclerosis: its clinical significance. *J Neurol Neurosurg Psychiatry* **40**, 464-469 (1977).

121. Ragagnin, A.M.G., Shadfar, S., Vidal, M., Jamali, M.S. & Atkin, J.D. Motor Neuron Susceptibility in ALS/FTD. *Front Neurosci* **13**, 532 (2019).

122. Kaplan, A., Spiller, K.J., Towne, C., Kanning, K.C., Choe, G.T., Geber, A., Akay, T., Aebischer, P. & Henderson, C.E. Neuronal matrix metalloproteinase-9 is a determinant of selective neurodegeneration. *Neuron* **81**, 333-348 (2014).

123. Pun, S., Santos, A.F., Saxena, S., Xu, L. & Caroni, P. Selective vulnerability and pruning of phasic motoneuron axons in motoneuron disease alleviated by CNTF. *Nat Neurosci* **9**, 408-419 (2006).

124. Kanning, K.C., Kaplan, A. & Henderson, C.E. Motor neuron diversity in development and disease. *Annu Rev Neurosci* **33**, 409-440 (2010).

125. Saxena, S., Roselli, F., Singh, K., Leptien, K., Julien, J.P., Gros-Louis, F. & Caroni, P. Neuroprotection through excitability and mTOR required in ALS motoneurons to delay disease and extend survival. *Neuron* **80**, 80-96 (2013).

126. Friese, A., Kaltschmidt, J.A., Ladle, D.R., Sigrist, M., Jessell, T.M. & Arber, S. Gamma and alpha motor neurons distinguished by expression of transcription factor Err3. *Proc Natl Acad Sci U S A* **106**, 13588-13593 (2009).

127. Powis, R.A. & Gillingwater, T.H. Selective loss of alpha motor neurons with sparing of gamma motor neurons and spinal cord cholinergic neurons in a mouse model of spinal muscular atrophy. *J Anat* **228**, 443-451 (2016).

128. Lalancette-Hebert, M., Sharma, A., Lyashchenko, A.K. & Shneider, N.A. Gamma motor neurons survive and exacerbate alpha motor neuron degeneration in ALS. *Proc Natl Acad Sci U S A* **113**, E8316-E8325 (2016).

129. Miller, R.G., Mitchell, J.D. & Moore, D.H. Riluzole for amyotrophic lateral sclerosis (ALS)/motor neuron disease (MND). *Cochrane Database Syst Rev*, CD001447 (2012).

130. Writing, G. & Edaravone, A.L.S.S.G. Safety and efficacy of edaravone in well defined patients with amyotrophic lateral sclerosis: a randomised, double-blind, placebo-controlled trial. *Lancet Neurol* **16**, 505-512 (2017).

131. Okada, M., Yamashita, S., Ueyama, H., Ishizaki, M., Maeda, Y. & Ando, Y. Long-term effects of edaravone on survival of patients with amyotrophic lateral sclerosis. *eNeurologicalSci* **11**, 11-14 (2018).

132. Liddelow, S.A., Guttenplan, K.A., Clarke, L.E., Bennett, F.C., Bohlen, C.J., Schirmer, L., Bennett, M.L., Munch, A.E., Chung, W.S., Peterson, T.C., Wilton, D.K., Frouin, A., Napier, B.A., Panicker, N., Kumar, M., Buckwalter, M.S., Rowitch, D.H., Dawson, V.L., Dawson, T.M., Stevens, B. & Barres, B.A. Neurotoxic reactive astrocytes are induced by activated microglia. *Nature* **541**, 481-487 (2017).

133. Turner, M.R., Cagnin, A., Turkheimer, F.E., Miller, C.C., Shaw, C.E., Brooks, D.J., Leigh, P.N. & Banati, R.B. Evidence of widespread cerebral microglial activation in amyotrophic lateral sclerosis: an [11C](R)-PK11195 positron emission tomography study. *Neurobiol Dis* **15**, 601-609 (2004).

134. Brettschneider, J., Toledo, J.B., Van Deerlin, V.M., Elman, L., McCluskey, L., Lee, V.M. & Trojanowski, J.Q. Microglial activation correlates with disease progression and upper motor neuron clinical symptoms in amyotrophic lateral sclerosis. *PLoS One* **7**, e39216 (2012).

135. Trias, E., Ibarburu, S., Barreto-Nunez, R., Babdor, J., Maciel, T.T., Guillo, M., Gros, L., Dubreuil, P., Diaz-Amarilla, P., Cassina, P., Martinez-Palma, L., Moura, I.C., Beckman, J.S., Hermine, O. & Barbeito, L. Post-paralysis tyrosine kinase inhibition with masitinib abrogates neuroinflammation and slows disease progression in inherited amyotrophic lateral sclerosis. *J Neuroinflammation* **13**, 177 (2016).

136. Gordon, P.H., Moore, D.H., Miller, R.G., Florence, J.M., Verheijde, J.L., Doorish, C., Hilton, J.F., Spitalny, G.M., MacArthur, R.B., Mitsumoto, H., Neville, H.E., Boylan, K., Mozaffar, T., Belsh, J.M., Ravits, J., Bedlack, R.S., Graves, M.C., McCluskey, L.F., Barohn, R.J., Tandan, R. & Western, A.L.S.S.G. Efficacy of minocycline in patients

with amyotrophic lateral sclerosis: a phase III randomised trial. *Lancet Neurol* **6**, 1045-1053 (2007).

137. Stommel, E.W., Cohen, J.A., Fadul, C.E., Cogbill, C.H., Graber, D.J., Kingman, L., Mackenzie, T., Channon Smith, J.Y. & Harris, B.T. Efficacy of thalidomide for the treatment of amyotrophic lateral sclerosis: a phase II open label clinical trial. *Amyotroph Lateral Scler* **10**, 393-404 (2009).

138. Dupuis, L., Dengler, R., Heneka, M.T., Meyer, T., Zierz, S., Kassubek, J., Fischer, W., Steiner, F., Lindauer, E., Otto, M., Dreyhaupt, J., Grehl, T., Hermann, A., Winkler, A.S., Bogdahn, U., Benecke, R., Schrank, B., Wessig, C., Grosskreutz, J., Ludolph, A.C. & Group, G.A.S. A randomized, double blind, placebo-controlled trial of pioglitazone in combination with riluzole in amyotrophic lateral sclerosis. *PLoS One* **7**, e37885 (2012).

139. Gosselin, D., Skola, D., Coufal, N.G., Holtman, I.R., Schlachetzki, J.C.M., Sajti, E., Jaeger, B.N., O'Connor, C., Fitzpatrick, C., Pasillas, M.P., Pena, M., Adair, A., Gonda, D.D., Levy, M.L., Ransohoff, R.M., Gage, F.H. & Glass, C.K. An environment-dependent transcriptional network specifies human microglia identity. *Science* **356**(2017).

140. Hansen, D.V., Hanson, J.E. & Sheng, M. Microglia in Alzheimer's disease. *J Cell Biol* **217**, 459-472 (2018).

141. Chiu, I.M., Morimoto, E.T., Goodarzi, H., Liao, J.T., O'Keeffe, S., Phatnani, H.P., Muratet, M., Carroll, M.C., Levy, S., Tavazoie, S., Myers, R.M. & Maniatis, T. A neurodegeneration-specific gene-expression signature of acutely isolated microglia from an amyotrophic lateral sclerosis mouse model. *Cell Rep* **4**, 385-401 (2013).

142. Yeh, F.L., Hansen, D.V. & Sheng, M. TREM2, Microglia, and Neurodegenerative Diseases. *Trends Mol Med* **23**, 512-533 (2017).

143. Ulrich, J.D., Ulland, T.K., Colonna, M. & Holtzman, D.M. Elucidating the Role of TREM2 in Alzheimer's Disease. *Neuron* **94**, 237-248 (2017).

144. Jonsson, T., Stefansson, H., Steinberg, S., Jonsdottir, I., Jonsson, P.V., Snaedal, J., Bjornsson, S., Huttenlocher, J., Levey, A.I., Lah, J.J., Rujescu, D., Hampel, H., Giegling, I., Andreassen, O.A., Engedal, K., Ulstein, I., Djurovic, S., Ibrahim-Verbaas, C., Hofman, A., Ikram, M.A., van Duijn, C.M., Thorsteinsdottir, U., Kong, A. & Stefansson, K. Variant of TREM2 associated with the risk of Alzheimer's disease. *N Engl J Med* **368**, 107-116 (2013).

145. Guerreiro, R., Wojtas, A., Bras, J., Carrasquillo, M., Rogaeva, E., Majounie, E., Cruchaga, C., Sassi, C., Kauwe, J.S., Younkin, S., Hazrati, L., Collinge, J., Pocock, J., Lashley, T., Williams, J., Lambert, J.C., Amouyel, P., Goate, A., Rademakers, R., Morgan, K., Powell, J., St George-Hyslop, P., Singleton, A., Hardy, J. & Alzheimer Genetic Analysis, G. TREM2 variants in Alzheimer's disease. *N Engl J Med* **368**, 117-127 (2013).

146. Evans, M.C., Couch, Y., Sibson, N. & Turner, M.R. Inflammation and neurovascular changes in amyotrophic lateral sclerosis. *Mol Cell Neurosci* **53**, 34-41 (2013).

147. Butovsky, O., Jedrychowski, M.P., Moore, C.S., Cialic, R., Lanser, A.J., Gabriely, G., Koeglsperger, T., Dake, B., Wu, P.M., Doykan, C.E., Fanek, Z., Liu, L., Chen, Z., Rothstein, J.D., Ransohoff, R.M., Gygi, S.P., Antel, J.P. & Weiner, H.L. Identification of a unique TGF-beta-dependent molecular and functional signature in microglia. *Nat Neurosci* **17**, 131-143 (2014).

148. Yin, Z., Raj, D., Saiepour, N., Van Dam, D., Brouwer, N., Holtman, I.R., Eggen, B.J.L., Moller, T., Tamm, J.A., Abdourahman, A., Hol, E.M., Kamphuis, W., Bayer, T.A., De Deyn, P.P. & Boddeke, E. Immune hyperreactivity of Abeta plaque-associated microglia in Alzheimer's disease. *Neurobiol Aging* **55**, 115-122 (2017).

149. Raj, D., Yin, Z., Breur, M., Doorduin, J., Holtman, I.R., Olah, M., Mantingh-Otter, I.J., Van Dam, D., De Deyn, P.P., den Dunnen, W., Eggen, B.J.L., Amor, S. & Boddeke, E. Increased White Matter Inflammation in Aging- and Alzheimer's Disease Brain. *Front Mol Neurosci* **10**, 206 (2017).

150. Mattsson, N., Insel, P., Nosheny, R., Zetterberg, H., Trojanowski, J.Q., Shaw, L.M., Tosun, D., Weiner, M. & Alzheimer's Disease Neuroimaging, I. CSF protein biomarkers predicting longitudinal reduction of CSF beta-amyloid42 in cognitively healthy elders. *Transl Psychiatry* **3**, e293 (2013).

151. Kiddle, S.J., Thambisetty, M., Simmons, A., Riddoch-Contreras, J., Hye, A., Westman, E., Pike, I., Ward, M., Johnston, C., Lupton, M.K., Lunnon, K., Soininen, H., Kloszewska, I., Tsolaki, M., Vellas, B., Mecocci, P., Lovestone, S., Newhouse, S., Dobson, R. & Alzheimers Disease Neuroimaging, I. Plasma based markers of [11C] PiB-PET brain amyloid burden. *PLoS One* **7**, e44260 (2012).

152. Fardo, D.W., Katsumata, Y., Kauwe, J.S., Deming, Y., Harari, O., Cruchaga, C., Alzheimer's Disease Neuroimaging, I. & Nelson, P.T. CSF protein changes associated with hippocampal sclerosis risk gene variants highlight impact of GRN/PGRN. *Exp Gerontol* **90**, 83-89 (2017).

153. A-Gonzalez, N., Bensinger, S.J., Hong, C., Beceiro, S., Bradley, M.N., Zelcer, N., Deniz, J., Ramirez, C., Diaz, M., Gallardo, G., de Galarreta, C.R., Salazar, J., Lopez, F., Edwards, P., Parks, J., Andujar, M., Tontonoz, P. & Castrillo, A. Apoptotic cells promote their own clearance and immune tolerance through activation of the nuclear receptor LXR. *Immunity* **31**, 245-258 (2009).

154. Mukundan, L., Odegaard, J.I., Morel, C.R., Heredia, J.E., Mwangi, J.W., Ricardo-Gonzalez, R.R., Goh, Y.P., Eagle, A.R., Dunn, S.E., Awakuni, J.U., Nguyen, K.D., Steinman, L., Michie, S.A. & Chawla, A. PPAR-delta senses and orchestrates clearance of apoptotic cells to promote tolerance. *Nat Med* **15**, 1266-1272 (2009).

155. Skerrett, R., Malm, T. & Landreth, G. Nuclear receptors in neurodegenerative diseases. *Neurobiol Dis* **72 Pt A**, 104-116 (2014).

156. Yamanaka, M., Ishikawa, T., Griep, A., Axt, D., Kummer, M.P. & Heneka, M.T. PPARgamma/RXRalpha-induced and CD36-mediated microglial amyloid-beta phagocytosis results in cognitive improvement in amyloid precursor protein/presenilin 1 mice. *J Neurosci* **32**, 17321-17331 (2012).

157. Cramer, P.E., Cirrito, J.R., Wesson, D.W., Lee, C.Y., Karlo, J.C., Zinn, A.E., Casali, B.T., Restivo, J.L., Goebel, W.D., James, M.J., Brunden, K.R., Wilson, D.A. & Landreth, G.E. ApoE-directed therapeutics rapidly clear beta-amyloid and reverse deficits in AD mouse models. *Science* **335**, 1503-1506 (2012).

158. Savage, J.C., Jay, T., Goduni, E., Quigley, C., Mariani, M.M., Malm, T., Ransohoff, R.M., Lamb, B.T. & Landreth, G.E. Nuclear receptors license phagocytosis by trem2+ myeloid cells in mouse models of Alzheimer's disease. *J Neurosci* **35**, 6532-6543 (2015).

159. Myers, K.V., Amend, S.R. & Pienta, K.J. Targeting Tyro3, Axl and MerTK (TAM receptors): implications for macrophages in the tumor microenvironment. *Mol Cancer* **18**, 94 (2019).

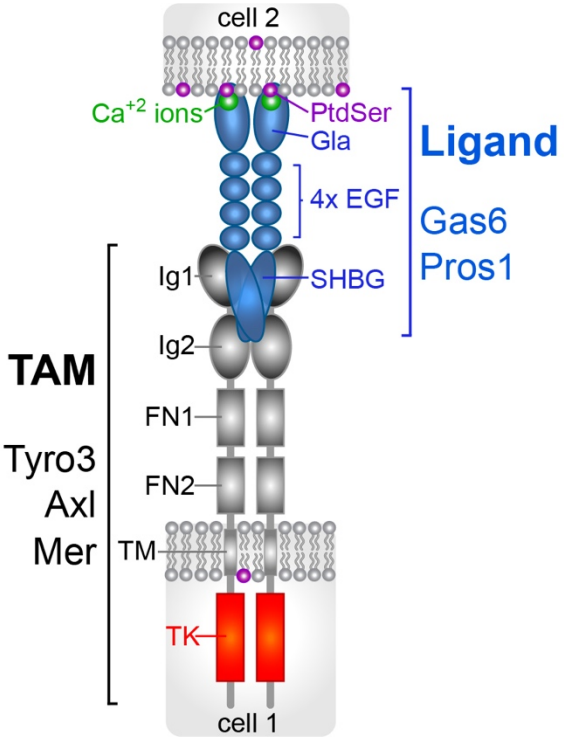

Figure 1.2-1 TAM receptors and their ligands

Tyro3, Axl, and Mer are receptor tyrosine kinases (TK) that are activated by the binding of the C-terminal 'SHBG' domains of the ligands Gas6 (which activates all three RTKs) and Pros1 (which activates Mer and Tyro3) via the N-terminal immunoglobulin domains (Ig1/2) of the receptors. TAM signaling absolutely requires the coincident binding of Ca^{2+} ions and phosphatidylserine (PtdSer, a common phospholipid) to the N-terminal 'Gla' domain of the ligands[52,54].

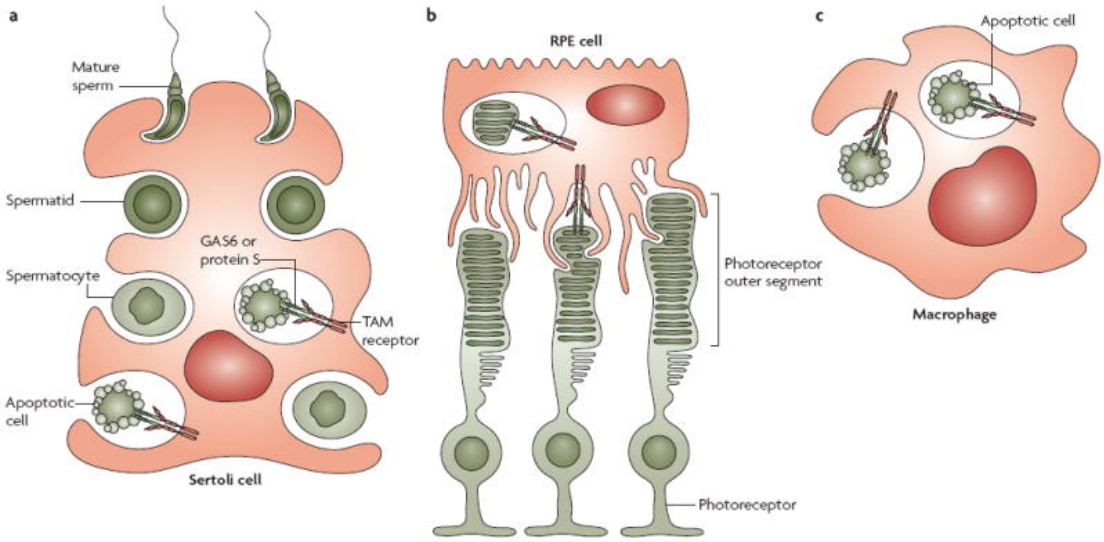

Figure 1.2-2 TAM receptors and the clearance of ACs and PtdSer-rich membranes

Sertoli cells (a), RPE cells (b), and microglia/ macrophages (c) all require TAM signaling to carry out PtdSer-dependent phagocytosis. TAM mutant mice display a pile-up of ACs in the testis, lymphoid organs, and brain, leading to infertility and severe autoimmune disease. Their PR outer segments are saturated with oxidized proteins, which leads to PR death and blindness. From (49).

Chapter 2: Investigating the role of microglial TAM receptors in Alzheimer's Disease

2.1 Introduction

The TAM receptor tyrosine kinases (RTKs) Axl and Mer (gene name *Mertk*) exert two key regulatory functions in macrophages and other immune sentinels[1,2]. First, these RTKs are absolutely required for the phagocytosis of apoptotic cells (ACs)[3-5]. The ACs that are eaten by TAM-expressing phagocytes include the $>10^{11}$ dead cells that are generated each day as a consequence of regular tissue renewal, as well as the added bolus of ACs that accumulate during disease[3]. Mer is expressed by all phagocytic tissue macrophages[3]. Second, both receptors, but most prominently Axl, function as intrinsic negative feedback inhibitors of Toll-like and cytokine receptor signaling in dendritic cells and macrophages subsequent to immune activation[1,2,6]. We have previously shown that both of these essential functions are TAM-controlled and TAM-dependent in microglia, the specialized tissue macrophages of the central nervous system (CNS)[7]. As genetic and cell biological analyses have revealed that many of the genes associated with increased risk for Alzheimer's disease (AD) and other neurodegenerative disorders are expressed in the CNS predominantly or exclusively by microglia, these macrophages have attracted increasing interest in the context of AD specifically and neurodegeneration generally[8,9].

Human and mouse microglia express high levels of Mer and low levels of Axl at steady-state[7,10], and we have previously shown that these RTKs, most notably Mer, play a critical role in microglial phagocytosis of the ACs that are generated during adult neurogenesis[7]. The third TAM receptor – Tyro3 – is not expressed by microglia[7,10], but is instead prominently expressed by neurons[11]. We and others have also shown that expression of the *Axl* gene is markedly up-regulated in microglia and all other tissue macrophages by nearly all inflammatory stimuli (e.g., type I and gamma interferons, poly I:C, and lipopolysaccharide)[5]; and that Axl up-regulation is also seen when macrophages are

activated during the course of infection, tissue trauma, or disease[3,7]. Correspondingly then, RNAseq analyses of laser-captured plaque-associated tissue from human AD, and single cell RNAseq analyses of 'disease-associated microglia' in the 5xFAD mouse model of AD, have both documented dramatic up-regulation of microglial *Axl* mRNA in late-stage disease[12,13]; and immunostaining of plaque-associated microglia in human AD has revealed marked Axl protein up-regulation specifically in these cells[14]. Subsequent to Axl up-regulation and catalytic activation, ADAM family metalloproteases cleave the Axl ectodomain from the cell surface[5], and elevated levels of this soluble Axl ectodomain (sAxl) in cerebrospinal fluid have been found to be predictive of disease development and progression in human AD[15,16]. All of the above observations have led to the classification of *Axl* as a prominent 'AD-associated gene'[13]. This classification notwithstanding, the roles that Axl and its closely-related receptor Mer might play in AD have not been studied, and are therefore unknown.

These considerations led us to examine the expression and function of microglial TAM receptors and their ligands in AD and its mouse models. We studied hemizygous *APP/PS1* mice, which carry a pathogenic, amyloidogenic 'Swedish mutation' of the human amyloid precursor protein (*APP*) gene and an activating (exon 9 deletion) mutation of the human presenilin 1 (PSEN1) gene[17,18], both as transgenes driven by the mouse prion protein promoter. In humans, these mutations result in familial AD, due to elevated proteolytic production of amyloid beta (Aβ) peptides from the amino terminus of APP. We also examined hemizygous *APP41* mice, which express a 'Swedish' + 'London' (V717I) mutant human APP under the control of the Thy-1 promoter[19,20]; and in addition examined TAM regulation in human AD. We find that the full TAM system, including its universal ligand Gas6 and essential co-ligand phosphatidylserine, is engaged concomitant with the deposition of Aβ plaques in the brain. Using single-cell, live two-photon imaging of compound mutant mice in

which both microglia and Aβ plaques are fluorescently labeled, we find that Axl/Mer-deficient microglia are unable to normally detect, respond to, organize, or phagocytose plaques. Remarkably, we further find that TAM-deficient *APP/PS1* mice have fewer plaques than their TAM-expressing counterparts. We propose a model to account for these results.

2.2 Material and Methods

Mice. The *Axl*$^{-/}$ [21], *Mertk*$^{-/-}$ [21], *Axl*$^{-/-}$*Mertk*$^{-/-}$ [21], and *Cx3cr1*$^{GFP/+}$ [22] strains have been described previously. *B6.Cg-Tg(APPSwePSEN1dE9)* hemizygous mice[17,18] (*APP/PS1*) (JAX number: 005864) were crossed with *Axl*$^{-/-}$, *Mertk*$^{-/-}$ and/or *Axl*$^{-/-}$*Mertk*$^{-/-}$ lines to generate *APP/PS1 Axl*$^{-/-}$, *APP/PS1Mertk*$^{-/-}$, and *APP/PS1Axl*$^{-/-}$*Mertk*$^{-/-}$ mice. For two-photon microscopy, *APP/PS1* mice were crossed with *Cx3cr1*$^{GFP/GFP}$ or *Cx3cr1*$^{GFP/GFP}$ *Axl*$^{-/-}$*Mertk*$^{-/-}$ strains. Only female *APP/PS1Cx3cr1*$^{GFP/+}$ WT or *Axl*$^{-/-}$*Mertk*$^{-/-}$ and healthy littermates were used in two-photon studies to avoid potential gender biases in pathology and microglial responses. *APP41* mice, which express a 'Swedish' + 'London' (V717I) mutant human APP under the Thy-1 promoter [19,20,23], were a kind gift of Drs. Kuo-Fen Lee and Jiqing Xu. All lines have been backcrossed for >10 generations to and maintained on a C57BL/6 background. All animal procedures were conducted according to protocols approved by the Salk Institute Animal Care and Use Committee (Protocol No. 17-00009). Mice of both genders were randomly allocated to experimental groups unless otherwise noted.

Reagents and antibodies. Antibodies used were as follows: anti-Axl (R&D AF854), anti-Mer (eBioscience DS5MMER and R&D AF591), anti-mouse Gas6 (R&D AF986), anti-human Gas6 (R&D AF885), anti-beta-amyloid, clone 6E10 (Biolegend 803001), anti-Iba1 (Wako 019-19741 and Novus NB100-1028), anti-GFAP (Dako z-334), cleaved Casp3 (Cell Signaling 9661), anti-CD68 (BioRad MCA1957), anti-NeuN (Chemicon MAB377), anti-Arc (Sysy #156003, Rabbit polyclonal), anti-RTN3 (EMD Millipore ABN1723), anti-Tmem119 (Abcam AB209064), anti-LAMP1 (BD Biosciences, Cat# 553792, clone 1D4B), and anti-Trem2 (R&D systems, AF1729). Secondary antibodies for immunohistochemistry were fluorophore-conjugated anti-rat (712- 545- 153 or 712- 165- 153 from Jackson ImmunoResearch), anti-goat (A-11056 from Life Technologies, or 705-166-147 from Jackson

ImmunoResearch), anti-rabbit (A-11071 or A-21206 from Life Technologies), anti-sheep (A21098 from Thermo Fisher Scientific) and anti-mouse (A-11029 from Life Technologies, 715-166-150 or 715- 176- 150 from Jackson ImmunoResearch). Antibodies used in the quantification of $A\beta_{42}$ peptides by ELISA were obtained as a kind gift from Dr. Marc Mercken from Janssen Pharmaceuticals: JRF AB042/26 for $A\beta_{42}$ and detection antibody JRF/AbN/25, unlabeled. Key reagents and their usage were as follows: Thio S (Acros organics 213150250); Hoechst 33258 in a 1% solution of bisbenzimide in water (Sigma Aldrich B-2883); TrueBlack® Lipofuscin Autofluorescence Quencher (Biotium #23007). For biotinylation of detection antibody JRF/AbN/25 (EZ link Sulfo-NHS-LC Biotin, Thermo Fisher, Cat #21217) and subsequent dialysis (Slide-A-lyzer dialysis cassette, Pierce 0728, prod # 66415). Synthetic human $A\beta_{1-42}$ peptides for ELISA standards (Anaspec Cat # 20276).pSIVA-IANBD™ was included in the pSIVA apoptotic detection kit (Novus Bio NBP2-29382) originally described in Kim et al.[24]. For in vivo amyloid plaque labeling, MX04 (Tocris 4920) was prepared and used as previously described[25], following the manufacturer's instructions. Stock MX04 was first dissolved in 100% DMSO then injected i.p. at a final concentration of 10 mg/kg in 10% DMSO, 45% propylene glycol, 45% PBS, pH 7.5) 24 h prior to imaging.

Immunohistochemistry and histochemistry. Routine perfusion procedures were as described previously [7]. Briefly, littermates of diseased and healthy mice of WT and *Axl*$^{-/-}$ *Mertk*$^{-/-}$ mice at P30 and at adult ages (2.5 -16 mo) were anesthetized with a final concentration of 100mg/kg Ketamine/10mg/kg Xylazine in accordance with IACUC guidelines. Mice were then transcardially perfused with 20U/ml heparin in PBS followed by freshly prepared 4% PFA in PBS. Both hemispheres were post-fixed in 4% PFA in PBS overnight and subsequently infiltrated in 30% sucrose in PBS for 1 day and flash frozen in TBS tissue freezing medium. The left hemisphere was sagittally cryo-sectioned at 15μm, air-

dried overnight and subsequently processed for staining. Antigen retrieval with citrate buffer was performed if needed by heating brain sections to 80°C for 3 min in pre-warmed citrate buffer and cooling to room temperature. Non-specific binding was blocked by 1h incubation in blocking buffer (PBS containing 0.3% Triton-X100, 0.1% Tween-20, 5% donkey serum and 2% IgG-free BSA). Sections were incubated overnight at 4°C with primary antibody diluted in blocking buffer, then washed in PBS 0.1% Tween-20, and incubated for 2 h at 22–24 °C in the dark with fluorophore-coupled secondary antibodies and subsequently in Hoechst for 5 min diluted in blocking buffer. Sections were washed, sealed with Fluoromount-G (SouthernBiotech) and stored at 4 °C. For synaptic staining, freshly sectioned fixed brain sections were blocked for 1 hr at room temp in blocking buffer containing 0.3% Triton-X100, 5% donkey in PBS. Primary antibodies diluted in antibody buffer (blocking buffer + 100mM lysine) were incubated overnight at 4 °C. The next day slides were washed in 3 x 5 min with PBS + 0.2% Triton X-100 and secondary antibodies diluted in the same antibody buffer were applied for 2 hr at room temp followed by nuclear staining and mounting as described above.

Cortical and hippocampal plaque density was quantified by staining with the fluorescent amyloid dye thioflavin S. Thio S binds to the β pleated sheets of dense-core senile amyloid plaques and provides for more reliable semi-automated quantification of plaques than immunostaining with 6E10. A serial set of 15μm sagittal sections (5 sections/mouse) were obtained 0.25mm-0.85mm from the midline, each spaced 0.15mm apart. Plaque abundance was quantified by histochemistry with Thio S staining using published protocols [26]. Image analysis of the number of cortical and hippocampal Thio S+ plaque was done blind with respect to genotypes and in a semi-automated fashion with set intensity thresholds for all conditions, using the ‘analyze particles’ function on ImageJ or FIJI software. For evaluating pSIVA-injected *APP/PS1* and WT mice, a serial set of 15μm sagittal

sections were obtained between 1mm-2mm from the midline (0.5mm before and after the corresponding pSIVA injection sites, 15 sections/mouse) from both PSIVA-injected and control hemispheres. Serially cut sections from both hemispheres and genotypes (*APP/PS1* vs WT) were further immunostained with 6E10 antibody and evaluated for co-localization of fluorescence emitted from pSIVA and amyloid.

Human postmortem AD brain sections. Paraffin-embedded thin sections of postmortem human brain tissues were obtained from the UCSD Alzheimer's Disease Research Center (ADRC), courtesy of Dr. Robert Rissman. Three age-matched pairs of AD BRAAK stage 6 and clinically normal brain sections were evaluated. Sections underwent standard deparaffinization and permeabilization with .3% Triton-X100 before treated for 5min with 1X TrueBlack in 70% Ethanol. Subsequent immunostaining for human Gas6 and Aβ plaques using the antibodies detailed above was done with the standard immunofluorescence protocol detailed above without detergents in the buffers.

RT-qPCR. RNA from snap-frozen cortex or hippocampal tissue was isolated with TRIzol (Thermo Fisher Scientific 15596026) according to the manufacturer's instructions. The RT Transcriptor First Strand cDNA Synthesis Kit (Roche) with anchored oligo(dT) primers (Roche) was used for reverse transcription. Quantitative PCR was run in a 384-well plate format on a QuantStudio Q5. Gas6 primer sequences used: forward primer 5'-3' AAC TGG CTG AAC GGG GAA G and reverse primer 5'-3' CTT CCC AGG TGG TTT CCG T. Arc (Arg3.1) primer sequences used: forward primer 5' – 3' GGAGGGAGGTCTTCTACCGTC and reverse primer 5' – 3' CCCCCACACCTAC AGAGACA. Relative expression of genes of interest was normalized to GAPDH (primer pairs: forward sequence 5'-3' AGG TCG GTG TGA ACG GAT TTG; reverse sequence 5'-3' GGG GTC GTT GAT GGC AAC).

Extraction of soluble Aβ and quantification of $A\beta_{42}$ by ELISA. Briefly, whole cortices and hippocampi were swiftly dissected from freshly extracted brains on an ice-cold platform and 'snap' frozen in liquid nitrogen. Tissues were lysed on ice in RIPA buffer [50mM Tris-HCl, pH =8.0, 150mM NaCl, 0.1% SDS, 1% Triton-X 100, 0.5% deoxycholate] with protease and phosphatase inhibitor (Roche, Sigma) at 4:1 RIPA volume/brain wet weight. Homogenates were spun at 5000g first to deplete debris and then ultracentrifuged at 100,000 rpm at 4°C for 1 hour. Supernatants (containing soluble Aβ) from the cortical and hippocampal preparation were aliquoted and stored at -80°C until further use. Extracts from APP/PS1 WT and *Axl*$^{-/-}$ *Mertk*$^{-/-}$ and their non-diseased littermates were prepared simultaneously and identically.

Standard sandwich ELISA measurements of soluble $A\beta_{42}$ were performed based on published protocols[27]. Briefly, 96-well plates were pre-coated with anti-$A\beta_{42}$ JRF AB042/26 capture antibody at a concentration of 1.5μg/ml 50ul per well overnight at 4°C. The following day, plates were blocked 150μl/well with 1% casein blocking buffer for 2 hours at room temperature. Plates were washed five times with PBS + 0.05%Tween-20. JRF/AbN/25 detection antibody against the N-terminus of Aβ had previously been biotinylated and dialyzed following manufacturer's instructions. 25μl biotinylated detection antibody was diluted in blocking buffer was mixed with either 25μl of standards (synthetic human $A\beta_{1-42}$ peptide) or 25μl extracellular media before loaded 50μl per well and in duplets. Following overnight incubation at 4°C, plates were rinsed and incubated in streptavidin-HRP at 50μl/well for 30min and developed in 1:1 mixture of Color Reagent A (H_2O_2) and Color Reagent B (Tetramethylbenzidine) (Cat # DY999). Plates were immediately measured on a TECAN Infinite® 200 PRO reader at 450nm.

Survival and home-cage video monitoring. Long-term (2 week) continuous digital videos of young adult AD mice (1.5-3 mo) housed in their home cages with clear cage lids (2 mice per cage) were collected at 25 fps using a high resolution, infrared equipped, digital video camera (Sony HandyCam HDR-XR520), set up in a top-down fixed angle for recording. The recording room was maintained on a 12h/12h light/red light cycle. Video monitoring of sporadic deaths and spontaneous convulsive seizures was performed by reviewing video footage via VLC player. Cages were checked every 12h to ensure proper air conduction and ample and accessible food and water, and to collect any mouse found dead. Brains from mice found dead during the study were freshly extracted, immersion-fixed, and immunostained for Arc expression.

pSIVA stereotaxic injections for in vivo PtdSer labeling. Stereotactic injections were performed following previously published protocols [28]. Briefly, thin wall glass pipettes were pulled on a Sutter Flaming/Brown puller and cut using sterile techniques resulting in tip diameters of 10-15μm. Adult APP/PS1 and WT control mice (15μmo) were anesthetized with isoflurane (4% for induction; 1%-2% during surgery). Mice were head-fixed in a computer-assisted stereotactic system with digital coordinate readout. Three sites were serially injected with pSIVA on the right hemisphere of each animal. Neocortical coordinates were (AP +1mm, ML+1.5mm, DV +1mm), (AP 0mm, ML+1.5mm, DV +1mm) and (AP -1mm, ML+1.5mm, DV +1mm) along the motor and somatosensory cortex around layer III/IV. First, craniotomy sites were marked and an electrical micro-drill with a fluted bit (0.5 mm tip diameter) was used to thin a 0.5–1 mm diameter part of the bone over the target injection site. Care was taken to ensure uninjured uplifting of the bone segment. Next, undiluted pSIVA dye was loaded into the glass pipette with sufficient volume and was gently lowered to the desired depth (using the DV coordinates). A total of 500μl pSIVA per injection site was injected slowly at

1nl/second over a period of 15-20min and with a 5-minute break halfway and at the end of each injection to avoid backflow before carefully retracting the injection pipette to the next target injection site (using AP and ML coordinates). At the end of the last injection, mice were sutured along the incision of the scalp, and given subcutaneous Buprenex SR (0.5mg/kg). Each mouse was allowed to recover before placement in their home cage for 1.5-2h before undergoing routine perfusion and processing of both PSIVA-injected hemisphere and control hemisphere (see previous section).

Surgery and animal preparation for *in vivo* two-photon imaging. Surgical procedures closely followed established protocols [7,28,29]. Briefly, mice were anesthetized with isoflurane (4-5% for induction; 1%-1.5% for maintenance), head-fixed with blunt ear bars, and kept at 36°C–37°C on a custom surgical bed (Thorlabs). Eyes were protected with vet ophthalmic ointment (Puralube). Depilator cream (Nair) was used to remove hair on top of the mouse's head. The scalp was thoroughly cleansed and disinfected with a two-stage scrub of betadine and 70% ethanol. A scalp portion was surgically removed to expose frontal, parietal, and interparietal skull segments. Scalp edges were attached to the lateral sides of the skull using tissue compatible adhesive (3M Vetbond). A custom-machined metal plate was affixed to the skull with dental cement (Coltene Whaledent, cat. no. H00335). Ear bars were removed and the head was stabilized by clamping the skull-attached plate with a custom holder. An approximately 3mm diameter craniotomy was made over somatosensory cortex (center coordinates: AP -1.5mm, ML 1.5mm). A 1.5% agarose solution and coverslip were applied to the exposed tissue, and the coverslip was fixed to the skull with dental cement to control tissue motion. Imaging commenced immediately after optical window preparation (corresponding to 13-14h after intraperitoneal MX04 injection). Depth of anesthesia was monitored throughout the experiment and adjusted as needed to maintain a breath rate of

approximately 55-65 breaths per minute. Animal temperature was maintained at 36°C–37°C and saline supplemented as needed to compensate for fluid loss.

Confocal microscopy. One-photon laser scanning confocal images were acquired with a Zeiss LSM 710 Confocal microscope using Plan-Apochromat 20x 0.8-NA air-matched or 63x 1.4-NA oil objectives (laser lines: 405 nm, 488nm, 594nm and 633nm). Image size was 1024 x 1024 pixels. Stack thickness is 15μm for mouse brain section and 5μm for postmortem paraffin-embedded sections. For synaptic quantification specifically, CA1 apical dendrites were imaged at 3 μm thickness and z stack image were obtained (optical slice 0.29 μm, 11 slices per 3μm stack). Exposure acquisition was set according to the WT or non-mutant samples in all experiments. Airyscan super-resolution images were acquired with a Zeiss LSM 880 Rear Port Laser Scanning Confocal and Airyscan FAST Microscope using 63x oil objective. Whenever possible, ≥ 3 images per section, ≥ 3-5 sections per animal. Images were obtained and processed via the Zen Black and Zen Blue editions. Images for cortical and hippocampal plaque quantification were acquired with Olympus VS-120 Virtual Slide Scanning Microscope using a 10x objective.

Two-photon microscopy. Live animal imaging was performed as previously described [7,28,29]. Briefly, a Sutter Movable Objective Microscope (MOM) equipped with a pulsed femtosecond Ti:Sapphire laser (Chameleon Ultra II, Coherent) with two fluorescence detection channels was used for imaging (dichroic beamsplitter: FF520-Di02 (Semrock); blue emission filter: FF01-452/45 (Semrock); green emission filter: ET525/70M (Chroma); photomultiplier tubes: H7422-40 GaAsP (Hamamatsu)). Laser excitation wavelength was set to 830nm. Average laser power was <10-15mW at the tissue surface and adjusted with depth as needed to compensate for signal loss due to scattering and absorption. An Olympus 20x

1.0-NA water immersion objective was used for light delivery and collection. Z-stacks included up to 350 images, acquired at 1μm axial step size, used a 2-frame average, 512 x 512 pixel resolution, and 2.0x-10x zoom (corresponding to 350μm-72μm fields of view). Time-lapse recordings typically included 60-70 images/stack, acquired at 1.0-1.2 μm axial step size, used a 2-frame average, 60 stack repeats (corresponding to approximately 94 min total recording duration), 512 x 512 pixel resolution, and 3.3x-5x zoom (corresponding to 212 μm - 142 μm fields of view). Up to thirteen z-stacks, and four to seven time-lapse recordings were acquired per animal in layers 1 and 2 of the somatosensory cortex.

Contextual fear condition behavior test. Only male mice were used in this study to limit gender-induced variability. 2 batches of animal cohorts were used (n=6-10/ group) and the data were analyzed separately for validation and then combined. Briefly, mice were habituated 5 consecutive days prior to fear acquisition. On the day of fear acquisition (day 1), mice were evaluated for their abilities to remember the association between a context and an aversive mild electrical stimulus. Freezing behavior calculated in form of "%freezing", i.e. time the mouse spent being immobile during the time period in the presence of the paired context (context test) even when the aversive stimulus is absent, is the readout of the memory tests and is monitored by an automated recording system[30]. After three paired stimuli of auditory cue and electric shock in fear acquisition, mice were monitored for their freezing behavior at 24h (Day 2) in the original context. To avoid estrogen-related variations, only male mice in cohorts with matching ages and group caged ones were use in these studies.

Data analysis. For fixed-brain thin sections, maximum intensity projection images of 212μm x 212μm (1024x1024 pixel resolution) were analyzed in FIJI. ~5-7 plaques per brain sections

(3-5 sections per animal) were randomly chosen in the prefrontal cortex using the 6E10 channel. Mean fluorescent intensity (MFI) for Mer, Axl, and Gas6 expression analysis, was calculated as the quotient of integrated density divided by region of interest, for example, Iba1 area or 6E10 area, respectively, which were gated based on their intensity and applied for all images in each experiment. Plaque-associated and non-plaque associated Iba1 areas were classified manually by investigator blind with respect to genotypes. For quantification of dystrophic neurite area using LAMP1 or RTN3, area above set fluorescent thresholds for either LAMP1 or RTN3-marked neuritic dystrophy and 6E10 immuno-positive area were calculated and summed using the FIJI 'analyze particle' tool, and the ratio of summed area (LAMP1 or RTN3 area/6E10 area) was calculated on per plaque basis. For LAMP1 analysis for convenience of binary categorization, dense-core plaques were defined as plaques that contain a single or solid (usually bright) 6E10-positive core area $\geq$ 100μm^2, and diffuse plaques were defined as the complement of these dense-core plaques that are characterized as those devoid of compact 6E10-positive area $\geq$ 100μm^2.

To assess excitatory synapse changes in hippocampus, co-localization of vGlut1 and PSD95 in the apical dendrite area of CA1 of mouse hippocampus was analyzed using Imaris software (Bitplane). 3D z stack images were background subtracted and positive puncta of vGlut1 and PSD95 were selected and built as 'spots' by uniformly thresholding size and intensity across all sections and genotypes analyzed. PSD95 spots were then transformed into distance vector using the 'distance transform' function, which was followed by a calculation of distance between vGlut1 spots and PSD95 spots. Puncta were considered colocalized if the distance between vGlut1 and PSD95 was $\leq$ 0.7 μm. Number of colocalized puncta from each image was averaged for one section or for one animal and compared

between the experimental groups that contain 3 animals. ≥ 3 images per section, ≥ 3-5 sections per animal were analyzed.

For analyses of two-photon image stacks, Imaris software (version 9.1.2; Bitplane, Zurich, Switzerland) was used for three-dimensional reconstruction of GFP microglia and MX04-labeled dense-core plaques, and also for the analysis of (a) the distance of the centroid of GFP^+ microglial cell bodies to the edge of a $MX04^+$ mass, (b) microglial cell body volume, and (c) intracellular Aβ,from 1μm-step z-series stack images of both genotypes. Two types of 'surfaces', as digital representations that capture the volume of either a microglia cell body or a dense-core (not diffuse) plaque for the GFP channel and MX04 channel, respectively, were created under the same threshold for all stack images. For MX04 objects, a surface cutoff was set to be at the clear-cut border of the outlining of dense-core plaques, exclusive of surrounding diffuse material. Only dense-core plaques whose diameters fell between 10μm-40μm were included in the following analysis. For GFP surfaces, filters for "Surface grain size", "Diameter of the largest sphere which fits into object", "Seed points diameter", "Quality for seed points" (e.g. to determine whether a structure belongs to the same or a neighboring cell), and volume cutoff were set to 0.3μm, 7.5μm, 3.75μm, 65a.u. and $65\mu m^3$, respectively, for capturing the structure of GFP microglial cell bodies in imaging volume of 142μm x142μm x 70μm for Fig. 3c and Supplementary Fig. 3a and a normalized imaging volume of 350μm x 350μm x 300μm in somatosensory cortex (512 x 512 pixel resolution). The same thresholds were applied to all images of both genotypes. Structures on edge and/or captured incompletely were manually deleted. Created surfaces were then used to determine distance of the centroid of individual GFP surfaces to the closest edge of MX04 objects with the build-in MATLAB function in Imaris.

For quantification of intracellular Aβ, a GFP 'cell-body only' channel was built with GFP surfaces as mask borders using the 'set outside voxel to 0' mask. MX04 and the 'cell-body only' GFP channel were then thresholded to capture the overlapping volume between MX04 and GFP channel using the 'co-localization' function in Imaris. The overlapping volume was then normalized to the total volume of GFP of the image as a representation of the percentage of GFP microglia cell body volume occupied by MX04 material. Primary process number, total length for PAM, and process polarization ratio for NPAM around dense-core plaques whose diameters fell between 10μm- 30μm were analyzed with FIJI based on maximum intensity projection stack images of 142μm x142μm x 60μm in volume. Measurements of these parameters were performed as described previously [31,32]. For primary process number and total length, PAM were defined as those whose cell body centroids were 0-5μm away from the edge of the nearest MX04 edge [33]. On average 3-5 microglia per plaque that were unambiguously distinct, showed clear process visibility, and were not between two plaques were selected. Primary process number and length from PAM were measured using the 'free-hand' line tool on FIJI. Z-stacks of these projected images were gone through to ensure processes continuity from the same cell across layers. Mainly distal primary processes were analyzed in this group of cells due to the fact that majority of their somata were next to or in direct contact with a plaque surface. For polarization index, NPAM were defined as those whose cell body centroids were 20-50μm from a dense-core MX04 edge and whose processes were clearly visible. Cells equidistant between two plaques were not included in the analysis. Calculation of this index was performed as described previously [32]. Briefly, processes oriented toward plaques were classified as those on the plaque side of a line drawn through the microglial cell body perpendicular to a line drawn to the nearest plaque. The polarization index for one microglia cell is the ratio of the summed length of all 'toward' primary processes divided by the summed length of all processes.

For structural dynamics of individual microglia processes, process velocity was assessed as previously described[29,34], by manually tracing process tips over time using the Manual Tracking plug-in on Fiji on Maximum Intensity Projected time lapse Videos, typically over 90-minute time spans that cover a FOV of 212μm x 212μm x 70μm in the somatosensory cortices of age-matched AD and healthy littermates of WT and *Axl*$^{-/-}$*Mertk*$^{-/-}$ mice. As mentioned in the previous section, measurements were made for AD microglia whose cell body centroids were within 5μm from the edge of dense-core MeX04 edge as measured on projected images (PAM), and for those whose centroids were over 20μm from any plaque in the FOV (NPAM). Resting microglia were microglia from non-AD age-matched littermates. At least 2-3 and 4-7 processes were quantified from PAM and NPAM, respectively, to obtain an average process velocity per microglia.

Statistical analysis. Statistics were performed with GraphPad Prism (version 8.0) software. All data in all figure panels of the paper are represented as mean ±1 standard deviation. In most cases, ‘‘n’’ is used to denote the number of mice per experimental group and ‘‘N’’ the number of brain sections/images/samples analyzed per mouse. Group sample sizes were chosen based on previous studies and/or power analysis. Datasets displayed normal distribution and equal standard deviations unless indicated by unequal variance test.

2.3 Results

2.3.1 TAM system expression in AD

Engagement of TAM receptors during disease

Consistent with earlier mRNA observations, we detected pronounced elevation of microglial Axl protein in *APP/PS1* mice. This Axl induction in microglia was very tightly plaque-associated, however, and was not seen early in disease prior to the deposition of Aβ plaques. We identified microglia as cells expressing Iba1 ('ionized calcium-binding adaptor molecule 1'), or alternatively, green fluorescent protein (GFP) in *Cx3cr1-eGFP* mice[7]. Microglia that were near but not touching Aβ plaques, identified with the 6E10 antibody specific to human APP, were Axl^- in aged *APP/PS1* mice, while those in direct contact with plaques were strongly Axl^+ (Fig. 2.3.1-1a). Importantly, Axl protein up-regulation specific to plaque-associated microglia has also been seen in human AD[14]. Quantification of Axl fluorescence in plaque-associated versus non-plaque-associated microglia - PAM and NPAM, respectively - in the cortex over the full course of disease in *APP/PS1* mice revealed a modest Axl increase in NPAM between 7 and 12 months; but strong Axl up-regulation was only seen in plaque-associated microglia (Fig. 2.3.1-1b). As documented previously, we did not detect reproducible plaque accumulation in *APP/PS1* mice until ~5 months, and we measured no microglial Axl up-regulation prior to this time (Fig. 2.3.1-1b,c). At 9.5 months of age, Axl protein levels were ~25-fold higher in PAM versus NPAM (Fig. 2.3.1-1b). In accordance with this, we also detected similar expression of Axl surrounding plaques in sections of human AD brain at BRAAK stage 6 (Fig. 2.3.1-3). In addition, we detected a similar Axl up-regulation in aged *APP41* mice, a second amyloidogenic model. In these mice, Axl immunoreactivity, in addition to being up-regulated in PAM, frequently displayed an interesting distribution that was concentrated at the very center of Aβ plaques (Fig. 2.3.1-4a).

Since strong Axl activation is always accompanied by cleavage of the Axl ectodomain and the generation of sAxl[5], this plaque-deposited Axl is almost certainly sAxl.

In contrast to Axl, Mer is abundant in microglia in non-diseased human and mouse brains[7,10], and also in the *APP/PS1* brain prior to the appearance of plaques. However, Mer expression was also up-regulated in PAM in aged *APP/PS1* (Fig. 2.3.1-2b) and *APP41* (Fig. 2.3.1-4b) mice. In the 9.5-month *APP/PS1* brain, we quantified an ~3.5-fold elevation in Mer protein levels in PAM versus NPAM (Fig. 2.3.1-2b). It is important to note that $Axl^{+}Mer^{hi}$ microglia were the same plaque-associated cells that also markedly up-regulated expression of Trem2 (Fig. 2.3.1-5), mutations in which increase the risk of developing human AD[35]. Although we observed that Axl, Mer, and Trem2 were always up-regulated in the same cells, Trem2 and the TAM receptors appeared to occupy distinct membrane domains (Fig. 2.3.1-5). Most $Axl^{+}Mer^{hi}Trem2^{+}$ microglia surrounding plaques in both *APP/PS1* and *APP41* mice were negative for TMEM119, a marker of homeostatic microglia[36], although in the *APP41* model particularly, 1-2 cells at the very center of plaques were often $TMEM119^{+}$ (Fig. 2.3.1-6). Plaque-associated astrocytes display reactive astrocytosis in AD and its mouse models, but unlike microglia, $GFAP^{+}$ and $S100b^{+}$ reactive astrocytes expressed no detectable Mer (Fig. 2.3.1-7 and Ref. 7).

Engagement of TAM ligand and co-ligand during disease

We found that expression of the obligate Axl and pan-TAM ligand Gas6[37] was also strongly up-regulated specifically on plaques in aged AD mice (Fig. 2.3.1-8a). This plaque-associated Gas6 has not been previously reported, and was not detected in earlier single cell RNAseq analyses of mouse AD models. This is because microglial expression of *Gas6*

mRNA, which is already very high in normal microglia and neurons[10], does not change over the course of disease in these models[12] - and the earlier analyses examined only mRNA. We found that the presence of plaque-associated Gas6 protein in *APP/PS1* mice was tied to an unusual feature of Gas6-Axl interaction: it has been shown that most or all Axl-expressing cells in normal wild-type (WT) mouse tissues are constitutively bound by Gas6, and that stable expression of Gas6 in these tissues is specifically Axl-dependent[5]. (Gas6 protein expression is lost in *Axl*$^{-/-}$ but not *Mertk*$^{-/-}$ tissues, even though *Gas6* mRNA levels are unchanged in these tissues between these mutants and WT[5].) Thus, Gas6 protein cannot be detected in normal, non-diseased *Gas6*-mRNA-rich brains because these brains express little or no Axl, and acquired Axl in plaque-associated microglia in AD models leads to acquired plaque-localized Gas6. Consistent with this observation, plaque-associated Gas6 was sharply reduced in *APP/PS1Axl*$^{-/-}$ mice and eliminated entirely in *APP/PS1Axl*$^{-/-}$*Mertk*$^{-/-}$ mice (Fig. 2.3.1-8a, quantified in Fig. 2.3.1-8b). Importantly, amyloid plaques did not develop, and Gas6 did not appear, in aged *Axl*$^{-/-}$*Mertk*$^{-/-}$ double mutants without the *APP/PS1* allele (Fig. 2.3.1-8b), and the level of *Gas6* mRNA was constant across WT, *APP/PS1*, *Axl*$^{-/-}$*Mertk*$^{-/-}$, and *APP/PS1Axl*$^{-/-}$*Mertk*$^{-/-}$ cortices at 12 months (Fig. 2.3.1-8c). We also detected expression of Gas6 surrounding plaques in sections of human AD brain at BRAAK stage 6, but not in age-matched controls (Fig. 2.3.1-9), indicating that acquired Gas6 expression also marks plaques in human AD. Gas6 activates both Axl and Mer, but Mer can also be activated by the closely-related ligand Protein S (Pros1)[37]. Although antibodies for high-resolution immunohistochemical detection of Pros1 in the mouse are not currently available, microglia express abundant *Pros1* mRNA[10,38], and recent deep proteomic profiling of the 5xFAD hippocampus over the course of disease has revealed that elevated Pros1 protein is a novel biomarker for disease severity in this model[39]. It is therefore very possible that amyloid plaques are also decorated with Pros1.

In addition to ligands and receptors, effective TAM signaling requires binding of the phospholipid phosphatidylserine (PtdSer) to the amino-terminal 'Gla' domains of the ligands Gas6 and Pros1[3,37]. For example, a 'Gla-less' truncation mutant of Gas6 has been shown to bind to Axl with the same sub-nanomolar affinity as the full-length ligand, but to be entirely incapable of activating the receptor[37]. With respect to TAM receptor interaction, PtdSer is generally externalized on the membrane surface of a cell that is apposed to a TAM-receptor-expressing cell[1]. Often this apposed cell is an AC or a membrane fragment thereof[3]. It is important to note that PtdSer is a common phospholipid component of every cell's plasma membrane, but that in all normal cells it is enzymatically confined to the inner (cytoplasm-facing) leaflet of the membrane[3]. Externalization of PtdSer on the plasma membrane surface (carried out by a set of PtdSer 'scramblases'[3] in response to apoptotic triggers, Ca^{2+} entry, viral infection, and disease stressors) is therefore the key to its action. During AC phagocytosis, Gas6 and/or Pros1 'bridge' PtdSer that is externalized on the AC surface to TAM receptors on the surface of microglia and other phagocytes[3]. To visualize externalization of PtdSer in the brains of *APP/PS1* mice, we stereotaxically injected their cortices with pSIVA, a 'polarity-sensitive indicator for viability and apoptosis' that fluoresces strongly only when bound to PtdSer[24]. Immediately next to the injection sites, we detected a 100% coincidence between $6E10^+$ Aβ plaques and $pSIVA^+$ externalized PtdSer but not with sham control on the other hemisphere of the subjects (Fig. 2.3.1-10). This PtdSer may mark the dystrophic neurites that are a feature of plaques and their immediate surroundings. Super-resolution microscopy suggested that Gas6 does indeed serve to 'bridge' $PtdSer^+$ Aβ plaques to TAM^+ microglia in the aged *APP/PS1* brain (Fig. 2.3.1-11). These results demonstrate that all of the essential components of TAM system signaling – the receptors themselves, their ligand Gas6, and the essential co-factor PtdSer – are specifically up-regulated in their expression on and around Aβ plaques in the *APP/PS1* AD brain

2.3.2 TAM activity in AD brains prior to plaques

Multiple whole-body TAM receptor antagonists – including small molecule inhibitors of the TAM tyrosine kinases – are currently in both development and clinical trials for the treatment of cancers[40]. We therefore thought it important to examine the consequences of genetic ablation of TAM signaling for the development of disease in *APP/PS1* mice, by crossing complete *Axl*$^{-/-}$ and *Mertk*$^{-/-}$ mouse mutants into this line. We observed striking phenotypes in these crosses, but the initial phenotype presented more than two months prior to the deposition of Aβ plaques and the up-regulation of Axl.

The *APP/PS1* line is subject to neuronal hyperexcitability and epileptic seizures, which occur from approximately postnatal day (P) 70 to P150 and result in the sudden death of 10-15% of these mice over this period[41,42]. As noted above, reproducible plaque deposition is not observed in *APP/PS1* mice until ~P150. Early seizure activity is also seen in other amyloidogenic AD mouse lines, such as TG2576, J9, J20, ARC48 and 5XFAD, etc[43-45], and importantly, epilepsy is a well-recognized comorbidity, especially at early stages of disease, in human AD[46-48]. Indeed, the incidence of spontaneous epileptiform seizures is 87-fold higher for early onset AD patients in early stages of disease[49-53] than in age-matched controls and up to 20% of patients with mild-to-moderate sporadic AD are estimated to have one unprovoked seizure[49,50,52]. When we crossed *Axl*$^{-/-}$*Mertk*$^{-/-}$ double mutants into *APP/PS1* mice, a large cohort of *APP/PS1 Axl*$^{-/-}$*Mertk*$^{-/-}$ compound homozygotes revealed an unexpected and dramatic decrease in viability compared to *APP/PS1* mice: by the time these mice are only 120 days old, more than 40% of the *APP/PS1 Axl*$^{-/-}$*Mertk*$^{-/-}$ population has died (**Fig. 2.3.2-1**). Essentially all of this enhanced lethality was due to mutation of *Mertk* alone (Fig. 2.3.2-1a) since we do not observe this phenomenon in *APP/PS1 Axl*$^{-/-}$ mice. Interestingly, *APP/PS1* mice with genetic ablation of TAM ligand Gas6 also phenocopy the mortality rate of the

Mertk-mutant *APP/PS1* mice and their mortality also peaks early in their disease, before the time of initial plaque deposition. This suggests a pivotal role of Gas6 signaling through Mer in the pre-plaque deposition stage in *APP/PS1* mice, the loss of which is at least partially responsible for the increased early sudden death cases. Sudden death in the *APP/PS1Axl*$^{-/-}$ *Mertk*$^{-/-}$ and *APP/PS1Mertk*$^{-/-}$ populations was first observed immediately after weaning and genotyping, sooner than was seen in *APP/PS1* (Fig. 2.3.2-1a), so the survival curves shown in Fig. 2.3.2-1a could even be an overestimation of the actual viability of all *Mertk*-mutant *APP/PS1* mice. Note that non-transgenic WT and *Axl*$^{-/-}$*Mertk*$^{-/-}$ littermate mice have essentially normal lifespans[21], and early death is not seen in these mice (Fig. 2.3.2a top panel). Video monitoring of *APP/PS1Axl*$^{-/-}$*Mertk*$^{-/-}$ and *APP/PS1Mertk*$^{-/-}$ mice (**Supplemental Videos 1, 2**, Fig 2.3.2-1b) suggested that sudden death in the compound mutants was, as has been well-documented for the *APP/PS1* allele alone[41,42], the result of lethal seizures.

Next, we sought to identify the mechanistic basis of the dramatic increase in lethality in Mer-mutant *APP/PS1* mice. In *APP/PS1Mertk*$^{-/-}$ individuals analyzed immediately after a lethal convulsive seizure, staining for the neuronal activity indicator Arc (Arg3.1)[54] demonstrated massive synchronous hyperactivation of granule cell neurons in the dentate gyrus (DG) of the hippocampus, a common initiating locus for temporal lobe epilepsy in humans and status epilepticus in mice[55] (**Fig. 2.3.2-2**). Arc expression was also detected in multiple additional loci throughout the brain (Fig. 2.3.2-2), and $\geq$99% of this expression was neuronal (**Fig. 2.3.2-3**). Arc was only sparsely expressed in DG neurons in similarly fixed WT and *Mertk*$^{-/-}$ brains (Fig. 2.3.2-3). It is important to note that this heightened large-scale Arc expression in DG neurons is a seizure-activity-induced neuronal response, as we found there is neither a difference in Arc-expressing cell number in the DG in regularly perfused AD transgenic mice comparing with their healthy littermates with and without the loss of TAM

receptors, nor is there difference in Arc mRNA in cortex among the above-mentioned genotypes (Fig. 2.3.2-4). Therefore, it is unlikely that the seizures are primed or enhanced by an over-activation of immediate early gene in DG neurons at basal levels, although the possibility that such phenomenon could occur in other relevant brain regions in non-convulsive *APP/PS1Mertk*$^{-/-}$ brains should not be excluded and warrants more investigation. For example, in *APP/PS1Mertk*$^{-/-}$ mice not experiencing an acute seizure, we again detected sparse Arc^{+} expression in the DG, but also more widely distributed Arc^{+} cells across several layers of the neocortex (Fig. 2.3.2-3), indicative of recent synchronous cortical hyperactivation.

For all *APP/PS1*-containing lines, lethal seizures and Aβ plaques were anti-correlated over time, in that the incidence of sudden death decreased precipitously with the first deposition of plaques at ~5 months of age (Fig. 2.3.2-1). In fact, our data suggest the increased mortality rate is related to other pre-plaque deficits in the *APP/PS1* mice that are additionally potentiated by the loss of *Mertk*, resulting in more disturbances in the excitatory/inhibitory (E/I) balance of their DG circuitry. The full mechanistic basis for TAM regulation of seizures in *APP/PS1* mice necessitates more investigation, but among some hypotheses we have tested, observations suggest that it is related to previously described TAM activity during adult neurogenesis[7].

We first asked whether unexpected death could be in part be explained by uncontrolled over-production of pro-inflammatory cytokines in the absence of TAM receptors, and therefore we looked at the mRNA expression for various pro-inflammatory cytokines. We have conducted preliminary RT-qPCR experiments to examine the expression of a few common pro-inflammatory cytokines and immune-regulatory genes, including IL-1β, TNFα,

IL-6, IFNα4, IFNβ, IFNγ and iNOS, in mRNA isolated from the cortices and hippocampi of APP/PS1 and *APP/PS1Axl*$^{-/-}$*Mertk*$^{-/-}$ mice together with age-matching non-diseased WT and *Axl*$^{-/-}$*Mertk*$^{-/-}$ mice at 2 months and 4 months of age. Despite the well-characterized immunosuppressive role of TAM receptors in all tissue macrophages, loss of TAM receptors in whole cortex-extract mRNA from APP/PS1 mice does not seem to advance or exacerbate the levels of expression of the tested pro-inflammatory genes in the brain (**Fig. 2.3.2-5**). Though we do not exclude the possibility of non-detectable subtle difference in pro-inflammatory cytokine production mediated by the loss of TAMs to have contributed to the mortality phenotype, the dramatic drop in viability seen between these ages in *APP/PS1Axl*$^{-/-}$ *Mertk*$^{-/-}$ mice is unlikely to be caused by a severe over-production of cytokines such as a cytokine storm, but instead corroborates with our observation that the exacerbated mortality rate is a direct result of lethal seizures.

The subgranular zone (SGZ) of the DG - a thin layer of cells immediately interior to the granule cell layer - is one of two principal centers of adult neurogenesis in the mouse brain, the other being the subventricular zone (SVZ); and we have previously shown that microglial Mer plays an essential role in the phagocytosis of ACs that are generated during this neurogenesis[7]. *Mertk*$^{-/-}$ and tamoxifen-injected *Mertk*$^{f/f}$*Cx3cr1*^{CreER} mice, in which *Mertk* is inactivated only in microglia, display substantial AC accumulation in the SVZ[7], and microglia in the *Axl*$^{-/-}$*Mertk*$^{-/-}$ SVZ display elevated expression of activation markers[7]. Despite the unchanged cytokine expression levels at 2 and 4 months from mRNA extracted from whole cortex and hippocampus among the genotypes tested (Fig. 2.3.2-5), we saw an increase in the expression level of Iba1 and the number of amoeboid-shaped microglia specifically in the DG of Axl- and Mer-deficient mice at 2.5 months, which indicates a region-specific hyperactivation state of microglia, an aberrant phenotype absent in the DG of WT and

APP/PS1 mice. This observation was further confirmed and quantified in the P30 SGZ of *Axl*$^{-/-}$*Mertk*$^{-/-}$ mice, where microglia expressed elevated levels of the lysosomal activation marker CD68 (**Fig. 2.3.2-6**). CD68 elevation was restricted specifically to the *Axl*$^{-/-}$*Mertk*$^{-/-}$ SGZ and DG, and no elevation was detected in *APP/PS1* mice relative to WT (Fig. 2.3.2f). At P30, the *Axl*$^{-/-}$*Mertk*$^{-/-}$ SGZ and DG also displayed accumulation of cleaved caspase 3-positive (cCasp3^{+}) ACs relative to WT, and *APP/PS1Axl*$^{-/-}$*Mertk*$^{-/-}$ mice displayed markedly higher levels of these ACs than either *APP/PS1* or *Axl*$^{-/-}$*Mertk*$^{-/-}$ mice alone (Fig. 2.3.2-6). In an independent set of collaborative studies, we have also measured decreased microglial phagocytic indices and elevated numbers of ACs in the *Mertk*$^{-/-}$, *Axl*$^{-/-}$*Mertk*$^{-/-}$ and tamoxifen-injected *Mertk*$^{f/f}$*Cx3cr1*^{CreER} dentate gyrus (relative to WT) using histochemical criteria[56], together with elevated numbers of newborn cells detected 24 hours after a systemic pulse of bromodeoxyuridine (BrdU)[56]. Enhanced lethality, again due entirely to epileptic seizures, has also been seen when the *APP/PS1* line is crossed with knock-outs for interleukin-18 (IL-18)[42], and perturbations in both hippocampal physiology and adult neurogenesis in the SGZ and dentate gyrus similar to those that we have detected in *Axl*$^{-/-}$*Mertk*$^{-/-}$ mice have also been reported for *IL18*$^{-/-}$ mice[57].

Soluble Aβ oligomers are known to be toxic for neurons[58,59], to some extent more than plaques, leading to excitotoxicity of neurons on a cellular level and contributing to aberrant neuronal activity on circuitry and network level [45,60]. We also asked whether *APP/PS1Axl*$^{-/-}$ *Mertk*$^{-/-}$ compared to *APP/PS1* mice have higher levels of soluble Aβ42, the most neurotoxic form of Aβ and the main component of neuritic plaques later on in disease, that might predispose the former with a more severe E/I imbalance in dentate circuitry. We prepared soluble fractions of cortical and hippocampal lysates from *APP/PS1* and *APP/PS1Axl*$^{-/-}$*Mertk*$^{-/-}$ mice by ultracentrifugation and measured the level of Aβ42 at 4 months with ELISA. There

was no significant difference in soluble Aβ42 levels in either cortex or hippocampus between the two genotypes. This suggests early production and clearance of soluble Aβ42 in these brain regions are likely not dependent upon TAM-mediated responses (**Fig. 2.3.2-7**). These results suggest no additional accumulation or lack of clearance of Aβ42 in soluble forms in TAM-deficient *APP/PS1* mice, and is therefore unlikely to serve as a cause of the worsened viability prior to plaque deposition seen in these mice.

Taken together, the above observations suggest that the inflammatory environment, AC accumulation, and aberrant newborn cells that continuously appear in the dentate gyrus of the *Axl*$^{-/-}$*Mertk*$^{-/-}$ mice may promote an excitation-inhibition imbalance, already perturbed in *APP/PS1* mice[41], which results in hippocampal detonation of the lethal seizures that occur in pre-plaque *APP/PS1Axl*$^{-/-}$*Mertk*$^{-/-}$ individuals.

2.3.3 TAM activity in AD brains during disease

Microglial TAM system activity at plaques

Is the up-regulation of TAM components of significance to microglial interaction with plaques? To address this question, we used live two-photon imaging to examine the role of TAM signaling in microglia in aged *APP/PS1* mice, when Axl was up-regulated and plaques were abundant. We analyzed hemizygous *APP/PS1* mice that also carried a single *Cx3cr1*^{GFP} allele[22] to label microglia. These compound mutants were then crossed with WT or *Axl*$^{-/-}$*Mertk*$^{-/-}$ mutant alleles. We labeled Aβ plaques in these mice using prior (overnight) intraperitoneal injection of Methoxy-X04[25] (MX04), a brain-penetrant fluorescent amyloid dye (see Methods). We then live-imaged 4-7 plaque-containing volumes per mouse in multiple mice, in layers 1/2 of somatosensory cortex, for ~90 min for each volume, using modifications of two-photon methods described previously[7,29] (see Methods).

Representative, side-by-side 90-minute time-lapse recordings of these analyses are shown in Supplementary Videos 3 and 4. Detailed quantification of microglial properties and behavior allowed us to establish multiple critical differences in plaque recognition and interaction between WT and *Axl*$^{-/-}$*Mertk*$^{-/-}$ microglia. First, we observed many fewer microglia encapsulating MX04-labeled Aβ plaques in *Cx3cr1*^{GFP}*APP/PS1Axl*$^{-/-}$*Mertk*$^{-/-}$ compared to *Cx3cr1*^{GFP}*APP/PS1* mice (**Fig. 2.3.3-1**a). Most plaques were completely enveloped by multiple, tightly bound, and dynamic microglia in *Cx3cr1*^{GFP}*APP/PS1* mice (Fig. 2.3.3-1a, left), whereas some plaques were entirely unattended by microglia in *Cx3cr1*^{GFP}*APP/PS1Axl*$^{-/-}$*Mertk*$^{-/-}$ mice (Fig. 2.3.3-1a, right). Surface building reconstruction and quantification of imaging volumes (Fig. 2.3.3-1b) yielded a flat distribution of microglia cell body distances from plaques in *Cx3cr1*^{GFP}*APP/PS1Axl*$^{-/-}$*Mertk*$^{-/-}$ mice, but showed a very pronounced bias for microglia to be in contact with (positioned 0-2μm from) plaques in *Cx3cr1*^{GFP}*APP/PS1* mice

(Fig. 2.3.3-1c). This distribution difference was independent of the size of the Aβ plaque, although in *Cx3cr1^{GFP}APP/PS1* mice, larger plaques were bound by more microglia (Fig. 2.3.3-1c; **Supplementary Fig. 2.3.3-1**a).

Similarly, there were obvious differences in both microglial morphology and motility between *Cx3cr1^{GFP}APP/PS1Axl$^{-/-}$Mertk$^{-/-}$* and *Cx3cr1^{GFP}APP/PS1* brains (Fig. 2.3.3-1a, d-g). *Cx3cr1^{GFP}APP/PS1Axl$^{-/-}$Mertk$^{-/-}$* microglia often displayed a typically ramified 'resting' configuration that was not substantially different from that seen in WT mice, particularly in regions between Aβ plaques (Fig. 2.3.3-1a, right; **Supplementary Video 3**). In marked contrast, microglia in *Cx3cr1^{GFP}APP/PS1* mice displayed a classically activated 'amoeboid' morphology, with larger cell bodies and fewer, shorter processes (Fig. 2.3.3-1a, left; Supplementary Video 3). Quantification revealed that *Cx3cr1^{GFP}APP/PS1Axl$^{-/-}$Mertk$^{-/-}$* PAM elaborated significantly more (Fig. 2.3.3-1d, Supplementary Fig. 2.3.3-1b) and longer (Fig. 2.3.3-1e, Supplementary Fig. 2.3.3-1c) primary processes per plaque and per cell than *Cx3cr1^{GFP}APP/PS1* PAM. At the same time, processes from NPAM – those microglia positioned >20μm from plaques - were strongly oriented toward plaques in the *Cx3cr1^{GFP}APP/PS1* cortex, but showed no orientation bias in the *Cx3cr1^{GFP}APP/PS1Axl$^{-/-}$Mertk$^{-/-}$* cortex (Fig. 2.3.3-1f, Supplementary Fig. 2.3.3-1d). In addition, microglial process motility – a reduction in which indicates microglial activation - was significantly reduced in *APP/PS1* mice relative to WT, even for microglia whose cell bodies were positioned >20μm from the edge of the nearest plaque (NPAM) (Fig. 2.3.3-1g). In stark contrast, process motility was only modestly lower than WT for *APP/PS1Axl$^{-/-}$Mertk$^{-/-}$* PAM (microglia <5 μm from the nearest plaque) (Fig. 2.3.3-1g), and was not statistically different from WT for *APP/PS1Axl$^{-/-}$Mertk$^{-/-}$* NPAM (Fig. 2.3.3-1g). Finally, microglia normally respond to disease development in both human AD and its mouse models by proliferating in the vicinity of

plaques, such that microglial numbers are elevated relative to normal brains in the plaque-burdened cortex and hippocampus. Mutation of *Trem2* in the context of the 5xFAD mouse AD model has been found to blunt this microgliosis ~2-fold[61,62], and we measured a similar loss in the number GFP$^+$ microglia, primarily those in close proximity to (0-10 μm from) plaques, in the cortex of *Cx3cr1^{GFP}APP/PS1Axl$^{-/-}$Mertk$^{-/-}$* mice relative to their *Cx3cr1^{GFP}APP/PS1* counterparts (Supplementary Fig. 2.3.3-1e). Thus, by all of the above measures, TAM-deficient microglia were dramatically deficient in their ability to detect, bind, and respond to amyloid plaques.

TAM-dependent phagocytosis and shaping of plaques

We have previously shown that microglia are unusually vigorous phagocytes that exhibit an absolute TAM receptor requirement for the phagocytosis of ACs[7]. In all phagocytic macrophages, the TAM receptors and their ligands become concentrated within a phagocytic cup that extends toward, contacts, and then surrounds the phagocytic target[5]. Since TAM-mediated phagocytosis of ACs is also entirely dependent on PtdSer externalization on the AC surface[3,37,63], and since we find that all Aβ plaques are decorated with both externalized PtdSer (Fig. 2.3.1-10) and Gas6 (Fig. 2.3.1-8), we used two-photon imaging to measure phagocytic engulfment of MX04-labeled amyloid plaque material into GFP$^+$ microglia that were either WT or *Axl$^{-/-}$Mertk$^{-/-}$*. We used volumetric reconstructions to quantify internalized MX04 signal both per normalized volume and per GFP volume (see Methods). These measurements revealed a striking deficit: we quantified ~10-fold lower levels of phagocytically engulfed MX04-labelled plaque material inside of *Axl$^{-/-}$Mertk$^{-/-}$* as compared to WT microglia by both measures (**Fig. 2.3.3-2**a, b). [Note that nearly 10% of GFP$^+$ WT microglial volume is occupied by MX04-labeled amyloid material (Fig. 2.3.3-2b).] These data

indicate that microglia cannot effectively phagocytose amyloid material without TAM receptors.

One consistent pathological feature of amyloid plaques, both dense-core neuritic and amorphous diffuse plaques, in both AD and its mouse models, is the presence of a surrounding halo of damaged, dystrophic neuronal membranes[64]. This membrane halo, which is thought to be shaped by microglial engagement with plaques and microglial phagocytic activity[33], is marked by the expression of several marker proteins, including the autophagic and endo-lysosomal vesicular marker LAMP1[65] (representative examples in Fig. 2.3.3-2c). As documented above (Fig. 2.3.1-10), the dystrophic membranes associated with plaques also display the externalized PtdSer required for TAM-mediated phagocytosis[3], and TAM-deficient microglia are compromised in their association with plaques (Fig. 2.3.3-1c). When we measured the area ratio of $LAMP1^+$ membranes to $6E10^+$ plaques, both dense-core and diffuse, over many plaques in multiple mice (**Supplementary Fig. 2.3.3-2**), we quantified a 10-fold increase in the area of the $LAMP1^+$ halo surrounding plaques, measured relative to the area of associated $6E10^+$ plaques, in *APP/PS1Axl*$^{-/-}$*Mertk*$^{-/-}$ versus *APP/PS1* mice at 12 months (Fig. 2.3.3-2d). This difference was primarily driven by a large expansion of LAMP1 expression surrounding weakly-staining, diffuse plaques (arrowheads in Fig. 2.3.3-2c), but was also seen for dense-core plaques (**Supplementary Fig. 2.3.3-3**a, b). A second protein that also displays a similar although more circumscribed distribution in dystrophic membranes surrounding plaques is the endoplasmic reticulum protein reticulon-3 (RTN3)[66]. When we performed a similar area ratio analysis for RTN3 expression surrounding 6E10-labeled plaques, we again measured a large increase in the RTN3/6E10 ratio in *APP/PS1Axl*$^{-/-}$*Mertk*$^{-/-}$ mice (Fig. 2.3.3-2e). As for LAMP1, this difference was primarily driven by a large expansion of RTN3 surrounding weakly-staining, diffuse plaques, but was also seen for

dense-core plaques (Supplementary Fig. 2.3.3-3c,d). Visual inspection of many 6E10$^+$ profiles in multiple mice gave the impression that diffuse, poorly-organized 6E10$^+$ plaques were more commonly seen in *APP/PS1Axl$^{-/-}$Mertk$^{-/-}$* than in *APP/PS1* mice (Supplementary Fig. 2.3.3-2), and quantification in *APP/PS1Mertk$^{-/-}$* and *APP/PS1* mice confirmed this impression (Supplementary Fig. 2.3.3-3e). Finally, and in further keeping with these phagocytic deficits, we always detected a field of uncleared cCasp3$^+$ debris surrounding 6E10$^+$ plaques in aged *APP/PS1Axl$^{-/-}$Mertk$^{-/-}$* mice, but never in *APP/PS1* mice (Supplementary Fig. 2.3.3-3f).

Dense-core plaque burden in the absence of TAM signaling

Microglial phagocytosis has heretofore been thought to constrain the growth of plaques[9]. Thus, a direct prediction from the almost complete inability of *APP/PS1Axl$^{-/-}$Mertk$^{-/-}$* microglia, which are also reduced in number, to recognize and engulf Aβ material is that aged TAM-deficient AD mice should display a much higher plaque burden than their AD counterparts with normal WT microglia. Our initial indication that this was not the case came from the observation that most of the volumes that we recorded in *APP/PS1Axl$^{-/-}$Mertk$^{-/-}$* mice in our two-photon imaging sessions contained *fewer* MX04-labeled plaques than *APP/PS1* volumes with WT microglia (representative examples in **Fig. 2.3.3-3**a). In order to measure plaque burden in these two mouse populations, we used semi-automated quantification of Thioflavin S (Thio S)-stained dense-core plaques in whole-brain sections to assess the effect of Axl and Mer deletion on cortical and hippocampal plaque accumulation, size, and number across disease development (see Methods for sample preparation and data collection). We also used the same methods to quantify dense-core plaques in the cortex and hippocampus of *APP/PS1Axl$^{-/-}$* and *APP/PS1Mertk$^{-/-}$* single compound mutant mice at 12 months. Representative Thio S-stained sagittal sections of *APP/PS1* and *APP/PS1Axl$^{-/-}$Mertk$^{-/-}$* brains,

at 12 months of age, are shown in Fig. 2.3.3-3b. Even prior to quantification, it was clear that *APP/PS1Axl*$^{-/-}$*Mertk*$^{-/-}$ mice displayed many fewer, not many more, plaques than *APP/PS1* mice, and that plaques were distributed over a wider expanse of the *APP/PS1* brain (Fig. 2.3.3-3b).

Quantification revealed that across the entirety of the time period examined, from initial plaque appearance to fulminant plaque deposition, the cortices of *APP/PS1Axl*$^{-/-}$*Mertk*$^{-/-}$ mice indeed displayed fewer Thio S^{+} dense-core plaques than those of *APP/PS1* mice (Fig. 2.3.3-3c). At 12 months of age, *APP/PS1Axl*$^{-/-}$*Mertk*$^{-/-}$ mice showed a 35% reduction in cortical Thio S^{+} plaque density relative to *APP/PS1* mice (Fig. 2.3.3-3d). This reduction was seen across all cross-sectional plaque sizes, but was most pronounced for smaller plaques (**Supplementary Fig. 2.3.3-4**a). A similar reduction was seen in the hippocampus, a second prominent site of plaque deposition in the *APP/PS1* line (Supplementary Fig. 2.3.3-4b). Importantly, these reductions in dense-core plaque density were not due to any change in the production of Aβ peptide, since measurement of soluble Aβ levels in the cortex and hippocampus at both 4 months (Fig. 2.3.2-7) and 12 months (Supplementary Fig. 2.3.3-4c) revealed no difference between *APP/PS1* and *APP/PS1Axl*$^{-/-}$*Mertk*$^{-/-}$ mice. Similarly, no change was apparent between these genotypes in the expression of the APP precursor protein in the cortex (Supplementary Fig. 2.3.3-4d). (Differences in the expression of APP or Aβ cannot occur cell-autonomously as a result of *Axl* and *Mertk* mutation, since these genes are not expressed in the CNS neurons that express the human *APP* transgene in *APP/PS1* mice.) Consistent with these findings of equivalent APP and Aβ levels between *APP/PS1* and *APP/PS1Axl*$^{-/-}$*Mertk*$^{-/-}$ mice, we detected equivalent reductions in a synaptogenesis index – the physically paired expression of the pre-synaptic marker vGlut1 and the post-synaptic

marker PSD95[67,68] – between these genotypes and wild-type mice within the CA1 region of the 15mo hippocampus (Supplementary Fig. 2.3.3-4e).

When we quantified dense-core plaque burden in the cortex and hippocampus of single compound mutants at 12 months, we found that nearly all of the observed effect was due to the action of Mer. *APP/PS1Mertk*$^{-/-}$ mice displayed reductions in dense-core plaque burden in both regions that were comparable to those seen in *APP/PS1Axl*$^{-/-}$*Mertk*$^{-/-}$ mice (Supplementary Fig. 2.3.3-4f), whereas *APP/PS1Axl*$^{-/-}$ mice, while displaying a statistically insignificant trend toward reduced plaque density in the hippocampus, displayed cortical plaque burdens that were equivalent to *APP/PS1* (Supplementary Fig. 2.3.3-4g). These data demonstrate that TAM, primarily Mer, signaling promotes the deposition of dense-core plaques.

Behavioral consequences of TAM deletion

The alteration in Aβ pathology in cortex and hippocampus and exacerbated level of neuritic damage in APP/PS1 *Axl*$^{-/-}$*Mertk*$^{-/-}$ mice led to the question of whether these pathological changes may reflect difference in the mice's cognitive abilities. However, ways to address this question are unfortunately limited and their results complicated. As *Mertk*$^{-/-}$ mice are blind due to photoreceptor degeneration[69], traditional measures relying on the ability of the mice to recognize surroundings in order to evaluate impairment of working memory, such as the Morris Water Maze, cannot be used. Aside from this, whole-body deficiency of Axl and Mer result in mice with a panoply of autoimmune phenotypes, including sickness behavior, that might affect interpretation of behavior data. Having in mind these potential complications, we carefully performed contextual and cued fear conditioning tests[70,71], which do not rely on visual cues or require energy- costly behaviors, on *APP/PS1*, *APP/PS1Axl*$^{-/-}$

Mertk$^{-/-}$ mice and their non-transgenic littermates at 12 months. The *APP/PS1* mouse has been shown to present defects in this model at 7-8 months of age, just after the plaque burden starts to become evident[72].

Mice were subject to three pairs of tone-shock on during fear acquisition trial (day 1) and subject context test in the same context 24 hrs after fear learning (day 2), during which freezing level as an index of mice fear learning and memory retention, respectively, was monitored. To our surprise, *APP/PS1* mice showed a dramatic reduction in their freezing level during and after three pairs of tone-shock, which suggests that the two AD groups have learning or working memory defects in acquiring the association of tone and shock. These results are not unprecedented; in fact, several reports on defects in learning in *APP/PS1* mice in other behavioral paradigms such as the Morris Water Maze[73,74], but few behavioral studies acknowledge learning defects during initial fear acquisition phase in fear conditioning experiment[75]. Statistical tests show that *APP/PS1 Axl*$^{-/-}$*Mertk*$^{-/-}$ mice spent even less time freezing during individual time components compared to *APP/PS1* mice (**Supplementary Fig. 2.3.3-5**), indicating an even more dramatic learning deficits. The immediate average motion during the 2s-electrical shocks, usually in manners of jumps or rapid running, was unchanged among all groups (data not shown), suggesting equal intensity of shocks are delivered and AD mice do not have impaired reflex. A Hargreaves test measuring pain threshold of these groups of mice is being carried out currently to ensure the difference in freezing level is not caused by a lack of pain sensitivity in the AD transgenic mice. Furthermore, our studies showed that *APP/PS1Axl*$^{-/-}$*Mertk*$^{-/-}$ have a trend of less freezing during day 2 context test compared to *APP/PS1* mice, suggesting worsened contextual fear memory in these mice (Fig. 2.3.3-5-c). Auditory cue tests showed no difference in freezing behavior between APP/PS1 *Axl*$^{-/-}$*Mertk*$^{-/-}$ and APP/PS1 (data not shown). Taken together,

these behavioral results are consistent with decreased cortical and hippocampal dense-core ThioS+ plaques and increased neuritic dystrophy phenotype that may reflect a multi-modal neurodegeneration and contribute to worsened learning and memory deficits in *APP/PS1Axl*$^{-/-}$*Mertk*$^{-/-}$ mice comparing to APP/PS1 mice and their non-transgenic littermates.

2.4 Conclusion & Discussion

Taken together, our findings reveal a novel and significant role of microglia TAM receptors, Axl and Mer in all of AD pathogenesis.

At pre-plaque stage, loss of TAMs – especially Mer –dramatically shortens the lifespan of *APP/PS1* mice due to lethal seizures. This decreased viability is unlikely to be due to a buildup or overproduction of neurotoxic soluble Aβ, or a 'cytokine storm' caused by a sudden rise of pro-inflammatory cytokines. Rather, it may be caused by an accumulation of ACs that contribute to a heightened hippocampal E/I imbalance as a secondary insult on top of a soluble Aβ disturbed neurocircuitry. Our results of TAM activity upon plaque deposition and thereafter lead to two principal conclusions. First, the TAM system is required for effective microglial recognition of, response to, and phagocytosis of Aβ plaques. And second, TAM-mediated microglial phagocytosis of Aβ material does not constrain, but rather promotes, the formation of dense-core plaques.

The first of these conclusions is consistent with extensive prior knowledge as to the biochemistry and cell biology of TAM action in microglia and other tissue macrophages[3,5,7]. All Aβ plaques are decorated by membranes that display the externalized phospholipid PtdSer, an essential TAM co-ligand[37] (Fig. 2.3.1-10). This PtdSer is bound by the amino terminal 'Gla' domain of the TAM ligand Gas6[37] (Fig. 2.3.1-8a,b). The C-terminal 'SHBG' domain of this ligand[1,37] then binds to the Axl and Mer that are expressed on the surface of phagocytic microglia (Fig. 2.3.1-1-4). In this arrangement (**Fig. 2.3.4-1**), the TAM ligand serves as a physical 'bridge' between a microglial cell and an Aβ plaque in the same way that TAM ligands bridge a phagocytic macrophage to a PtdSer-expressing apoptotic cell during TAM-dependent engulfment[1,3-5,7,37]. In the absence of Axl and Mer, microglia are

compromised in their attachment to plaques (Fig. 2.3.3-1a-c), do not re-orient their processes toward plaques (Fig. 2.3.3-1f), are blunted in their proliferative response to plaques (Supplementary Fig. 2.3.3-1e), and are not activated by plaques, as assessed by process reduction, retraction, and motility (Fig. 2.3.3-1d, e, g). Most strikingly, *Axl*$^{-/-}$*Mertk*$^{-/-}$ microglia display a 10-fold reduction in their ability to phagocytically engulf Aβ plaque material as measured directly *in vivo* (Fig. 2.3.3-2a, b).

There are some similarities between the phenotypes we describe for *APP/PS1Axl*$^{-/-}$ *Mertk*$^{-/-}$ mice and those seen when *Trem2*$^{-/-}$ mice are crossed into amyloidogenic AD mouse models – either 5xFAD or an alternative *APP/PS1* line[35,61,62,76-78] – but in general the TAM phenotypes are far stronger. The closest similarities are seen with respect to (a) blunted microgliosis of plaque-associated cells, which is reduced ~2-fold in the *Trem2*$^{-/-}$ compound mutants[62,76] (also ~2-fold for *Axl*$^{-/-}$*Mertk*$^{-/-}$ compound mutants) and (b) a 2-4-fold reduction in the number of microglia that associate with plaques in the *Trem2*$^{-/-}$ compound mutants[61,62,76,77] (~5-fold in the *Axl*$^{-/-}$*Mertk*$^{-/-}$ compound mutants). Loss of Trem2 from the *APP/PS1-21* line results in a ~3.5-fold increase in the volume of the halo of dystrophic LAMP1^{+} membranes surrounding 'filamentous' (diffuse) plaques and a ~1.5-fold increase for compact plaques in late-stage disease[78], whereas these numbers for the *APP/PS1Axl*$^{-/-}$*Mertk*$^{-/-}$ mice are ~8-fold and ~4-fold at a comparable stage of disease. Since dystrophic neurites arise around plaques devoid of microglial coverage[33], the paucity of microglial plaque association seen in *APP/PS1Axl*$^{-/-}$*Mertk*$^{-/-}$ mice (Fig. 2.3.3-1a-c) may unleash significant collateral axonal damage.

There is no consensus among research groups as to the effect of Trem2 deletion on Aβ plaque burden over time in amyloidogenic AD models (reviewed in refs. [35] and [76]), with

different groups reporting either marginal increases or decreases, or no changes, in plaque density (measured with Thio S, 6E10, or amyloid dyes) that vary with the model employed and the age analyzed, and that are not consistently seen between the cortex and hippocampus. In contrast, *APP/PS1Axl*$^{-/-}$*Mertk*$^{-/-}$ mice display a consistent reduction in dense-core plaque density, in both the cortex and the hippocampus, across the full course of disease in *APP/PS1* mice. Most strikingly, *Trem2*$^{-/-}$ microglia exhibit a ~2-fold reduction in their ability to phagocytose MX04-labeled Aβ material[62] and display entirely normal phagocytosis of ACs in *in vitro* assays[61], whereas *Axl*$^{-/-}$*Mertk*$^{-/-}$ microglia exhibit a 10-fold drop in their ability to phagocytose MX04-labeled Aβ material *in vivo* (Fig. 2.3.3-2a,b), and are completely incapable of *any* AC phagocytosis in *in vitro* assays[7]. Together, these results argue that Mer and Axl are the main receptors that microglia use to detect, engage, and engulf amyloid plaques. Indeed, it is possible that some of phenotypes observed in *Trem2*$^{-/-}$ mice are in part TAM-mediated, since single cell RNA seq analyses have suggested that up-regulation of *Axl* mRNA in the 5xFAD model is Trem2-dependent[12].

The second of our principal conclusions is contrary to expectation. How is it possible that a 10-fold reduction in phagocytic capacity (Fig. 2.3.3-2a,b), coupled with a 2-fold reduction in microglial numbers (Supplementary Fig. 2.3.3-1e) and a 5-fold reduction in plaque binding to microglia (Fig. 2.3.3-1c), results in 35% *fewer* dense-core plaques (Fig. 2.3.3-3d)? This remarkable finding should be considered in light of two sets of prior analyses in the 5xFAD mouse model[79-81]. First, using two-photon imaging methods similar to those outlined above, Baik and colleagues found that microglial extrusion and deposition, via exocytosis or microglial cell death, of *previously-phagocytosed* Aβ material was essential for the growth of plaques in the 5xFAD brain[79]. An acidic environment, such as that found in the microglial lysosomes into which engulfed Aβ materially is deposited[82], is known to promote

the formation and compaction of large, densely-packed, protease-resistant Aβ fibrils[79,83,84] (Fig. 2.3.4-1). A second, key observation is provided by recent studies in which microglia were killed by pharmacological inhibition of the CSF1 receptor[80,81], which is constitutively required for microglial survival. These studies demonstrated that plaques never develop in the 5xFAD brain when microglia are killed, except in those limited regions where microglia are spared from death, where there is a 100% spatial correspondence between the presence of surviving microglia and the presence of Aβ plaques[80]. Together with our results, these findings suggest that phagocytic microglia are required for the aggregation, organization, and compaction of dense-core Aβ plaques from loosely-organized Aβ material, and that the TAM receptors Axl and Mer are fundamental components of the molecular machinery through which this is achieved (Fig. 2.3.4-1). They are consistent with the hypothesis that plaque formation may represent a defense mechanism that limits the dissemination of highly toxic, pre-plaque Aβ oligomers throughout the AD brain, and may in part explain why agents that disaggregate plaques but do little to halt the production of Aβ peptides have for the most part failed as AD therapeutics[9,85].

2.5 Acknowledgements

This Chapter is largely adapted from the material as it appears in **Huang, Y.,** Happonen, K.E., Burrola, P.G., O'Connor, C., Hah N., Huang, L., Nimmerjahn, A. & Lemke, G. Microglia use TAM receptors to detect and engulf amyloid beta plaques. *Nature Immunology*, In revision. (2020). The dissertation author was a primary investigator and the first author of this material. The authors would like to thank Joseph Hash for excellent technical assistance; Dr. Marc Mercken (Janssen Pharmaceuticals) for $A\beta_{42}$ antibodies; Dr. Robert Rissman and the Alzheimer's Disease Research Center at UCSD for AD brain sections; Dr. Maxim Shokhirev for advice on bioinformatic analyses; Shijia Liu (Han lab) for technical assistance; Dr. Sarah Parylak (Gage lab), Dr. Isabel Salas and Jillybeth Burgado (Allen lab), for technical assistance and useful discussion; and members of the Lemke laboratory, Molecular Neurobiology Laboratory and Nomis Center for helpful discussions. Supported by grants from the US National Institutes of Health (RF1 AG060748 and R01 AI101400 to G.L., DP2 NS083038, R01 NS108034, and U01 NS103522 to A.N., P30 AG062429 to the UCSD ADRC, and P30 CA014195 and S10-OD023689 to the Salk Institute), the Cure Alzheimer's Fund (to G.L.), and the Leona M. and Harry B. Helmsley Charitable Trust (to the Salk Institute); by Marguerite Vogt and H.A and Mary K. Chapman Charitable Trust graduate and Goeddel Chancellor's graduate fellowships (to Y.H.), and by Anderson, Nomis, and Sweden-America Foundation postdoctoral fellowships (to K.E.H.).

2.6 References

1. Lemke, G. Biology of the TAM receptors. *Cold Spring Harbor Perspectives* **5(11)**, doi: 10.1101/cshperspect.a009076. (2013).

2. Lu, Q. & Lemke, G. Homeostatic regulation of the immune system by receptor tyrosine kinases of the Tyro 3 family. *Science* **293**, 306-311 (2001).

3. Lemke, G. How macrophages deal with death. *Nat Rev Immunol* **19**, 539-549 (2019).

4. Scott, R.S., McMahon, E.J., Pop, S.M., Reap, E.A., Caricchio, R., Cohen, P.L., Earp, H.S. & Matsushima, G.K. Phagocytosis and clearance of apoptotic cells is mediated by MER. *Nature* **411**, 207-211 (2001).

5. Zagórska, A., Través, P.G., Lew, E.D., Dransfield, I. & Lemke, G. Diversification of TAM receptor tyrosine kinase function. *Nat Immunol* **15**, 920-928 (2014).

6. Rothlin, C.V., Ghosh, S., Zuniga, E.I., Oldstone, M.B. & Lemke, G. TAM receptors are pleiotropic inhibitors of the innate immune response. *Cell* **131**, 1124-1136 (2007).

7. Fourgeaud, L., Traves, P.G., Tufail, Y., Leal-Bailey, H., Lew, E.D., Burrola, P.G., Callaway, P., Zagorska, A., Rothlin, C.V., Nimmerjahn, A. & Lemke, G. TAM receptors regulate multiple features of microglial physiology. *Nature* **532**, 240-244 (2016).

8. Labzin, L.I., Heneka, M.T. & Latz, E. Innate Immunity and Neurodegeneration. *Annu Rev Med* **69**, 437-449 (2018).

9. Long, J.M. & Holtzman, D.M. Alzheimer Disease: An Update on Pathobiology and Treatment Strategies. *Cell* **179**, 312-339 (2019).

10. ImmGen, C. Open-source ImmGen: mononuclear phagocytes. *Nat Immunol* **17**, 741 (2016).

11. Lai, C. & Lemke, G. An extended family of protein-tyrosine kinase genes differentially expressed in the vertebrate nervous system. *Neuron* **6**, 691-704 (1991).

12. Keren-Shaul, H., Spinrad, A., Weiner, A., Matcovitch-Natan, O., Dvir-Szternfeld, R., Ulland, T.K., David, E., Baruch, K., Lara-Astaiso, D., Toth, B., Itzkovitz, S., Colonna,

M., Schwartz, M. & Amit, I. A Unique Microglia Type Associated with Restricting Development of Alzheimer's Disease. *Cell* **169**, 1276-1290 e1217 (2017).

13. Yin, Z., Raj, D., Saiepour, N., Van Dam, D., Brouwer, N., Holtman, I.R., Eggen, B.J.L., Moller, T., Tamm, J.A., Abdourahman, A., Hol, E.M., Kamphuis, W., Bayer, T.A., De Deyn, P.P. & Boddeke, E. Immune hyperreactivity of Abeta plaque-associated microglia in Alzheimer's disease. *Neurobiol Aging* **55**, 115-122 (2017).

14. Roy, E.R., Wang, B., Wan, Y.W., Chiu, G., Cole, A., Yin, Z., Propson, N.E., Xu, Y., Jankowsky, J.L., Liu, Z., Lee, V.M., Trojanowski, J.Q., Ginsberg, S.D., Butovsky, O., Zheng, H. & Cao, W. Type I interferon response drives neuroinflammation and synapse loss in Alzheimer disease. *J Clin Invest* (2020).

15. Fardo, D.W., Katsumata, Y., Kauwe, J.S., Deming, Y., Harari, O., Cruchaga, C., Alzheimer's Disease Neuroimaging, I. & Nelson, P.T. CSF protein changes associated with hippocampal sclerosis risk gene variants highlight impact of GRN/PGRN. *Exp Gerontol* **90**, 83-89 (2017).

16. Mattsson, N., Insel, P., Nosheny, R., Zetterberg, H., Trojanowski, J.Q., Shaw, L.M., Tosun, D., Weiner, M. & Alzheimer's Disease Neuroimaging, I. CSF protein biomarkers predicting longitudinal reduction of CSF beta-amyloid42 in cognitively healthy elders. *Transl Psychiatry* **3**, e293 (2013).

17. Jankowsky, J.L., Fadale, D.J., Anderson, J., Xu, G.M., Gonzales, V., Jenkins, N.A., Copeland, N.G., Lee, M.K., Younkin, L.H., Wagner, S.L., Younkin, S.G. & Borchelt, D.R. Mutant presenilins specifically elevate the levels of the 42 residue beta-amyloid peptide in vivo: evidence for augmentation of a 42-specific gamma secretase. *Hum Mol Genet* **13**, 159-170 (2004).

18. Jankowsky, J.L., Slunt, H.H., Ratovitski, T., Jenkins, N.A., Copeland, N.G. & Borchelt, D.R. Co-expression of multiple transgenes in mouse CNS: a comparison of strategies. *Biomol Eng* **17**, 157-165 (2001).

19. Hutter-Paier, B., Huttunen, H.J., Puglielli, L., Eckman, C.B., Kim, D.Y., Hofmeister, A., Moir, R.D., Domnitz, S.B., Frosch, M.P., Windisch, M. & Kovacs, D.M. The ACAT inhibitor CP-113,818 markedly reduces amyloid pathology in a mouse model of Alzheimer's disease. *Neuron* **44**, 227-238 (2004).

20. Rockenstein, E., Mallory, M., Mante, M., Sisk, A. & Masliaha, E. Early formation of mature amyloid-beta protein deposits in a mutant APP transgenic model depends on levels of Abeta(1-42). *J Neurosci Res* **66**, 573-582 (2001).

21. Lu, Q., Gore, M., Zhang, Q., Camenisch, T., Boast, S., Casagranda, F., Lai, C., Skinner, M.K., Klein, R., Matsushima, G.K., Earp, H.S., Goff, S.P. & Lemke, G. Tyro-3 family receptors are essential regulators of mammalian spermatogenesis. *Nature* **398**, 723-728 (1999).

22. Jung, S., Aliberti, J., Graemmel, P., Sunshine, M.J., Kreutzberg, G.W., Sher, A. & Littman, D.R. Analysis of fractalkine receptor CX(3)CR1 function by targeted deletion and green fluorescent protein reporter gene insertion. *Mol Cell Biol* **20**, 4106-4114 (2000).

23. Imbimbo, B.P., Hutter-Paier, B., Villetti, G., Facchinetti, F., Cenacchi, V., Volta, R., Lanzillotta, A., Pizzi, M. & Windisch, M. CHF5074, a novel gamma-secretase modulator, attenuates brain beta-amyloid pathology and learning deficit in a mouse model of Alzheimer's disease. *Br J Pharmacol* **156**, 982-993 (2009).

24. Kim, Y.E., Chen, J., Langen, R. & Chan, J.R. Monitoring apoptosis and neuronal degeneration by real-time detection of phosphatidylserine externalization using a polarity-sensitive indicator of viability and apoptosis. *Nat Protoc* **5**, 1396-1405 (2010).

25. Klunk, W.E., Bacskai, B.J., Mathis, C.A., Kajdasz, S.T., McLellan, M.E., Frosch, M.P., Debnath, M.L., Holt, D.P., Wang, Y. & Hyman, B.T. Imaging Abeta plaques in living transgenic mice with multiphoton microscopy and methoxy-X04, a systemically administered Congo red derivative. *J Neuropathol Exp Neurol* **61**, 797-805 (2002).

26. Ly, P.T., Cai, F. & Song, W. Detection of neuritic plaques in Alzheimer's disease mouse model. *J Vis Exp* (2011).

27. Schmidt, S.D., Mazzella, M.J., Nixon, R.A. & Mathews, P.M. Abeta measurement by enzyme-linked immunosorbent assay. *Methods Mol Biol* **849**, 507-527 (2012).

28. Tufail, Y., Cook, D., Fourgeaud, L., Powers, C.J., Merten, K., Clark, C.L., Hoffman, E., Ngo, A., Sekiguchi, K.J., O'Shea, C.C., Lemke, G. & Nimmerjahn, A. Phosphatidylserine Exposure Controls Viral Innate Immune Responses by Microglia. *Neuron* **93**, 574-586 e578 (2017).

29. Nimmerjahn, A., Kirchhoff, F. & Helmchen, F. Resting microglial cells are highly dynamic surveillants of brain parenchyma in vivo. *Science* **308**, 1314-1318 (2005).

30. Shoji, H., Takao, K., Hattori, S. & Miyakawa, T. Contextual and cued fear conditioning test using a video analyzing system in mice. *J Vis Exp* (2014).

31. Koenigsknecht-Talboo, J., Meyer-Luehmann, M., Parsadanian, M., Garcia-Alloza, M., Finn, M.B., Hyman, B.T., Bacskai, B.J. & Holtzman, D.M. Rapid microglial response around amyloid pathology after systemic anti-Abeta antibody administration in PDAPP mice. *J Neurosci* **28**, 14156-14164 (2008).

32. Bolmont, T., Haiss, F., Eicke, D., Radde, R., Mathis, C.A., Klunk, W.E., Kohsaka, S., Jucker, M. & Calhoun, M.E. Dynamics of the microglial/amyloid interaction indicate a role in plaque maintenance. *J Neurosci* **28**, 4283-4292 (2008).

33. Condello, C., Yuan, P., Schain, A. & Grutzendler, J. Microglia constitute a barrier that prevents neurotoxic protofibrillar Abeta42 hotspots around plaques. *Nature communications* **6**, 6176 (2015).

34. Bernier, L.P., Bohlen, C.J., York, E.M., Choi, H.B., Kamyabi, A., Dissing-Olesen, L., Hefendehl, J.K., Collins, H.Y., Stevens, B., Barres, B.A. & MacVicar, B.A. Nanoscale Surveillance of the Brain by Microglia via cAMP-Regulated Filopodia. *Cell Rep* **27**, 2895-2908 e2894 (2019).

35. Ulland, T.K. & Colonna, M. TREM2 - a key player in microglial biology and Alzheimer disease. *Nat Rev Neurol* **14**, 667-675 (2018).

36. Bennett, M.L., Bennett, F.C., Liddelow, S.A., Ajami, B., Zamanian, J.L., Fernhoff, N.B., Mulinyawe, S.B., Bohlen, C.J., Adil, A., Tucker, A., Weissman, I.L., Chang, E.F., Li, G., Grant, G.A., Hayden Gephart, M.G. & Barres, B.A. New tools for studying microglia in the mouse and human CNS. *Proc Natl Acad Sci U S A* **113**, E1738-1746 (2016).

37. Lew, E.D., Oh, J., Burrola, P.G., Lax, I., Zagórska, A., Través, P.G., Schlessinger, J. & Lemke, G. Differential TAM receptor-ligand-phospholipid interactions delimit differential TAM bioactivities. *eLife* **3:e03385**(2014).

38. Butovsky, O., Jedrychowski, M.P., Moore, C.S., Cialic, R., Lanser, A.J., Gabriely, G., Koeglsperger, T., Dake, B., Wu, P.M., Doykan, C.E., Fanek, Z., Liu, L., Chen, Z., Rothstein, J.D., Ransohoff, R.M., Gygi, S.P., Antel, J.P. & Weiner, H.L. Identification of a unique TGF-beta-dependent molecular and functional signature in microglia. *Nat Neurosci* **17**, 131-143 (2014).

39. Kim, D.K., Han, D., Park, J., Choi, H., Park, J.C., Cha, M.Y., Woo, J., Byun, M.S., Lee, D.Y., Kim, Y. & Mook-Jung, I. Deep proteome profiling of the hippocampus in the 5XFAD mouse model reveals biological process alterations and a novel biomarker of Alzheimer's disease. *Exp Mol Med* **51**, 1-17 (2019).

40. Myers, K.V., Amend, S.R. & Pienta, K.J. Targeting Tyro3, Axl and MerTK (TAM receptors): implications for macrophages in the tumor microenvironment. *Mol Cancer* **18**, 94 (2019).

41. Minkeviciene, R., Rheims, S., Dobszay, M.B., Zilberter, M., Hartikainen, J., Fulop, L., Penke, B., Zilberter, Y., Harkany, T., Pitkanen, A. & Tanila, H. Amyloid beta-induced neuronal hyperexcitability triggers progressive epilepsy. *J Neurosci* **29**, 3453-3462 (2009).

42. Tzeng, T.C., Hasegawa, Y., Iguchi, R., Cheung, A., Caffrey, D.R., Thatcher, E.J., Mao, W., Germain, G., Tamburro, N.D., Okabe, S., Heneka, M.T., Latz, E., Futai, K. & Golenbock, D.T. Inflammasome-derived cytokine IL18 suppresses amyloid-induced seizures in Alzheimer-prone mice. *Proc Natl Acad Sci U S A* **115**, 9002-9007 (2018).

43. Scharfman, H.E. Alzheimer's disease and epilepsy: insight from animal models. *Future Neurol* **7**, 177-192 (2012).

44. Palop, J.J., Chin, J., Roberson, E.D., Wang, J., Thwin, M.T., Bien-Ly, N., Yoo, J., Ho, K.O., Yu, G.Q., Kreitzer, A., Finkbeiner, S., Noebels, J.L. & Mucke, L. Aberrant excitatory neuronal activity and compensatory remodeling of inhibitory hippocampal circuits in mouse models of Alzheimer's disease. *Neuron* **55**, 697-711 (2007).

45. Palop, J.J. & Mucke, L. Epilepsy and cognitive impairments in Alzheimer disease. *Arch Neurol* **66**, 435-440 (2009).

46. Powell, G., Ziso, B. & Larner, A.J. The overlap between epilepsy and Alzheimer's disease and the consequences for treatment. *Expert Rev Neurother* **19**, 653-661 (2019).

47. Vossel, K.A., Tartaglia, M.C., Nygaard, H.B., Zeman, A.Z. & Miller, B.L. Epileptic activity in Alzheimer's disease: causes and clinical relevance. *Lancet Neurol* **16**, 311-322 (2017).

48. Zarea, A., Charbonnier, C., Rovelet-Lecrux, A., Nicolas, G., Rousseau, S., Borden, A., Pariente, J., Le Ber, I., Pasquier, F., Formaglio, M., Martinaud, O., Rollin-Sillaire, A., Sarazin, M., Croisile, B., Boutoleau-Bretonniere, C., Ceccaldi, M., Gabelle, A., Chamard, L., Blanc, F., Sellal, F., Paquet, C., Campion, D., Hannequin, D., Wallon, D. & Collaborators, P.G. Seizures in dominantly inherited Alzheimer disease. *Neurology* **87**, 912-919 (2016).

49. Hauser, W.A., Morris, M.L., Heston, L.L. & Anderson, V.E. Seizures and myoclonus in patients with Alzheimer's disease. *Neurology* **36**, 1226-1230 (1986).

50. Mendez, M.F., Catanzaro, P., Doss, R.C., R, A.R. & Frey, W.H., 2nd. Seizures in Alzheimer's disease: clinicopathologic study. *J Geriatr Psychiatry Neurol* **7**, 230-233 (1994).

51. Hesdorffer, D.C., Hauser, W.A., Annegers, J.F., Kokmen, E. & Rocca, W.A. Dementia and adult-onset unprovoked seizures. *Neurology* **46**, 727-730 (1996).

52. Amatniek, J.C., Hauser, W.A., DelCastillo-Castaneda, C., Jacobs, D.M., Marder, K., Bell, K., Albert, M., Brandt, J. & Stern, Y. Incidence and predictors of seizures in patients with Alzheimer's disease. *Epilepsia* **47**, 867-872 (2006).

53. Lozsadi, D.A. & Larner, A.J. Prevalence and causes of seizures at the time of diagnosis of probable Alzheimer's disease. *Dement Geriatr Cogn Disord* **22**, 121-124 (2006).

54. Plath, N., Ohana, O., Dammermann, B., Errington, M.L., Schmitz, D., Gross, C., Mao, X., Engelsberg, A., Mahlke, C., Welzl, H., Kobalz, U., Stawrakakis, A., Fernandez, E., Waltereit, R., Bick-Sander, A., Therstappen, E., Cooke, S.F., Blanquet, V., Wurst, W., Salmen, B., Bosl, M.R., Lipp, H.P., Grant, S.G., Bliss, T.V., Wolfer, D.P. & Kuhl, D. Arc/Arg3.1 is essential for the consolidation of synaptic plasticity and memories. *Neuron* **52**, 437-444 (2006).

55. Scharfman, H.E. The Dentate Gyrus and Temporal Lobe Epilepsy: An "Exciting" Era. *Epilepsy Curr* **19**, 249-255 (2019).

56. Diaz-Aparicio, I., Paris, I., Sierra-Torre, V., Plaza-Zabala, A., Rodríguez-Iglesias, N., Márquez-Ropero, M., Beccari, S., Abiega, O., Alberdi, E., Matute, C., Bernales, I., Schulz, A., Otrokocsi, L., Sperlagh, B., Happonen, K.E., Lemke, G., Maletic-Savatic, M., Valero, J. & Sierra, A. Microglia actively remodel adult hippocampal neurogenesis through the phagocytosis secretome. *J. Neurosci.*, In press (2019).

57. Yamanishi, K., Doe, N., Mukai, K., Ikubo, K., Hashimoto, T., Uwa, N., Sumida, M., El-Darawish, Y., Gamachi, N., Li, W., Kuwahara-Otani, S., Maeda, S., Watanabe, Y., Hayakawa, T., Yamanishi, H., Matsuyama, T., Yagi, H., Okamura, H. & Matsunaga, H. Interleukin-18-deficient mice develop hippocampal abnormalities related to possible depressive-like behaviors. *Neuroscience* **408**, 147-160 (2019).

58. Ugalde, C.L., Finkelstein, D.I., Lawson, V.A. & Hill, A.F. Pathogenic mechanisms of prion protein, amyloid-beta and alpha-synuclein misfolding: the prion concept and neurotoxicity of protein oligomers. *J Neurochem* (2016).

59. Benilova, I., Karran, E. & De Strooper, B. The toxic Abeta oligomer and Alzheimer's disease: an emperor in need of clothes. *Nat Neurosci* **15**, 349-357 (2012).

60. Palop, J.J., Chin, J. & Mucke, L. A network dysfunction perspective on neurodegenerative diseases. *Nature* **443**, 768-773 (2006).

61. Wang, Y., Cella, M., Mallinson, K., Ulrich, J.D., Young, K.L., Robinette, M.L., Gilfillan, S., Krishnan, G.M., Sudhakar, S., Zinselmeyer, B.H., Holtzman, D.M., Cirrito, J.R. & Colonna, M. TREM2 lipid sensing sustains the microglial response in an Alzheimer's disease model. *Cell* **160**, 1061-1071 (2015).

62. Wang, Y., Ulland, T.K., Ulrich, J.D., Song, W., Tzaferis, J.A., Hole, J.T., Yuan, P., Mahan, T.E., Shi, Y., Gilfillan, S., Cella, M., Grutzendler, J., DeMattos, R.B., Cirrito, J.R., Holtzman, D.M. & Colonna, M. TREM2-mediated early microglial response limits diffusion and toxicity of amyloid plaques. *J Exp Med* **213**, 667-675 (2016).

63. Dransfield, I., Zagorska, A., Lew, E.D., Michail, K. & Lemke, G. Mer receptor tyrosine kinase mediates both tethering and phagocytosis of apoptotic cells. *Cell Death Dis* **6**, e1646 (2015).

64. Nixon, R.A., Wegiel, J., Kumar, A., Yu, W.H., Peterhoff, C., Cataldo, A. & Cuervo, A.M. Extensive involvement of autophagy in Alzheimer disease: an immuno-electron microscopy study. *J Neuropathol Exp Neurol* **64**, 113-122 (2005).

65. Hassiotis, S., Manavis, J., Blumbergs, P.C., Hattersley, K.J., Carosi, J.M., Kamei, M. & Sargeant, T.J. Lysosomal LAMP1 immunoreactivity exists in both diffuse and neuritic amyloid plaques in the human hippocampus. *Eur J Neurosci* **47**, 1043-1053 (2018).

66. Hu, X., Shi, Q., Zhou, X., He, W., Yi, H., Yin, X., Gearing, M., Levey, A. & Yan, R. Transgenic mice overexpressing reticulon 3 develop neuritic abnormalities. *EMBO J* **26**, 2755-2767 (2007).

67. Blanco-Suarez, E., Liu, T.F., Kopelevich, A. & Allen, N.J. Astrocyte-Secreted Chordin-like 1 Drives Synapse Maturation and Limits Plasticity by Increasing Synaptic GluA2 AMPA Receptors. *Neuron* **100**, 1116-1132 e1113 (2018).

68. Hong, S., Beja-Glasser, V.F., Nfonoyim, B.M., Frouin, A., Li, S., Ramakrishnan, S., Merry, K.M., Shi, Q., Rosenthal, A., Barres, B.A., Lemere, C.A., Selkoe, D.J. & Stevens, B. Complement and microglia mediate early synapse loss in Alzheimer mouse models. *Science* **352**, 712-716 (2016).

69. Burstyn-Cohen, T., Lew, E.D., Traves, P.G., Burrola, P.G., Hash, J.C. & Lemke, G. Genetic dissection of TAM receptor-ligand interaction in retinal pigment epithelial cell phagocytosis. *Neuron* **76**, 1123-1132 (2012).

70. Kitamura, T., Pignatelli, M., Suh, J., Kohara, K., Yoshiki, A., Abe, K. & Tonegawa, S. Island cells control temporal association memory. *Science* **343**, 896-901 (2014).

71. Suh, J., Rivest, A.J., Nakashiba, T., Tominaga, T. & Tonegawa, S. Entorhinal cortex layer III input to the hippocampus is crucial for temporal association memory. *Science* **334**, 1415-1420 (2011).

72. Cramer, P.E., Cirrito, J.R., Wesson, D.W., Lee, C.Y., Karlo, J.C., Zinn, A.E., Casali, B.T., Restivo, J.L., Goebel, W.D., James, M.J., Brunden, K.R., Wilson, D.A. & Landreth, G.E. ApoE-directed therapeutics rapidly clear beta-amyloid and reverse deficits in AD mouse models. *Science* **335**, 1503-1506 (2012).

73. Volianskis, A., Kostner, R., Molgaard, M., Hass, S. & Jensen, M.S. Episodic memory deficits are not related to altered glutamatergic synaptic transmission and plasticity in the CA1 hippocampus of the APPswe/PS1deltaE9-deleted transgenic mice model of ss-amyloidosis. *Neurobiol Aging* **31**, 1173-1187 (2010).

74. Lalonde, R., Kim, H.D., Maxwell, J.A. & Fukuchi, K. Exploratory activity and spatial learning in 12-month-old APP(695)SWE/co+PS1/DeltaE9 mice with amyloid plaques. *Neurosci Lett* **390**, 87-92 (2005).

75. Knafo, S., Venero, C., Merino-Serrais, P., Fernaud-Espinosa, I., Gonzalez-Soriano, J., Ferrer, I., Santpere, G. & DeFelipe, J. Morphological alterations to neurons of the amygdala and impaired fear conditioning in a transgenic mouse model of Alzheimer's disease. *J Pathol* **219**, 41-51 (2009).

76. Jay, T.R., Hirsch, A.M., Broihier, M.L., Miller, C.M., Neilson, L.E., Ransohoff, R.M., Lamb, B.T. & Landreth, G.E. Disease Progression-Dependent Effects of TREM2 Deficiency in a Mouse Model of Alzheimer's Disease. *J Neurosci* **37**, 637-647 (2017).

77. Jay, T.R., Miller, C.M., Cheng, P.J., Graham, L.C., Bemiller, S., Broihier, M.L., Xu, G., Margevicius, D., Karlo, J.C., Sousa, G.L., Cotleur, A.C., Butovsky, O., Bekris, L., Staugaitis, S.M., Leverenz, J.B., Pimplikar, S.W., Landreth, G.E., Howell, G.R., Ransohoff, R.M. & Lamb, B.T. TREM2 deficiency eliminates TREM2+ inflammatory macrophages and ameliorates pathology in Alzheimer's disease mouse models. *J Exp Med* **212**, 287-295 (2015).

78. Yuan, P., Condello, C., Keene, C.D., Wang, Y., Bird, T.D., Paul, S.M., Luo, W., Colonna, M., Baddeley, D. & Grutzendler, J. TREM2 Haplodeficiency in Mice and Humans Impairs the Microglia Barrier Function Leading to Decreased Amyloid Compaction and Severe Axonal Dystrophy. *Neuron* **90**, 724-739 (2016).

79. Baik, S.H., Kang, S., Son, S.M. & Mook-Jung, I. Microglia contributes to plaque growth by cell death due to uptake of amyloid beta in the brain of Alzheimer's disease mouse model. *Glia* **64**, 2274-2290 (2016).

80. Spangenberg, E., Severson, P.L., Hohsfield, L.A., Crapser, J., Zhang, J., Burton, E.A., Zhang, Y., Spevak, W., Lin, J., Phan, N.Y., Habets, G., Rymar, A., Tsang, G., Walters, J., Nespi, M., Singh, P., Broome, S., Ibrahim, P., Zhang, C., Bollag, G., West, B.L. & Green, K.N. Sustained microglial depletion with CSF1R inhibitor impairs parenchymal plaque development in an Alzheimer's disease model. *Nat Commun* **10**, 3758 (2019).

81. Sosna, J., Philipp, S., Albay, R., 3rd, Reyes-Ruiz, J.M., Baglietto-Vargas, D., LaFerla, F.M. & Glabe, C.G. Early long-term administration of the CSF1R inhibitor PLX3397 ablates microglia and reduces accumulation of intraneuronal amyloid, neuritic plaque deposition and pre-fibrillar oligomers in 5XFAD mouse model of Alzheimer's disease. *Mol Neurodegener* **13**, 11 (2018).

82. Fu, H., Liu, B., Frost, J.L., Hong, S., Jin, M., Ostaszewski, B., Shankar, G.M., Costantino, I.M., Carroll, M.C., Mayadas, T.N. & Lemere, C.A. Complement component C3 and complement receptor type 3 contribute to the phagocytosis and clearance of fibrillar Abeta by microglia. *Glia* **60**, 993-1003 (2012).

83. Hu, X., Crick, S.L., Bu, G., Frieden, C., Pappu, R.V. & Lee, J.M. Amyloid seeds formed by cellular uptake, concentration, and aggregation of the amyloid-beta peptide. *Proc Natl Acad Sci U S A* **106**, 20324-20329 (2009).

84. Klug, G.M., Losic, D., Subasinghe, S.S., Aguilar, M.I., Martin, L.L. & Small, D.H. Beta-amyloid protein oligomers induced by metal ions and acid pH are distinct from those generated by slow spontaneous ageing at neutral pH. *Eur J Biochem* **270**, 4282-4293 (2003).

85. Panza, F., Lozupone, M., Logroscino, G. & Imbimbo, B.P. A critical appraisal of amyloid-beta-targeting therapies for Alzheimer disease. *Nat Rev Neurol* **15**, 73-88 (2019).

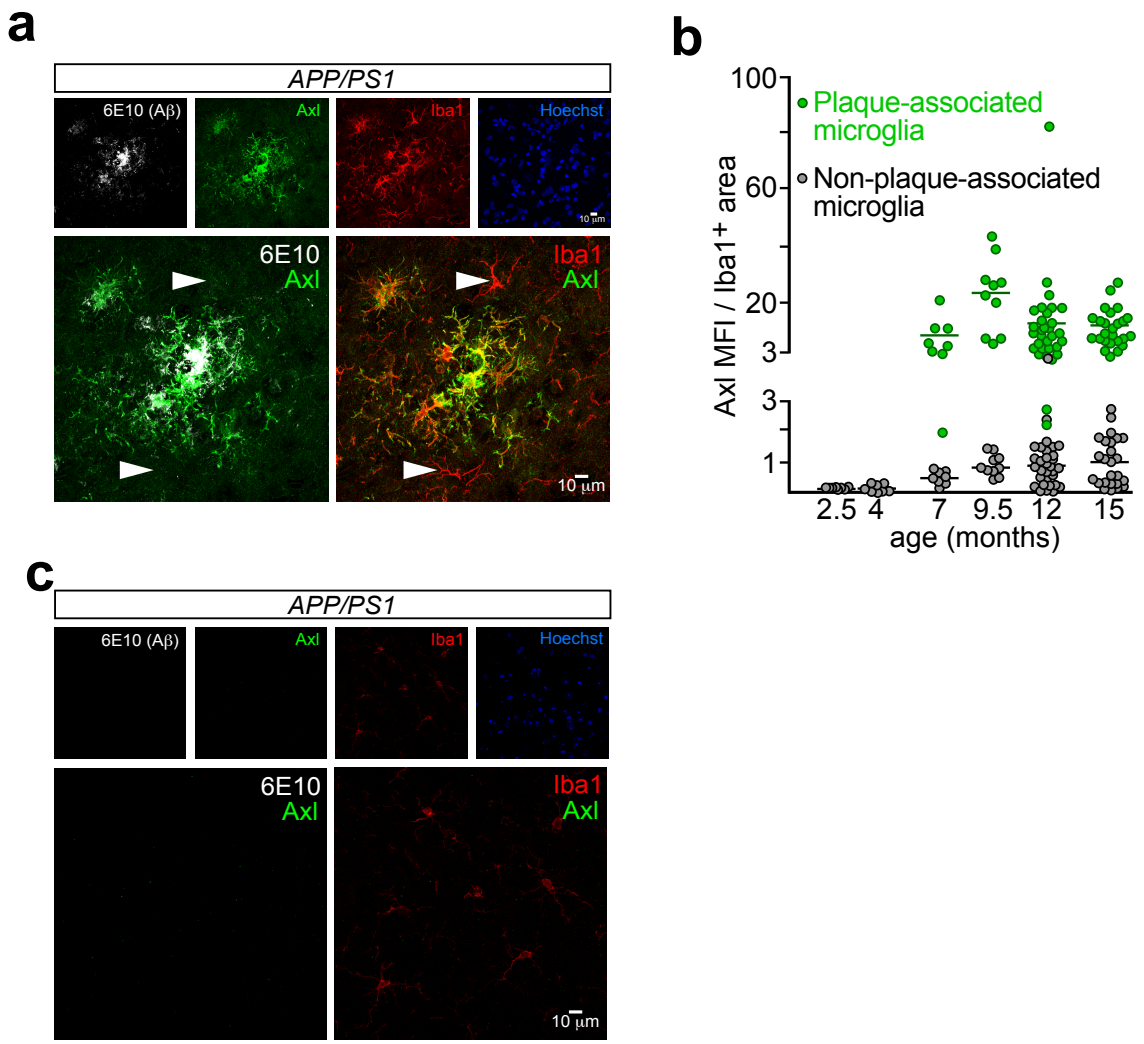

Figure 2.3.1-1. Axl upregulation is strictly plaque-associated.

Axl protein (green) in 9.5 mo *APP/PS1* mice (**a**), but not in 4 mo *APP/PS1* mice (**c**), is up-regulated in microglia (Iba1, red) that are in contact with Aβ plaques (6E10, white), but not in microglia not contacting plaques (arrowheads in lower panels). Iba1 expression is also up-regulated in plaque-associated microglia. Hoechst stains nuclei. (**b**) Quantification of Axl mean fluorescence intensity (MFI) in cortical Iba1$^+$ microglia in *APP/PS1* mice over time reveals Axl up-regulation co-incident with the first deposition of plaques at ~5 mo, only in plaque-associated Iba1$^+$ cells (green points). Lower panels in **a**, **c** are enlargements of upper panels. **a** and **c** contain representative images from N $\geq$ 3 sections per mouse from n $\geq$ 3 mice. Data in **b** were measured from N $\geq$ 3 images per mouse from n $\geq$ 3 mice per timepoint. Scale bars 10μm.

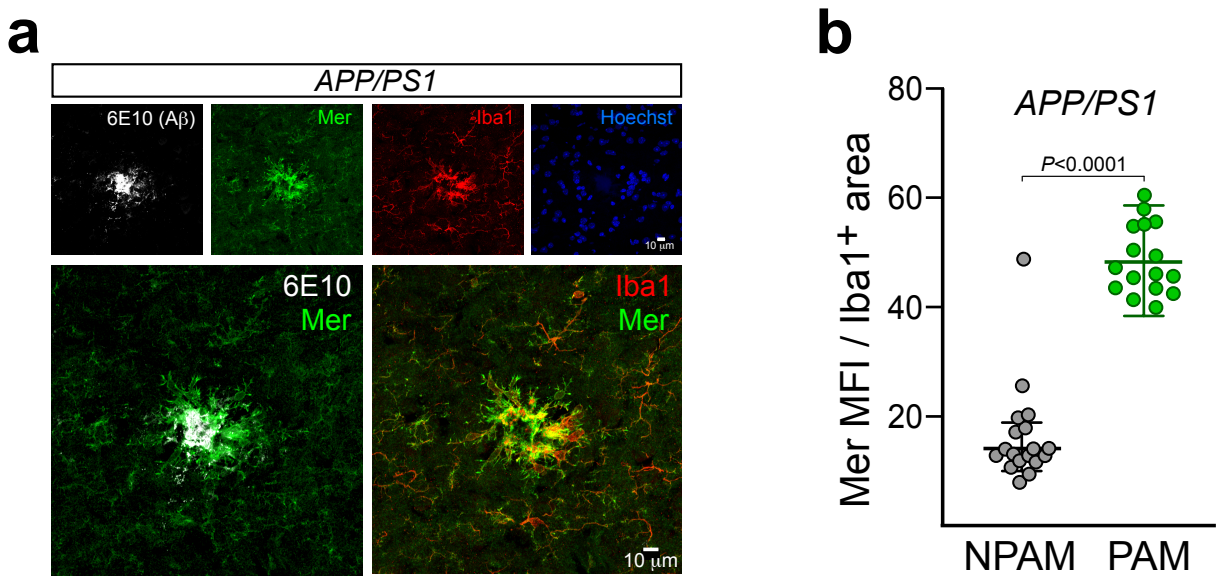

Figure 2.3.1-2 Mer upregulation in plaque-associated microglia

(**a**) Expression of Mer protein (green) in 9.5 mo *APP/PS1* mice is seen in all cortical microglia (Iba1, red), but is further upregulated in microglia that invest Aβ plaques (6E10, white). (**b**) Quantification of Mer protein up-regulation in cortical Iba1^{+} microglia in *APP/PS1* mice at 9.5 months. **a** contain representative images from N $\geq$ 3 sections per mouse from n $\geq$ 3 mice. Data in **b** were measured from N $\geq$ 3 images per mouse from n $\geq$ 3 mice. Scale bar 10μm. P values as shown. Mann-Whitney test.

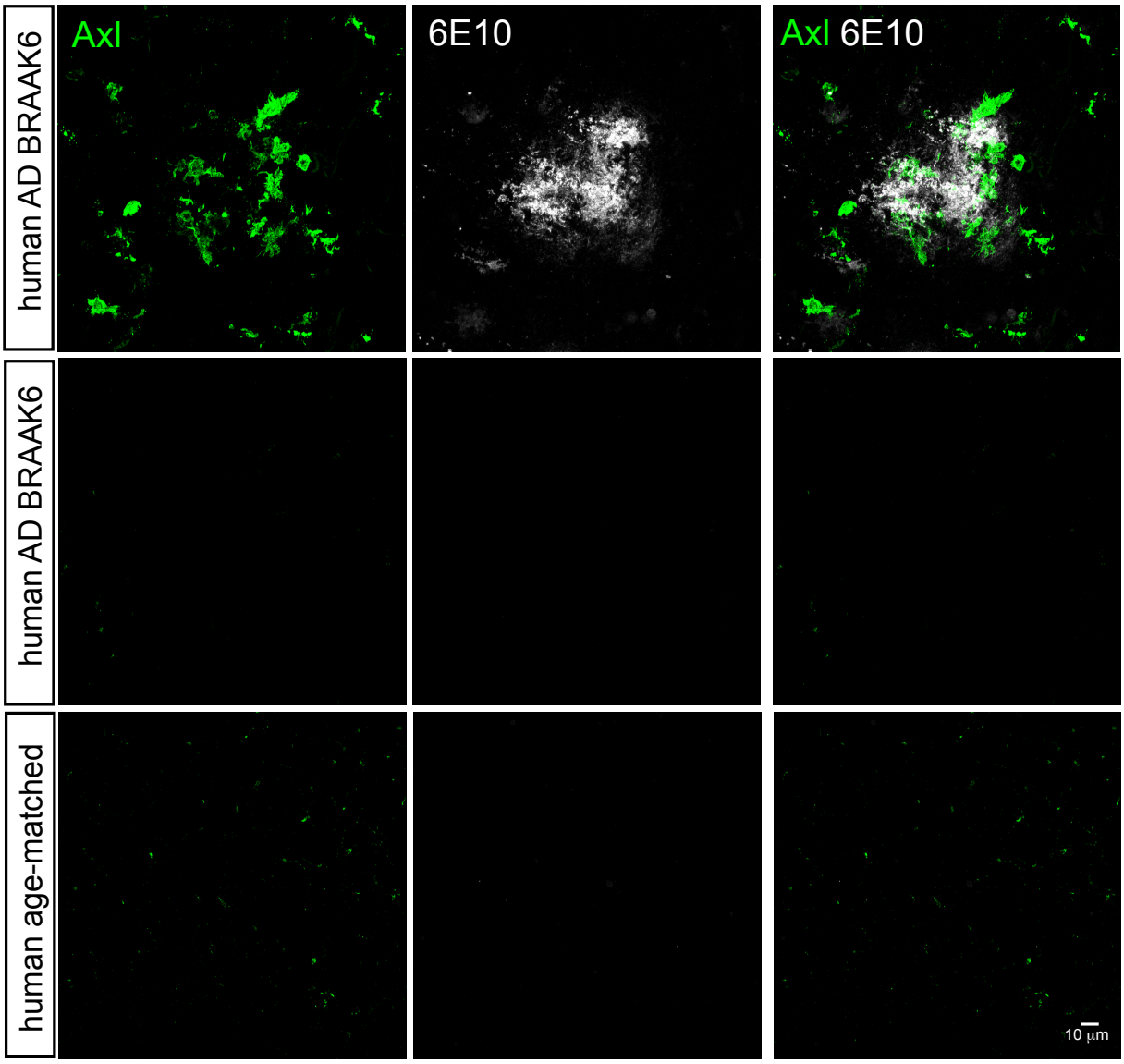

Figure 2.3.1-3 Axl upregulation specifically in plaque-affected area in AD human postmortem brain

Axl protein (green) also is induced highly around $6E10^{+}$ plaques (white) on sections of postmortem cortex from human patients with advance (BRAAK stage 6) AD at plaque-affected areas (top panels), but not at plaque-free areas (middle panels) or in cognitively healthy age-matching controls (bottom panels). Representative images obtained from immunostaining of $\geq$ 3 sections from 3 individuals of each condition. Scale bar 10μm.

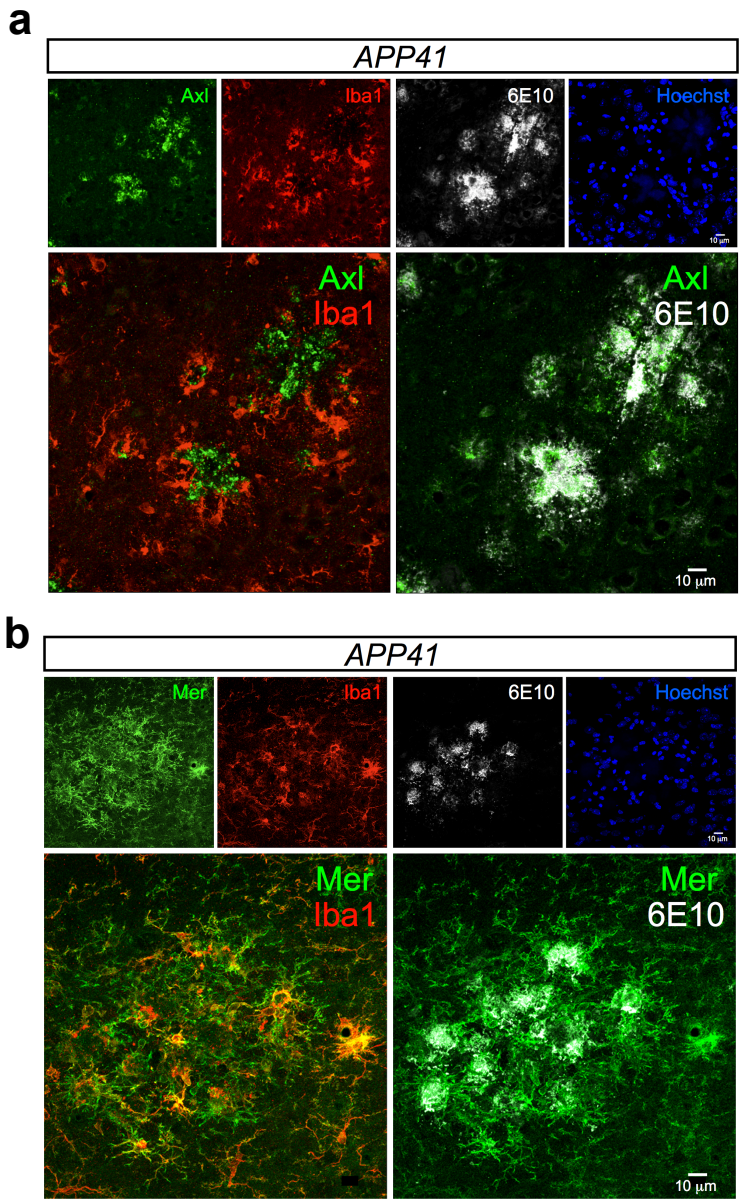

Figure 2.3.1-4 Expression of Axl and Mer in plaque-burdened areas in APP41 mouse model of AD

(**a**) Immunohistochemical analyses demonstrate that Axl protein (green) in 15 mo *APP41* mice is up-regulated in cortical microglia (Iba1, red) that are in contact with Aβ plaques (6E10, white), and is also often concentrated in plaque centers, consistent with strong prior activation of Axl and subsequent cleavage of its ectodomain. (As is seen for other RTKs, robust activation of Axl results in nearly complete cleavage of the ectodomain from the cell surface.) Hoechst 33258 stains nuclei. (**b**) Expression of Mer protein (green) in 15 mo *APP41* mice is seen in all cortical microglia (Iba1, red), but is further up-regulated in microglia that invest Aβ plaques (6E10, white). Representative images obtained from immunostaining of $N \geq 3$ sections from $n \geq 2$ mice of each genotype. Scale bars 10μm.

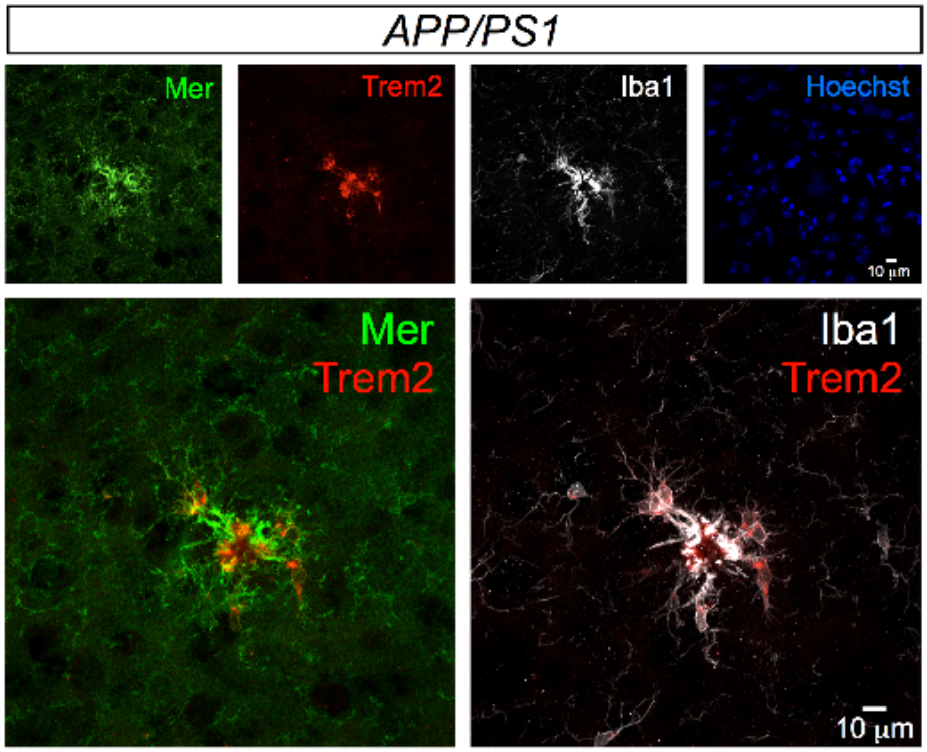

Figure 2.3.1-5 Mer and Trem2 are co-upregulated but not in colocalization in the same ensemble of plaque-associated microglia

The same cortical microglia that up-regulate Mer (green) and Iba1 (white) protein expression in 9.5 mo *APP/PS1* mice also up-regulate expression of Trem2 (red). Lower panels are enlargements of upper panels. Representative images obtained from N $\geq$ 3 sections per mouse from n $\geq$ 3 mice. Scale bar 10μm.

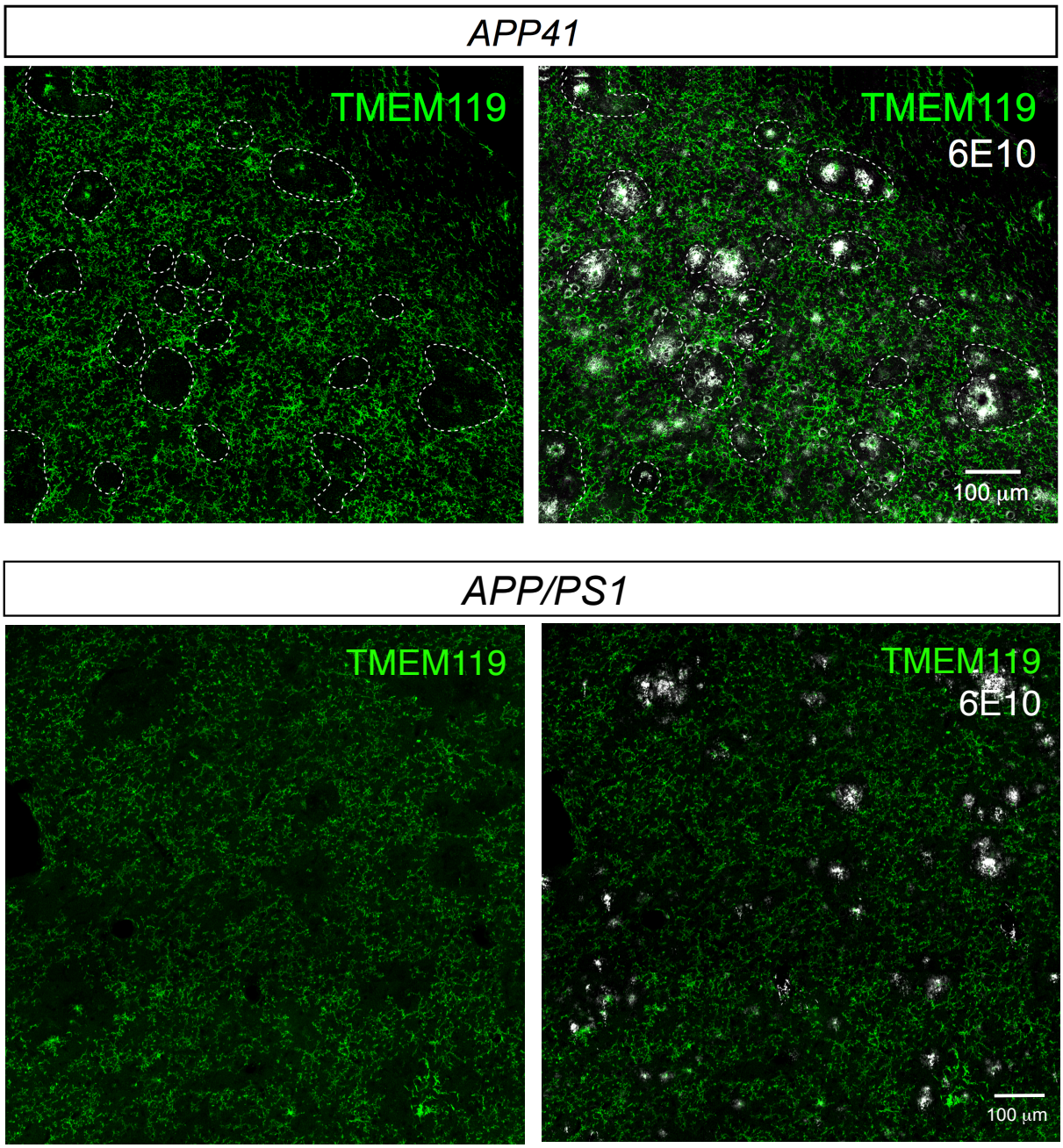

Figure 2.3.1-6 Expression of Tmem119 is downregulated in plaque-affected areas in AD brains

Expression of the homeostatic microglial marker TMEM119 (green) is lost in cortical microglia that surround plaques (6E10, white) in 15 mo *APP41* mice (**a**) and in 15 mo *APP/PS1* (**b**), except for 1-2 cells at the very center of plaques. Representative images obtained from immunostaining of N $\geq$ 3 sections from n $\geq$ 2 mice of each genotype. Scale bars 100μm.

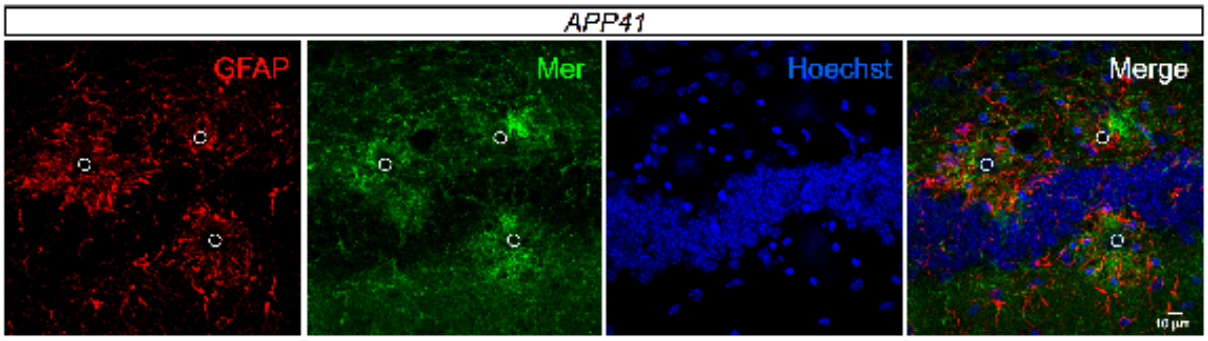

Figure 2.3.1-7 Plaque-induced up-regulation of Mer is not present in reactive astrocytes
The up-regulated Mer expression (green) seen in 15 mo *APP41* mice is not present in $GFAP^+$ reactive astrocytes (red). (Activated $S100b^+$ astrocytes are also negative for Mer expression by IHC depicted in Fourgeaud et al., 2016). Circles mark the position of Aβ plaques. Representative images obtained from immunostaining of $N \geq 3$ sections from $n \geq 2$ mice of each genotype. Scale bar 10μm.

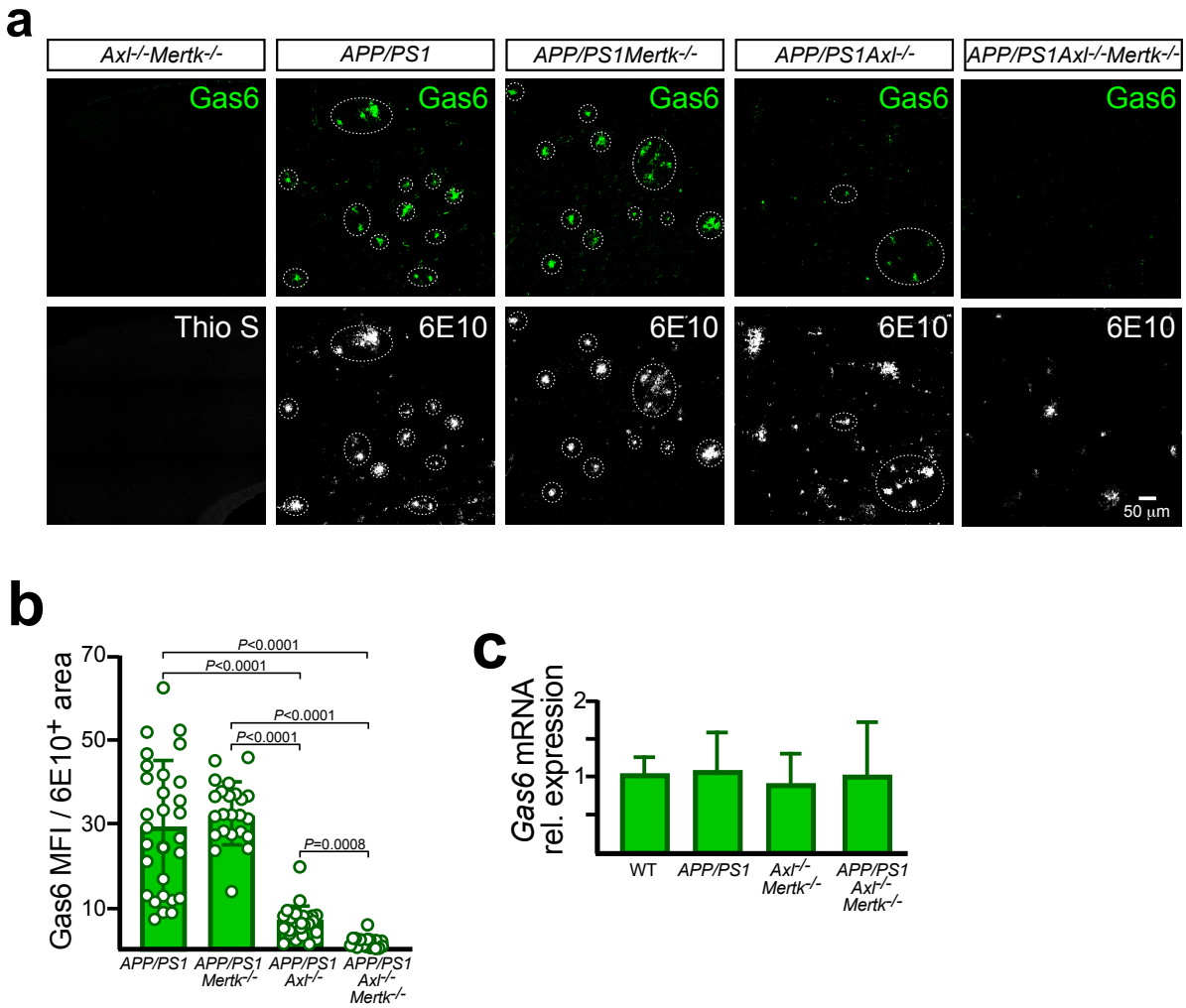

Figure 2.3.1-8 TAM ligand Gas6 decorate all Aβ plaques

(**a**) There is no Gas6 protein (green) and are no plaques (Thio S, white, since 6E10 is human-specific) in the cortex of 12 mo WT (not shown) or *Axl*$^{-/-}$*Mertk*$^{-/-}$ mice (left panels), but abundant Gas6 specifically associated with Aβ plaques (6E10, white) in *APP/PS1* mice (second panels). Plaque-associated Gas6 is unchanged in *APP/PS1Mertk*$^{-/-}$ mice (third panels), severely reduced in *APP/PS1Axl*$^{-/-}$ mice (fourth panels), and eliminated entirely in *APP/PS1Axl*$^{-/-}$*Mertk*$^{-/-}$ mice (fifth panels). Dotted ovals mark Gas6/6E10 coincidence. (**b**) Quantification of results in **a** expressed as Gas6 MFI per 6E10+ area. (**c**) There is no change in the expression of cortical *Gas6* mRNA between the indicated genotypes (n = 6 mice per group). **a** contain representative images from N ≥ 3 sections from n ≥ 3 mice of each genotype, quantified in **b**. Error bars in **b**, **c** and all subsequent panels in the thesis are ±1 standard deviation. P values as shown. One-way ANOVA test.

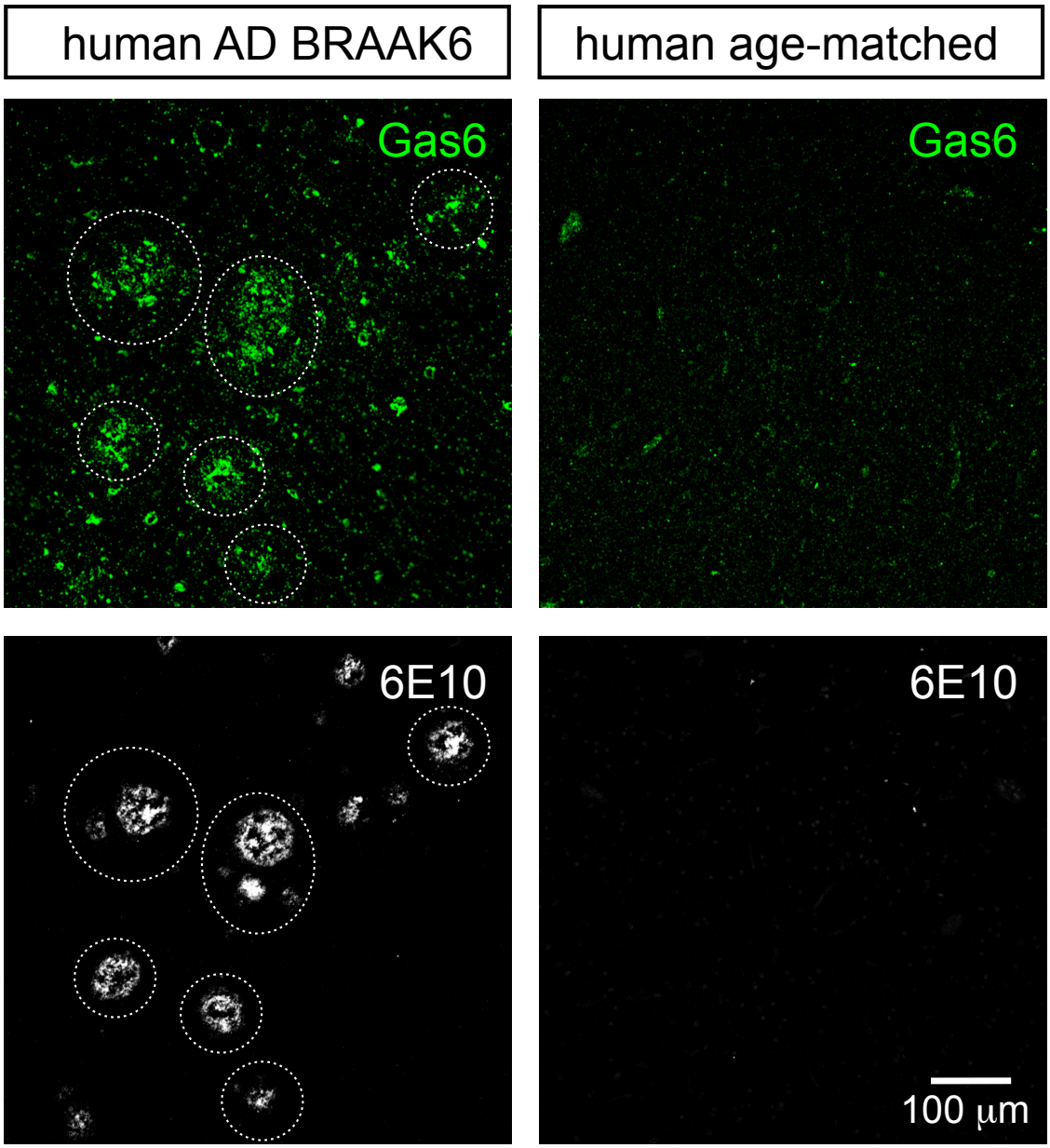

Figure 2.3.1-9 Gas6 decoration of Aβ plaques

Gas6 protein (green) also decorates 6E10^{+} plaques (white) on sections of postmortem cortex from human patients with advanced (BRAAK stage 6) AD (left panels), but is not evident in the plaque-free cortex of cognitively normal age-matched controls (right panels). Representative images obtained from immunostaining of $\geq$3 sections from 3 individuals of each condition. Scale bar 100μm.

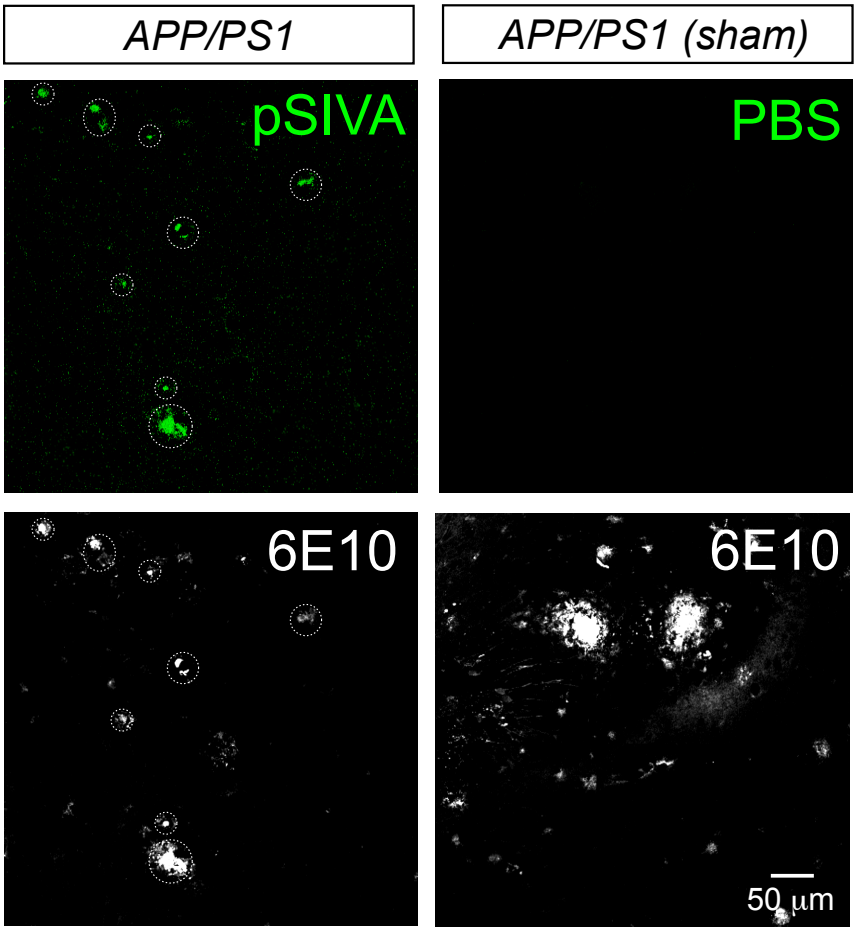

Figure 2.3.1-10 TAM co-ligand phosphatidylserine similarly labels majority of Aβ plaques Externalization of PtdSer (detected with pSIVA, green, upper left panel) in the cortex of 15 mo *APP/PS1* mice is specific to $6E10^{+}$ Aβ plaques (lower left panel). PBS-injected sham control shows no specific plaque-associated fluorescence (right panels). Scale bar 50μm.

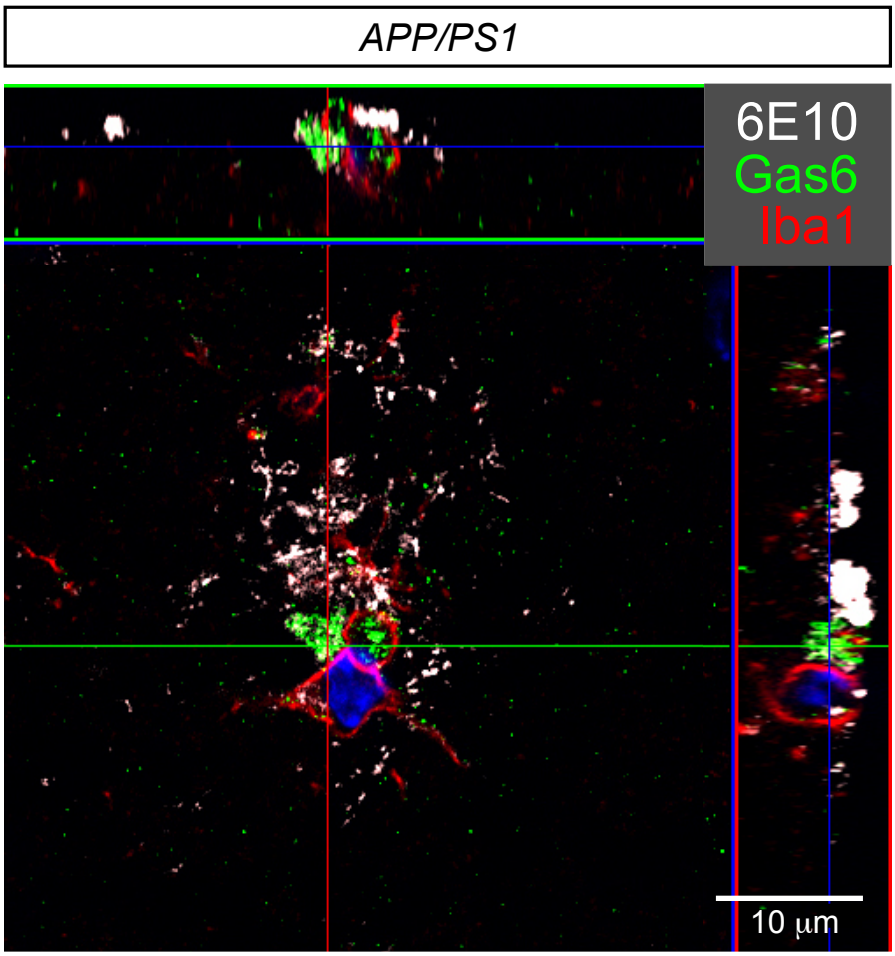

Figure 2.3.1-11 Gas6 bridges plaque-associated microglia and Aβ plaques

Airyscan super-resolution image of the juxtaposition of plaque-associated microglia (Iba1, red), Gas6 (green), and Aβ plaque (6E10, white) in 12 mo *APP/PS1* mice. Representative images obtained from immunostaining of ≥3 sections from 3 *APP/PS1* mice. Scale bar 10μm.

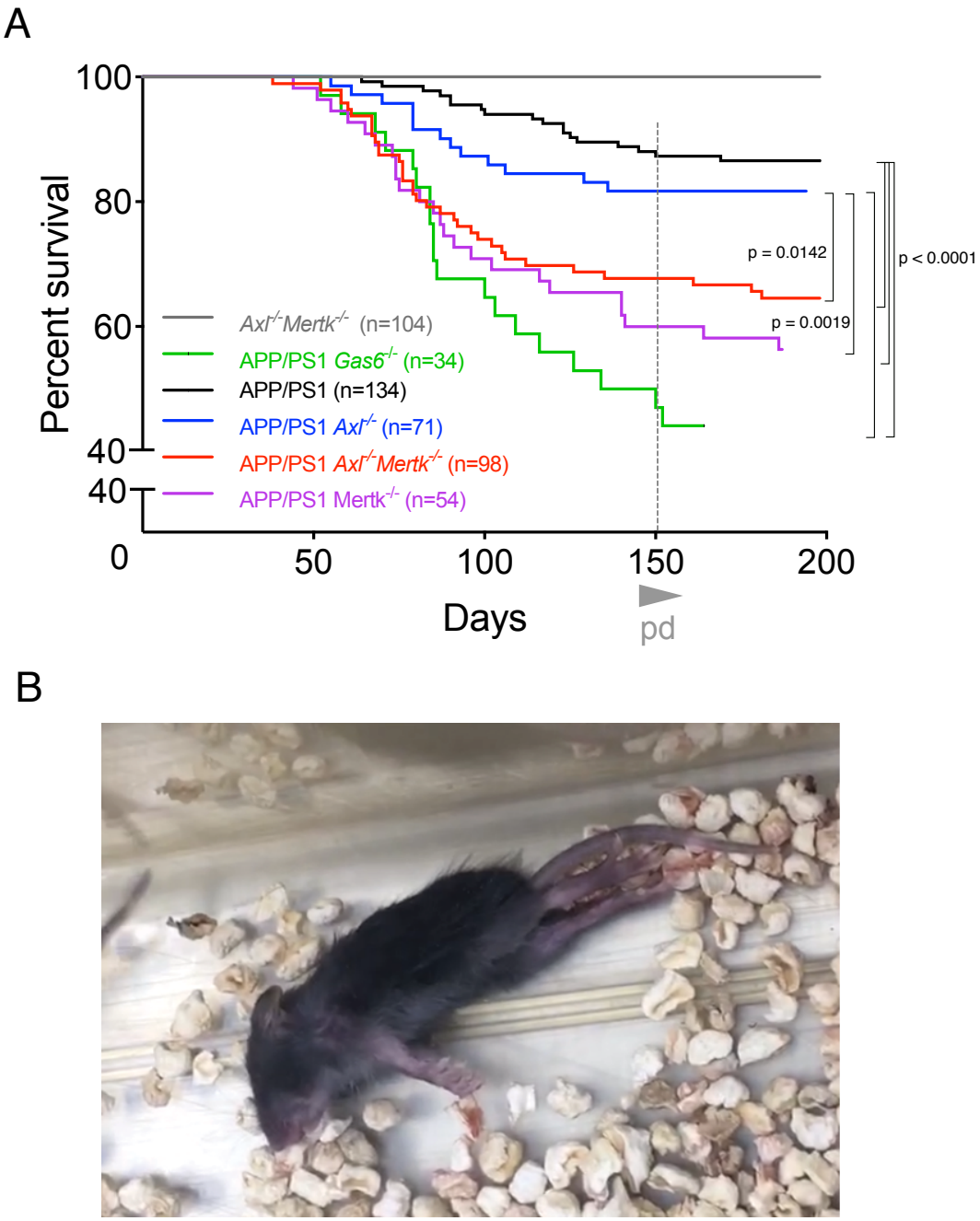

Figure 2.3.2-1 Genetic deletion of Mer and TAM ligand Gas6 exacerbates lethal epileptic seizures

(**a**) Survival curves for the indicated genotypes. The onset of plaque deposition (pd) occurs at ~P150. *P* values calculated by log-rank (Mantel-Cox) test. (The *APP/PS1* versus *APP/PS1Axl*$^{-/-}$ and *APP/PS1Mertk*$^{-/-}$ versus *APP/PS1Axl*$^{-/-}$*Mertk*$^{-/-}$ differences are not significant: *P*=0.3012 and 0.3608, respectively.) n, number of mice per population. (**b**), Young (18 d) *APP/PS1Mertk*$^{-/-}$ mice immediately after death from seizure. Note the distended hindlimbs, which are a typical posture subsequent to this event.

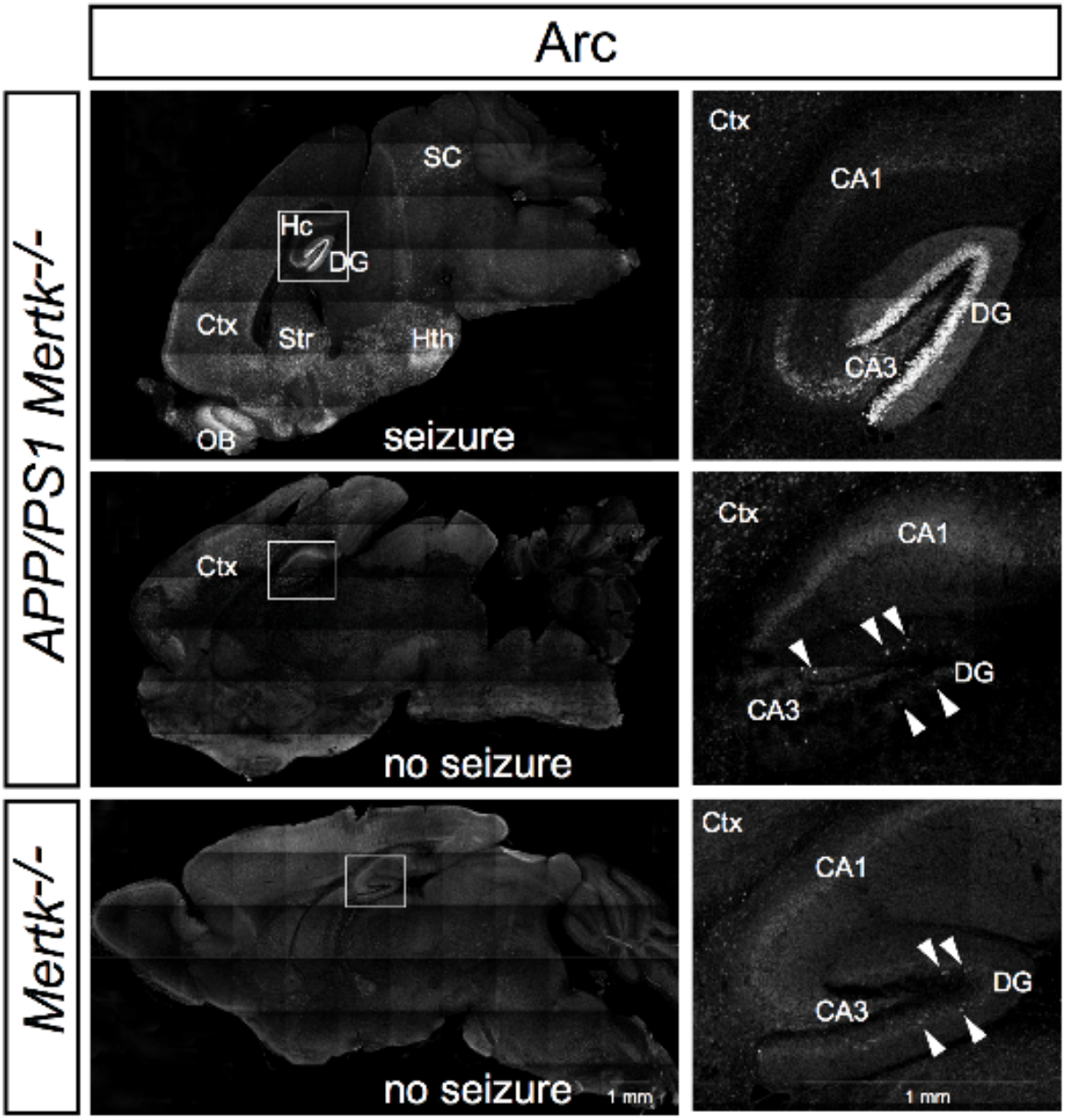

Figure 2.3.2-2 Post-seizure *APP/PS1Mertk*$^{-/-}$ brain present widely distributed Arc expression
Arc expression in the brain (left three panels) and hippocampus (right three panels) of *APP/PS1Mertk*$^{-/-}$ and *Mertk*$^{-/-}$ mice. Top two panels show Arc expression in the olfactory bulb (OB), cortex (Ctx), striatum (Str), hypothalamus (Hth), superior colliculus (SC), and hippocampus (Hc), especially in the DG, of a P18 *APP/PS1Mertk*$^{-/-}$ individual immediately after lethal seizure. An age-matched *APP/PS1Mertk*$^{-/-}$ mouse but without lethal seizure displays occasional Arc^{+} cells in the DG and cortex (middle panels). *Mertk*$^{-/-}$ mice, which never experience lethal seizures, display occasional Arc^{+} cells in the DG (lower panels).

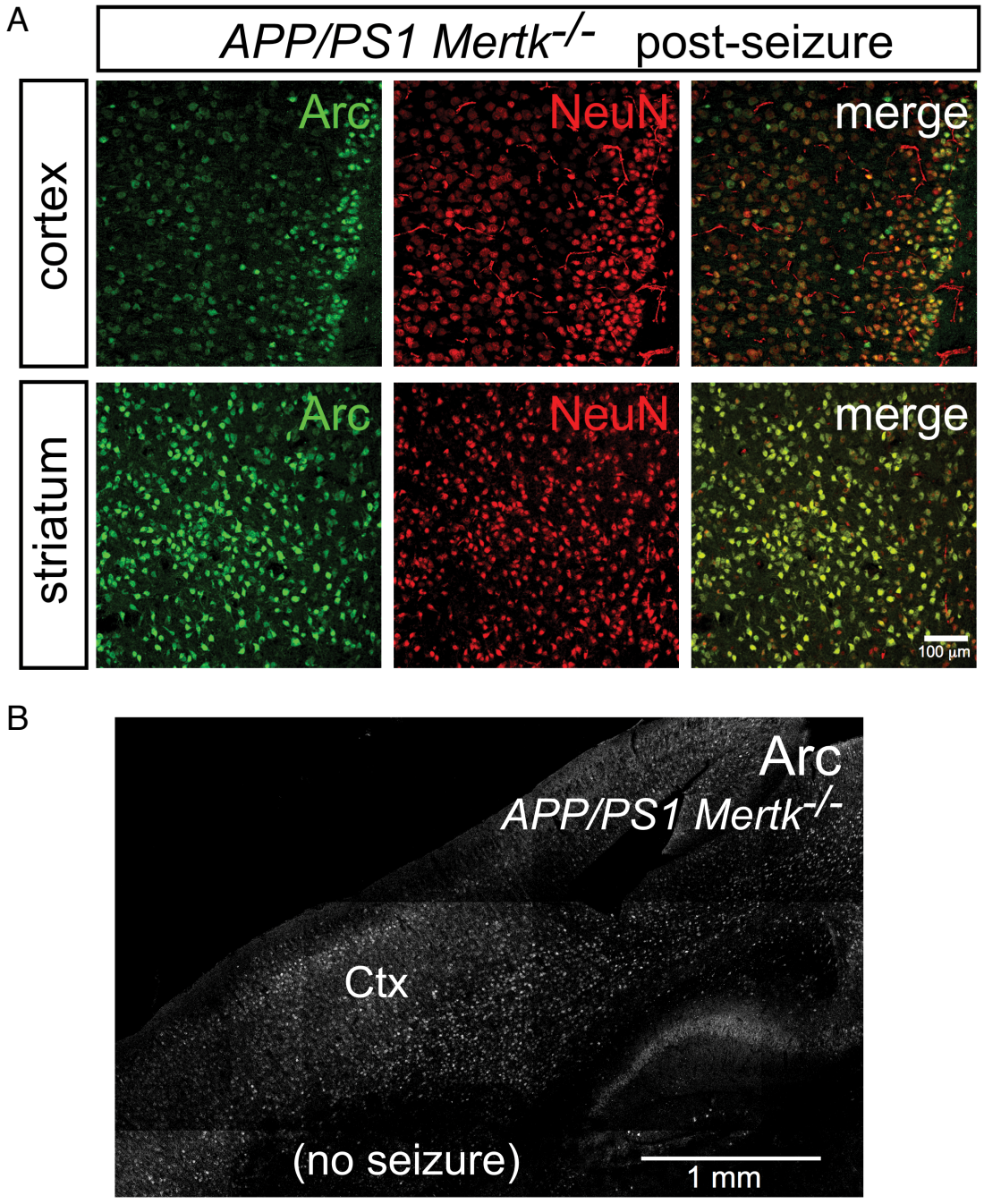

Figure 2.3.2-3 Large-scale Arc expression in young *APP/PS1Mertk*$^{-/-}$ brain

(**a**) Nuclear Arc expression (green, left panels) and expression of the neuronal nuclear marker NeuN (red, middle panels) in the cortex (top panels) and striatum (bottom panels) of the *APP/PS1Mertk*$^{-/-}$ brain shown in **Fig. 2.3.2-2** (top) are co-incident (right panels). (**b**) Arc expression (white) in the cortex in an P18 *APP/PS1Mertk*$^{-/-}$ mouse in the absence of apparent seizure.

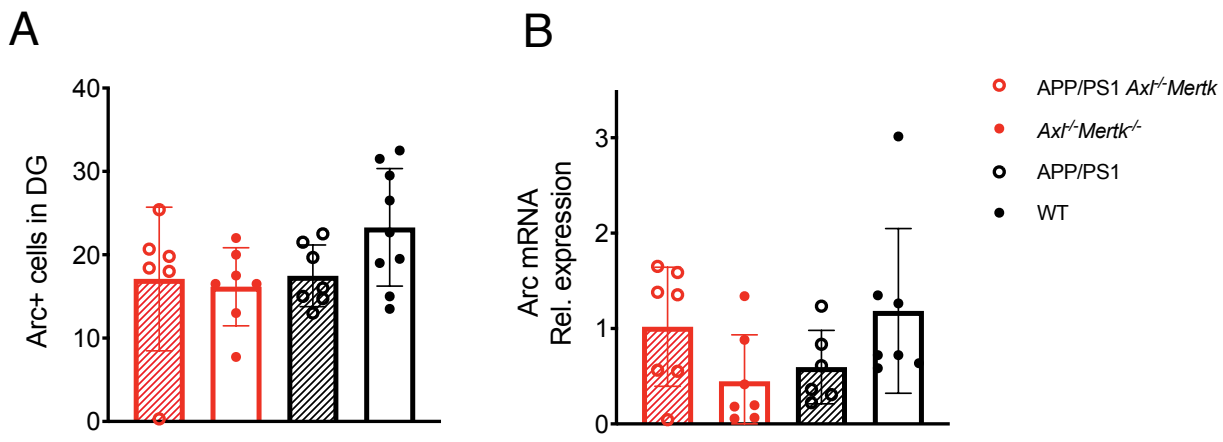

Figure 2.3.1-4 Baseline Arc expression in the hippocampus is unchanged in the absence of overt seizure

(**a**) Arc-expressing cell number is unchanged in DG of regularly perfused WT or *Mertk*$^{-/-}$ APP/PS1 and their healthy littermates without apparent seizures at 2 mo (**b**) No significant difference were detected in Arc mRNA extracted from whole hippocampus among the above-mentioned genotypes (n = 6-8 mice per group). **a** data points represent averaged number of Arc+ cells quantified from N $\geq$3 sections from n= 6-8 mice of each indicated genotype. One-way ANOVA test.

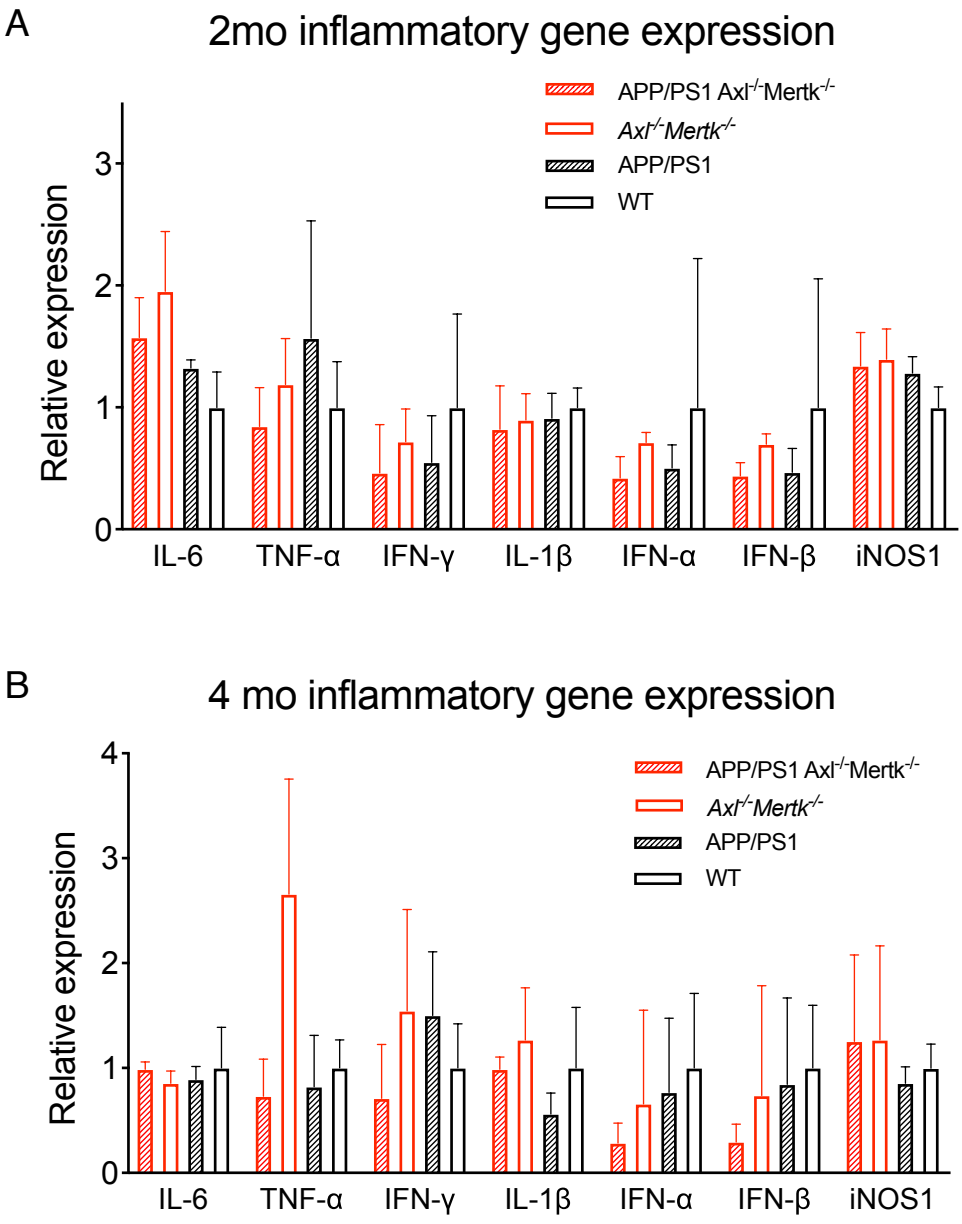

Figure 2.3.2-5 Inflammatory-related gene expression is unchanged in young AD mice

Inflammatory-related gene expression as indicated is unchanged in mRNA extracted from whole cortex of 2 mo (**a**) and 4 mo (**b**) mice with indicated genotypes. Relative expression (y-axis) of each gene was first normalized to housekeeping gene *Gapdh* and then presented in relative to the mean of the WT group for each respective gene. n ≥ 5 per genotype. No significance shown for any gene expression. One-way ANOVA test.

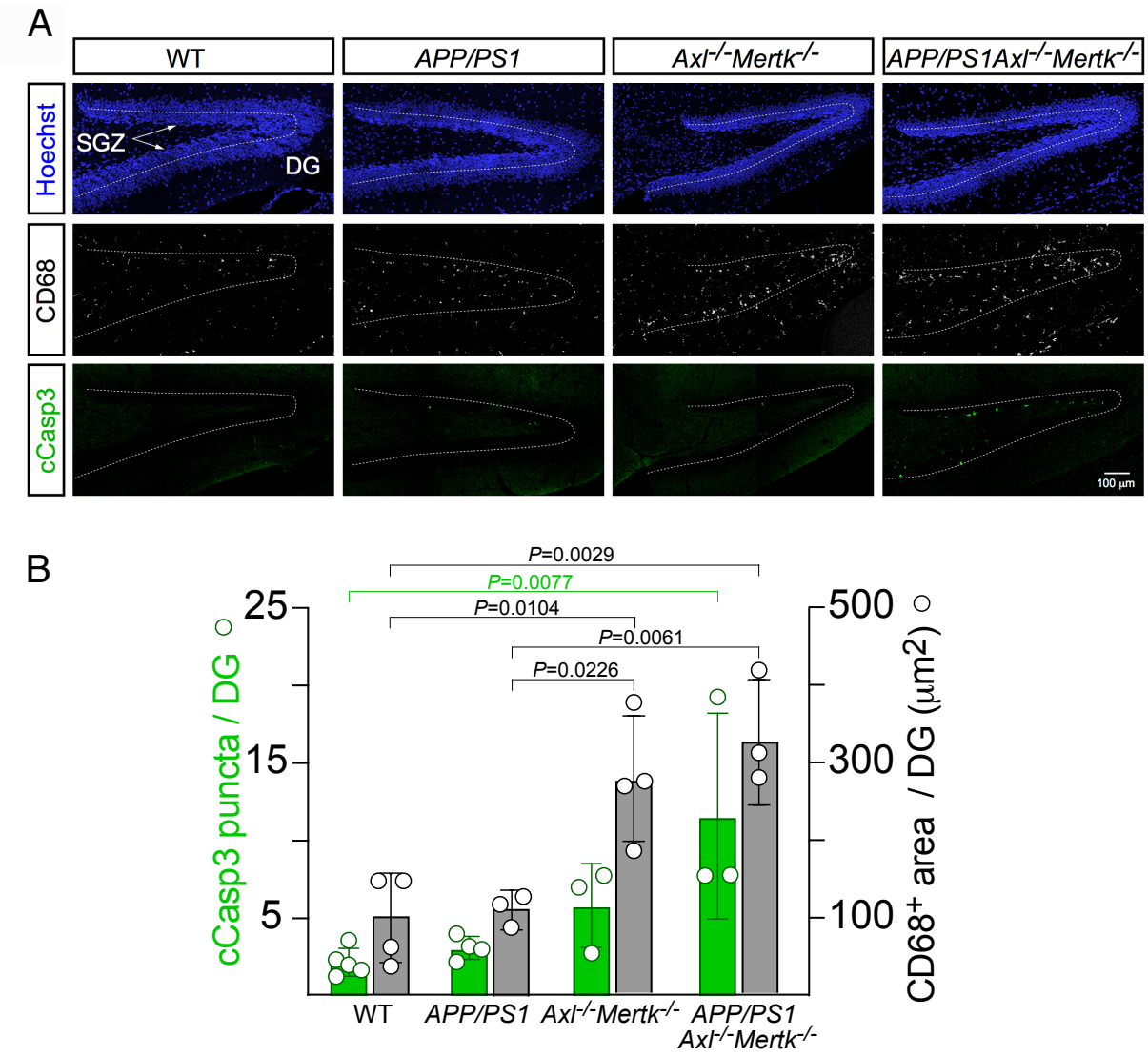

Figure 2.3.2-6 AD-predisposed induction of microglial CD68 expression and accumulation of cCasp3 in SGZ of P 30 *APP/PS1 Axl*$^{-/-}$ *Mertk*$^{-/-}$

(**a**) Hoechst staining (top panels), CD68 expression (middle panels), and cleaved caspase 3^{+} ACs (lower panels) of the P30 DG, whose SGZ is a site of neurogenesis. Panels are representative images from ≥3 sections from ≥3 mice of each genotype. (**b**) Quantification of results in **a**. Points are average signal from 4-5 sections per mouse; 3-5 mice per genotype. *P* values calculated using Kruskal-Wallis with Dunn's posthoc test (cCasp3) and one-way ANOVA with Holm-Sidak multiple comparison test (CD68).

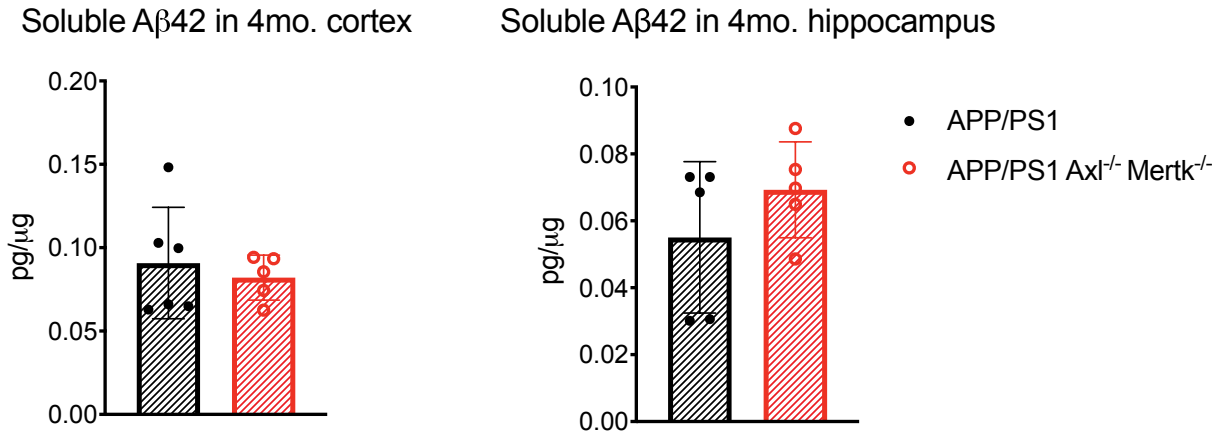

Figure 2.3.2-7 Soluble Aβ42 levels are unchanged at 4 mo in *APP/PS1Axl*$^{-/-}$*Mertk*$^{-/-}$

Soluble Aβ42 levels quantified in *APP/PS1* (gray) versus *APP/PS1Axl*$^{-/-}$*Mertk*$^{-/-}$ (red) cortex (left) and hippocampus (right) at 4 months. Data points represent levels of soluble Aβ42 in n ≥ 5 mice of each genotype.

Figure 2.3.3-1 Microglia use Axl and Mer to detect, engage, and react to Aβ plaques
(**a**) Representative video stills from two-photon imaging of microglia (GFP signal, white) and amyloid plaques (MX04 signal, red) in 16 mo *APP/PS1* and *APP/PS1Axl*$^{-/-}$*Mertk*$^{-/-}$ cortex. (**b**) Imaris surface builds of microglial volumes at 0-5μm (white) and 5-20μm (green) from the edge of nearest plaque (red) in *APP/PS1* and *APP/PS1Axl*$^{-/-}$*Mertk*$^{-/-}$ cortex. (**c**) Distribution of distances of microglial cell body centroids from the edge of Aβ plaques in *APP/PS1* and *APP/PS1Axl*$^{-/-}$*Mertk*$^{-/-}$ cortex. A total of 22 and 37 plaques were investigated from 3 and 4 mice for *APP/PS1* and *APP/PS1Axl*$^{-/-}$*Mertk*$^{-/-}$, respectively. (**d**) Primary microglial processes per nearest plaque for PAM (microglia <5μm from plaques) in *APP/PS1* (*A/PS*) and *APP/PS1Axl*$^{-/-}$*Mertk*$^{-/-}$ (*A/PS A/M*$^{-/-}$) cortex. (**e**) Summed length of primary microglial processes per nearest plaque for PAM in *APP/PS1* and *APP/PS1Axl*$^{-/-}$*Mertk*$^{-/-}$ cortex. (**f**) Process polarization to nearest plaque (ratio of summed length of primary processes oriented toward plaque to summed length of all primary processes) for NPAM (microglia >20μm from plaques) in *APP/PS1* and *APP/PS1Axl*$^{-/-}$*Mertk*$^{-/-}$ cortex. (**g**) Process motility for cortical PAM, NPAM, and non-diseased microglia in mice of the indicated genotypes. Data points are from 7-29 representative plaques from n = 3 mice from both genotypes (**d**-**f**), and 18-52 microglia from 2 (WT and *Axl*$^{-/-}$*Mertk*$^{-/-}$) and 3 (*APP/PS1* and *APP/PS1Axl*$^{-/-}$*Mertk*$^{-/-}$) mice (**g**).

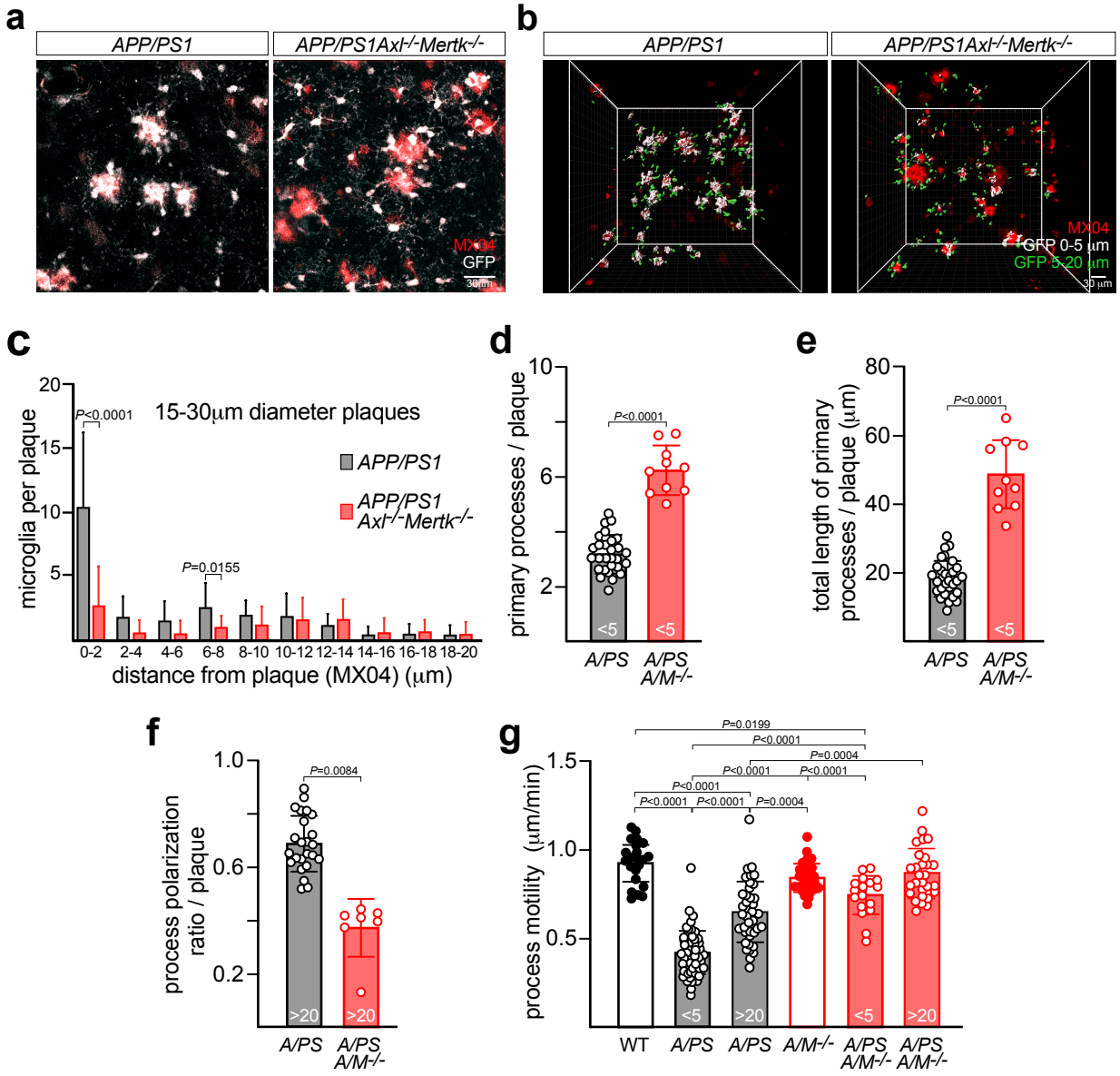
a
APP/PS1
APP/PS1Axl-/-Mertk-/-
MX04
GFP
30µm
b
APP/PS1
APP/PS1Axl-/-Mertk-/-
MX04
GFP 0-5 µm
GFP 5-20 µm
30 µm
c
microglia per plaque
15-30µm diameter plaques
APP/PS1
APP/PS1 Axl-/-Mertk-/-
P<0.0001
P=0.0155
0-2
2-4
4-6
6-8
8-10
10-12
12-14
14-16
16-18
18-20
distance from plaque (MX04) (µm)
d
primary processes / plaque
P<0.0001
<5
<5
A/PS
A/PS A/M-/-
e
total length of primary processes / plaque (µm)
P<0.0001
<5
<5
A/PS
A/PS A/M-/-
f
process polarization ratio / plaque
P=0.0084
>20
>20
A/PS
A/PS A/M-/-
g
process motility (µm/min)
P=0.0199
P<0.0001
P=0.0004
P<0.0001
P<0.0001
P<0.0001
P<0.0001
P<0.0001
P=0.0004
<5
>20
<5
>20
WT
A/PS
A/PS
A/M-/-
A/PS A/M-/-
A/PS A/M-/-

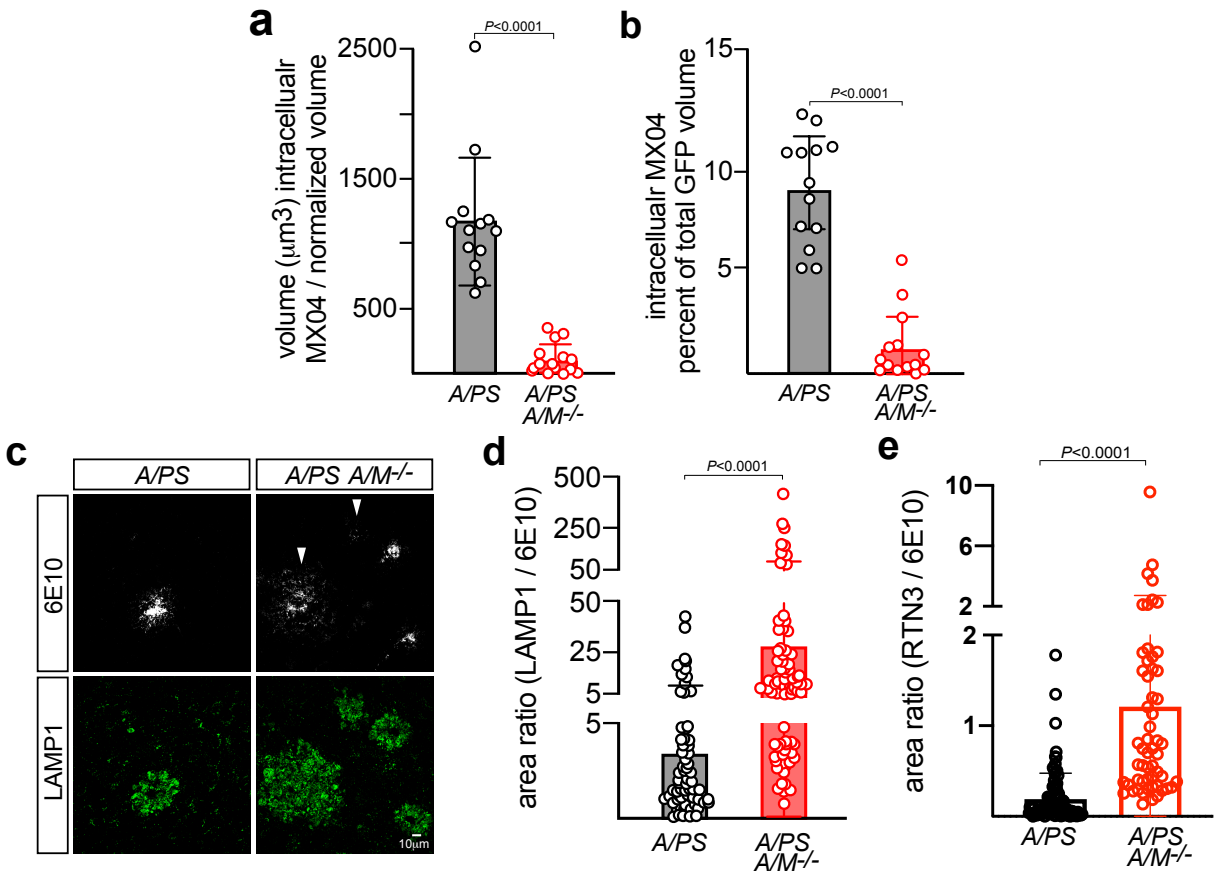

Figure 2.3.3-2 TAM-deficient microglia can neither phagocytose nor organize plaques

(**a**, **b**) MX04-labeled Aβ plaque material engulfed within GFP$^+$ microglia, imaged *in vivo*, in 16 mo. *APP/PS1* (*A/PS*) versus *APP/PS1Axl$^{-/-}$Mertk$^{-/-}$* (*A/PS A/M$^{-/-}$*) cortex, normalized to imaging volume (**a**) and the volume of GFP$^+$ cells (**b**). (**c**) Representative images of the halo of LAMP1$^+$ dystrophic membranes (green, lower panels) that surround 6E10$^+$ plaques in 12 mo. *APP/PS1* (*A/PS*; left) versus *APP/PS1Axl$^{-/-}$Mertk$^{-/-}$* (*A/PS A/M$^{-/-}$*; right) cortex. Arrowheads mark weakly-staining, diffuse 6E10$^+$ plaques, which are more common in the *APP/PS1Axl$^{-/-}$Mertk$^{-/-}$* brain (see also Supplementary Fig. 2.3.3-2). (**d**) Quantification of the ratio of LAMP1$^+$ area to 6E10$^+$ plaque area for all plaque sizes, both dense-core and diffuse. (**e**) Quantification of ratio RTN3$^+$ area to 6E10$^+$ plaque area for all plaque sizes, both dense-core and diffuse. Data are 13-15 volumetric images from n= 3 and 4 mice for *APP/PS1* and *APP/PS1Axl$^{-/-}$Mertk$^{-/-}$*, respectively (**a-b**). Data are 94-113 plaques (**d**) and 56-96 plaques (**e**) investigated from N $\geq$ 3 sections per mouse from n = 3 mice of each genotype.

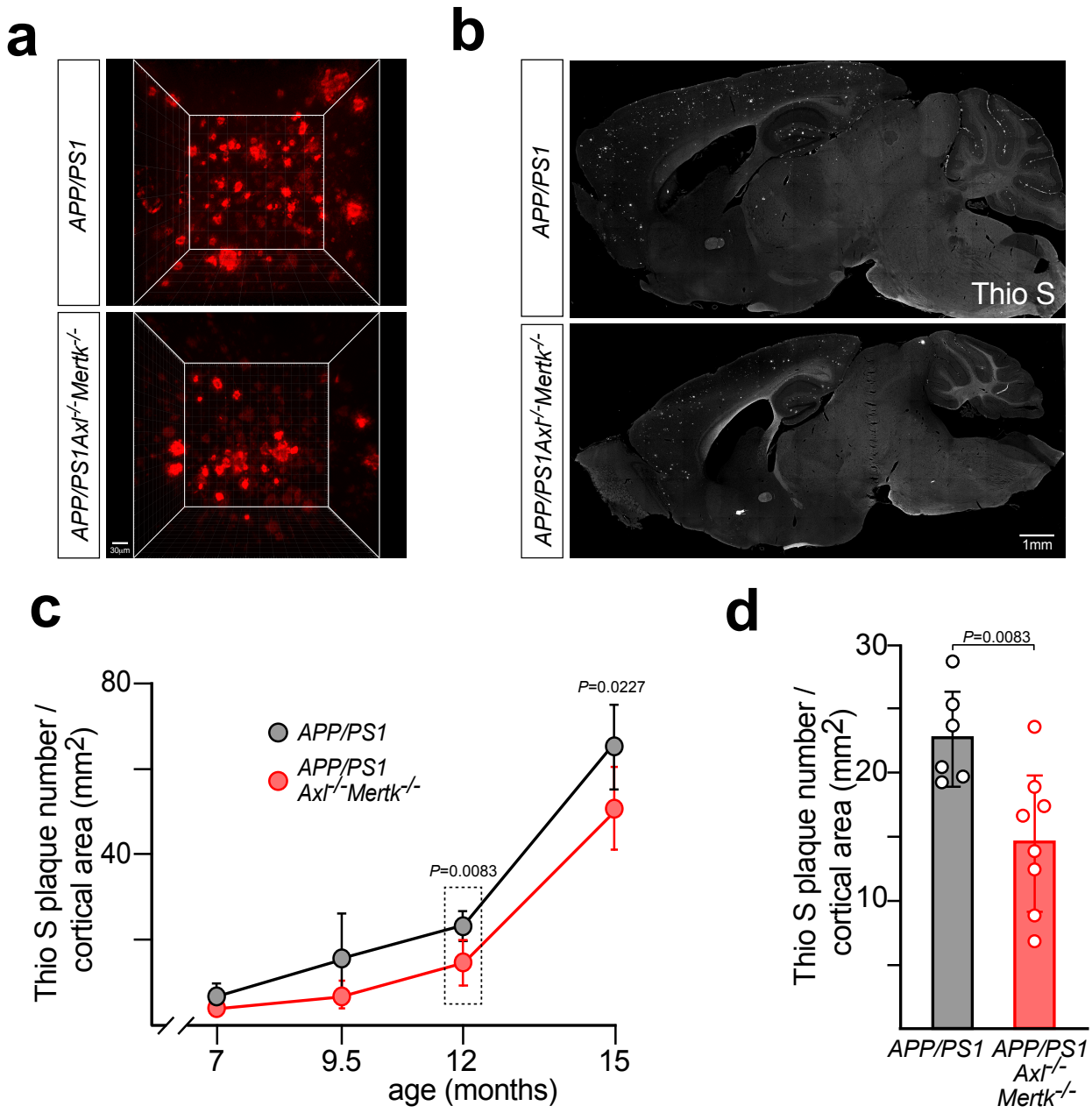

Figure 2.3.3-3 TAM-driven microglial phagocytosis favors plaque formation

(**a**) Representative two-photon imaging volumes (X and Y 350μm, Z 300μm) of MX04-labeled plaques in 16 mo *APP/PS1* and *APP/PS1Axl*$^{-/-}$*Mertk*$^{-/-}$ cortex. (**b**) Representative sagittal sections from 12 mo *APP/PS1* (top) and *APP/PS1Axl*$^{-/-}$*Mertk*$^{-/-}$ (bottom) brains, stained for dense-core plaques with thioflavin S (Thio S). (**c**) Quantification (see Methods) of Thio S-labeled dense-core Aβ plaque density, for cross-sectional plaque areas of all sizes, in *APP/PS1* (gray) and *APP/PS1Axl*$^{-/-}$*Mertk*$^{-/-}$ (red) cortex over time. Boxed data at 12 months are detailed in **d**. (**d**) Thio S-labeled plaque density in cortex (of *APP/PS1* (gray) and *APP/PS1Axl*$^{-/-}$*Mertk*$^{-/-}$ (red) mice at 12 mo. Data points represent plaque density in n= 6-8 mice of the indicated genotypes averaged from N ≥ 5 cortical sections of each brain.

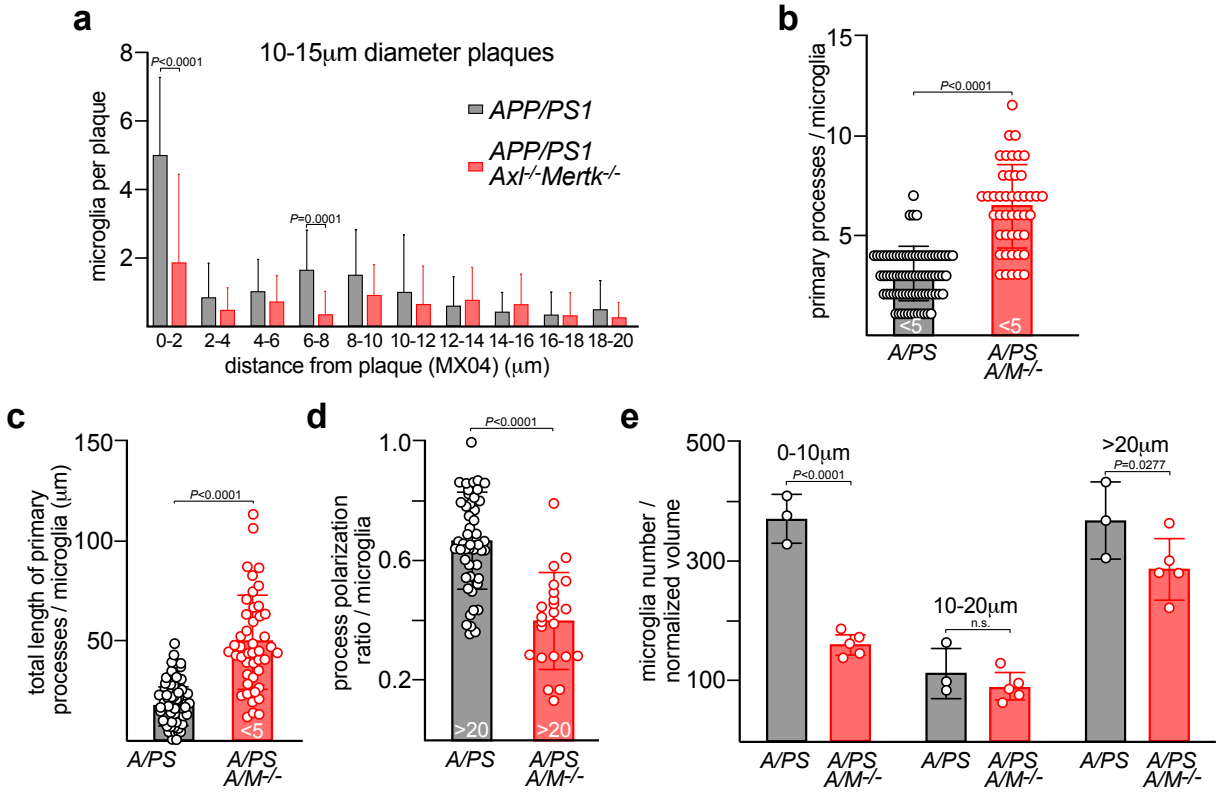

Supplementary Figure 2.3.3-1 *APP/PS1Axl*$^{-/-}$*Mertk*$^{-/-}$ microglia are unresponsive to Aβ plaques

(**a**) Distribution of distance of microglial cell body centroids, in 2μm bins, from the edge of MX04-labeled Aβ plaques with diameters of 10-15μm in *APP/PS1* (gray) and *APP/PS1Axl*$^{-/-}$ *Mertk*$^{-/-}$ (red) cortex. Values obtained for 56 and 23 plaques from 3 and 4 mice for *APP/PS1* and *APP/PS1Axl*$^{-/-}$*Mertk*$^{-/-}$, respectively. (**b**) Number of imaged GFP^{+} primary processes per PAM (microglia <5μm from plaques) in *APP/PS1* (gray, *A/PS*) and *APP/PS1Axl*$^{-/-}$*Mertk*$^{-/-}$ (red, *A/PS A/M*$^{-/-}$) cortex. (**c**) Summed length of primary microglial processes per PAM in *APP/PS1* (gray) and *APP/PS1Axl*$^{-/-}$*Mertk*$^{-/-}$ (red) cortex. (**d**) Process polarization ratio to nearest plaque per NPAM (microglia >20μm from plaques; see Materials and Methods) in *APP/PS1* (gray) and *APP/PS1Axl*$^{-/-}$*Mertk*$^{-/-}$ (red) cortex. (**e**) Quantification of microglial cell density in the cortex of 16 month *APP/PS1* (gray) and *APP/PS1Axl*$^{-/-}$*Mertk*$^{-/-}$ (red) mice for microglia 0-10 μm, 10-20 μm, and >20 μm from the edge of the nearest plaque. Data points are from 45-129 measured PAM investing 10-29 plaques (**b**, **c**), 21-49 cells peripheral to 7-24 plaques (**e**), and 3-5 imaging volumes (**e**) from 2 (*APP/PS1*) and 3-4 (*APP/PS1Axl*$^{-/-}$*Mertk*$^{-/-}$) mice. For all supplementary figure panels, errors bars are ±1 STD.

Supplementary Figure 2.3.3-2 Expansive areas of plaque-associated dystrophic LAMP1$^+$ membrane and poorly compacted plaques in the *APP/PS1Axl$^{-/-}$Mertk$^{-/-}$* brain

A collection of 24 sections in both *APP/PS1* (top six rows) and *APP/PS1Axl$^{-/-}$Mertk$^{-/-}$* (bottom six rows) cortex, each stained with antibodies to both LAMP1 (green) and 6E10 (white). This montage, which is a subset of the images used to generate the data in Fig. 2.3.3-2d, is composed of images taken from three different mice of each genotype at 12 months. Note that: (a) 6E10$^+$ Aβ plaques are in general more compact and brightly stained in *APP/PS1* mice and more diffuse and weakly stained in *APP/PS1Axl$^{-/-}$Mertk$^{-/-}$* mice; and (b) the area occupied by LAMP1$^+$ membrane is in general much larger in *APP/PS1Axl$^{-/-}$Mertk$^{-/-}$* mice. Scale bars, 10μm.

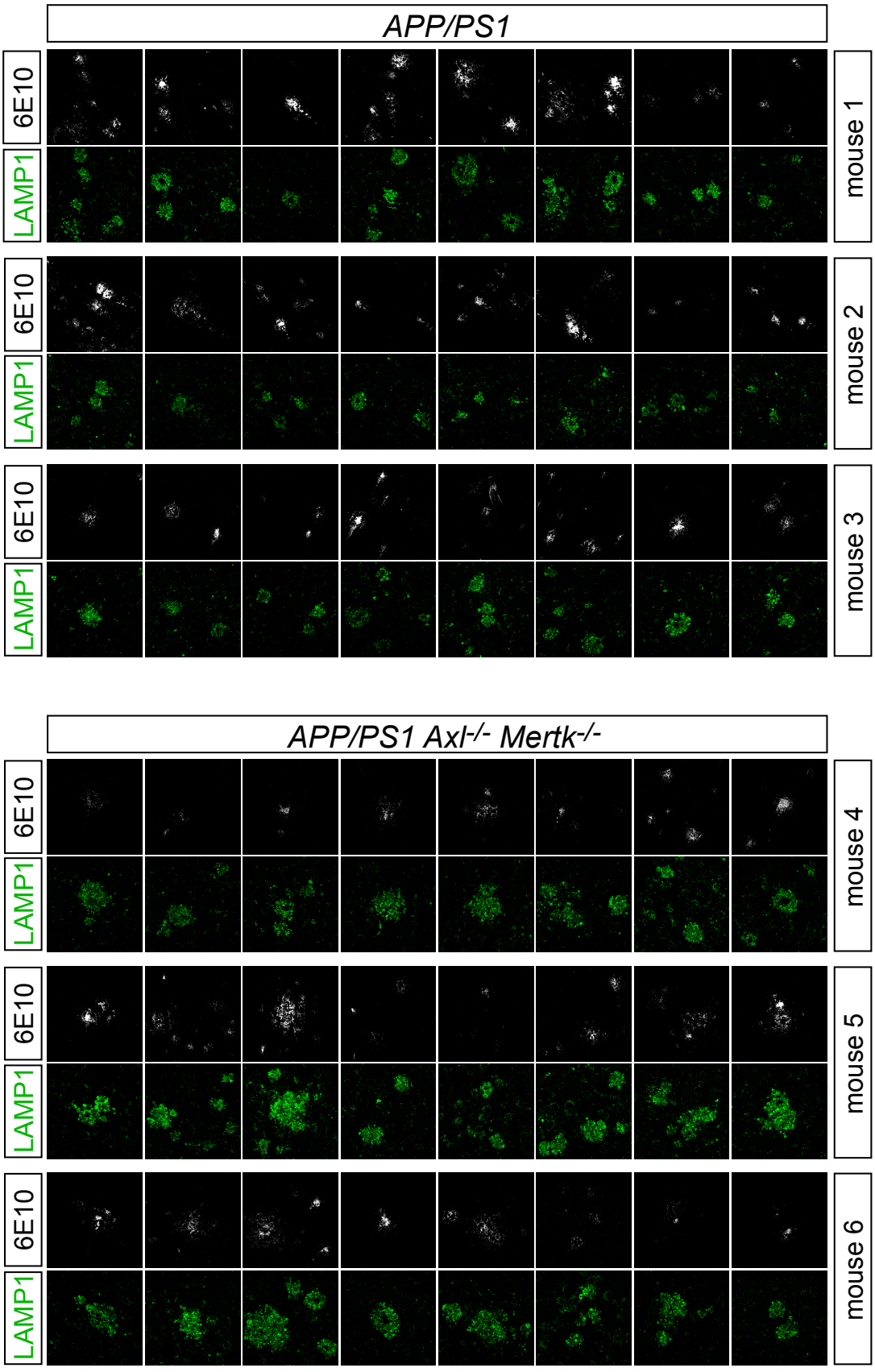
APP/PS1
APP/PS1 Axl-/- Mertk-/-
6E10
LAMP1
mouse 1
mouse 2
mouse 3
mouse 4
mouse 5
mouse 6

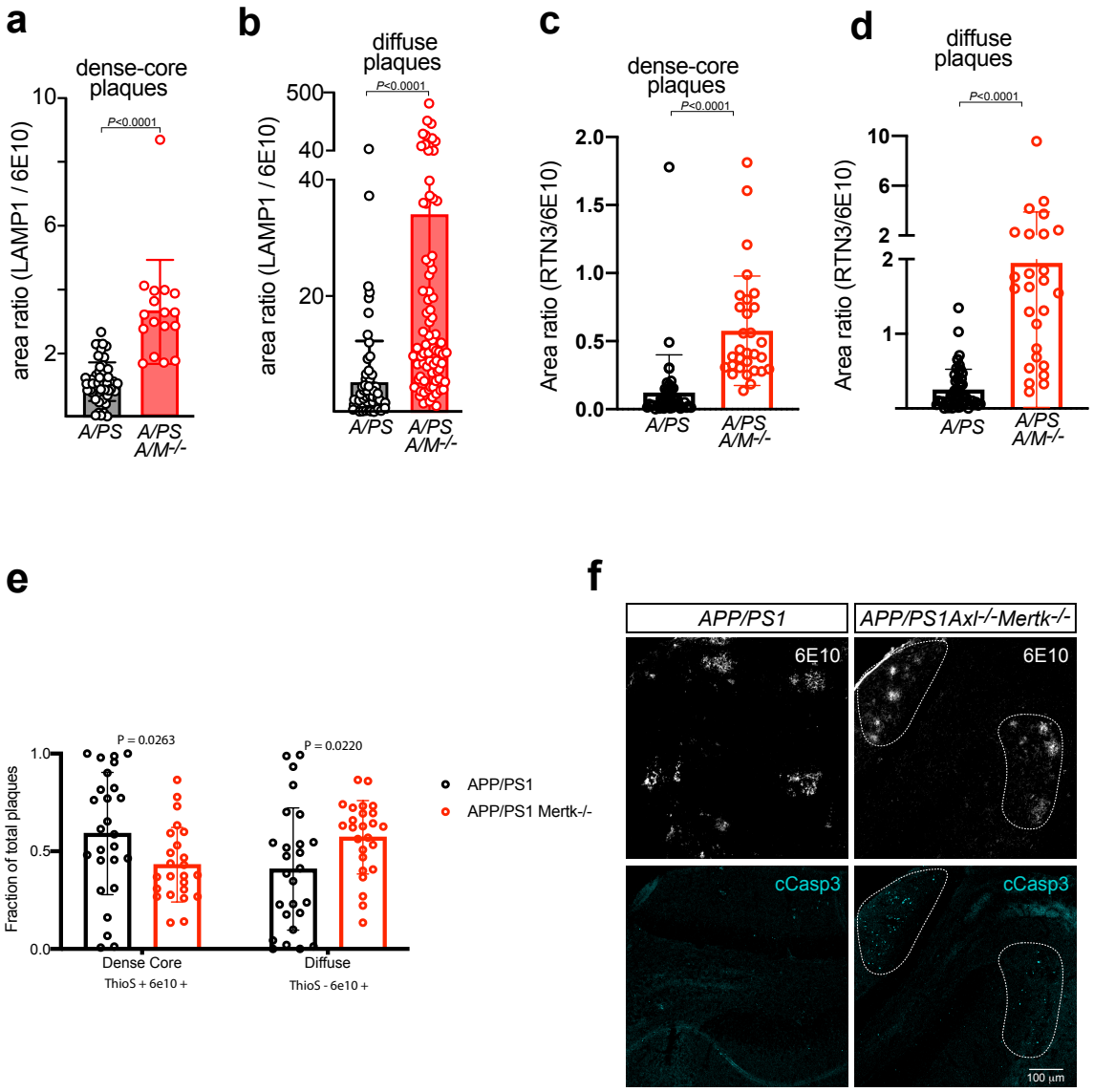

Supplementary Figure 2.3.3-3 Accumulation of LAMP1^{+} dystrophic membrane and apoptotic cell debris in the *APP/PS1Axl$^{-/-}$Mertk$^{-/-}$* brain

(**a**) Quantification of LAMP1/6E10 area ratio as in Fig. 4d, but only for dense-core plaques (plaques with solid 6E10^{+} cores with areas > 100µm^{2}). (**b**) Quantification of LAMP1/6E10 area ratio as in Fig. 2.3.3-2d, but only for diffuse plaques (plaques without solid 6E10^{+} cores with areas > 100µm^{2}). Quantification of RTN3/6E10 area ratio as in Fig. 2.3.3-2e for dense-core (**c**) and diffuse plaques (**d**) by the same criteria noted above. (**e**) Number of dense-core (ThioS+ 6E10+) and diffuse plaque (ThioS- 6E10+) was represented as fraction of total plaques in prefrontal cortex of 12 mo *APPP/PS1* and *APP/PS1 Mertk$^{-/-}$* mice. Data points represent images analyzed collected from n ≥ 6 mice/group. (**f**) cCasp3^{+} apoptotic debris (cyan, lower panels) accumulates around 6E10^{+} Aβ plaques (upper panels) in the *APP/PS1Axl$^{-/-}$Mertk$^{-/-}$* (right panels) but not the *APP/PS1* (left panels) hippocampus. Scale bar, 100µm.

Supplementary Figure 2.3.3-4 TAM (Mer) signaling promotes Aβ plaque accumulation

(**a**)Thio S^+ plaque density in *APP/PS1* (gray) versus *APP/PS1Axl*$^{-/-}$*Mertk*$^{-/-}$ (red) cortex for plaques of the indicated size at 12 months. (**b**) Thio S^+ plaque density (all plaque sizes) in *APP/PS1* (gray) versus *APP/PS1Axl*$^{-/-}$*Mertk*$^{-/-}$ (red) hippocampus at 12 months. (**c**) Soluble Aβ42 levels quantified in *APP/PS1* (gray) versus *APP/PS1Axl*$^{-/-}$*Mertk*$^{-/-}$ (red) cortex and hippocampus at 12 months. (**d**) Li-Cor immunoblot of human amyloid precursor protein (APP) at 100kDa using human-specific antibody 6E10 (upper) quantification relative to loading control protein GAPDH as fold changes to intensity of the non-transgenic WT group (lower) shows no difference in APP protein level between *APP/PS1* and *APP/PS1Axl*$^{-/-}$*Mertk*$^{-/-}$ group. Each lane and data point represent individual animal. (**e**) Quantification of immunostaining of excitatory pre- and post-synaptic puncta, vGlut1 and PSD95, respectively, in 15 mo CA1 region of mice with genotypes noted. Co-localization analysis shows similar synaptic deficits in *APP/PS1* and *APP/PS1Axl*$^{-/-}$*Mertk*$^{-/-}$ mice comparing to their non-diseased littermates. Fold changes (y axis) of co-localized puncta number of each animal are normalized to that of WT. Data points represent individual animals that are an average of data from N $\geq$ 9 images out of $\geq$ 3 hippocampal sections/animal. (**f**) ThioS^+ plaque density (all plaque sizes) in *APP/PS1* (gray) versus *APP/PS1Mertk*$^{-/-}$ (pink) cortex and hippocampus at 12 months. (**g**) Thio S^+ plaque density (all plaque sizes) in *APP/PS1* (gray) versus *APP/PS1Axl*$^{-/-}$ (white) cortex and hippocampus at 12 months. Data points represent plaque density in n= 6-8 mice of the indicated genotypes averaged from N $\geq$ 5 cortical sections for each brain.

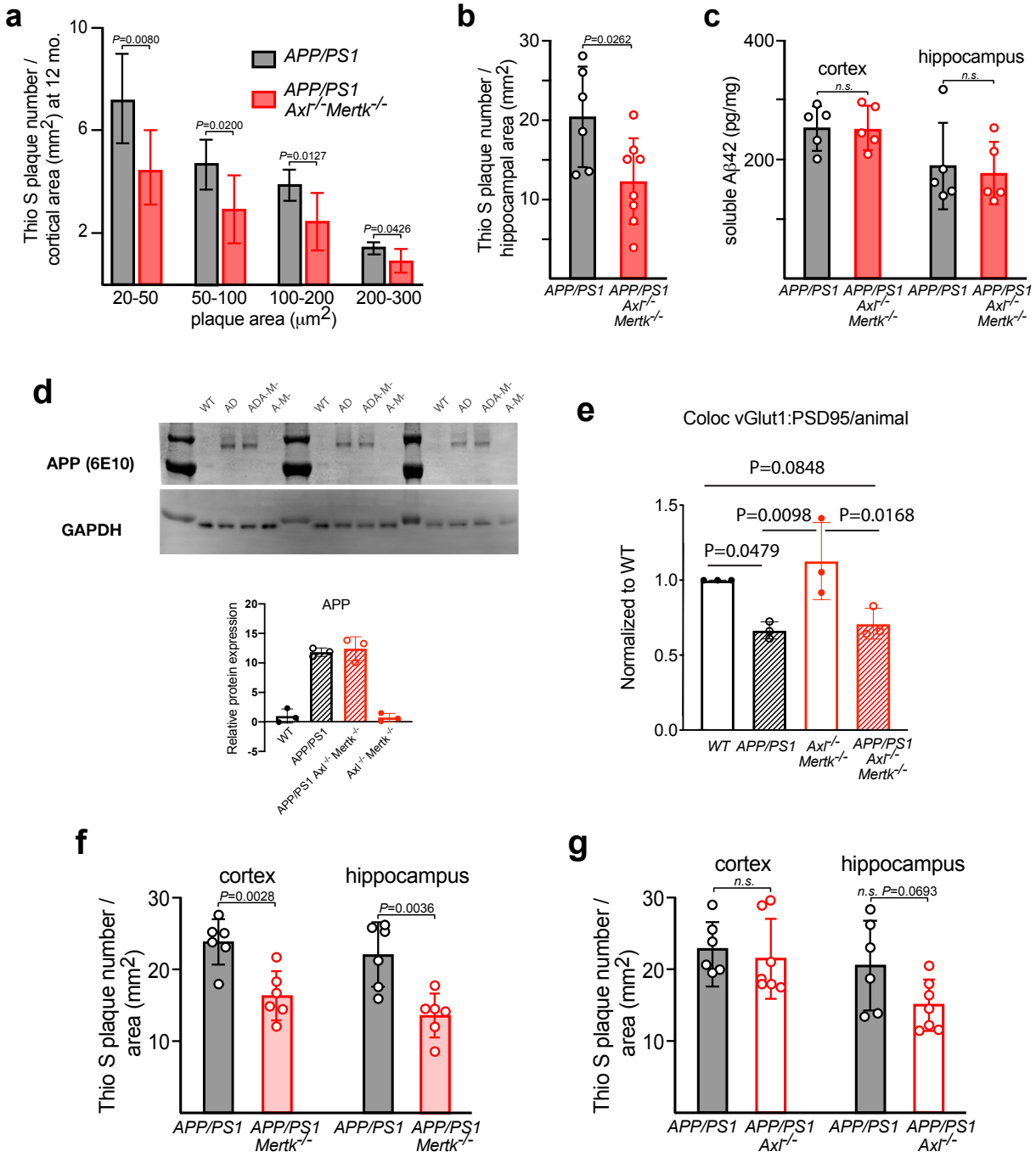
a
Thio S plaque number / cortical area (mm2) at 12 mo.
APP/PS1
APP/PS1 Axl-/-Mertk-/-
P=0.0080
P=0.0200
P=0.0127
P=0.0426
20-50
50-100
100-200
200-300
plaque area (μm2)
b
Thio S plaque number / hippocampal area (mm2)
P=0.0262
APP/PS1
APP/PS1 Axl-/- Mertk-/-
c
soluble Aβ42 (pg/mg)
cortex
hippocampus
n.s.
d
APP (6E10)
GAPDH
WT
AD
ADA-M-A-M-
APP
Relative protein expression
e
Coloc vGlut1:PSD95/animal
Normalized to WT
P=0.0848
P=0.0098
P=0.0168
P=0.0479
WT
APP/PS1
Axl-/- Mertk-/-
f
Thio S plaque number / area (mm2)
P=0.0028
P=0.0036
Mertk-/-
g
n.s. P=0.0693
Axl-/-

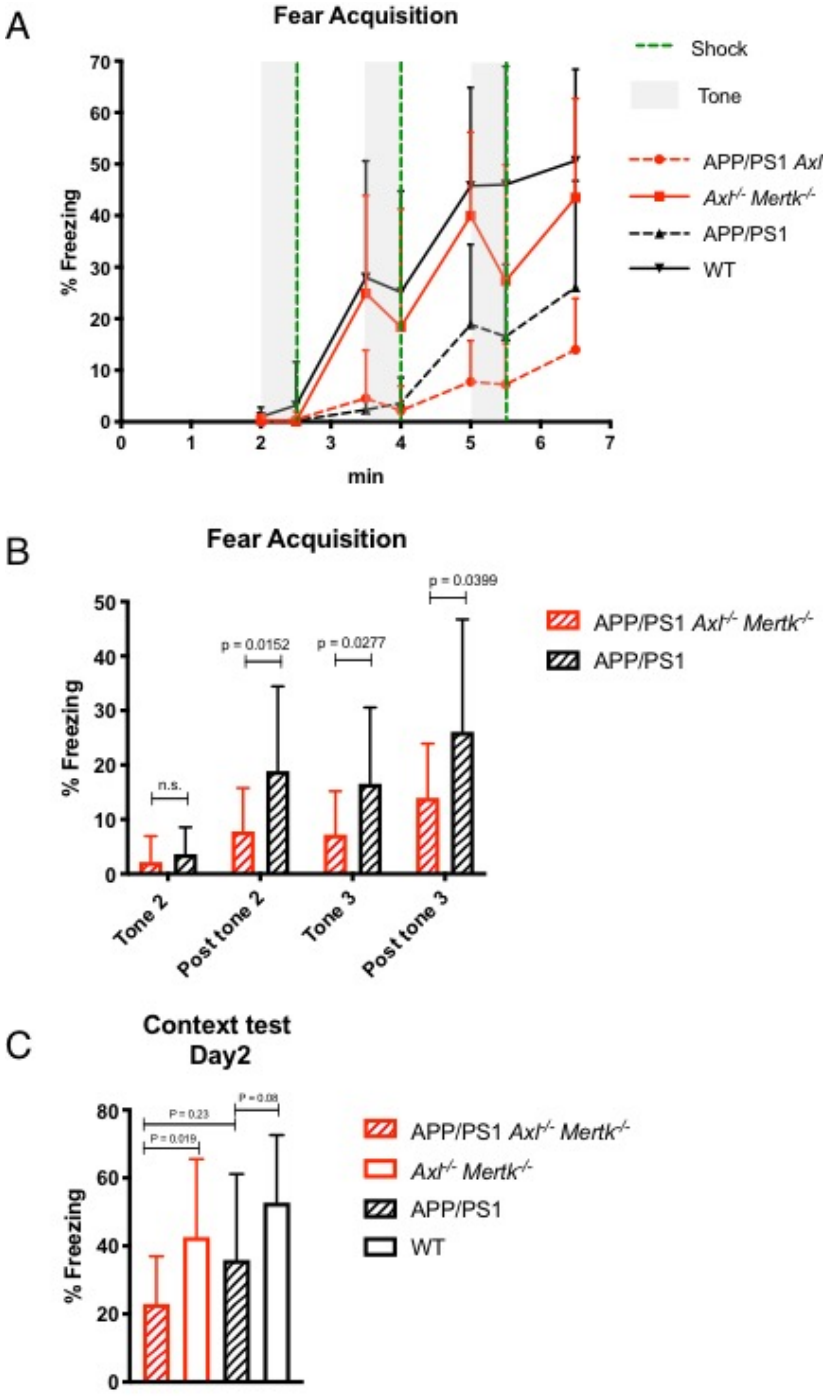

Supplementary Figure 2.3.3-5 APP/PS1 mice lacking TAM receptors show worsened cognitive deficits compared to age-matched APP/PS1 mice

(**a,b**) 12mo *APP/PS1 Axl*$^{-/-}$*Mertk*$^{-/-}$ mice show significantly less freezing response during and after tone-shock-paired fear acquisition and (**c**) a slight trend of less freezing response in context test 24hrs after fear acquisition compared to 12mo. *APP/PS1* mice. n=12-18 per genotype, males only. One-way ANOVA test.

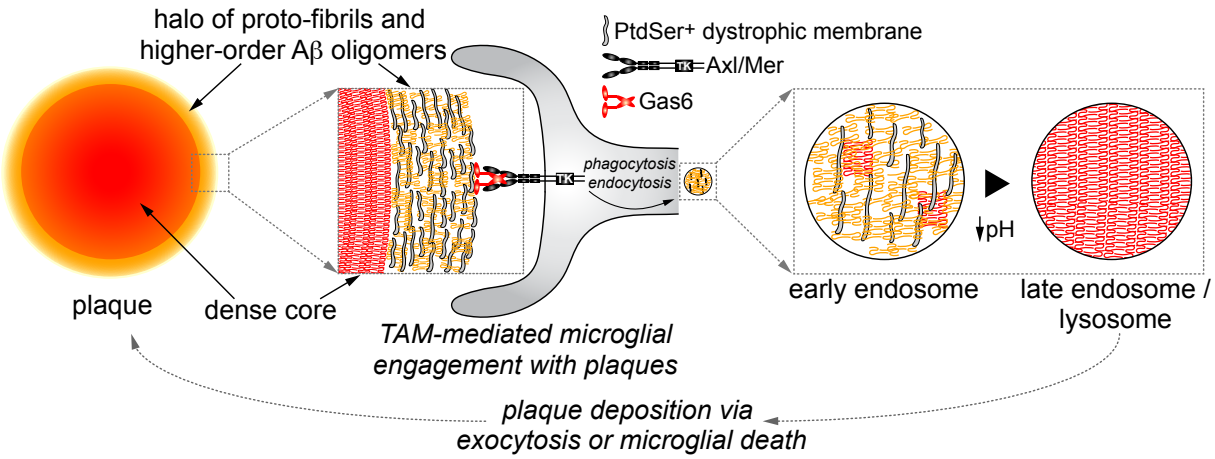

Figure 2.3.4-1 Mer upregulation in plaque-associated microglia

Microglial Axl and Mer do not bind plaques directly, but are bridged to the PtdSer-rich dystrophic membranes of plaques via TAM ligands (Fig. 2.3.1-8,10a,b), whose N-terminal and C-terminal domains bind PtdSer and Axl/Mer, respectively[3, 37]. Gas6 is shown, but a role for the Mer ligand Pros1[37] is not excluded. The PtdSer-TAM ligand-TAM receptor complex is an essential component of the mechanism through which microglia detect and respond to plaques. Engagement of this complex activates the TAM tyrosine kinases (TK), which drives remodeling of the microglial actin cytoskeleton, phagocytosis, and internalization of forming plaque material. Internalized phagocytic cargo is eventually transferred to lysosomes, whose acidic interiors promote the aggregation of large Aβ fibrils. Exocytosis or microglial death then delivers this aggregated material to growing dense-core plaques.

Supplemental Movie Legends

Movie S1. Continuous home cage monitoring set-up. A representative video clip illustrating continuous top-down recording of home cage activity of a mouse cohort. Recording for this sequence was performed during dark cycle housing, under red light illumination (see Materials and Methods). In this example, an *APP/PS1Mertk*$^{-/-}$ mouse (age 2.5 mo) in the cage at the lower right displays a series of abnormal, seizure-like motor behaviors that led to its death shortly after the end of the clip.

Movie S2. *APP/PS1Mertk*$^{-/-}$ mutants develop lethal seizures. A video montage of distinct seizure activities exhibited by two different individuals. First, an *APP/PS1Mertk*$^{-/-}$ mouse (P18), the individual shown in Fig. S3A, at the end of a lethal seizure. Second, an *APP/PS1Axl*$^{-/-}$*Mertk*$^{-/-}$ mouse (P20) in a tonic-clonic seizure. Third, the same individual alternating between frozen distended postures in which its body is elevated. Fourth, the same individual exhibiting tremor and pronounced hyperactivity. This mouse died from seizure after the recording.

Movie S3. Microglia show reduced interaction with amyloid plaques in somatosensory cortical layer 1 of 16mo *APP/PS1Axl*$^{-/-}$*Mertk*$^{-/-}$ as compared to *APP/PS1* mice. Left, example two-photon time-lapse recording showing microglia (GFP signal, white) and amyloid plaques (MX04 signal, red) in somatosensory cortical layer 1 of an anesthetized *APP/PS1Cx3cr1*$^{GFP/+}$ mouse. Each image is a maximum-intensity projection of a 70 μm-thick z-stack (1.2μm axial step size) recorded every ~93s between 100μm and 30μm depth below the pia. Right, example two-photon time-lapse recording showing microglia (GFP signal, white) and amyloid plaques (MX04 signal, red) in somatosensory cortical layer 1 of an age- and gender-matched anesthetized *APP/PS1Axl*$^{-/-}$*Mertk*$^{-/-}$*Cx3cr1*$^{GFP/+}$ mouse. Each image is a maximum-intensity projection of a 70μm-thick z-stack (1.2μm axial step size) recorded every

~93s between 94μm and 24μm depth below the pia. Elapsed time is indicated in the upper right corner. Amyloid plaques are closely encapsulated by highly polarized microglia in *APP/PS1* but not *APP/PS1Axl*$^{-/-}$*Mertk*$^{-/-}$ mice. Additionally, microglia near plaques typically show fewer and less elaborate processes, higher process polarization, and reduced process motility in *APP/PS1* as compared to *APP/PS1Axl*$^{-/-}$*Mertk*$^{-/-}$ mice. Supplemental movies 3 and 4 were prepared using Fiji and custom-written scripts in Igor Pro (version 6.04; WaveMetrics). Scale bar, 30 μm.

Movie S4. Microglia show reduced interaction with amyloid plaques in somatosensory cortical layers 1/2 of 16mo *APP/PS1Axl*$^{-/-}$*Mertk*$^{-/-}$ as compared to *APP/PS1* mice. Left, example two-photon time-lapse recording showing microglia (GFP signal, white) and amyloid plaques (MX04 signal, red) in somatosensory cortical layers 1/2 of an anesthetized *APP/PS1Cx3cr1*$^{GFP/+}$ mouse. Each image is a maximum-intensity projection of a 70μm-thick z-stack (1.2μm axial step size) recorded every ~93s between 148μm and 78μm depth below the pia. Right, example two-photon time-lapse recording showing microglia (GFP signal, white) and amyloid plaques (MX04 signal, red) in somatosensory cortical layers 1/2 of an age-and gender-matched anesthetized *APP/PS1Axl*$^{-/-}$*Mertk*$^{-/-}$*Cx3cr1*$^{GFP/+}$ mouse. Each image is a maximum-intensity projection of a 70μm-thick z-stack (1.2μm axial step size) recorded every ~93s between 135μm and 65μm depth below the pia. Elapsed time is indicated in the upper right corner. Amyloid plaques are closely encapsulated by highly polarized microglia in *APP/PS1* but not *APP/PS1Axl*$^{-/-}$*Mertk*$^{-/-}$ mice. Additionally, microglia near plaques typically show fewer and less elaborate processes, higher process polarization, and reduced process motility in *APP/PS1* as compared to *APP/PS1Axl*$^{-/-}$*Mertk*$^{-/-}$ mice. Scale bar, 30μm.

Chapter 3: Expression and function of the TAM system in a mouse model of ALS

3.1 Introduction

In light of our findings in AD, we further explored the potential role of the microglial TAM receptors Axl and Mer in ALS, another deadly and irreversible neurodegenerative disease. It is characterized by progressive muscle weakness and paralysis resulting from the death of motor neurons (MNs) predominantly[1,2,3,4,5]. Over 5000 people in the U.S. are diagnosed with ALS each year, and the life expectancy of an ALS patient averages 2 to 5 years from the time of diagnosis. There are currently no therapies that halt or reverse this deadly disease.

Though the exact mechanism of selective MN death is still unclear in ALS, glutamate-mediated excitotoxicity underlying disrupted calcium homeostasis has long been recognized as one of the major and early-occurring pathological features contributing to MN degeneration in sporadic and familial ALS patients [6-9]. Indeed, Riluzole, one of the two FDA-approved drugs[10], aims at dampening this exact phenomenon serving as a glutamate antagonist. Interestingly, ALS-prone neurons, such as MMP9+ FF alpha MNs that express calcium-permeable glutamate receptors, are especially more susceptible to aberrantly elevated intracellular calcium and higher rates of neuronal firing due to a lack of intracellular calcium-binding components such as calbindin D28K and parvalbumin[11 12,13]. Undoubtedly, dampening MN excitotoxicity especially in ALS-susceptible MNs may alleviate the MN degenerative process and preservation of motor functions in ALS.

ALS is but a MN-autonomous disease. Patients with ALS carrying mutations in *SOD1*, C9orf72 and *TARDBP* present with dramatic inflammation in the CNS, particularly in but not limited to the ventral horn of spinal cord and motor cortex. Transgenic mice with mutations in these genes also develop ALS-like symptoms and profound immune dysfunction. Although it

is widely appreciated that immune dysregulation is a key feature of ALS pathogenesis and there is little doubt that microglia are the master regulators of neuroinflammation in ALS, whether immune responses drive or protect against ALS progression is yet to be addressed. Indeed, studies in patients with ALS and in its transgenic mouse models suggest a seemingly contradictive, dual action role for neuroinflammation – an initial protective, anti-inflammatory response is followed by a subsequent chronic toxic response. These reactive microglia can lose their surveillance role when chronically activated, and secrete proinflammatory cytokines and toxic agents[14,15] that worsen MN axonal dieback, death, and disease progression in ALS[16,17]. Furthermore, TNF-α secreted by activated microglia can promote an E/I imbalance in MN which potentiates MN susceptibility to excitotoxicity[18,19].

The TAM receptors Axl and Mer play major roles in the phagocytic clearance of apoptotic cells[20-24] and the feedback inhibition of the innate immune response[23-27] in macrophages and other immune sentinels, activities that are closely related to pathological changes in ALS. Importantly, recent evidence suggests that Axl is a prominent component of a 'disease-associated microglia' gene signature in SOD1 mice at late stage of disease[28,29]. This evidence notwithstanding, an understanding of whether and how microglia act through TAM receptors to regulate ALS progression is yet to be experimentally addressed.

Our aim is to study the role of TAM receptors in microglia at various timepoints along the disease progression of ALS in mice. To do this, we have crossed mice genetically deficient for both or single microglial TAM receptors - Axl and Mer - into the $SOD1^{G93A}$ (SOD1) mouse model of ALS[30]. We have evaluated these mice in comparison to SOD1 mice for changes in disease course[31], MN death, and inflammation, in order to assess the impact of loss of microglial TAM signaling in ALS. New studies using microglia-specific conditional

knockout mice are also underway to validate key findings from whole-body knock-outs. Outcomes from our studies will advance our understanding of the engagement of the TAM signaling pathway and its role in microglia in the development of ALS. Microglial TAM pathway-targeted therapies may ameliorate microglial local immune responses and motor circuitry degeneration in disease. As TAM receptors are already drug targets in the clinic, treating symptomatic patients with TAM inhibitors may hold promise with respect to improving quality of life.

3.2 Material and Methods

Mice

The *Axl*$^{-/}$ [32], *Axl*$^{-/-}$*Mertk*$^{-/-}$ [32] strains have been described previously. We employ a congenic B6 version of the most widely studied model – the SOD1^{G93A} (SOD1) mouse [30] – which we have obtained from Jackson Laboratory (JAX number: 004435). This mouse has been the most extensively studied rodent model; it displays clinical symptoms of ALS and motor neuron death[31]. Its B6 version displays a spectrum of ALS-associated phenotypes similar to that of the original B6SJL hybrid, but with an ~30d later age of onset and an average lifespan of ~157 d. The B6.SOD1 mice were crossed with *Axl*$^{-/-}$ and/or *Axl*$^{-/-}$*Mertk*$^{-/-}$ lines to generate SOD1 *Axl*$^{-/-}$ and SOD1 *Axl*$^{-/-}$ *Mertk*$^{-/-}$ mice. All lines have been backcrossed for >10 generations to and maintained on a C57BL/6 background. All animal procedures were conducted according to protocols approved by the Salk Institute Animal Care and Use Committee (Protocol No. 17-00009). Mice of both genders were randomly allocated to experimental groups unless otherwise noted.

Tail suspension behavior scoring

To objectively score the severity of ALS disease phenotype for SOD1 transgenic mice, we have modified the 5-point phenotype scoring system of Solomon et al.[33] to monitor disease progression. Briefly, score 1 = shaking or splaying of both hindlimbs when suspended by tail (symptomatic phase) while score 0 represents time prior to appearance of symptomatic phase; score 2= unable to extend of both hindlimbs and/or changes for gait in two days in a row (disease onset); 3= minimal joint movement in show of extreme weakness or paralysis in both hind limbs; score 4 or end point (E.P.) = mouse unable to right to sternum after being placed on its side for more than 20 seconds.

Histology and immunohistochemistry

Mice at day 80, day 120 and day 160 were routinely anesthetized with ketamine/xylazine and perfused with 4% PFA in PBS as described in Chapter 2.2. Spinal cords were dissected out under a dissection microscope, separated into cervical, thoracic and lumbar segments and post-fixed in 4% PFA in PBS solution overnight before switching to 30% sucrose in PBS for 1 day and flash frozen in TBS tissue freezing medium. Cross-sections of cords were cryo-sectioned at 25μm, air-dried overnight before staining. For lumbar motor neuron quantification, spinal cord cross-sections were evaluated for at least 3 sections per spinal cord level that contain at least 6 ventral horns per animal. Immunohistochemistry procedures were previously described in section 2.2.

RT-qPCR

RNA from snap-frozen whole spinal cord tissue was isolated with TRIzol (Thermo Fisher Scientific 15596026) according to the manufacturer's instructions and following the procedure listed in Ch 2.2. The following primer sequences were used:

TNFα primer sequences used were forward primer 5'-3' GCC ACC ACG CTC TTC TGT CT and reverse primer 5'-3' CAG CTG CTC CTC CAC TTG GT.

IFNα4 forward primer 5'-3' CCC ACA GCC CAG AGA GTG AC and reverse primer 5'-3' GCC CTC TTG TTC CCG AGG T.

IL-6 forward primer AGA CAA AGC CAG AGT CCT TCA GA and reverse primer 5'-3' GCC ACT CCT TCT GTG ACT CCA.

IL-1β forward primer 5'-3' CCT CTC CAG CCA AGC TTC C reverse primer 5'-3' CTCA TCA GGA CAG CCC AGG T.

IFNγ forward primer CAA TCA GGC CAT CAG CAA CA and reverse primer 5'-3' AAC AGC TGG TGG ACC ACT CG.

IL-4 forward primer 5'-3' AGGAGCCATATCCACGGATGCGA and reverse primer 5'-3' TGTTCTTCGTTGCTGTGAGGACGT.

Relative expression of genes of interest was normalized to GAPDH with forward sequence 5'-3' AGG TCG GTG TGA ACG GAT TTG and reverse sequence 5'-3' GGG GTC GTT GAT GGC AAC.

Immunoblot analysis

Tissues were 'snap frozen' in liquid nitrogen. Frozen tissues were lysed using RIPA buffer and phosphatase protease inhibitor (Roche, Sigma) for 30min on ice. Supernatants were stored at −80°C after samples were spun down at 12 000rpm for 5min. Immunoblotting followed previously a published protocol[34]. Briefly, equal amounts of protein (10ug) in 3XLaemmli buffer and 0.1M DTT were separated by electrophoresis through 4-12% Bis-Tris polyacrylamide gels (Novex, Life Technologies) and were transferred to PVDF membranes. Membranes were blocked with blocking buffer (1% casein block in PBS) (Biorad) and subsequently incubated with primary and secondary antibodies and washed with TBST (50mM Tris-HCl pH7.5, 0.15M NaCl and 0.25% Tween-20) in between. Blots were developed using an Odyssey Gel Imaging System (Li-Cor). Immunoblot were quantified using ImageStudio using GAPDH and beta-actin as loading control.

Antibodies and reagents

For immunohistochemistry, antibodies used were as follows: anti-Axl (R&D AF854), anti-Mer (eBioscience DS5MMER and R&D AF591), anti-mouse Gas6 (R&D AF986), anti-misfolded human mutant SOD1 B8H10 (misSOD1) (Medilabs MM-0070-P), anti-MMP9 (Abcam Ab38898), anti-NeuN (Chemicon MAB377), anti-Iba1 (Wako 019-19741 and Novus NB100-1028), anti-CD68 (BioRad MCA1957), anti-Tmem119 (Abcam AB209064), anti-cleaved Casp3 (cCasp3) (Cell Signaling 9661), anti-Choline-Acetyl Transferase (ChAT) (Millipore AB1444P). Same fluorophore-conjugated antibodies were used as described in Ch 2.2. For immunoblotting, additional antibodies besides those listed above are anti-GAPDH (Millipore MAB374) and anti-beta-actin (Li-Cor 926-42210), both used as loading control. For Li-Cor detection, IRDye 680RG IgG secondary antibodies of the corresponding species were used.

Confocal microscopy

Confocal images of ventral horn or tilescan of lumbar spinal cord were acquired with a Zeiss LSM 710 Confocal microscope using Plan-Apochromat 20x 0.8-NA air-matched or 63x 1.4-NA oil objectives (laser lines: 405 nm, 488nm, 594nm and 633nm). Image size was 1024 x 1024 pixels. Images were obtained and processed via the Zen Black and Zen Blue editions.

Data analysis

For lumbar spinal cord sections, maximum intensity projection images were analyzed in FIJI. At least 3 sections containing 6 ventral horns per lumbar spinal cord level per animal were quantified in each analysis. At least 3 animals per genotype at each disease stage were used in each analysis. Cross sections from lumbar level L4-L5 were pooled for Iba1 and CD68 expression analysis. Both were calculated as the quotient of their respective occupied area

divided by area of ventral horn, which were gated based on their intensity and applied for all images in each experiment. For motor neuron and subtypes quantification analysis, lumbar spinal cord between L1-2 and L3-5 were quantified separately and in both lateral and medial motor columns. Co-localization of ChAT, NeuN and MMP9, markers for generic motor neurons, alpha motor neurons and fast-fatigable motor neurons that are to susceptible to ALS, respectively.

Statistics

Data analysis and statistical tests were performed using GraphPad Prism (version 8.0) software. All data in all figure panels of the paper are represented as mean ±1 standard deviation. In most cases, ‘‘n’’ is used to denote the number of mice per experimental group and ‘‘N’’ the number of brain sections/images/samples analyzed per mouse. Datasets displayed normal distribution and equal standard deviations unless indicated by unequal variance test.

3.3 Results

3.3.1 Characterization of microglial response and TAM system expression along the disease progression in the SOD1 mice

We first initiated studies of TAM system regulation in microglia during disease progression in the SOD1 mouse model for ALS, where we have adopted a multi-point phenotype scoring system of Solomon et al.[33] to monitor disease progression. As for human AD[35-38] and mouse models of PD[20] and AD[29] (Chapter 2), we again observed dramatic up-regulation of TAM expression in sick *SOD1* mice (**Fig. 3.3.1-1**). Increased Mer and Axl expression is strong enough to be detected easily on western blots of cervical, thoracic, and lumbar spinal cord extracts from *SOD1* mice, at both disease stage 3 (extreme weakness in both hind limbs/minimal joint movement) and at end point (E.P., mouse unable to right to sternum after being placed on its side), as well as in SOD1 brain lysates. This suggests a strong pan-induction of TAMs across the CNS at late and end stage of disease, even in regions of only mild degeneration such as the thoracic portion of the spinal cord.

We further investigated the onset and extent of TAM expression upregulation in whole spinal cord during ALS disease development at progressive disease stages or at various timepoints, postnatal (P) 80, P120 and P160 as well as at end point (**Fig. 3.3.1-2a & b**, respectively). These results suggest that TAM receptors – Axl and Mer – are both expressed at steady state in mouse spinal cord, however, their expression upregulation precedes the symptomatic stage of the disease (score 1, hind limb trembling) - typically between P80 and P120 - and this robust increase of expression for both TAM receptors persists throughout the disease course. Interestingly, we also found that the ligand of both Axl and Mer receptors, Gas6, also acquires increasingly higher expression in ALS lumbar spinal cord after symptomatic phase (score 1) but before score 2, and further peaks at E.P. (Fig. 3.3.1 -2b). In line with the knowledge in the field that long before symptoms appear,

immune dysregulation is tied with the pathogenesis of ALS[39], we find that the TAM system is involved early and persistently throughout the disease progression.

We next investigated the cellular specificity and spatial distribution of these TAM receptors and their ligand Gas6. We examined these questions at score 3 of SOD1 mice, a timepoint with extensive upregulation of TAM receptors and their ligand Gas6 expression and corresponding to complete hindlimb paralysis. Immunostaining of sections from lumbar spinal cord demonstrated that essentially all Axl upregulation occurred in Iba1-labeled microglia, and nearly all Iba1 positive cells were also Axl positive (**Fig. 3.3.1-3a,b**). Similarly, despite a high basal level of expression, robust Mer expression also was seen exclusively in Iba1+ cells, suggesting that an elevated TAM receptor response was restricted to microglia (**Fig. 3.3.1-3c**). Upon further examination, we noticed overall more heightened Iba1 expression in the ventral horn than that of in the dorsal horn. These Iba1-high microglia assumed a typical activated morphology with enlarged cell body and few ramified processes and were distributed near ChAT+ MNs. We found higher TAM expression in these activated Iba1+ cells in the ventral horn (Fig. 3.3.1-3a-c). Interestingly, Gas6, the obligate Axl ligand, only partially co-localized with Iba1 and Axl+ microglia in the diseased cord. These $Axl^{hi}Iba1^{hi}$ activated microglia were usually found in immediate proximity to these unique Gas6-positive puncta (**Fig. 3.3.1-3d**). Although the exact cellular identity of these other Gas6-expressing cells is yet to be identified, they may be stressed/apoptotic MNs that have externalized PtdSer, a co-ligand of TAM receptors, and are thus coated with Gas6 on their surfaces. Section 3.3.5 will elaborate further with this working hypothesis.

3.3.2 Functional role of TAMs in disease progression of ALS

To evaluate whether ALS disease progression is altered by the lack of TAM receptors, we crossed SOD1 mice with *Axl*$^{-/-}$*Mertk*$^{-/-}$ mice to determine overall impact of microglial TAMs on disease course. We also crossed the SOD1 mice with single *Axl*$^{-/-}$ mice to determine contribution of Axl receptor alone. We have characterized the entire disease course using unbiased cohort behavioral scoring, and have investigated changes in immune dysregulation, microgliosis, phagocytic response, and survival of MNs and their subtypes at various timepoints of ALS development.

Involvement of TAMs in ALS disease course

To assess potential alternation at the onset of disease stages, we monitored the clinical score on a tri-weekly basis in cohorts of SOD1, SOD1 *Axl*$^{-/-}$ and SOD1 *Axl*$^{-/-}$*Mertk*$^{-/-}$ mice**.** Following the objective scoring system by Solomon et al.[33] for disease progression, we found that SOD1 mice on B6 background in our hands, reached symptomatic phase (clinical score 1) around day 110, disease onset (clinical score 2) around day 140, and clinical end point (E.P. or score 4) on average at day 154 (**Fig. 3.3.2-1a**), which is consistent with published results on for SOD1^{G93A} mice on B6 background [30,40]. Through preliminary studies, we also found no significant difference between genders in terms of latency to reach each disease stage (**Fig. 3.3.2-1b**), so for all behavioral testing based on tail suspension motor symptoms, cohorts with equal percentage of both sexes were studied and compared.

Interestingly, SOD1 *Axl*$^{-/-}$*Mertk*$^{-/-}$ mice showed a very different course of disease progression (**Fig. 3.3.2-2**). Initially, these *Axl*$^{-/-}$*Mertk*$^{-/-}$ mutant SOD1 mice displayed a significantly earlier occurrence of the symptomatic phase (clinical score 1, SOD1 mice 109.6

± 16.55 days; SOD1 *Axl*$^{-/-}$*Mertk*$^{-/-}$ 81.87 ± 9.325 days, p<0.0001, **Fig. 3.3.2-3a**), and also showed a slightly more rapid disease progression period until reaching disease onset (clinical score 2, SOD1 mice 138.9 ± 12.01 days, SOD1 *Axl*$^{-/-}$*Mertk*$^{-/-}$ 128.2 ± 17.52 days, p=0.0006, **Fig. 3.3.2-3b**). However, at later stages of the disease, mutant *Axl*$^{-/-}$*Mertk*$^{-/-}$ SOD1 mice showed a trend of delayed onset of clinical score 3 and a significantly late arrival at end stage in comparison to SOD1 mice (for score 3, SOD1 mice 154.3 ± 12.84 days, SOD1 *Axl*$^{-/-}$ *Mertk*$^{-/-}$ 163.8 ± 12.44 days, p = 0.0516. And for E.P., SOD1 mice 154.7 ± 13.66 days, SOD1 *Axl*$^{-/-}$*Mertk*$^{-/-}$ 178.2 ± 13.12 days, p < 0.0001, **Fig. 3.3.2-3c**,**d**). Consequently, despite showing earlier motor symptoms, SOD1 *Axl*$^{-/-}$*Mertk*$^{-/-}$ mice have a mean extension of life span by ~15% compared to SOD1 mice. They also displayed an almost twice as prolonged mean length of disease course, from symptomatic phase to E.P., compared to the SOD1 mice (Fig. 3.3.2-3d).

Of note, SOD1 mice that are only deficient of Axl receptor (SOD1 *Axl*$^{-/-}$) demonstrate a latency to E.P. that falls in between that of SOD1 *Axl*$^{-/-}$*Mertk*$^{-/-}$ and SOD1 cohorts (SOD1 *Axl*$^{-/-}$ mice 163.7 ± 10.12 days; SOD1 mice 154.7 ± 13.66 days; SOD1 *Axl*$^{-/-}$*Mertk*$^{-/-}$ 178.2 ± 13.12 days. Log-rank tests, p = 0.0188 between SOD1 and SOD1 *Axl*$^{-/-}$ curves; p = 0.0004 between SOD1 *Axl*$^{-/-}$*Mertk*$^{-/-}$ and SOD1 *Axl*$^{-/-}$ curves) (Fig. 3.3.2-3d). It is noteworthy that these SOD1 *Axl*$^{-/-}$ mice also show a modest advancement of symptomatic phase compared to SOD1 mice, although to significantly less extent than that in SOD1 *Axl*$^{-/-}$*Mertk*$^{-/-}$ mice. This indicates that Axl alone, which has been implicated as one of the top upregulated signature gene in 'disease associated microglia' and prominent 'neurodegenerative genes'[41], cannot fully account for the alteration of disease course phenotype seen in SOD1 mice lacking both Axl and Mer, suggesting a synergistic effect of both TAM receptors in restraining disease onset and contributing to its progression.

These confounding but intriguing observations demonstrate that TAM receptors may play differential roles at different stages of the disease – initial upregulation of TAM receptors seen in Fig. 3.3.1-1 prior to score 1 and 2 may act to constrain and protect against the onset of motor symptoms such as loss of fine motor control and splaying of hindlimbs. However at later stages, the chronically high expression of Axl and Mer may be related to detrimental mechanisms that accelerate the worsening of paralysis and deterioration of the organisms. Further investigation with SOD1^{G93A} *Mertk*$^{-/-}$ mice is warranted to confirm the role of Mer in ALS onset and progression.

TAM activity in early stage of ALS

Next, we set out to investigate the mechanistic basis for altered disease course in SOD1 *Axl*$^{-/-}$*Mertk*$^{-/-}$ mice. We asked whether deficiency of TAM receptors may result in differential composition of motor neurons and preferentially affect ALS-susceptible MN subpopulation such as FF alpha MNs. If so, this may account for the advancement of earlier onset of motor weakness -- hindlimb splaying (clinical score 1) and gait changes among others (score 2) -- observed in TAM-deficient mice compared to SOD1 mice.

In order to profile and quantify MN number and the ALS-susceptible FF MN subpopulation, we performed immunohistochemistry using combinations of antibodies for choline acetyl transferase (ChAT), NeuN[42,43] and MMP9[4,44,45] for co-labeling the cell bodies of MNs, alpha MNs and FF alpha MNs, respectively. Lumbar spinal cord sections were matched and selected from SOD1 mice collected at day 80, prior to symptomatic phase (score 1), in comparison to SOD1 *Axl*$^{-/-}$*Mertk*$^{-/-}$ mice at the same age. Both motor pools in

lumbar spinal cord, lateral motor column (LMC) and medial motor column (MMC), were analyzed but only data from LMC is shown (**Fig. 3.3.2-4**) since in our hands majority of MMP9+ cells are present in the LMC. Data from lumbar L1-2 and L3-5 were separated due to differential number of MNs at these levels (**Fig. 3.3.2-4b-c and -4e-g**). Firstly, we found that at day 80, although there was a trend toward fewer ChAT+ cells at both L1-2 and L3-5 in SOD1 mice, there was no statistical difference in the total number of ChAT + cells in the ventral horn (VH) among WT, SOD1, and SOD1 *Axl*$^{-/-}$*Mertk*$^{-/-}$ mice (Fig. 3.3.2-4b, 4d), suggesting that a severe loss of MN soma was absent at this age. When co-labeling with NeuN as a marker for mature alpha MNs, however, we saw a statistically significant, albeit modest, decrease in the number of ChAT+NeuN+ MNs in the VH from L3-5 specifically in the SOD1 *Axl*$^{-/-}$*Mertk*$^{-/-}$ group compared to SOD1 group (Fig. 3.3.2-4c, 4e). This suggests that a potential loss of function of mature alpha MNs or even their death, occurred in TAM-deficient mice already at day 80, an age when motor symptoms such as hindlimb trembling are absent in SOD1 mice but are present in almost 50% of SOD1 animals. Next, we focused on the VH in L3-5 for quantifying MMP9-expressing alpha MNs. Co-immunoreactivity analyses of MMP9, NeuN, and ChAT revealed that the SOD1 spinal cord also showed a trend of decrease in the number of triple positive cells (MMP9+ChAT+NeuN+) compared to WT and SOD1 mice (Fig. 3.3.2-4f). These results suggest that TAM deficiency in microglia may trigger an acceleration of the degeneration of ALS-vulnerable FF alpha MNs already at day 80, worsening the denervation of the fast-fatigable muscle groups. However, since the total number of ChAT+ MN was unchanged (Fig. 3.3.2-4b, 4d, 4g), whether the specific decrease in the number and percentage of MMP9+ and NeuN+ MN population in TAM-mutant spinal cords was due to a downregulation of MMP9 and NeuN expression in MNs or an early onset of death of these MNs (Fig. 3.3.2-4e and 4f) is still to be evaluated.

To follow up, we next investigated how TAM-deficiency can result in a specific reduction of the ALS-vulnerable FF alpha MNs subpopulation. Given the immunosuppressive role of TAM receptors in DCs and macrophages and the strong upregulation of microglial TAM expression in late-stage disease (Fig. 3.3.1-1 and 3.3.1-2), we hypothesized that microglial TAM receptors might regulate the neuroinflammation that arises prior to the symptomatic phase of ALS. If so, a loss of TAM receptors in these crucial disease-activated microglia might result in uncontrolled cytokine and chemokine dysregulation and an exacerbated pro-inflammatory environment already at day 80 in *Axl*$^{-/-}$ *Mertk*$^{-/-}$*SOD1*$^{G93A+}$ compound mutants. We performed RT-qPCR on mRNA extracted from whole spinal cord from SOD1 and SOD1 *Axl*$^{-/-}$*Mertk*$^{-/-}$ and their non-diseased littermates at day 80 for a battery of pro- and anti-inflammatory cytokines and agents and quantified their mRNA relative expression (**Fig. 3.3.2-5**). Contrary to our hypothesis, we did not find any statistically significant difference from whole spinal cord extracts among the above-mentioned genotypes in any of the cytokine mRNAs tested. Though we do not exclude the possibility that subtle or regional changes in cytokine production by local microglia with and without TAMs may have been overshadowed by the coarse whole-tissue mRNA extraction in the initial stage (day 80), dramatic changes in the expression of certain cytokines in later stages of disease (day 120 and 160), such as TNF-α and IL-1β, are after all detectable in whole tissues (Fig. 3.3.2-6).

TAM activity at late stages of disease

We next aimed to study how the absence of TAMs confers a delay in the mice reaching clinical end stage and thereby prolonging their lifespan. We first evaluated inflammatory responses in spinal cord by measuring the expression of a battery of cytokine mRNAs using RT-qPCR during disease development, both after symptomatic stage (day 120) and at late stage (day 160) in terms of SOD1 mice disease course. In accordance with

published results, the main neuroinflammatory agents in SOD1 transgenic mice, TNF-α and IL-1β, present a trend of increasing expression at day 120 and are dramatically upregulated at the end stage of disease (day 160) compared with their WT littermates (**Fig. 3.3.2-6**). Surprisingly, despite a well-described immunosuppressive role of TAMs as negative feedback inhibitors of Toll-like and cytokine receptor signaling in other immune sentinels following immune activation[25-27], at late stage of disease (day 160) in SOD1 mice, we found instead that SOD1 *Axl*$^{-/-}$*Mertk*$^{-/-}$ mice have significantly, albeit modestly, lower level of specifically TNF-α expression comparing to SOD1 mice at this same age. To note, we did not observe a change in type I IFN response measured by expression level of IFNα (Fig. 3.3.2-6), which TAM receptors are known to suppress in antigen presenting cells such as DCs[27], at either time points during the chronic neuroinflammation in SOD1 mice lacking TAM receptors. As paralysis, along with other aspects of the disease, is less progressed in these SOD1 *Axl*$^{-/-}$*Mertk*$^{-/-}$ compared to SOD1 mice that have survived to day 160, investigation is underway to find out whether this decreased TNF-α expression at day 160 in TAM-mutant spinal cord is causal to the delayed E.P. phenotype or is a mere reflection of the stage of disease progression.

We then asked whether this altered inflammatory environment in TAM-mutant SOD1 mice at day 160 indicates an altered microglial activation and response towards pathology. For this, we first characterized the microglial activation state by performing immunostaining on spinal cord sections that contain L4-5 from SOD1 and SOD1 *Axl*$^{-/-}$*Mertk*$^{-/-}$ mice at day 160 since this is the age not only with a more robust inflammatory response but also with a fair enough portion of SOD1 mice still alive (though morbid). We quantified the percent area occupied by Iba1 in the VH area (**Fig. 3.3.2-7a**). As expected, both SOD1 and SOD1 *Axl*$^{-/-}$ *Mertk*$^{-/-}$ mice spinal cords compared with their non-transgenic littermates, showed a robust

increase in Iba1-occupied area and number of Iba1+ cells that display the characteristic activated 'amoeboid' morphology, as opposed to the 'resting'-like ramified morphology at physiological conditions. To note, Iba1 area and microglia morphology do not show a baseline difference in WT and *Axl*$^{-/-}$*Mertk*$^{-/-}$ spinal cord in non-diseased setting (Fig. 3.3.2-7a). However, we found SOD1 *Axl*$^{-/-}$*Mertk*$^{-/-}$ mice have notably less Iba1 coverage comparing to the SOD1 mice at day 160, indicating lower microglia activation, proliferation and/or other myeloid cell infiltration, which is consistent with our cytokine expression analysis at the same age (Fig. 3.3.2-6). Furthermore, co-localization analysis of the immunoreactivity of Iba1 and CD68, a marker of lysosomes specific to microglia, shows a markedly lower level of CD68 occupied area in VH of SOD1 *Axl*$^{-/-}$*Mertk*$^{-/-}$ mice in comparison to SOD1 mice at day 160 (**Fig. 3.3.2-7b**).

These results suggest that, in addition to the reduction of microglial activation that may contribute to the modestly ameliorated pro-inflammatory environment observed in SOD1 *Axl*$^{-/-}$*Mertk*$^{-/-}$ mice at late stage, microglia in SOD1 *Axl*$^{-/-}$*Mertk*$^{-/-}$ mice also present with a reduction of phagocytic capacity as indicated by a reduction of CD68 immunoreactivity. Based on these findings, we subsequently evaluated the severity of motor neuron degeneration in SOD1 mice at late stage (day 160). As TAM receptor/ligand activation is dependent on the regulated display of externalized PtdSer[46,47], we reasoned that microglia that are *Axl*$^{-/-}$*Mertk*$^{-/-}$ would have impaired detection of PtdSer and clearance of these target cells. Interestingly, recent studies have uncovered various PtdSer exposure events in a non-apoptotic manner[56-58], subjecting them to be 'eaten alive' in challenging settings, a process that can be dependent on TAM receptors. In the case of ALS, this loss of TAMs in SOD1 mice may spare some stressed PtdSer-displaying but still living MNs at late stage, which would be consistent with the delayed latency to reach E.P. phenotype observed in TAM-

mutant SOD1 mice (Fig. 3.3.2-2). To test this hypothesis, we again assessed the number and percentage of MNs, alpha MNs and the most ALS-susceptible FF alpha MNs by labeling and co-labeling with ChAT, NeuN and MMP9, respectively. We showed that on L1-2 for both LMC and MMC, there is a reduction in the number of total ChAT+ cells and in NeuN+ ChAT+ co-labeled alpha MNs in SOD1 and SOD1 *Axl*$^{-/-}$*Mertk*$^{-/-}$ compared to WT (**Fig. 3.3.2-8a-c**), but no difference was detected between the two transgenic groups. On level L3-5 for LMC specifically where large alpha MN soma are abundant physiologically, we did see a significant though modest restoration of both ChAT+ and ChAT+NeuN+ co-labeled cell number in SOD1 *Axl*$^{-/-}$*Mertk*$^{-/-}$ mice compared to SOD1 mice (**Fig. 3.3.2-8e-f**). Similarly, for the number of MMP9+ FF alpha MNs, we saw a consistent though minor rescue of the number of MMP9+ NeuN+ ChAT+ (triple+) cells in SOD1 *Axl*$^{-/-}$*Mertk*$^{-/-}$ compared to SOD1 mice (**Fig.3.3.2-8g**). Considering the fact that SOD1 *Axl*$^{-/-}$*Mertk*$^{-/-}$ mice have an almost twice longer disease course and an early loss of MMP9+ ALS-susceptible MNs compared to SOD1 mice (Fig. 3.3.2-4g), the rate of MN loss was dramatically diminished in TAM-mutant SOD1 mice. These results suggest that TAM-mediated phagocytosis partially contributes to MN loss and faster neurodegeneration.

3.4 Conclusion

Taken together, our results indicate that TAM receptors Axl and Mer are crucially involved in the pathogenesis of ALS. We found that both receptors, together with their ligand Gas6, are upregulated in the spinal cord of SOD1 mice prior to disease onset, which persists and peaks at end-stage. High-resolution confocal analysis showed that Axl and Mer are located exclusively in microglia. Interestingly, we found that TAMs play differential roles at early and late stages of ALS. Whole body genetic knockout of Axl and Mer resulted in an earlier occurrence of symptomatic phase but significantly slowed the loss of motor function and prolonged the lifespan in $SOD1^{G93A}$ mice. We have not fully explored the mechanistic basis of such a dramatic alteration in the disease course due to TAM deficiency, but observations suggest that it may be related to the previously described TAM-mediated phagocytosis in microglia and other tissue macrophages [20,34,48]. We showed that both Iba1 and CD68, a macrophage-specific phagocytic marker, are expressed at a lower level in the absence of TAMs at late stage, suggesting a dampening of aberrant activation and phagocytic capacity in these TAM-mutant myeloid populations in the spinal cord. Correspondingly, we detected diminished expression of TNF-α, known to contribute to MN excitotoxicity and to drive the worsening of ALS, which suggests an ameliorated pro-inflammatory environment in spinal cord of SOD1 $Axl^{-/-}Mertk^{-/-}$ mice compared to SOD1 mice. Consistent with these findings, despite showing an initial loss of ALS-vulnerable MNs, TAM-mutant mice show a comparatively much slower rate of MN degeneration until the late stage compared to that in SOD1 mice expressing TAMs.

Despite many efforts in drug development and clinical trials for the past 20 years, ALS remains uniformly intractable, irreversible, and fatal. We lack therapeutic targets that are accessible in the CNS and whose mode of action is understood. Importantly, our findings

suggest the TAMs may be such targets with translatable potential. As small-molecule and monoclonal antibody inhibitors of TAM receptors are already in clinical trials as cancer therapeutics[49-53] and readily cross the BBB[53], our findings may provide insights into TAM receptors as therapeutic targets whose perturbation may extend the lifespan of ALS patients.

3.5 Discussion and Future Directions

I. Glutamate-mediate excitotoxicity-induced PtdSer exposure as a potential mechanism of TAM-mediated phagocytosis of ALS-vulnerable MNs

TAM receptors, expressed at high abundance by professional phagocytes, have been shown to be critical for the clearance of PtdSer-externalized ACs in multiple tissues[22,34,54,55]. This process is critically mediated by the bridging of TAM ligands, Gas6 and Pros1, between membranes with externalized PtdSer and TAM receptors expressed by phagocytes (Fig. 1.2-2). Interestingly, recent studies have uncovered various PtdSer exposure events in a non-apoptotic manner[56-58]. Besides ACs, distressed but nonetheless living cells may also present externalized PtdSer on surface, subjecting them to be 'eaten alive' in challenging settings, such as adult neurogenesis, viral-infected astrocytes, or in stroke-induced penumbra[20,59,60]. This is a process that has been termed 'phagoptosis' in which TAM-dependent phagocytosis has been recognized to be responsible for the clearance of these non-apoptotic PtdSer-presenting cells. In addition, synapse-localized exposed PtdSer is found in a more transient manner during synaptic pruning and elimination[61-63]. One of the main components in the regulatory machinery of PtdSer asymmetry is through Ca^{2+}-dependent scramblases[48,59,64]. Conceivably, an abnormally high intracellular calcium concentration due to excessive firing could theoretically induce exposure of PtdSer on MNs or locally at neuromuscular junctions (NMJs) in events of glutamate-mediated excitotoxicity in ALS.

Together with our results, our current working hypothesis is as follows (**Fig. 3.3.3-1**): in SOD1 mice, an abnormally heightened intracellular Ca^{2+} as a result of excitotoxicity in Ca^{2+}-sensitive FF alpha MNs may trigger an increased externalization of the 'eat-me' signal PtdSer locally at NMJs and/or on MN cell bodies in the VH. In recognition of exposed PtdSer,

TAM ligands, such as Gas6, may tag these cells and their processes, surrendering them to be phagocytosed 'live' or at least preemptively before their apoptosis by TAM-expressing microglia. This may cause a selective loss of Ca^{2+} dysregulation-prone MNs and dissociation of NMJs (the separation of the terminal Schwann cells and motor axon from the motor endplate of the muscle) followed by subsequent axonal dieback and muscle denervation. Our studies in late stage are consistent with this hypothesis. Firstly, we found that Gas6 expression does not co-localize completely with Axl in SOD1 cord but these non-colocalizing Gas6 surfaces, though entities non yet defined, are very often adjacent to Axl-expressing Iba1+ cells (Fig. 3.3.1-3d). We would like to examine further whether such phenomenon suggests an interaction between stressed PtdSer-exposing MNs coated with the TAM ligand Gas6 and TAM-expressing microglia in ALS spinal cord. Secondly, at late stage SOD1 *Axl*$^{-/-}$ *Mertk*$^{-/-}$ mice have reduced level of TNF-α expression (Fig. 3.3.2-6) possibly due to a decreased microglial activation (Fig. 3.3.2-7), and a more benign microenvironment that may ameliorate calcium dysregulation in MNs comparing to SOD1 mice. Moreover, TAM-deficient microglia, blind from PtdSer externalized on MNs, indeed show a reduction phagocytic capacity (Fig. 3.3.2-7). Converging evidence suggest a TAM absence results in microglia with inefficient 'phagoptosis' and a delay in the eventual death of these alpha motor neurons as a consequence (Fig. 3.3.2-8). Altogether this promotes preservation of some basic motor function of ALS mice and contributes to the extension the lifespan of SOD1 mice in the absence of Axl and Mer (Fig. 3.3.2-2).

II. Investigation of TAM activity in inflammatory response and skeletal muscle denervation in the periphery

We will be continuing our endeavors in searching for a full mechanistic basis for the above-mentioned selectively early loss of markers for FF alpha MNs (Fig. 3.3.2-4e,f) and the foreshown hindlimb weaknesses (Fig. 3.3.2-2a) in TAM-mutant SOD1 mice. One lead for us is to pin down other potential localities of TAM action at this stage of disease besides in the CNS. As TAMs are expressed in almost all tissue resident macrophages[23,24], we speculate a role for TAMs in the peripheral nervous system that includes the intramuscular nerves, the NMJs, and the skeletal muscles, regulating the progressive motor denervation in ALS.

Studies demonstrate an early peripheral inflammatory response and macrophage activation near NMJs that persist throughout ALS disease course[65-67]. This peripheral response coincides with NMJ dissociation and skeletal muscle denervation that may precede symptom onset in ALS rodent models and human patients, though whether these macrophages play a protective/resolving or detrimental role remains unclear[68 69]. Given the concomitant functions of TAMs in mediating phagocytosis and pleiotropic immunosuppression in numerous tissue resident macrophages, we speculate that TAM-expressing resident macrophages near NMJs play a pivotal but similarly divergent role at different stages of disease: restraining local inflammation in the early stage of the disease and dutifully clearing degenerating overexcited NMJs as disease progresses, thereby accelerating loss of motor function in later stage of disease. We will evaluate this possibility experimentally.

III. On TAM-mediated selective loss of MMP9 expression in the spinal cord at early stage

Our results on ALS-vulnerable cells in the spinal cord (Fig. 3.3.2-4) suggest that while the total ChAT+ cell number are unchanged, a selective loss of MMP9/NeuN/ChAT (triple positive) cell number is reduced in TAM-mutant SOD1 mice at pre-symptomatic phase. It is unclear if this is a reflection of simple downregulation of MMP9 in alpha MNs or whether this signifies an early death of this subset of ALS-vulnerable cells already at this stage. Of note, Kaplan et al.[4] found that in the presence of mutant SOD1, MMP-9 expressed by fast motor neurons themselves enhances activation of ER stress and is sufficient to trigger axonal die-back and death of these alpha MNs. Further studies from C. Henderson group[4] and V. Lee group[70], using multiple mouse models of ALS with different genetic predispositions and various targeting strategies, uncover that downregulation or inactivation of MMP9 can not only improve motor symptoms but also lengthen the average life span of these mice. We are now curious whether microglial TAMs play a role in regulating neuronal MMP9 expression and therefore, the loss of TAM mediating a downregulation of MMP9 in response to misfolded SOD1 as a MN-intrinsic self-preservation mechanism for longer survival of this ALS-susceptible subset and of the diseased organism.

IV. Caveats

One caveat to our studies concerns the cell type specificity of TAM receptors. In the CNS, we and others have shown that besides microglia, TAMs are also expressed on brain microvascular endothelial cells (BMECs)[71]. Brain endothelial Mer is particularly important for maintenance of blood brain barrier (BBB) integrity, especially upon pathological challenge such as viral infection. ALS concerns both upper motor neurons, the majority of which are in the motor cortex and brain stem, as well as lower motor neurons whose cell bodies dwell in the ventral horns of the cervical and lumbar spinal cord. Numerous studies have shown

impairment of BBB and blood spinal cord barrier (BSCB) in SOD1 mouse models[72-74] and patients [75,76], including signs of IgG deposition and increased leukocyte infiltration into the CNS. Thus, how much the phenotypes described above are the result of a leaky blood-brain barrier in the absence of TAMs rather than microglial TAMs alone needs to be further investigated. In the peripheral nervous system, Axl and Mer are also expressed by Schwann cells, a subset of which, the perisynaptic Schwann cells, makes up the tripartite synapse of NMJs. Though Brosius Lutz et al.[77] showed both Axl and Mer mediate myelin clearance by Schwann cells after CNS axotomy, we have no knowledge of whether Axl and Mer are similarly expressed in perisynaptic Schwann cells and their role in maintaining integrity of NMJs, especially in neurodegenerative disease settings. Moreover, reports suggest that apart from microglia, infiltrating blood-derived monocytes, which may also be TAM expressing, may contribute to neuroinflammation and worsening of disease[78]. Our current study is not optimized for discerning these two myeloid populations. We have speculated that the majority of TAM action in the SOD1 ALS model occurs in microglia at least in the CNS. To delineate the role of microglial TAMs (or rather, myeloid TAMs) in ALS pathogenesis, we have generated floxed alleles of Axl and Mer on the SOD1 animal model, and plan to cross them with tamoxifen-inducible cell type-specific driver, including the Cx3cr1-Cre^{ERT} line for myeloid cell-specific deletion[79]and VECadh5-Cre^{ERT} line for endothelial-specific deletion[80]. One of the beauties of this setup is that we can achieve conditionally inactivation of the *Mertk* and *Axl* genes in only one population at different stages of disease, e.g. prior to symptomatic onset and at later stage, and thus attempt to differentiate the dual action of TAMs along the disease course on top of cell type-specific ablation of TAMs. Since lineage tracing studies showed muscle resident macrophages originate from both yolk-sac and bone-marrow[81], we plan to re-treat the mice with tamoxifen every month since the start point in order to maintain a stable knockdown of TAMs.

A second caveat is that our studies are only conducted on the SOD1^{G93A} mouse model of ALS. We chose this model because SOD1^{G93A} was the first ALS mouse model established[30] is by far the most frequently used model for in vivo experiments. Its disease course is stable with low variance on the B6 background. However, mutations in SOD1 are not the most represented in ALS patients: only 20% of familial and 1% of sporadic patients carry SOD1 mutations[10]. Therefore, results in mutant SOD1 transgenic mice may not exactly be translatable to human disease, which may underlie the failure of several ALS clinical trials predicated on results obtained in this model[10,82]. Other ALS mouse models that involve mutations in more pathologically prevalent genes, such as mice that present cytoplasmic accumulation of TDP43 (rNLS8, JAX number: 028412)[83] must be evaluated.

Finally, besides the above-listed future directions, we will also use pharmacological methods to validate the motor symptom findings in corroboration with our genetic knockout animals. We will treat SOD1 with a Mer inhibitor, UNC2025 [53], in SOD1 mice both before (day 60 onwards) and after disease onset (day 100 onwards). We expect after-onset inhibitor-treated SOD1 mice to develop motor symptoms the same time as vehicle-treated control mice but have delayed disease progression and extended life span similar to or even longer than SOD1 *Axl*$^{-/-}$ *Mertk*$^{-/-}$ mice. Outcome from our studies would suggest the optimal window and strategy to treat ALS mice, and perhaps also ALS patients, with TAM inhibitors.

3.6 Acknowledgements

Chapter 3, in part, is currently being prepared for submission for publication of the material. The working citation is: **Huang, Y** and Lemke, G. TAM receptors are crucial mediators of ALS pathology. The dissertation author was a primary investigator and the first author of this material. The authors would like to thank Joseph Hash for excellent technical assistance; Dr. L.Sweeney (Kintner lab, now at IST Austria) for providing MMP9 antibody and useful discussion, Dr. Graziana Gatto and Xiangyu Ren (Goulding lab) for antibodies and useful discussion. Supported by grants from the US National Institutes of Health (RF1 AG060748 and R01 AI101400 to G.L., and P30CA014195 to the Salk Institute), the Leona M. and Harry B. Helmsley Charitable Trust (to the Salk Institute) and by Marguerite Vogt, H.A and Mary K. Chapman Charitable Trust, Goeddel Chancellor's graduate fellowships and Salk Women and Science award (to Y.H.).

3.7 References

1. Cleveland, D.W. & Rothstein, J.D. From Charcot to Lou Gehrig: deciphering selective motor neuron death in ALS. *Nat Rev Neurosci* **2**, 806-819 (2001).

2. D'Ambrosi, N., Finocchi, P., Apolloni, S., Cozzolino, M., Ferri, A., Padovano, V., Pietrini, G., Carri, M.T. & Volonte, C. The proinflammatory action of microglial P2 receptors is enhanced in SOD1 models for amyotrophic lateral sclerosis. *J Immunol* **183**, 4648-4656 (2009).

3. Ilieva, H., Polymenidou, M. & Cleveland, D.W. Non-cell autonomous toxicity in neurodegenerative disorders: ALS and beyond. *J Cell Biol* **187**, 761-772 (2009).

4. Kaplan, A., Spiller, K.J., Towne, C., Kanning, K.C., Choe, G.T., Geber, A., Akay, T., Aebischer, P. & Henderson, C.E. Neuronal matrix metalloproteinase-9 is a determinant of selective neurodegeneration. *Neuron* **81**, 333-348 (2014).

5. de Waard, M.C., van der Pluijm, I., Zuiderveen Borgesius, N., Comley, L.H., Haasdijk, E.D., Rijksen, Y., Ridwan, Y., Zondag, G., Hoeijmakers, J.H., Elgersma, Y., Gillingwater, T.H. & Jaarsma, D. Age-related motor neuron degeneration in DNA repair-deficient Ercc1 mice. *Acta Neuropathol* **120**, 461-475 (2010).

6. Rothstein, J.D., Tsai, G., Kuncl, R.W., Clawson, L., Cornblath, D.R., Drachman, D.B., Pestronk, A., Stauch, B.L. & Coyle, J.T. Abnormal excitatory amino acid metabolism in amyotrophic lateral sclerosis. *Ann Neurol* **28**, 18-25 (1990).

7. Rothstein, J.D., Kuncl, R., Chaudhry, V., Clawson, L., Cornblath, D.R., Coyle, J.T. & Drachman, D.B. Excitatory amino acids in amyotrophic lateral sclerosis: an update. *Ann Neurol* **30**, 224-225 (1991).

8. Rothstein, J.D. Excitotoxicity hypothesis. *Neurology* **47**, S19-25; discussion S26 (1996).

9. Trotti, D., Aoki, M., Pasinelli, P., Berger, U.V., Danbolt, N.C., Brown, R.H., Jr. & Hediger, M.A. Amyotrophic lateral sclerosis-linked glutamate transporter mutant has impaired glutamate clearance capacity. *J Biol Chem* **276**, 576-582 (2001).

10. Wobst, H.J., Mack, K.L., Brown, D.G., Brandon, N.J. & Shorter, J. The clinical trial landscape in amyotrophic lateral sclerosis-Past, present, and future. *Med Res Rev* **40**, 1352-1384 (2020).

11. Alexianu, M.E., Ho, B.K., Mohamed, A.H., La Bella, V., Smith, R.G. & Appel, S.H. The role of calcium-binding proteins in selective motoneuron vulnerability in amyotrophic lateral sclerosis. *Ann Neurol* **36**, 846-858 (1994).

12. Ince, P., Stout, N., Shaw, P., Slade, J., Hunziker, W., Heizmann, C.W. & Baimbridge, K.G. Parvalbumin and calbindin D-28k in the human motor system and in motor neuron disease. *Neuropathol Appl Neurobiol* **19**, 291-299 (1993).

13. Pasinelli, P., Houseweart, M.K., Brown, R.H., Jr. & Cleveland, D.W. Caspase-1 and -3 are sequentially activated in motor neuron death in Cu,Zn superoxide dismutase-mediated familial amyotrophic lateral sclerosis. *Proc Natl Acad Sci U S A* **97**, 13901-13906 (2000).

14. Boillee, S., Vande Velde, C. & Cleveland, D.W. ALS: a disease of motor neurons and their nonneuronal neighbors. *Neuron* **52**, 39-59 (2006).

15. McCombe, P.A. & Henderson, R.D. The Role of immune and inflammatory mechanisms in ALS. *Curr Mol Med* **11**, 246-254 (2011).

16. Spiller, K.J., Restrepo, C.R., Khan, T., Dominique, M.A., Fang, T.C., Canter, R.G., Roberts, C.J., Miller, K.R., Ransohoff, R.M., Trojanowski, J.Q. & Lee, V.M. Microglia-mediated recovery from ALS-relevant motor neuron degeneration in a mouse model of TDP-43 proteinopathy. *Nat Neurosci* **21**, 329-340 (2018).

17. Taylor, J.P., Brown, R.H., Jr. & Cleveland, D.W. Decoding ALS: from genes to mechanism. *Nature* **539**, 197-206 (2016).

18. Olmos, G. & Llado, J. Tumor necrosis factor alpha: a link between neuroinflammation and excitotoxicity. *Mediators Inflamm* **2014**, 861231 (2014).

19. Moisse, K. & Strong, M.J. Innate immunity in amyotrophic lateral sclerosis. *Biochim Biophys Acta* **1762**, 1083-1093 (2006).

20. Fourgeaud, L., Traves, P.G., Tufail, Y., Leal-Bailey, H., Lew, E.D., Burrola, P.G., Callaway, P., Zagorska, A., Rothlin, C.V., Nimmerjahn, A. & Lemke, G. TAM receptors regulate multiple features of microglial physiology. *Nature* **532**, 240-244 (2016).

21. Nagata, S., Hanayama, R. & Kawane, K. Autoimmunity and the clearance of dead cells. *Cell* **140**, 619-630 (2010).

22. Lemke, G. & Burstyn-Cohen, T. TAM receptors and the clearance of apoptotic cells. *Ann N Y Acad Sci* **1209**, 23-29. PMC3061224 (2010).

23. Lemke, G. & Lu, Q. Macrophage regulation by Tyro 3 family receptors. *Curr Opin Immunol* **15**, 31-36 (2003).

24. Lemke, G. & Rothlin, C.V. Immunobiology of the TAM receptors. *Nat Rev Immunol* **8**, 327-336; PMC2856445 (2008).

25. Lemke, G. Biology of the TAM receptors. *Cold Spring Harbor Perspectives* **5(11)**, doi: 10.1101/cshperspect.a009076. (2013).

26. Lu, Q. & Lemke, G. Homeostatic regulation of the immune system by receptor tyrosine kinases of the Tyro 3 family. *Science* **293**, 306-311 (2001).

27. Rothlin, C.V., Ghosh, S., Zuniga, E.I., Oldstone, M.B. & Lemke, G. TAM receptors are pleiotropic inhibitors of the innate immune response. *Cell* **131**, 1124-1136 (2007).

28. Chiu, I.M., Morimoto, E.T., Goodarzi, H., Liao, J.T., O'Keeffe, S., Phatnani, H.P., Muratet, M., Carroll, M.C., Levy, S., Tavazoie, S., Myers, R.M. & Maniatis, T. A neurodegeneration-specific gene-expression signature of acutely isolated microglia from an amyotrophic lateral sclerosis mouse model. *Cell Rep* **4**, 385-401 (2013).

29. Keren-Shaul, H., Spinrad, A., Weiner, A., Matcovitch-Natan, O., Dvir-Szternfeld, R., Ulland, T.K., David, E., Baruch, K., Lara-Astaiso, D., Toth, B., Itzkovitz, S., Colonna, M., Schwartz, M. & Amit, I. A Unique Microglia Type Associated with Restricting Development of Alzheimer's Disease. *Cell* **169**, 1276-1290 e1217 (2017).

30. Gurney, M.E., Pu, H., Chiu, A.Y., Dal Canto, M.C., Polchow, C.Y., Alexander, D.D., Caliendo, J., Hentati, A., Kwon, Y.W., Deng, H.X., Chen, W., Ping, Z., Sufit, R.L. & Siddique, T. Motor neuron degeneration in mice that express a human Cu,Zn superoxide dismutase mutation. *Science* **264**, 1772-1775 (1994).

31. Philips, T. & Rothstein, J.D. Rodent Models of Amyotrophic Lateral Sclerosis. *Curr Protoc Pharmacol* **69**, 5 67 61-65 67 21 (2015).

32. Lu, Q., Gore, M., Zhang, Q., Camenisch, T., Boast, S., Casagranda, F., Lai, C., Skinner, M.K., Klein, R., Matsushima, G.K., Earp, H.S., Goff, S.P. & Lemke, G. Tyro-3 family receptors are essential regulators of mammalian spermatogenesis. *Nature* **398**, 723-728 (1999).

33. Solomon, J.A., Tarnopolsky, M.A. & Hamadeh, M.J. One universal common endpoint in mouse models of amyotrophic lateral sclerosis. *PLoS One* **6**, e20582 (2011).

34. Zagórska, A., Través, P.G., Lew, E.D., Dransfield, I. & Lemke, G. Diversification of TAM receptor tyrosine kinase function. *Nat Immunol* **15**, 920-928 (2014).

35. Raj, D., Yin, Z., Breur, M., Doorduin, J., Holtman, I.R., Olah, M., Mantingh-Otter, I.J., Van Dam, D., De Deyn, P.P., den Dunnen, W., Eggen, B.J.L., Amor, S. & Boddeke, E. Increased White Matter Inflammation in Aging- and Alzheimer's Disease Brain. *Front Mol Neurosci* **10**, 206 (2017).

36. Yin, Z., Raj, D., Saiepour, N., Van Dam, D., Brouwer, N., Holtman, I.R., Eggen, B.J.L., Moller, T., Tamm, J.A., Abdourahman, A., Hol, E.M., Kamphuis, W., Bayer, T.A., De Deyn, P.P. & Boddeke, E. Immune hyperreactivity of Abeta plaque-associated microglia in Alzheimer's disease. *Neurobiol Aging* **55**, 115-122 (2017).

37. Kiddle, S.J., Thambisetty, M., Simmons, A., Riddoch-Contreras, J., Hye, A., Westman, E., Pike, I., Ward, M., Johnston, C., Lupton, M.K., Lunnon, K., Soininen, H., Kloszewska, I., Tsolaki, M., Vellas, B., Mecocci, P., Lovestone, S., Newhouse, S., Dobson, R. & Alzheimers Disease Neuroimaging, I. Plasma based markers of [11C] PiB-PET brain amyloid burden. *PLoS One* **7**, e44260 (2012).

38. Mattsson, N., Insel, P., Nosheny, R., Zetterberg, H., Trojanowski, J.Q., Shaw, L.M., Tosun, D., Weiner, M. & Alzheimer's Disease Neuroimaging, I. CSF protein biomarkers predicting longitudinal reduction of CSF beta-amyloid42 in cognitively healthy elders. *Transl Psychiatry* **3**, e293 (2013).

39. Glass, C.K., Saijo, K., Winner, B., Marchetto, M.C. & Gage, F.H. Mechanisms underlying inflammation in neurodegeneration. *Cell* **140**, 918-934 (2010).

40. Wooley, C.M., Sher, R.B., Kale, A., Frankel, W.N., Cox, G.A. & Seburn, K.L. Gait analysis detects early changes in transgenic SOD1(G93A) mice. *Muscle Nerve* **32**, 43-50 (2005).

41. Krasemann, S., Madore, C., Cialic, R., Baufeld, C., Calcagno, N., El Fatimy, R., Beckers, L., O'Loughlin, E., Xu, Y., Fanek, Z., Greco, D.J., Smith, S.T., Tweet, G., Humulock, Z., Zrzavy, T., Conde-Sanroman, P., Gacias, M., Weng, Z., Chen, H., Tjon, E., Mazaheri, F., Hartmann, K., Madi, A., Ulrich, J.D., Glatzel, M., Worthmann, A., Heeren, J., Budnik, B., Lemere, C., Ikezu, T., Heppner, F.L., Litvak, V., Holtzman, D.M., Lassmann, H., Weiner, H.L., Ochando, J., Haass, C. & Butovsky, O. The TREM2-APOE Pathway Drives the Transcriptional Phenotype of Dysfunctional Microglia in Neurodegenerative Diseases. *Immunity* **47**, 566-581 e569 (2017).

42. Friese, A., Kaltschmidt, J.A., Ladle, D.R., Sigrist, M., Jessell, T.M. & Arber, S. Gamma and alpha motor neurons distinguished by expression of transcription factor Err3. *Proc Natl Acad Sci U S A* **106**, 13588-13593 (2009).

43. Powis, R.A. & Gillingwater, T.H. Selective loss of alpha motor neurons with sparing of gamma motor neurons and spinal cord cholinergic neurons in a mouse model of spinal muscular atrophy. *J Anat* **228**, 443-451 (2016).

44. Nijssen, J., Comley, L.H. & Hedlund, E. Motor neuron vulnerability and resistance in amyotrophic lateral sclerosis. *Acta Neuropathol* **133**, 863-885 (2017).

45. Lalancette-Hebert, M., Sharma, A., Lyashchenko, A.K. & Shneider, N.A. Gamma motor neurons survive and exacerbate alpha motor neuron degeneration in ALS. *Proc Natl Acad Sci U S A* **113**, E8316-E8325 (2016).

46. Lew, E.D., Oh, J., Burrola, P.G., Lax, I., Zagórska, A., Través, P.G., Schlessinger, J. & Lemke, G. Differential TAM receptor-ligand-phospholipid interactions delimit differential TAM bioactivities. *eLife* **3:e03385**(2014).

47. Lemke, G. Phosphatidylserine Is the Signal for TAM Receptors and Their Ligands. *Trends Biochem Sci* **42**, 738-748 (2017).

48. Lemke, G. How macrophages deal with death. *Nat Rev Immunol* **19**, 539-549 (2019).

49. Akassoglou, K., Probert, L., Kontogeorgos, G. & Kollias, G. Astrocyte-specific but not neuron-specific transmembrane TNF triggers inflammation and degeneration in the central nervous system of transgenic mice. *J Immunol* **158**, 438-445 (1997).

50. Holland, S.J., Pan, A., Franci, C., Hu, Y., Chang, B., Li, W., Duan, M., Torneros, A., Yu, J., Heckrodt, T.J., Zhang, J., Ding, P., Apatira, A., Chua, J., Brandt, R., Pine, P., Goff, D., Singh, R., Payan, D.G. & Hitoshi, Y. R428, a selective small molecule inhibitor of Axl kinase, blocks tumor spread and prolongs survival in models of metastatic breast cancer. *Cancer Res* **70**, 1544-1554 (2010).

51. Myers, K.V., Amend, S.R. & Pienta, K.J. Targeting Tyro3, Axl and MerTK (TAM receptors): implications for macrophages in the tumor microenvironment. *Mol Cancer* **18**, 94 (2019).

52. Sinik, L., Minson, K.A., Tentler, J.J., Carrico, J., Bagby, S.M., Robinson, W.A., Kami, R., Burstyn-Cohen, T., Eckhardt, S.G., Wang, X., Frye, S.V., Earp, H.S., DeRyckere,

D. & Graham, D.K. Inhibition of MERTK Promotes Suppression of Tumor Growth in BRAF Mutant and BRAF Wild-Type Melanoma. *Mol Cancer Ther* **18**, 278-288 (2019).

53. Zhang, W., DeRyckere, D., Hunter, D., Liu, J., Stashko, M.A., Minson, K.A., Cummings, C.T., Lee, M., Glaros, T.G., Newton, D.L., Sather, S., Zhang, D., Kireev, D., Janzen, W.P., Earp, H.S., Graham, D.K., Frye, S.V. & Wang, X. UNC2025, a potent and orally bioavailable MER/FLT3 dual inhibitor. *J Med Chem* **57**, 7031-7041 (2014).

54. Scott, R.S., McMahon, E.J., Pop, S.M., Reap, E.A., Caricchio, R., Cohen, P.L., Earp, H.S. & Matsushima, G.K. Phagocytosis and clearance of apoptotic cells is mediated by MER. *Nature* **411**, 207-211 (2001).

55. Rothlin, C.V., Carrera-Silva, E.A., Bosurgi, L. & Ghosh, S. TAM receptor signaling in immune homeostasis. *Annu Rev Immunol* **33**, 355-391 (2015).

56. Segawa, K., Kurata, S., Yanagihashi, Y., Brummelkamp, T.R., Matsuda, F. & Nagata, S. Caspase-mediated cleavage of phospholipid flippase for apoptotic phosphatidylserine exposure. *Science* **344**, 1164-1168 (2014).

57. Segawa, K., Suzuki, J. & Nagata, S. Constitutive exposure of phosphatidylserine on viable cells. *Proc Natl Acad Sci U S A* **108**, 19246-19251 (2011).

58. Smrz, D., Lebduska, P., Draberova, L., Korb, J. & Draber, P. Engagement of phospholipid scramblase 1 in activated cells: implication for phosphatidylserine externalization and exocytosis. *J Biol Chem* **283**, 10904-10918 (2008).

59. Tufail, Y., Cook, D., Fourgeaud, L., Powers, C.J., Merten, K., Clark, C.L., Hoffman, E., Ngo, A., Sekiguchi, K.J., O'Shea, C.C., Lemke, G. & Nimmerjahn, A. Phosphatidylserine Exposure Controls Viral Innate Immune Responses by Microglia. *Neuron* **93**, 574-586 e578 (2017).

60. Neher, J.J., Emmrich, J.V., Fricker, M., Mander, P.K., Thery, C. & Brown, G.C. Phagocytosis executes delayed neuronal death after focal brain ischemia. *Proc Natl Acad Sci U S A* **110**, E4098-4107 (2013).

61. Gyorffy, B.A., Kun, J., Torok, G., Bulyaki, E., Borhegyi, Z., Gulyassy, P., Kis, V., Szocsics, P., Micsonai, A., Matko, J., Drahos, L., Juhasz, G., Kekesi, K.A. & Kardos, J. Local apoptotic-like mechanisms underlie complement-mediated synaptic pruning. *Proc Natl Acad Sci U S A* **115**, 6303-6308 (2018).

62. Sapar, M.L., Ji, H., Wang, B., Poe, A.R., Dubey, K., Ren, X., Ni, J.Q. & Han, C. Phosphatidylserine Externalization Results from and Causes Neurite Degeneration in Drosophila. *Cell Rep* **24**, 2273-2286 (2018).

63. Scott-Hewitt. N, P.F., Morini. R, Erreni. M, Mahoney M, Witkowska. A, Carey. A, Faggiani. E, Theresia Schuetz. L, Mason. S, Tamborini. M, Bizzotto. M, Passoni. L, Filipello. F, Jahn. R, Stevens. B and Matteoli. M. Local externalization of phosphatidylserine mediates developmental synaptic pruning by microglia. *BioRxiv* (2020).

64. Cory, S. Phosphatidylserine hide-and-seek. *Proc Natl Acad Sci U S A* **115**, 12092-12094 (2018).

65. Graber, D.J., Hickey, W.F. & Harris, B.T. Progressive changes in microglia and macrophages in spinal cord and peripheral nerve in the transgenic rat model of amyotrophic lateral sclerosis. *J Neuroinflammation* **7**, 8 (2010).

66. Zhang, R., Gascon, R., Miller, R.G., Gelinas, D.F., Mass, J., Hadlock, K., Jin, X., Reis, J., Narvaez, A. & McGrath, M.S. Evidence for systemic immune system alterations in sporadic amyotrophic lateral sclerosis (sALS). *J Neuroimmunol* **159**, 215-224 (2005).

67. Chiu, I.M., Phatnani, H., Kuligowski, M., Tapia, J.C., Carrasco, M.A., Zhang, M., Maniatis, T. & Carroll, M.C. Activation of innate and humoral immunity in the peripheral nervous system of ALS transgenic mice. *Proc Natl Acad Sci U S A* **106**, 20960-20965 (2009).

68. Dupuis, L. & Loeffler, J.P. Neuromuscular junction destruction during amyotrophic lateral sclerosis: insights from transgenic models. *Curr Opin Pharmacol* **9**, 341-346 (2009).

69. Krakora, D., Macrander, C. & Suzuki, M. Neuromuscular junction protection for the potential treatment of amyotrophic lateral sclerosis. *Neurol Res Int* **2012**, 379657 (2012).

70. Spiller, K.J., Khan, T., Dominique, M.A., Restrepo, C.R., Cotton-Samuel, D., Levitan, M., Jafar-Nejad, P., Zhang, B., Soriano, A., Rigo, F., Trojanowski, J.Q. & Lee, V.M. Reduction of matrix metalloproteinase 9 (MMP-9) protects motor neurons from TDP-43-triggered death in rNLS8 mice. *Neurobiol Dis* **124**, 133-140 (2019).

71. Miner, J.J., Daniels, B.P., Shrestha, B., Proenca-Modena, J.L., Lew, E.D., Lazear, H.M., Gorman, M.J., Lemke, G., Klein, R.S. & Diamond, M.S. The TAM receptor

Mertk protects against neuroinvasive viral infection by maintaining blood-brain barrier integrity. *Nat Med* **21**, 1464-1472 (2015).

72. Garbuzova-Davis, S., Haller, E., Saporta, S., Kolomey, I., Nicosia, S.V. & Sanberg, P.R. Ultrastructure of blood-brain barrier and blood-spinal cord barrier in SOD1 mice modeling ALS. *Brain Res* **1157**, 126-137 (2007).

73. Zhong, Z., Deane, R., Ali, Z., Parisi, M., Shapovalov, Y., O'Banion, M.K., Stojanovic, K., Sagare, A., Boillee, S., Cleveland, D.W. & Zlokovic, B.V. ALS-causing SOD1 mutants generate vascular changes prior to motor neuron degeneration. *Nat Neurosci* **11**, 420-422 (2008).

74. Miyazaki, K., Ohta, Y., Nagai, M., Morimoto, N., Kurata, T., Takehisa, Y., Ikeda, Y., Matsuura, T. & Abe, K. Disruption of neurovascular unit prior to motor neuron degeneration in amyotrophic lateral sclerosis. *J Neurosci Res* **89**, 718-728 (2011).

75. Garbuzova-Davis, S. & Sanberg, P.R. Blood-CNS Barrier Impairment in ALS patients versus an animal model. *Front Cell Neurosci* **8**, 21 (2014).

76. Henkel, J.S., Beers, D.R., Wen, S., Bowser, R. & Appel, S.H. Decreased mRNA expression of tight junction proteins in lumbar spinal cords of patients with ALS. *Neurology* **72**, 1614-1616 (2009).

77. Brosius Lutz, A., Chung, W.S., Sloan, S.A., Carson, G.A., Zhou, L., Lovelett, E., Posada, S., Zuchero, J.B. & Barres, B.A. Schwann cells use TAM receptor-mediated phagocytosis in addition to autophagy to clear myelin in a mouse model of nerve injury. *Proc Natl Acad Sci U S A* **114**, E8072-E8080 (2017).

78. Meyer-Luehmann, M. & Prinz, M. Myeloid cells in Alzheimer's disease: culprits, victims or innocent bystanders? *Trends Neurosci* **38**, 659-668 (2015).

79. Parkhurst, C.N., Yang, G., Ninan, I., Savas, J.N., Yates, J.R., 3rd, Lafaille, J.J., Hempstead, B.L., Littman, D.R. & Gan, W.B. Microglia promote learning-dependent synapse formation through brain-derived neurotrophic factor. *Cell* **155**, 1596-1609 (2013).

80. Wang, Y., Nakayama, M., Pitulescu, M.E., Schmidt, T.S., Bochenek, M.L., Sakakibara, A., Adams, S., Davy, A., Deutsch, U., Luthi, U., Barberis, A., Benjamin, L.E., Makinen, T., Nobes, C.D. & Adams, R.H. Ephrin-B2 controls VEGF-induced angiogenesis and lymphangiogenesis. *Nature* **465**, 483-486 (2010).

81. Wang, X., Sathe, A.A., Smith, G.R., Ruf-Zamojski, F., Nair, V., Lavine, K.J., Xing, C., Sealfon, S.C. & Zhou, L. Heterogeneous origins and functions of mouse skeletal muscle-resident macrophages. *Proc Natl Acad Sci U S A* **117**, 20729-20740 (2020).

82. Mitsumoto, H., Brooks, B.R. & Silani, V. Clinical trials in amyotrophic lateral sclerosis: why so many negative trials and how can trials be improved? *Lancet Neurol* **13**, 1127-1138 (2014).

83. Neumann, M., Sampathu, D.M., Kwong, L.K., Truax, A.C., Micsenyi, M.C., Chou, T.T., Bruce, J., Schuck, T., Grossman, M., Clark, C.M., McCluskey, L.F., Miller, B.L., Masliah, E., Mackenzie, I.R., Feldman, H., Feiden, W., Kretzschmar, H.A., Trojanowski, J.Q. & Lee, V.M. Ubiquitinated TDP-43 in frontotemporal lobar degeneration and amyotrophic lateral sclerosis. *Science* **314**, 130-133 (2006).

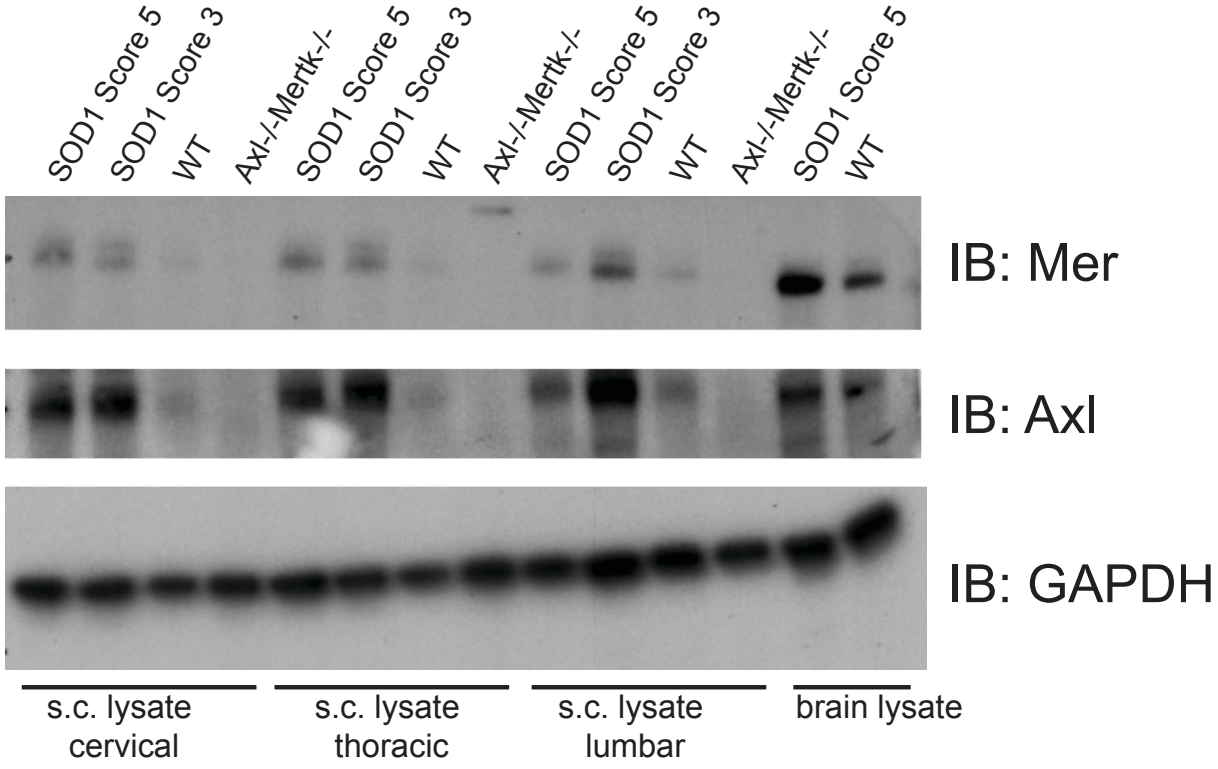

Figure 3.3.1-1. TAM upregulation is throughout all levels of SOD1 mouse spinal cord at late stages of ALS

Extracts of cervical, thoracic and lumbar spinal cord and brain of WT and two SOD1 mice at disease score 3 and end point (E.P.) immunoblotted for Mer and Axl. SOD1 spinal cord lysates demonstrate robust up-regulation of Axl and Mer at all levels of spinal cord as well as in brain at late and end stage of disease. *Axl*$^{-/-}$*Mertk*$^{-/-}$ extracts are antibody specificity controls; GAPDH is a loading control.

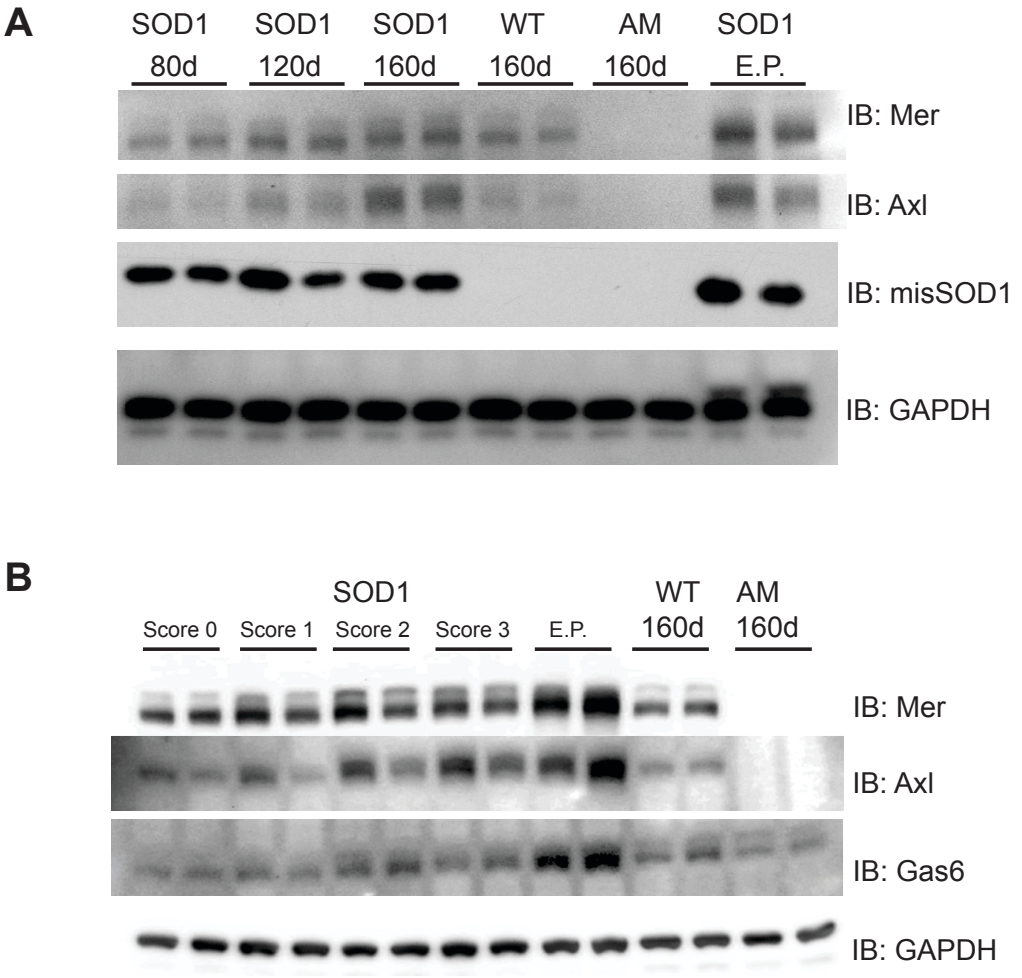

Figure 3.3.1-2. Time course of TAM upregulation in the development of ALS

Extracts of whole spinal cord of two biological replicates of SOD1, WT and *Axl*$^{-/-}$*Mertk*$^{-/-}$ genotypes at indicated time point (**A**) or indicated ALS score according to Solomon et al., 2011 (**B**) immunoblotted for Mer, Axl, Gas6 or misfolded SOD1 (B8H10) and GAPDH as a loading control. Data are representative of two independent experiments each with two technical replicates for a total of n = 4 biological replicates/genotype/timepoint or disease score.

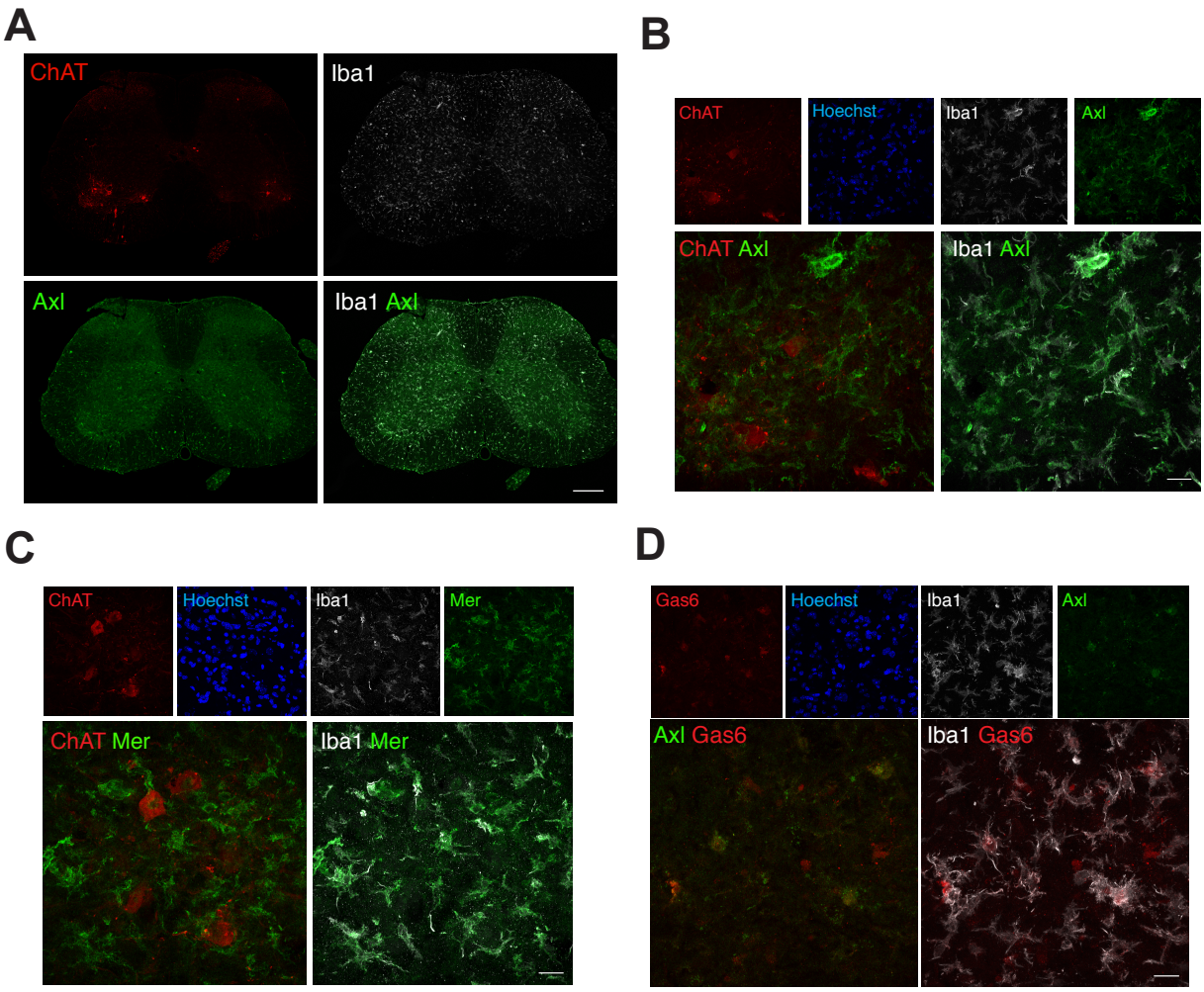

Figure 3.3.1-3. TAM receptors are up-regulated specifically in microglia in the spinal cord

Sections of SOD1 lumbar L4 spinal cord at stage 3, stained with the indicated antibodies for Iba1, ChAT and Axl (**A**) at low magnification overview and at high magnification at ventral horn of these sections for Axl (**B**), Mer (**C**) and TAM ligand Gas6 (**D**). Lower panels of B-D are enlargements of the upper panels. Expression of Mer and Axl at non-diseased baseline is seen at low levels in spinal microglia in healthy WT mice or prior to motor symptom onset in SOD1 mice (data not shown) and their expression up-regulation is exclusively in Iba1-labeled microglia at late stage of disease and Gas6 expression is in large in colocalization with Iba1 and Axl, or in juxtaposition with them. Scale bar = 200μm(A), and 20μm (B-D). A-D contain representative images from N $\geq$ 3 sections per mouse from n $\geq$ 3 mice.

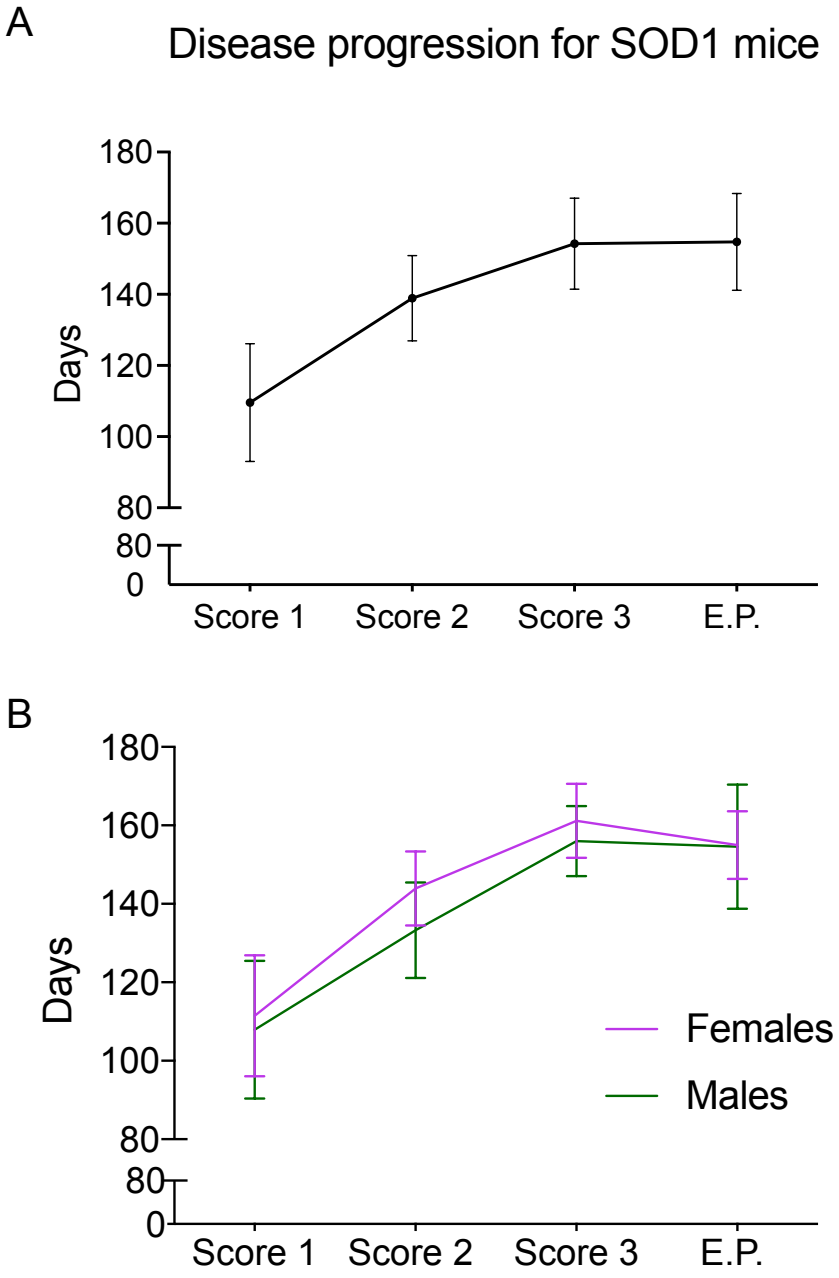

Figure 3.3.2-1. Disease progression of SOD1 mice.

(**A**) SOD1 mice of both males and females are evaluated for the onset day of key motor symptoms for reaching each disease stage based on a modified objective scoring system. Averaged days of arrival at each disease stage from pooled 3 cohorts of a total of 64 SOD1 mice are shown (A) or of 30 females and of 34 males (**B**). No statistically significant difference between genders was observed as for the average day to arrival at each individual disease score or overall disease progression. Mann-Whitney test and two-way ANOVA. $P > 0.05$. Mean ± SD is shown and applies to all subsequent panels in this chapter.

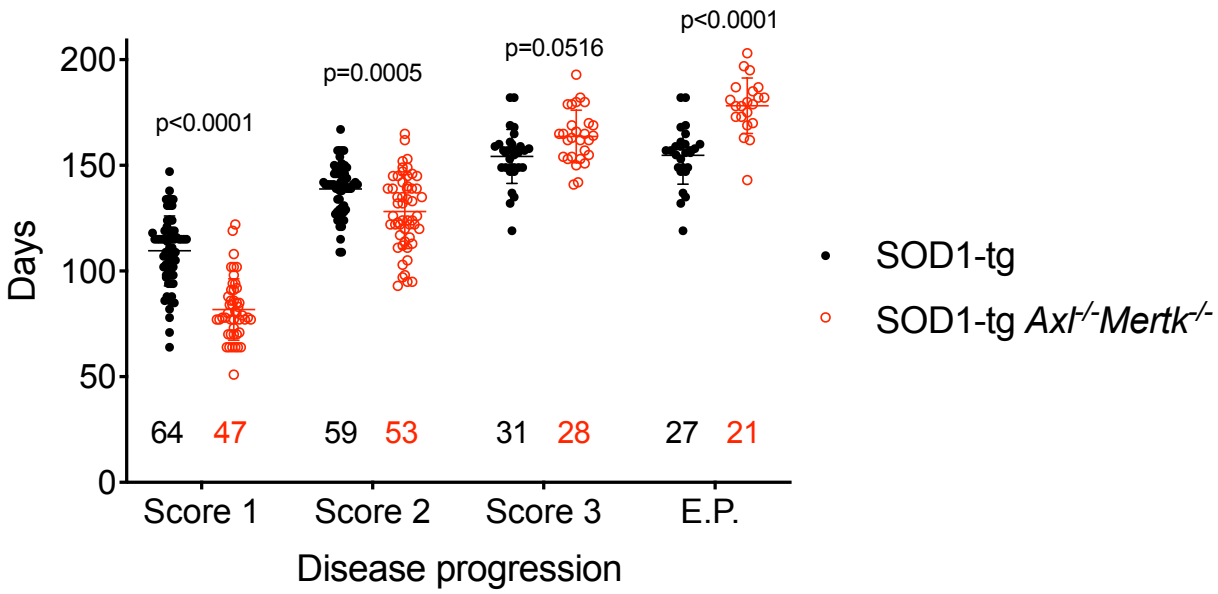

Figure 3.3.2-2. Comparison of disease progression of SOD1 and SOD1 *Axl*$^{-/-}$*Mertk*$^{-/-}$ mice. Pooled cohorts of SOD1 and SOD1 *Axl*$^{-/-}$*Mertk*$^{-/-}$ mice are evaluated for the onset day of reaching disease stage. Animal numbers n for each group at each disease stage are noted on the graph. SOD1 *Axl*$^{-/-}$*Mertk*$^{-/-}$ mice show markedly advanced arrival of early stages of disease (score 1 and 2) but significantly delayed appearance of E.P. in comparison to SOD1 mice. Two-way ANOVA with Sidak's multiple comparison test, P values as noted.

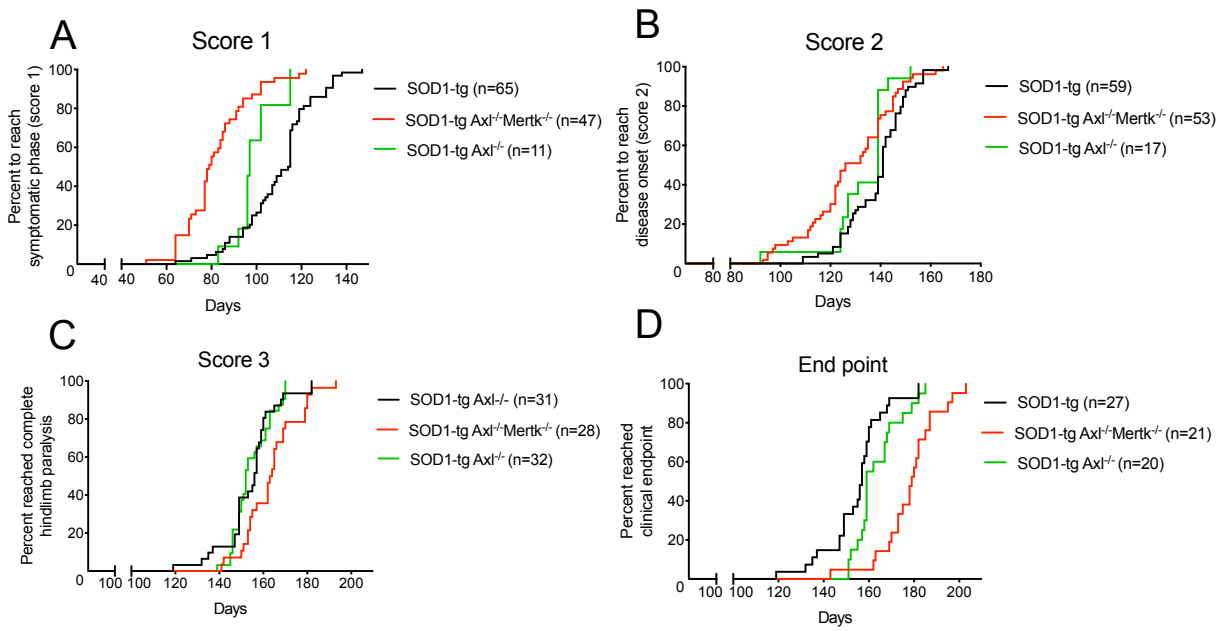

Figure 3.3.2-3. Comparisons of latency to reach individual disease stages among SOD1, SOD1 *Axl*$^{-/-}$, SOD1 *Axl*$^{-/-}$*Mertk*$^{-/-}$ mice.

Reverse Kaplan-Meier plots showing the cumulative probability (expressed in percentage) to reach clinical score 1 (**A**), 2 (**B**), 3 (**C**) and end point (E.P.) (**D**) of each indicated genotype. P < 0.0001 (A), = 0.0072 (B), 0.0151 (C), <0.0001 (D) between SOD1 and SOD1 *Axl*$^{-/-}$*Mertk*$^{-/-}$, P = 0.0023 (A), 0.0209 (B), 0.02010 (C), 0.0550 (D) between SOD1 and SOD1 *Axl*$^{-/-}$ curves and P = 0.0115 (A), 0.1087 (B), 0.0020 (C), 0.0003 (D) between SOD1 *Axl*$^{-/-}$and SOD1 *Axl*$^{-/-}$ *Mertk*$^{-/-}$. Log-rank test. n number as noted.

Figure 3.3.1-1. Direct electrical interaction drives lateral inhibition between ORNs.

Sections of lumbar spinal cord featuring ventral horn (VH) labeled with antibodies as indicated in representative images (**A**) and quantified for ChAT+ total MN number on L1-2 level (**B**) and on L3-5 level (**D**), and for co-localization analysis with alpha MN marker NeuN (**C, E**) and fast fatigable (FF) alpha MN marker MMP9 at L3-5 level (**F**), where the majority of FF MNs are found. All MMP9 MNs are NeuN+, though some NeuN+ cells are not MMP9+. Since almost MMP9+ cells are preferentially found in lateral motor column (LMC), only LMC data is shown at this stage of disease. MN composition of lumbar LMC in spinal sections L3-5 from the indicated genotypes is visualized in **G** for the three populations of ChAT+ MNs: NeuN-MMP9- (non-alpha MNs), NeuN+MMP9- (non-FF alpha MNs) and NeuN+MMP9+ MNs (FF alpha MNs). A non-significant reduction of MMP9+ MNs percentage was seen specifically in SOD1 *Axl*$^{-/-}$*Mertk*$^{-/-}$ but not in SOD1 mice at day 80 (F,G). Data points represent cell number per VH pooled from n ≥ 3 per genotype. One-way ANOVA test. P values as noted. n.s., not significant.

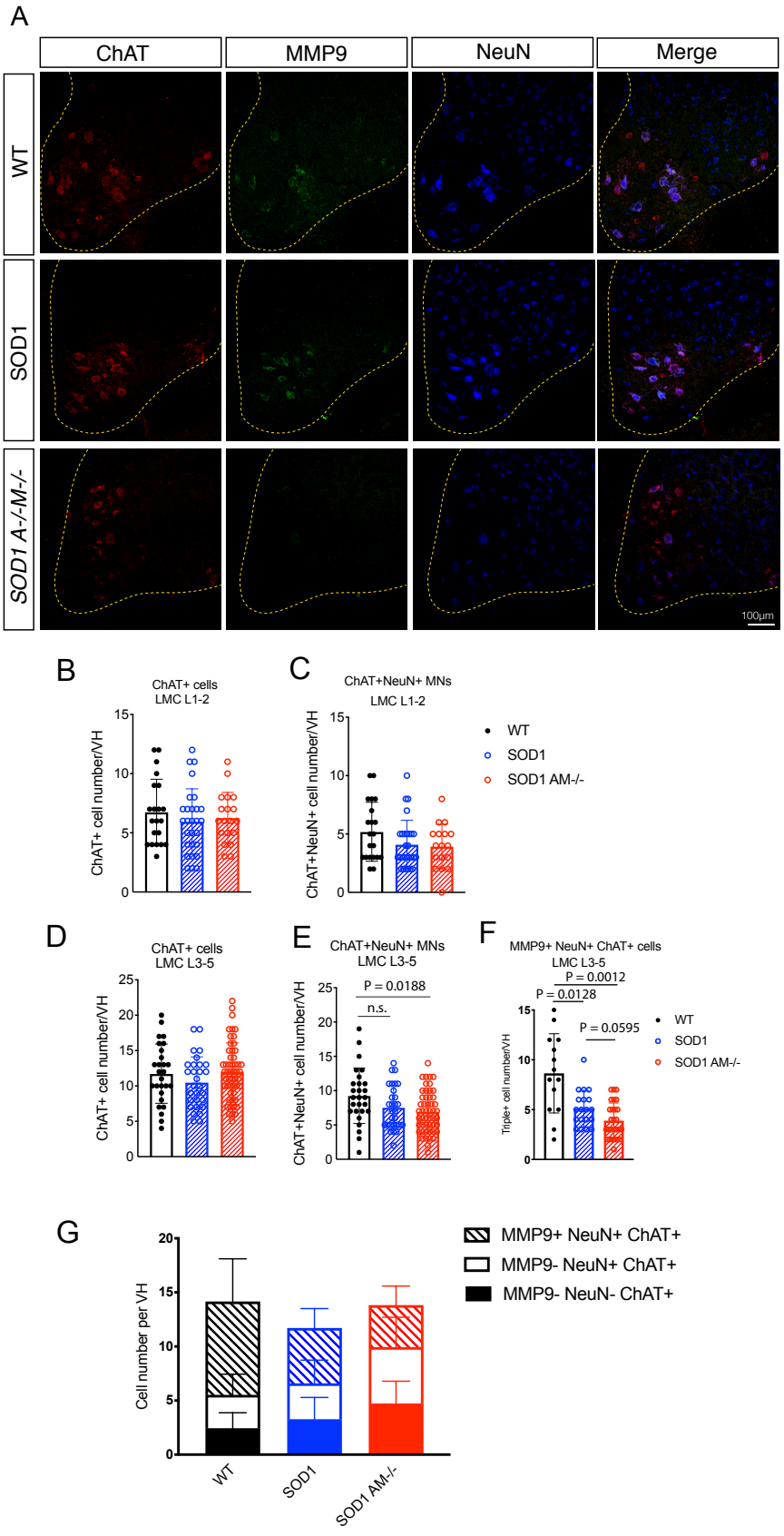
A
ChAT
MMP9
NeuN
Merge
WT
SOD1
SOD1 A-/-M-/-
100µm
B
ChAT+ cells
LMC L1-2
ChAT+ cell number/VH
C
ChAT+NeuN+ MNs
LMC L1-2
ChAT+NeuN+ cell number/VH
WT
SOD1
SOD1 AM-/-
D
ChAT+ cells
LMC L3-5
ChAT+ cell number/VH
E
ChAT+NeuN+ MNs
LMC L3-5
P = 0.0188
n.s.
ChAT+NeuN+ cell number/VH
F
MMP9+ NeuN+ ChAT+ cells
LMC L3-5
P = 0.0012
P = 0.0128
P = 0.0595
Triple+ cell number/VH
WT
SOD1
SOD1 AM-/-
G
Cell number per VH
MMP9+ NeuN+ ChAT+
MMP9- NeuN+ ChAT+
MMP9- NeuN- ChAT+
WT
SOD1
SOD1 AM-/-

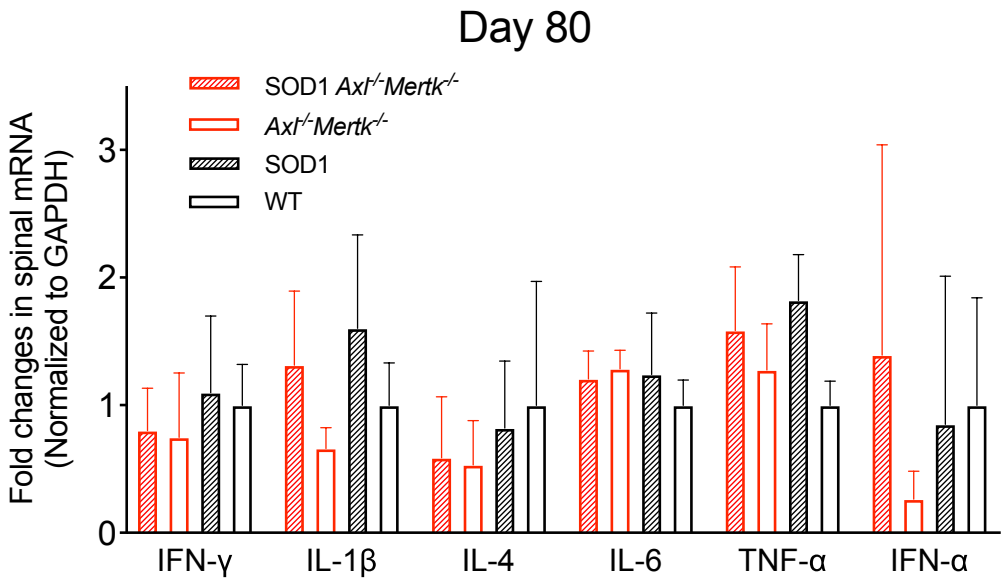

Figure 3.3.2-5. Inflammation-related gene expression analysis reveals no detectable level of neuroinflammation in either SOD1 group at day 80

Gene expression of the indicated cytokines were measured from mRNA prepared from whole spinal cord of the indicated genotypes at day 80 and quantified by qPCR after being normalized to housekeeping gene *Gapdh*. Relative expression (y-axis) of each gene in different groups is relative to the mean of the WT group for the respective gene. n ≥ 5 per genotype. One-way ANOVA test.

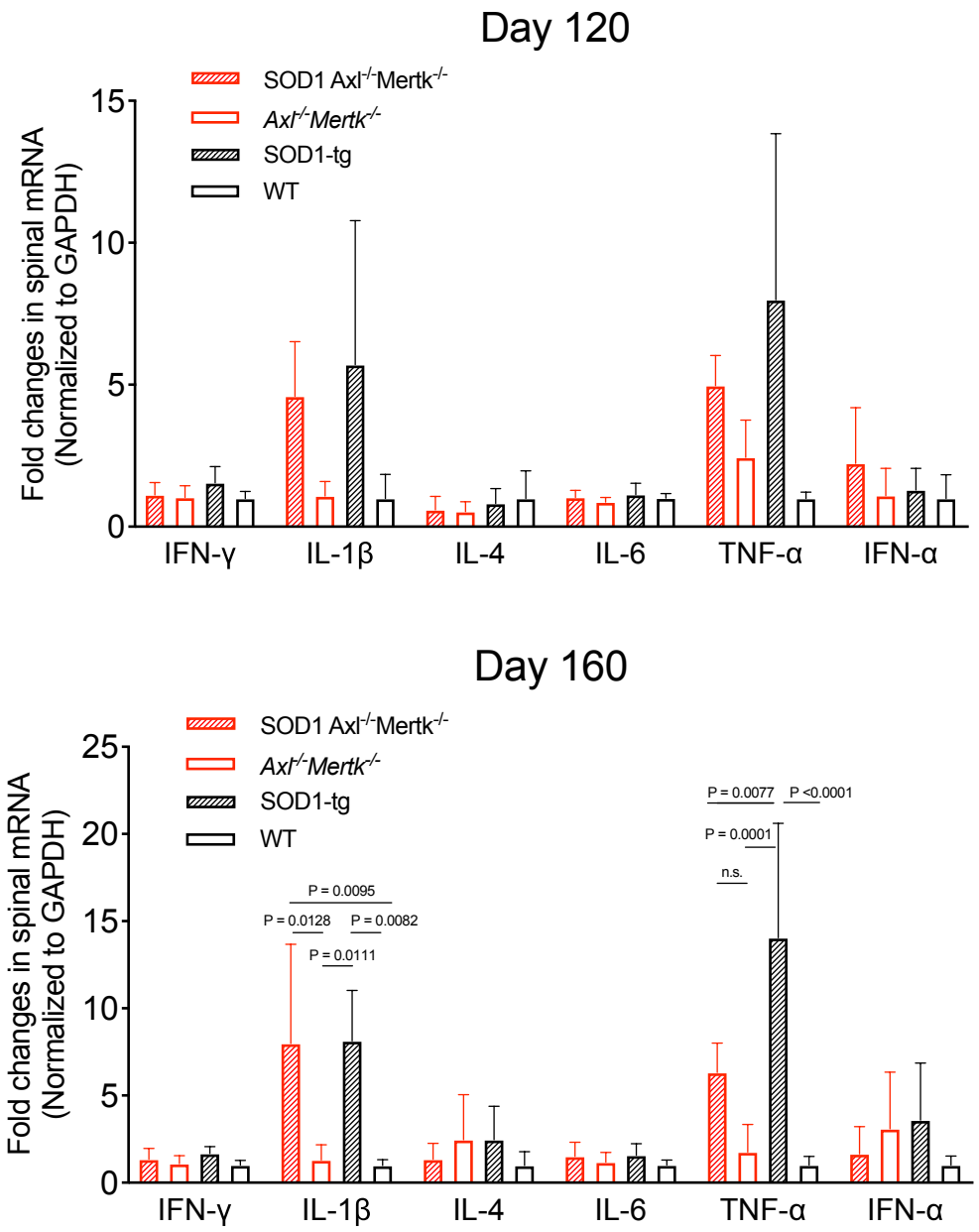

Figure 3.3.2-6. TAM deficiency in SOD1 mice leads to reduced level of inflammatory response through gene expression analysis at day 120 and day 160

Gene expression of the above-mentioned cytokines in the indicated genotypes after symptomatic onset (day 120, **A**) and at late stage (day 160, **B**) were measured and quantified by qPCR relative to WT group. SOD1 *Axl*$^{-/-}$*Mertk*$^{-/-}$ group shows ameliorated level of TNF-α expression comparing to SOD1 mice at day 160 and a similar trend at day 120 though not significant. n ≥ 5 per genotype. One-way ANOVA test. Statistically significant P values as noted.

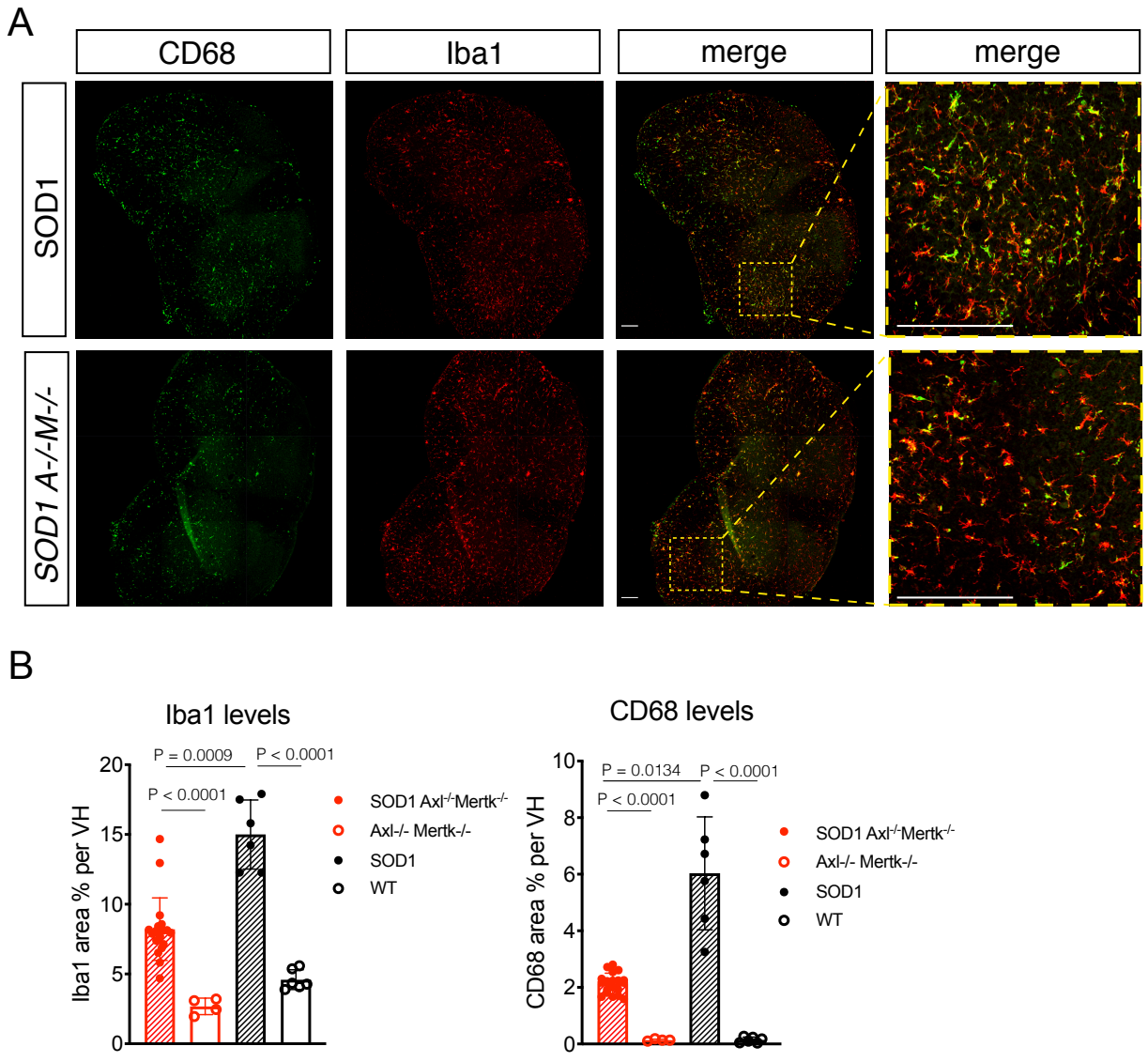

Figure 3.3.2-7. Direct electrical interaction drives lateral inhibition between ORNs.

(**A**) Representative lumbar spinal cord at day 160 overview (left three sets of panels) and enlarged zoom-in view of VH (right yellow boxed panels) co-labeled with Iba1, generic myeloid cell marker whose expression increases upon activation and CD68, a myeloid-specific lysosomal marker indicative of phagocytic capacity. (**B**) Quantification of the percent area of VH occupied by Iba1 (left) and CD68 (right) in the genotypes indicated. SOD1 *Axl*$^{-/-}$ *Mertk*$^{-/-}$ group shows a notable reduction of both Iba1+ as well as co-localizing CD68+ area comparing to SOD1 mice. Data points represent area percentage per VH averaged bilaterally per cord section pooled from n = 3 per genotype. One-way ANOVA test. Statistically significant P values as noted. Scale Bar = 200μm.

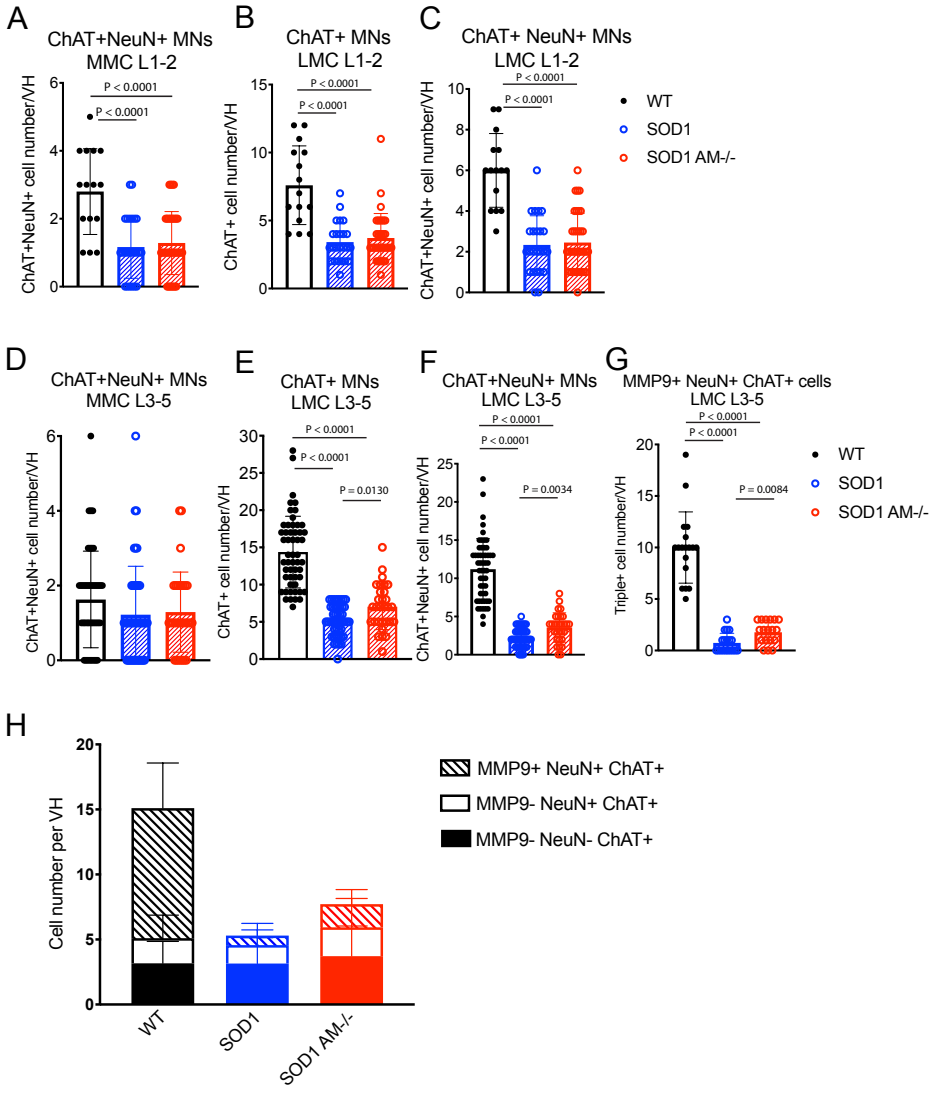

Figure 3.3.2-8. Delayed loss of MN and ALS-vulnerable MN subsets in spinal lumbar sections of SOD1 *Axl*$^{-/-}$*Mertk*$^{-/-}$ mice comparing to at day 160

Quantification of ChAT+ NeuN+ MN number in medium motor column (MMC) and LMC on L1-2 level (**A**, **C**) and on L3-5 level (**D, F**), respectively. Quantification of FF alpha MN number is also quantified with MMP9 co-labeling with NeuN and ChAT at L3-5 (**G**). ChAT+ total MN number is significantly reduced at late stage of disease comparing with WT on both L1-2 and L3-5 levels in LMC as quantified in (**B, E**), though there is a modest rescue effect in total ChAT+ MN number in TAM-mutant SOD1 mice. The same phenotype is seen in both quantification of ChAT+ NeuN+ alpha MNs and MMP9+ChAT+NeuN+ (triple positive) cells on L3-5 LMC where MMP9+ cells are abundantly encountered in WT mice. MN composition of lumbar LMC in spinal sections L3-5 from the indicated genotypes is visualized in **H** for the three populations of ChAT+ MNs: NeuN-MMP9- (non-alpha MNs), NeuN+MMP9- (non-FF alpha MNs) and NeuN+MMP9+ MNs (FF alpha MNs). An overall preservation of total ChAT+ MNs as well as a specific rescue of ALS-vulnerable FF alpha MNs is seen in SOD1 *Axl*$^{-/-}$ *Mertk*$^{-/-}$ comparing with in SOD1 mice at day 160 (E-H). Data points represent cell number per VH pooled from n ≥ 3 per genotype. One-way ANOVA test. P values as noted.